UNIVERSITY OF SZCZECIN

INSTITUTE OF PHYSICS

ENRICO LAUDATO

A DHOST MODEL TO UNIFY THEM ALL

PHD THESIS
WRITTEN UNDER SUPERVISION OF
DR HAB. VINCENZO SALZANO, PROF. US

SZCZECIN 2024

INSTYTUT FIZYKI
UNIWERSYTETU SZCZECIŃSKIEGO

STATEMENT 1

I declare that I wrote the submitted doctoral dissertation myself. This means that when writing the dissertation entitled — **"A DHOST model to unify them all"** — apart from the necessary consultations, I did not use the help of other people, and in particular, I did not commission other persons to prepare the dissertation or its parts, and I did not copy the dissertation or its parts from other people. At the same time, I acknowledge that if the above statement turns out to be untrue, the resolution awarding me the doctoral degree will be withdrawn.

Szczecin, 13/03/2024 .....

signature

STATEMENT 2

I consent to the disclosure of my dissertation entitled — **"A DHOST model to unify them all".**

Szczecin, 13/03/2024 .....

signature

ul. Wielkopolska 15
70-451 Szczecin
tel. +48 91 444 12 27
www.fiz.usz.edu.pl

Acknowledgements

I would like to express my sincere gratitude to my supervisor, dr. hab. Vincenzo Salzano, professor at US, for supervising and guiding me over these four years, for igniting my passion, for our inspiring conversations, and, last but not least, for the great patience he has shown. I am well aware that it was sometimes incredibly hard to work with me.

I would also like to thank Dr. Hussain Gohar, a collaborator and friend, for the insightful discussions and for every moment we shared.

During my PhD, I experienced tough moments. However, if I was always able to get through these, it was only thanks to Andrea, Ricci, Gali, Tang, Alessandra, Fabian, Sam, Paolo, Saboura, and many more who were always there for me.

I also wish to thank my PhD companions, Fabian, Filippo, Ilim, Marcello, Paolo, Saboura, and Sam for the ideas and feedback we shared. It was enriching not only from a professional but also from a human point of view.

I express my heartfelt gratitude to my family for the unwavering support you provided, continuously saying how proud you were of me.

The most important part comes last to my life partner Nora. When I began to doubt the realization of my PhD aspirations, your support and love spurred me on to persevere and pursue my goal. Without you, I wouldn't be standing here today. Your attitude and passion towards every situation in life have always been

an inspiration to me. I am deeply grateful because not only you have always supported me, but also for your immense patience in handling difficult situations with me. Without you, I would not be the person who I am today.

Abstract

The Λ Cold Dark Matter model, although able to provide a satisfactory description of most of the data collected at cosmological and astrophysical scales, faces both theoretical and observational problems. Its foundation is the assumption of General Relativity as the definitive theory of gravity. Once Einstein's theory is accepted, the content of 95% of the Universe must be "dark". Dark Energy, which accounts for 68% of the universe's energy budget, drives the late-time accelerated expansion phase of the universe, while Dark Matter, which accounts for the 27%, manifests itself as the additional gravitational attraction observed at astrophysical scales.

Today, however, we have no idea about the nature of both the Dark Energy and the Dark Matter. Because of that, cosmologists are looking for solutions. One approach is to consider General Relativity as a special case of a more general theory of gravity. Such approach leads to the so-called Extended Theories of Gravity. However, all new gravitational models must be reduced to General Relativity on the scale of the Solar system, where it has been found to be fully valid. The safe mechanism that allows Extended Gravity Theories to reproduce the effect of Dark Energy at cosmological scales and reduce to General Relativity at Solar System scales is generally defined as a screening mechanism.

Interestingly, in some of these Extended Theories, this screening mechanism

is partially broken. Thus, General Relativity is also modified inside a source of matter, such as clusters and galaxies, where Dark Matter plays a key role.

This partial breaking of the screening mechanism may provide a way to consider Extended Theories of Gravity as a viable mechanism to realise a unification of Dark Energy at cosmological scales and Dark Matter at astrophysical scales. The aim of this work is to shed light on this possibility by adopting a specific model belonging to the domain of Degenerate Higher-Order Scalar Tensor theories with a broken screening mechanism, and testing it by trying to use the most complete observational data at astrophysical scales involving galaxy clusters and galaxies.

In the first part we focus on the scales of galaxy clusters. We have tested a dataset of 16 clusters selected from the *CLASH* programme. Our analysis includes two independent probes, X-ray and gravitational lensing observations, combining both strong and weak lensing effects.

A multi-component approach has also been taken. This means that the cluster masses have been modelled taking into account not only the Dark Matter and hot X-ray gas component, but also the contribution from the Brightest Cluster Galaxy and other galaxy components.

The chosen Degenerate Higher-Order Scalar Tensor theory model is characterised by a partially broken Vainshtein screening. Two different scenarios were considered. In the first scenario, the model was used to replace only Dark Energy. We therefore assume that Dark Matter is also included in the cluster mass budget. In the second scenario, the model is assumed to also play the role of Dark Matter due to the partial breaking of the Vainshtein screen.

We show that the this model has a slight statistical advantage over General Relativity in mimicking the Dark Energy component. In addition, it reduces the discrepancy between the X-ray and gravitational lensing masses. When the model acts as both Dark Energy and Dark Matter, it shows a statistical disadvantage when compared with general relativity.

In the second part, we continue our investigation of the same model at galactic scales. In particular, we analyse the kinematics of a sub-sample of so-called Ultra Diffuse Galaxies (UDGs) observed with the Dragonfly Telescope Array. These systems are very interesting in the context of testing Extended Theories of Gravity,

as they show very different properties, including galaxies with a very low Dark Matter content, such as NGC 1052-DF2 and NGC 1052-DF4, and others that are Dark Matter dominated, such as Dragonfly 44.

The model has been taken into account to study firstly the velocity dispersion of NGC 1052-DF2, whose observational data have been derived using associated globular clusters. The same analysis was then extended to NGC 1052-DF4 and to Dragonfly 44. We consider three scenarios: one in which the galaxies are entirely baryonic systems, a second in which the model mimics Dark Energy, and a third one in which the model also plays the role of the Dark Matter component. In the latter case, the galaxy masses were modelled using only the stellar component.

For NGC 1052-DF2 and NGC 1052-DF4, we confirm that the best agreement with the data in the General Relativity framework occurs when these two galaxies are considered as almost entirely baryonic systems. For a Dark Matter dominated system such as Dragonfly 44, this scenario is strongly disfavoured compared to one in which a Dark Matter component is assumed to be the main dominant mass component.

When the model mimics Dark Energy, the General Relativity reference case is still favoured. This result is largely expected, since Dark Energy does not play a relevant role on galactic scales. When the model plays the role of an "effective" Dark Matter component, we show that for NGC 1052-DF2 and NGC 1052-DF4 this scenario is as successful as General Relativity. In contrast, Dragonfly 44 still requires a Dark Matter component.

Table of Contents

CHAPTER 1

Introducing the consensus cosmology: pros and cons

Twenty-four years have passed since one of the most important discoveries for modern cosmology: that our Universe is in a phase of accelerated expansion [1, 2]. According to the standard *consensus* approach, which fully relies on Einstein's General Relativity, recognized as the most reliable theory of gravity, such accelerated expansion should be caused by an unknown form of energy, which has been purposely called Dark Energy (DE). Its existence and crucial role in the dynamics of our Universe has been successively confirmed by the most up-to-date measurements of the Cosmic Microwave Background (CMB) anisotropies realised by the *Planck* telescope [3] and by a set of different types of cosmological and astrophysical data, such as the Baryon Acoustic Oscillations (BAO), galaxy clustering and cosmic weak lensing, among the most relevant lately [4–7]. All of this data have set that DE should account for $\sim 68\%$ of the total energy-matter content of the Universe.

In addition to DE, a further $\sim 27\%$ of the Universe's composition is also unknown [3]. This second dark component, referred to as Dark Matter (DM), has been "known" (i.e. there has been evidence for its existence) for a longer time,

starting from the studies of Zwicky [8] in the early thirties of the previous century. Shreds of evidence of such kind of matter, which interacts only through gravity with baryonic "standard" matter (estimated to contribute for only $\sim 5\%$ to the matter in our Universe), have been collected once again by multiple types of observations at astrophysical scales, as in the case of the pioneering works about the flattening of the rotation curves of spiral galaxies [9], and, at cosmological scales, from the same *Planck* satellite [3].

1.1 ΛCDM, or the *consensus* model

It is important to emphasize that the current cosmological *consensus* model is built on the crucial assumption of General Relativity (GR) as the "final" theory of gravity. As it is well known, the Hilbert-Einstein action, which determines its role in the dynamics of all structures in our Universe and of the entire Universe itself, reads

$$S_{HE} = \int d^4x\sqrt{-g}\left[\frac{c^4}{16\pi G}(R-2\Lambda)+\mathscr{L}_m(\phi_i)\right], \tag{1.1}$$

where: G is the Newtonian universal gravitational constant; c is the speed of light; R is the Ricci scalar; g is the determinant of the metric, $g_{\mu\nu}$; $\mathscr{L}(\phi_i)$ is the matter Lagrangian which includes all the matter species ϕ_i; and Λ is Einstein's *"biggest blunder"*, the Cosmological Constant responsible for the late-time accelerated expansion phase of the Universe (and whose role and alternatives will be discussed in more detail in the next sections).

Once a variational principle is applied to the above action with respect to the metric, we arrive at the famous Einstein equations,

$$R_{\mu\nu}-\frac{1}{2}Rg_{\mu\nu}+\Lambda g_{\mu\nu}=\frac{8\pi G}{c^4}T_{\mu\nu}, \tag{1.2}$$

where the geometrical effects of GR are fully contained and described by the metric tensor $g_{\mu\nu}$, the Ricci tensor $R_{\mu\nu}$ and the Ricci scalar R, whilst the stress-energy tensor, $T_{\mu\nu}$, incorporates all the properties of the energy and matter components which are in the Universe.

To proceed further in the use of Einstein's equations, further assumptions have to be made. One of them, and surely one of the most important, is the so-called

Cosmological Principle, namely, the assumption that the Universe is homogeneous and isotropic on sufficiently large scales. Although studies intended to verify at which scale this assumption can be considered satisfied are still ongoing [10], it is generally assumed that our Universe is homogeneous and isotropic at scales larger than $\sim 250 \div 300$ Mpc. As a consequence of the assumption of the Cosmological Principle, the metric $g_{\mu\nu}$ can be represented by the Friedman-Robertson-Lemaitre-Walker (FRLW) metric, under which a line element can be expressed as

$$ds^2 = g_{\mu\nu}dx^\mu dx^\nu = -c^2dt^2 + a^2(t)\left[\frac{dr^2}{1-kr^2} + r^2 d\Omega^2\right] \tag{1.3}$$

where: $d\Omega^2 = d\theta^2 + \sin^2\theta d\phi^2$ is the solid angle; k is a constant, generally expressed in the units of $[length]^{-2}$, representing the curvature of the spacetime, and that can assume the values $\{1, 0, -1\}$ whether the Universe is, respectively, closed (sphere), spatially flat (Euclidean), and open (hyperboloid). Finally, the function $a(t)$ is the scale factor (which we assume here to be dimensionless) describing how the Universe expands.

Together with the metric, we also need to set some general properties for the energy-matter content. It is generally assumed, in the consensus scenario, that the matter distribution in the Universe is in the form of a perfect cosmological fluid. This leads to defining the stress-energy tensor, $T^{\mu\nu}$ as

$$T^{\mu\nu} = (\rho c^2 + p)\, u^\mu u^\nu + p g^{\mu\nu}, \tag{1.4}$$

where ρ represents the density of the cosmological fluid(s), p is their pressure and u is their four-velocity in a comoving frame.

With all these ingredients, Einstein's equations can be cast in a form that is more easily handled when compared with observational data. This form is known as the Friedmann equations:

$$H^2 \equiv \left(\frac{\dot{a}}{a}\right)^2 = \frac{8\pi G}{3}\sum_i \rho_i + \frac{\Lambda c^2}{3} - \frac{kc^2}{a^2}, \tag{1.5}$$

$$\frac{\ddot{a}}{a} = -\frac{4\pi G}{3}\sum_i \left(\rho_i + \frac{3p}{c^2}\right) + \frac{\Lambda c^2}{3} \tag{1.6}$$

where we have introduced the Hubble parameter, $H(a)$, and where ρ_i and p_i are, obviously, the density and the pressure of each energy-matter species. The combination of these two equations leads to another equally fundamental equation (which can also be obtained independently from them from the assumption of conservation of energy-mass applied directly to the stress-energy tensor), the continuity equation which, in its most general form, reads as

$$\sum_i \rho_i + 3H \sum_i \left(\rho_i + \frac{p_i}{c^2}\right) = 0\,. \tag{1.7}$$

In the case of the absence of any interaction among the various energy-matter components, the previous equation can be decoupled ending with a similar expression valid for each component separately.

Introducing the critical density of the Universe, namely the density of the Universe if there were no Λ and a spatially flat geometry, $\rho_c = \frac{3H_0}{8\pi G}$, we can define the dimensionless density parameters $\Omega_i = \rho_i/\rho_c$, after which the first Friedman equation can be rewritten as

$$H^2(a) = H_0^2 \left(\Omega_{m,0} a^3 + \Omega_{r,0} a^4 + \Omega_k a^2 + \Omega_\Lambda\right) \tag{1.8}$$

where: H_0 is the Hubble constant; $\Omega_{m,0}$ is the density parameter associated with the matter (baryon and dark) component evaluated today (thus the suffix 0); $\Omega_{r,0}$ is related to radiation (photons and neutrinos); Ω_k is connected to the spatial curvature; and $\Omega_\Lambda \equiv 1 - \Omega_{m,0} - \Omega_{r,0} - \Omega_k$ is the dimensionless density parameter of the Cosmological Constant, Λ. This equation provides in a quite clear way the main ingredients and their role in the global background evolution of the Universe through the Hubble parameter, i.e. its expansion rate.

The second Friedman equation, instead, provides information about the acceleration (or deceleration) of the Universe's expansion. We can easily see how the Cosmological Constant (which is generally considered a positive quantity) leads to acceleration, while any other type of "standard" contribution (whether radiation, baryons or dark matter) leads to deceleration.

All the above equations, and the components we have included so far in them, make the *consensus* cosmological model named ΛCDM.

1.2 ΛCDM: successes and failures

The ΛCDM model has been proven to successfully explain several cosmological observations. However, its validity is still under examination due to various observational and theoretical problems, which we will briefly review in the following pages.

1.2.1 ΛCDM vs. observations

From an observational point of view, in recent years there has been an intensification of the debate within the cosmological community regarding the effective role of the ΛCDM model as a consensus model, due to newly updated and more precise measurements from independent cosmological probes, which have exacerbated the now (in)famous "cosmological tensions" [11]. The two most discussed tensions in this context are the Hubble (H_0) tension and the S_8 tension. The state of the art relating to the two aforementioned tensions will be reported below, highlighting the main results.

The H_0 tension. We have compelling statistical evidence of an inconsistency between the values of the Hubble constant obtained by the *Planck* measurements of the CMB [3] (the so-called early-times value, at $z \sim 1100$), and the low redshift (the late-times value, for $z < 1$) ones [12], obtained by using local standard candles such as Cepheids and Type Ia Supernovae (SNeIa) [13].

The latest results from the *Planck* satellite provide a value[1] for the Hubble constant, $H_0 = 67.27 \pm 0.60$ km s^{-1} Mpc^{-1} [3]. The key point is that CMB data cannot be analysed without assuming a cosmological model. The baseline value provided by the mission is based on the assumption of a flat ΛCDM model, which is also the most statistically favoured model with respect to other standard extensions that the mission has considered. However, even such extensions do not provide a value of H_0 much greater than $68 \div 69$.

It should be noted that the previous CMB mission, the Wilkinson Microwave Anisotropy Probe (WMAP) preferred a value of $H_0 = 70.0 \pm 2.0$ km s^{-1} Mpc^{-1} [14] which is still consistent with the *Planck* value but also less in tension with the

[1] All uncertainties reported in this thesis are at 1σ confidence level, if not explicitly reported differently.

local value. Ground-based CMB experiments, such as the South Pole Telescope (SPT) initially found $H_0 = 71.3 \pm 2.1$ km s^{-1} Mpc^{-1} [15] which, after technical improvements, has been later updated to $H_0 = 68.8 \pm 1.5$ km s^{-1} Mpc^{-1} [16]). The Atacama Cosmology Telescope (ACT) [17] measured $H_0 = 67.9 \pm 1.5$ km s^{-1} Mpc^{-1}. A combination of several ground-based experiments on CMB (SPT, SPT-Pol, ACTPol) led to a Hubble constant value $H_0 = 69.72 \pm 1.63$ km s^{-1} Mpc^{-1} [18].

BAO are another probe known to be sensitive to the same early physics as the CMB. However, they can only constrain the product of the Hubble constant H_0 and the sound horizon scale r_s[2]. Due to this degeneracy, measuring H_0 solely using BAO data is not possible. The degeneracy can be broken once a fiducial model is provided or when BAO measurements are combined with other independent data, for example, by fixing the sound horizon r_s with the CMB power spectrum. The analysis of the Data Release 12 (DR12) of the Baryon Oscillation Spectroscopic Survey (BOSS), assuming a prior on the baryon density Ω_b [19], provided $H_0 = 67.9 \pm 1.1$ km s^{-1} Mpc^{-1} [20]. The study of DR12 of BOSS using the Effective Field Theory of Large-Scale Structure (EFTofLSS) produced $H_0 = 68.5 \pm 2.2$ km s^{-1} Mpc^{-1} [21]. Additionally, when BAO data from the Main Galaxy Sample, are combined with BOSS and eBOSS a value of $H_0 = 67.35 \pm 0.97$ km s^{-1} Mpc^{-1} is obtained.

Late-time measurements of the Hubble constant H_0 mostly rely on distance ladder methods, which appear to be cosmology-insensitive [22]. Distances of standard candles, such as Cepheids, are usually calibrated using geometric anchors (e.g. Milky Way, Large Magellanic Cloud, NGC 4258), and can be determined using several approaches among which geometry parallax is the most commonly used (other calibration methods are presented in [23–25]). Once the distances of Cepheids are known, the luminosity of SNIa, residing in the same galaxies, can be determined.

The Supernovae H_0 for the Equation of State (SH0ES) group has provided multiple measurements of the Hubble constant in recent years, with the most

[2]The sound horizon r_s is the standard ruler in any cosmological model and corresponds to the comoving distance that a sound wave (in cosmology, the photon-baryon plasma) could travel from the beginning of the Universe to the recombination epoch

updated and upgraded estimation, obtained by combining Early Data Release 3 (EDR3) from the ESA Gaia mission with the Milky Way's Cepheids multiband photometry from the Hubble Space Telescope (HST), being $H_0 = 73.04 \pm 1.04$ km s^{-1} Mpc^{-1} [12]. This result shows a $\sim 5\sigma$ tension with the one derived by *Planck* assuming the ΛCDM scenario. Further re-analysis of the SH0ES data seems to confirm this trend from the local environment, having $H_0 = 73.75 \pm 2.11$ km s^{-1} Mpc^{-1} (using Bayesian hyper-parameters) [26], $H_0 = 75.35 \pm 1.68$ km s^{-1} Mpc^{-1} (cosmographic expansion of luminosity distance) [27], $H_0 = 72.8 \pm 1.6$ km s^{-1} Mpc^{-1} (SNIa sample measured in near-infrared) [28], and $H_0 = 73.2 \pm 2.3$ km s^{-1} Mpc^{-1} (data from Carnegie Supernova Project I) [29].

Cepheids are not the only calibrators for SNIa. Indeed, other distance ladder methods involve the Tip of Red Giant Branch (TRGB) stars and Mirae, which result in the estimation of H_0 lying in the range of $H_0 \sim 70 - 74$ km s^{-1} Mpc^{-1} [24, 30–35], albeit with much larger uncertainties than the Cepheids-SNIa based values. This same trend is common to other approaches applied to late-time data which involve, for example, the Surface Brightness Fluctuations (SBF) method [36, 37], the Tully Fisher [38] and the Baryonic Tully Fisher [39] relations, Type II Supernovae [40] and the Megamaser Cosmology Project (MCP) [41].

Time delay effects due to strong gravitational lens phenomena can be used to assess the H_0 value through model-dependent characterization of mass distributions. These measurements show agreement with low redshift H_0 determinations and a slight tension with *Planck* ones. For instance, the H0 Lenses in COSMOGRAIL's Wellspring (H0LiCOW) collaboration, without involving distance ladder methods, achieved an estimation of $H_0 = 72.5^{+2.1}_{-2.3}$ km s^{-1} Mpc^{-1} [42] and $H_0 = 73.3^{+1.7}_{-1.8}$ km s^{-1} Mpc^{-1} [43] (further details regarding re-analysis of H0LiCOW or combination with other measurements are explained in [11]).

Early-type galaxies that undergo passive evolution and exhibit a characteristic feature in their spectra, i.e. the so-called 4000 break, are generally defined as cosmic chronometers. Indeed, they have been extensively shown to act as "clocks" [44–46] and can provide measurements of the Hubble parameter $H(z)$ without relying on early-times physics or on distance ladder methods. In [47], using 28 measurements of $H(z)$, extrapolated then at $z = 0$, the authors reported $H_0 = 68.3^{+2.7}_{-2.6}$ km s^{-1} Mpc^{-1}. More updated measurements relying on Cosmic

Chronometers combined with other probes such as BAO and SNIa, provide a wide range (considering the errors) for the value of the Hubble constant $H_0 = 66 - 73$ km s^{-1} Mpc^{-1} [48–56]. This broad range of H_0 values prevents, for now, from exploiting this method to alleviate the Hubble tension.

Finally, standard and dark sirens (gravitational waves with and without an electromagnetic counterpart) can also be used as probes to determine the luminosity density up to cosmological scales without requiring any distance ladders. From the first attempt using the crucial GW170817 (standard siren) event, in [57] the authors reported a value $H_0 = 70.0^{+12.0}_{-8.0}$ km s^{-1} Mpc^{-1}. Re-analysis of this same event has been conducted: after correction for the source's peculiar velocity, in [58] they get $H_0 = 68.3^{+4.6}_{-4.5}$ km s^{-1} Mpc^{-1}; treating it as a dark-like siren, namely, combining the redshifts from each galaxy with the distance estimate from GW170817, in [59] it is obtained $H_0 = 77^{+37}_{-18}$ km s^{-1} Mpc^{-1} [59]. The first measurement of the Hubble constant from purely dark sirens is described in [60], with an obvious degradation of the signal and dependence on the applied prior, which in the best case leads to $H_0 = 75.2^{+39.5}_{-32.4}$ km s^{-1} Mpc^{-1}. If the dark siren is well localised, the constraints are slightly improved, $H_0 = 77.96^{+23.0}_{-5.03}$ km s^{-1} Mpc^{-1} [61]. A combination of both standard and dark sirens can improve the constraints slightly, with $H_0 = 68.84^{+15.51}_{-7.74}$ km s^{-1} Mpc^{-1} [62]. However, it is evident that gravitational waves are currently not yet able to provide decisive assistance in solving the H_0 tension, although the forecasts for the future are promising [63].

The S_8 tension. This second tension is connected to the measured values of the $S_8 = \sigma_{8,0}\sqrt{\Omega_{m,0}/0.3}$ parameter, which combines (and correlates) two cosmological parameters, $\Omega_{m,0}$, which we have introduced in the previous section, and $\sigma_{8,0}$, the amplitude (evaluated today) of the power spectrum on scales of $8h^{-1}$ Mpc. There is actually a discrepancy between the values from *Planck* ($S_8 = 0.834 \pm 0.016$) versus those obtained from cosmic weak lensing surveys [64], cluster counts [65], and redshift space distortion [66].

Cosmic shear [67–70], which is the distortion of images of background distant galaxies due to weak gravitational lensing by the foreground (line-of-sight) large-scale structure in the Universe, represents a powerful tool to test cosmological models. Cosmic shear outcomes from the Canada France Hawaii Telescope Lensing Survey (CFHTLenS) showed a tension with *Planck* CMB results [71]. Cos-

mic shear analysis from the ~ 450 deg^2 of the Kilo Degree Survey (KiDS-450) [72–75], was performed to shed the light on the S_8 tension between *Planck* and CFHTLenS data, reporting $S_8 = 0.745 \pm 0.039$ (over 2σ tension with *Planck*). The combination of the cosmic shear data from KiDS-450 with the galaxy-galaxy lensing tomography and redshift-space power spectra of the spectroscopic surveys, 2-degree Field Lensing Survey (2dFLenS) and BOSS, produced $S_8 = 0.742 \pm 0.035$ [76]. When KiDS-450 data are combined with the VISTA Kilo-Degree Infrared Galaxy Survey (VIKING) a value of $S_8 = 0.737^{+0.040}_{-0.036}$ [77] has been found. More recently, the analysis of the fourth release of the KiDS data of ~ 1000 deg^2 increases the tension with Planck data up to $\sim 3\sigma$ ($S_8 = 0.766^{+0.020}_{-0.014}$) [78]. Once KiDS-450 data are combined with the first release of DES [79, 80], the tension, with Planck data, reaches 3.2σ ($S_8 = 0.755^{+0.019}_{-0.021}$). Finally, the combination of KiDS-450 and BOSS data produces an $S_8 = 0.728 \pm 0.026$. The most updated result comes from a joint cosmic shear analysis of the Dark Energy Survey (DES Y3) and the Kilo-Degree Survey (KiDS-1000) leading to $S_8 = 0.790^{+0.018}_{-0.014}$, which is "only" at 1.7σ tension with *Planck*.

Galaxy cluster abundances (as a function of mass and redshift) can be used to constrain the matter density $\Omega_{m,0}$, and the amplitude of the matter power spectrum $\sigma_{8,0}$. Constraints on $\sigma_{8,0}$ can also be combined with CMB data, assessing the growth of cosmic structures. In [65], the authors analysed a catalogue of galaxy clusters identified with the AMICO algorithm [81] in the third release of the KiDS data. They used the cluster number counts and the stacked weak lensing analysis to constrain the cosmological parameters $\Omega_{m,0}$, $\sigma_{8,0}$, and S_8. They reported $S_8 = 0.78 \pm 0.04$ which is compatible at 1σ CL with the results provided by *WMAP* and *Planck*. However, the matter density $\Omega_{m,0} = 0.24 \pm 0.24^{+0.03}_{-0.04}$ agrees at 1σ with *WMAP* one but it shows a 2σ tension with *Planck*.

Lyman-α absorption lines of quasars spectra represent a powerful tool to understand the clustering of the Universe at $z \sim 2-4$. In [82], Lyman-α measurements, based on BOSS and E-BOSS data consisting of 43751 quasars, have been used to put constraints on the set of cosmological parameters comparing the results with the *Planck* ones. Regarding the parameter S_8, a tension of $\sim 2.6\sigma$ has been found.

1.2.2 ΛCDM vs. theory

The *ΛCDM* model relies on the crucial assumption of GR as the ultimate theory of gravity. This is a strong hypothesis since Einstein's theory has been *directly* tested only on Solar System scales. As explained in the previous section, the adoption of the ΛCDM model leads to tensions that arise when we compare inference from cosmological probes related to the latest stages in the evolution of our Universe to the early stages. We might then conclude that the ΛCDM model is unable to provide a unified description of our Universe evolution. Additionally, the ΛCDM model is unable to explain comprehensively the nature of DE and DM.

A huge variety of solutions have been introduced in the effort to reduce the differences between independent cosmological probes and to understand the nature of the dark components that, after all, constitute the $\sim 95\%$ of the Universe's energy-matter content. In the following pages, we provide a general state-of-the-art and we will be focusing in particular on modifications of Einstein's theory of gravity which represent the basis of this work.

Dark Energy

As we have seen, the "easiest" (from an Occam's razor perspective) way to explain the accelerated expansion of our Universe is, according to the ΛCDM scenario, through the introduction of a Cosmological Constant (CC), Λ. The most credited hypothesis about the nature of such a constant is that it would represent the expected value of the energy density of the vacuum [83]. However, there is a discrepancy of about ~ 120 orders of magnitude between the observed value of Λ and the one derived from theory. This problem is known as the *Cosmological Constant problem* [83].

Furthermore, the CC present value of the energy density ρ_Λ seems to be approximately equal to the present matter density $\rho_{m,0}$, namely we measure $\rho_\Lambda \sim \rho_{m,0}$. Nonetheless, these two densities scale differently with the size of the Universe ($\rho_\Lambda = const$ and $\rho_m \propto a^{-3}$). This problem in literature is known as the *coincidence problem.*

The above-mentioned issues (a more detailed list is presented in [84]) and cosmological tensions [11], have pushed the scientific community to look for alternatives to the ΛCDM model.

The first path still assumes GR. It relies on the introduction of modifications in the right-hand side of the Einstein field equations, namely, introducing (new) energy or matter fields in the stress-energy tensor. Usually, in the most standard case, matter and energy fields are treated and introduced as perfect fluids, so that their equations of state connecting pressure p with density ρ can be parametrised as $p = w\rho$, with the equation of state (EoS) parameter, w, being only function of time (or scale factor). For instance, although the CC was initially introduced as a geometrical term (thus, on the left-hand side of Einstein's equations), it can be equivalently (at least from a formal mathematical point of view) described by an equation of state $p_\Lambda = -\rho_\Lambda$, i.e. with $w_\Lambda = -1$. It is not pedantic to remind here that for this reason, when talking about *dark energy*, we generally refer to models in which the density of the fluid is a function of time.

Of course, other more general choices are possible [85]. Quintessence models, or *wCDM*, have $w = const. \neq -1$. The Chevallier-Polarski-Linder (CPL) model, the simplest two-parameters generalisation for $w(a)$, a straight line (in the scale factor) interpolating late and early-times EoS, $w_{CPL} = w_0 + (1-a)w_a$ [86, 87]. DE models characterized by two parameters in the EoS have been extensively studied by the proposal of other (and most varied) parametrizations [88–90].

While such models are hardly more than phenomenological proposals, one can even build more physically based scenarios: quintessence models have a scalar field minimally coupled with gravity and whose potential can reproduce the late-time accelerated expansion of the Universe; *K-essence* [91] models, where we recover the accelerated expansion by modifying the kinetic term of the additional degree of freedom; or even *ghost* fields, that is, scalar degrees of freedom with an equation of state $w < -1$ and therefore negative kinetic energy [92]. A more recent possibility, introduced to address the H_0 tension [93], is represented by a DE fluid with a phantom crossing, namely moving from a ghost-field behaviour exhibiting $w < -1$ to a standard quintessence with $w > -1$. This phantom crossing is supposed to happen for a certain value of the scale factor $a = a_m$ (or redshift equivalently) at which the DE conservation equation changes sign.

Early Dark Energy (EDE) models have been introduced to try to reconcile the SNIa and *Planck* measurements on H_0. These models introduce a "primordial" DE which, contrary to a CC, has a more relevant role and prominence also at early times. Several EDE models have been proposed, for example, based on a scalar field with an anharmonic potential [94] or with a power-law potential [95, 96], ultralight axion-like particles [97] also interacting with dilatons [98]. Other possibilities are represented by phenomenological EDE with an Anti-de Sitter phase [99], or by a dark fluid, defined as Acoustic Dark Energy, impacting acoustic oscillations imprinted in the CMB [100].

Beyond that, we can also consider a less conservative approach whereby GR represents a specific instance of a more general theory of gravity. Under this perspective, the left-hand side of the Einstein field equations is modified. This approach introduces an even larger number of possible theories of gravity that expand upon GR. Their quantity is so large that it is unmanageable (and outside the scope of this thesis) to detail all of them fully.

Although the number of theories is large, one must not make the mistake of thinking that consistently modifying Einstein's theory is an easy task to accomplish. From a theoretical point of view, for example, Lovelock's theorem [101, 102] states that GR is the only local theory of gravity with equations of motion in the second order in the metric $g_{\mu\nu}$. On one hand, this limits the possibility to generalise GR in this context but also provides a hint about which paths to follow. Then, a crucial step to check the consistency of a theory is that it has to be stable [103, 104].

With these quite general and not exhaustive prescriptions, we can classify the ETGs zoo into four macro families:

- theories with extra degrees of freedom. These can be additional fields of various kind: scalar [105–109], vector [110, 111], tensor [112–115] or even mixed [116, 117];

- theories with higher (than second) order derivatives in the Hilbert-Einstein action, like: $f(R)$ theories [118–123], $f(Q)$ theories (with Q being the non-metricity tensor, equal to zero in GR) [124], $f(T)$ theories (with T being the

torsion tensor, equal to zero in GR) or tele-parallel theories [125], Horava-Lifshitz gravity [126], or Conformal Gravity [127];

- nonlocal theories, whose Lagrangians contain nonlocal differential operators trying to create a bridge between gravity and the formalism of quantum mechanics [128–130]. Some examples are Infinite Derivatives of Theories of Gravity [131, 132], which introduce functions of the Dalambertian operator $\Box$ in the action, or Integral Kernel Theories of Gravity which rely on the adoption of the inverse of the Dalambertian operator $\Box^{-1}$ [128, 130];

- theories in which space-time has higher dimensionality and GR is a particular case of a more general theory embedded in a manifold with a dimension greater than four [133–135], like Kaluza-Klein theory [136] or Cascading gravity [137].

In the next chapter, we will focus our attention on the first group and, in particular, on a specific sub-family of scalar-tensor theories of gravity which we have used in our works.

One main obstacle on the road to building a successful ETG is that it has to be as successful as GR in explaining the data and cannot spoil GR's successes. This means that all the modifications of GR must pass, for example, the well-known Solar System constraints [138, 139]. Indeed, GR has been proven to work perfectly at these scales. This has a main consequence: all ETGs, in one way or another, introduce a new kind of interaction, generally called a fifth force. Therefore, a mechanism must exist which, at the same time, turns off GR's modifications at Solar System scales and maintains such modifications at larger scales of the right order of magnitude to drive the Universe's acceleration. Such "safety" mechanisms for ETGs are usually called *screening mechanisms*.

A phenomenological classification of screening mechanisms is possible (a force classification is also possible [140]). We can distinguish three major groups:

1. chameleon type – screening based on the properties of the scalar field [105, 106], whose mass depends on the density of the local environment: on cosmological scales, where the density is low, the mass is small and its interaction length is large (possibly reproducing DE on such scales); on smaller

scales, like in the Solar System, where the density is much higher, the field's mass is large and its interaction length is very small, making it basically ineffective and undetectable;

2. symmetron type [107, 108, 141] – screening based on the first derivatives of the scalar field: the screening is again dominated by the form of the potential of the new field, but now it is the coupling of the new field with the matter which screens the new forces: on cosmological scales it is large, and the effects of the field are measurable; on smaller higher density scales, the coupling is much smaller and the effects of the field are much weaker, thus satisfying all the local constraints;

3. Kinetic type – the screening is controlled by the kinetic contribution of the field: when the first-order derivatives of the fields are dominant, the effects of the field are turned off when the local gravitational acceleration is larger than some critical value set by the theory (this is the base for the phenomenological behaviour of MOND theory); when the second order derivatives dominate, then we have the so-called Vainshtein screening [142].

Dark Matter

The other unknown component, which represents the $\sim 27\%$ of the matter content in the Universe, is DM. Historically, the term DM was coined in 1933 by the Swiss astronomer Fritz Zwicky [8] who discovered a discrepancy between the observed matter and what theoretical arguments should be expected in order to explain the dynamics of the Coma Cluster. This new matter should have had the peculiarity to interact with the baryonic one only through gravity. For this reason, as the properties of this matter were different from the baryonic one and since it was not luminous, it was defined as "dark matter".

This discrepancy was later confirmed by the American astronomer Vera Rubin, who observed the rotation curve of spiral galaxies [9, 143]. The rotation curves at larger radii were expected to decrease with a Keplerian trend. The exact opposite was observed, i.e., the rotation curves flattened at larger radii. The conclusion was that the baryonic matter alone should not be able to support the formation of the cosmological structures we see today (e.g. galaxies and galaxy clusters).

At the present day, a particle nature is attributed to DM, which is thus tentatively explained using the Standard Model without introducing any form of "extremely" exotic new types of matter.

According to the ΛCDM model, DM should be represented by *cold* particles (CDM) whose velocity is much lower than the speed of light. These particles should be able to form small clumps that then aggregate through gravity into larger ones. Since CDM can fit the data better, its candidates are usually preferred. A detailed list is provided in [144], with some of them being: Weakly Interactive Massive Particles (WIMPs) [145] interacting with baryonic matter through gravity and the weak force; axions [146], originally introduced as a possible solution to the strong interaction CP violation problem [147]; Feebly Interactive Massive Particles (FIMPs) [148]; Supersymmetric (SUSY) particles [149] like gravitino and neutralino.

In addition to the standard scenario represented by the CDM, two other categories of DM can be defined, based on the velocity of the hypothetical particles. Ultra-relativistic particles like neutrinos may characterize Hot Dark Matter (HDM). HDM should be responsible for forming large mass clumps that surround galaxy clusters. However, multiple observations seem to kill this possibility, as this kind of dark matter should not be able to form structures at small scales like galaxies. We can also have Warm Dark Matter (WDM) particles [150, 151] that lie between the previous two categories.

Nevertheless, since DM is defined as a particle, it should be detectable using the already existing experiments such as ATLAS at the Large Hadron Collider (LHC[3]) in Geneva, and Darkside[4], Xenon100[5] (updated to XENONnT [152]) at Gran Sasso in Italy. But despite all these experiments searching for DM, we have not detected any statistically significant and strikingly positive signal so far.

New DM models have been introduced recently trying to ease the S_8 tension. For example, in [153], the authors have shown that a "cannibal dark matter" (CanDM), which is a matter with number-changing interactions, might alleviate

[3] https://home.cern/science/accelerators/large-hadron-collider
[4] https://www.lngs.infn.it/en/darkside
[5] http://www.xenon1t.org/

the S_8 tension (and not the H_0 one) between CMB and weak lensing measurements. Another possibility is represented by a decaying dark matter according to which CDM particles could decay into a massive WDM particle and dark radiation (DR) [154]. Additionally, this peculiar kind of DM might be able to explain the excess registered in the Xenon-1T experiment [155, 156].

A third option may be represented by a dark component mimicking both DM and DE. With this purpose, in [157], it has been shown that a unified dark matter or *quartessence* model tested with a combination of *Planck*, SDSS DR12 and cosmic shear data from KiDS could ease the existing tension between the total matter density and the structure clustering.

As introduced in the previous section, the H_0 and the S_8 tensions are not the only observational problems affecting the ΛCDM model. A third one related to our understanding of the DM's nature is the so-called cuspy-core problem [158–162]. It refers to the discrepancy of DM distribution in dwarf galaxies, assessed from cosmological simulations and observations. According to N-body simulations (based on the ΛCDM paradigm), DM haloes seem to be characterized by a cuspy density profile $\rho_{DM} \propto r^{-\alpha}$ that increases steeply when $r \to 0$. Examples of density profile describing cuspy DM haloes are the Navarro-Frenck-White profile (NFW) [163], Einasto profile [164], Moore profile [165]. All these profiles can be generalised with the profile proposed by [166, 167]. However, results from observations [160, 161, 168, 169] state that in the inner region of dwarf galaxies, the density of dark matter haloes is approximately constant $\rho_{DM} \propto r^0$ ($\alpha = 0$).

The missing satellite problem [170, 171] highlights the disparity between the sub-halo structures inferred from N-body simulations and the number of dwarf satellite galaxies in the Local Group. Specifically, in the ΛCDM gravitational scenario the predicted number of satellites is ~ 1000, while observations reveal only a fraction of that amount, ~ 50 [172, 173].

Finally, the recent study of the kinematics of a particular class of low surface brightness galaxies, called Ultra-diffuse galaxies (UDGs) [174] unveiled that some of them, for instance, NGC 10552-DF2 and NGC1052-DF4 [175, 176] are characterized by a low amount of DM. This lack of DM makes these galaxies outliers in the standard cosmological background provided by the ΛCDM model.

Explanations of these problems, at the present day, are not known and they could lead to an overcoming of the GR in favour of other solutions represented, for example, by ETGs.

1.3 Motivation: unification of Dark Energy and Dark Matter

It emerges quite clearly from the previous sections, which, we remark here, are just a quick and non-detailed summary of a much more complex and large state-of-the-art, that DM and DE, whose origin and nature are still a big question mark, are among the most pressing problems to be solved in modern cosmology. We claim we are now living in the era of so-called "precision cosmology" [177]; a statement which is quite true if we consider the advances in technology we have witnessed over the last few years and the higher technological level and conditions under which the astronomical community can now think to plan next future observations [178]. And even more exciting times are ahead of us thanks to a new and fast-developing window of multi-messenger observations, opened by the recent discoveries made in the gravitational waves field [179, 180]. But this freshly achieved high precision, instead of helping us to solve those big issues, has done nothing more than further deepen the mystery behind them.

So that, now, here we stand: we have no idea of what could be DM, and we have no idea of what could be DE. To be more precise, we do have a plethora of candidates for both DM [144] and DE [181, 182]. However, regarding DM, none of them has been detected directly in laboratories so far. And for DE the situation is even more troublesome, because the same intrinsic physical properties of DE which we have been able to infer so far, push us to a far deeper break in our understanding of the Universe. In fact, even in the most conservative case, we need a cosmological ingredient whose properties run away from every possible interpretation of what we have taken for granted in our physical interpretation of the Universe to date. In the less conservative approaches, we can push even further: dealing with DE's nature is equivalent to dealing with a new theory of gravity. In this case, we generally speak about "extended" theories of gravity [181].

This seemingly exotic terminology is actually more appropriate than one might think because both DM and DE emerge as "problems" in a context where GR is assumed to be the final and ultimate theory of gravity. So we are left with two choices: we can face a Universe where we assume GR as the universal law of gravity, but then we need to uncover and understand the nature of two missing quantities which sum up to about 95% of the energy-matter content in our Universe [3]; or, we can try to relax the GR assumption and find a more general way to explain DM and DE, but at the expense of basically ignoring which should be the effective way to describe the behaviour of gravity at all possible scales [84].

In this very wide and complex scenario, our research would aim to make up our personal contribution to the topic by asking and tentatively answering the following questions.

- *Why?* The main spur would be to pursue an old goal with new instruments. The "old goal" refers to a "Theory of Everything" which unifies all the fundamental interactions; the "new instruments" refer to ETGs and, more specifically, to those having and fulfilling some specific properties and requirements. Thus, our main goal will be to contribute to answering the question: *can we unify dark energy and dark matter in one single theoretical background?* They have completely different properties, but *is it possible that they are different manifestations of the same kind of (new) interaction?* After all, the same nature of gravity, as a fundamental force, is unclear and highly debated.

- *What?* We will turn on ETGs as the theoretical arena in which to perform our studies, but not all ETGs are feasible for such a goal. ETGs are mostly formulated in order to give meaning to DE, not to DM. All of them have to fulfil some basic requirements: they have to reduce to GR at local and Solar System scales, where we know that GR works perfectly well. This constraint must require a *screening mechanism* which prevents the large cosmological scale effects of ETGs mimicking DE from affecting the smaller astrophysical ones. What we propose here is the idea that *the partial breaking of such screening mechanisms at astrophysical scales, could be the key*

to unifying DM and DE as two different sides of the same gravitational theory.

- *How? (observations)* The tests for such a hypothesis will span the full range of scales of the large-scale structure of the Universe. We will make use of the most diverse sets of observational probes which can be retrieved from literature and databases. A preliminary list might include: gravitational lensing events (both weak and strong); X-ray observations; stellar dynamics and kinematics. We will also look for distinctive and peculiar features which might be indicative of a departure from GR, and which could be related to ETGs' screening mechanisms.

The lines of investigation which have been delineated above, stem from a series of studies which show how a specific family of ETGs, the DHOST theories which will be described in more detail in the next chapter, exhibit a partial breaking of the Vainshtein screening mechanism [183]. For this reason, they have been selected as the class of theories which we have analysed in our works.

A Vainshtein screening partially broken may represent the *trait d'union* between cosmological and astrophysical scales. Indeed, gravity modifications that should be effectively working only at cosmological scales whilst being partially screened at astrophysical scales, could leak to these scales where the DM component should play a fundamental role. In this sense, there would be a unification of DE and DM. Due to the partial breaking of the Vainshtein screening mechanism, a DHOST theory may reproduce, at cosmological scales, the effect we associate with DE and at astrophysical scales the ones we attribute to DM. According to this idea, DM would no longer be described by a hypothetical particle but would become a gravitational effect induced by an ETG (a DHOST theory in this work).

Typically, modifications of Einstein's theory have been developed as alternatives to DE. DM, which is characterized by entirely different properties, is usually described with models (a list is provided in [144]) that do not require a gravity modification.

However, a potentially new and compelling idea, which represents the foundation of the works on which this thesis is based on, might be considered. DE and DM are considered distinct physical components because they possess different

properties. However, they might be different sides of the same gravitational interaction. Following this hypothesis, with one model, instead of many, it could be possible, depending on the scales, to describe the effects we associate with DM and DE. This model, to be suitably tested, might therefore provide a unification of DM and DE.

It is crucial to understand at which scale such unification may happen and consequently look for the observational data required to test the above-mentioned idea.

This thesis is organised as follows. In Chapter 2, we introduce all the theoretical properties of the ETG model which have been used to test the possible unification of DE and DM. In Chapter 3, we will explain which kind of observational data have been used in our publications, which gravitational structures have been chosen for our analysis and how they have been modelled. We will also briefly illustrate the statistical tools used to derive and corroborate the results of our research. Such results will be discussed in Chapter 4 regarding the galaxy cluster scale, and in Chapter 5 for the galactic scales. Finally, in Chapter 6 we summarise the main consequences and impact of our works and possible future developments.

CHAPTER 2

Degenerate Higher-Order Scalar Tensor (DHOST) theories

One of the "easiest" ways to modify Einstein's theory of gravity is to introduce an additional scalar degree of freedom in the Hilbert-Einstein action. For this reason, theories that follow this approach are defined in the literature as scalar-tensor theories (where "tensor" clearly refers to the metric tensor). The most common expression of the action for such theories is described in [184] and can be written as

$$S_{ST} = \frac{1}{16\pi G_*}\int d^4x\sqrt{-g}\left[F(\phi)R - Z(\phi)g^{\mu\nu}\partial_\mu\phi\partial_\nu\phi - 2U(\phi)\right] + S_m[\psi_m; g_{\mu\nu}], \tag{2.1}$$

where: ϕ is the new scalar field; G_* is the bare gravitational constant, different from the experimentally measured one, the "standard" G_N; S_m is the action of the standard matter field(s) ψ_m; and F, Z and U are general functions and potential of the new minimally coupled scalar field ϕ that completely describe its dynamics. However, not all of these functions are independent, and their form depends on a case-by-case basis.

In 1974, Gregory Horndeski introduced the most general scalar-tensor theory of gravity [185] (later called Horndeski theory) with a Lagrangian contain-

ing second-order derivatives of the scalar field (which is the only propagating scalar degree of freedom) and satisfying the specific constraint of leading to Euler-Lagrange equations which are at most second order. This theory was a bit forgotten until very recently when it was somehow "rediscovered" after the Galileon theories. The Galileon scalar fields [109, 186] owe their name to the fact that they are characterised by the Galilean symmetry $\phi(x) \to \phi(x) + b_\mu x^\mu + c$. Even though these theories have been introduced within a Minkowskian background [186], they were later extended by adding gravity and promoting the operators to their covariant version. Thus, the so-called covariant Galileon theories came out, which are described by the following Lagrangian [186]

$$\begin{aligned}\mathscr{L} =& c_1\phi + c_2 X - c_3 X\Box\phi + \frac{c_4}{2}X^2 R + c_4 X\left[(\Box\phi)^2 - \phi^{\mu\nu}\phi_{\mu\nu}\right] \\ &+ c_5 X^2 G^{\mu\nu}\phi_{\mu\nu} - \frac{c_5}{3}X\left[(\Box\phi)^3 - 3\Box\phi\phi^{\mu\nu}\phi_{\mu\nu} + 2\phi_{\mu\nu}\phi^{\nu\lambda}\phi^{\mu}_{\lambda}\right]\end{aligned} \tag{2.2}$$

where: R is the Ricci scalar; $G^{\mu\nu}$ is the Einstein tensor; $\phi_\mu = \nabla_\mu\phi$ and $\phi_{\mu\nu} = \nabla_\mu\nabla_\nu\phi$ with ∇ which denotes the covariant derivative. In the Lagrangian (2.2), the fourth and the sixth terms are those that prevent the theory from having higher-order derivatives in the equations of motion, which are second-order, and thus suffering instabilities (this point is discussed later in this section). Covariant Galileon theories have been introduced within a four-dimensional spacetime, however, they can be further extended to higher dimensional spacetime [187].

The action that is currently most used for Horndeski theory is not written exactly as the one initially defined in [185] but as it emerged in the Galileon theories, although it is, of course, fully equivalent from a physical point of view. This action looks like

$$S_H = \int d^4x\sqrt{-g}\left\{\frac{1}{8\pi G_N}\mathscr{L}_i[g_{\mu\nu},\phi]\right\} + S_m[\psi_m; g_{\mu\nu}]\,, \tag{2.3}$$

with:

$$\mathscr{L}_2 = G_2(\phi, X), \tag{2.4}$$

$$\mathscr{L}_3 = G_3(\phi, X)\Box\phi, \tag{2.5}$$

$$\mathscr{L}_4 = G_4(\phi, X)R + G_{4,X}(\phi, X)\left[(\Box\phi)^2 - \phi_{\mu\nu}\phi^{\mu\nu}\right], \tag{2.6}$$

$$\mathscr{L}_5 = G_5(\phi, X)G_{\mu\nu}\phi^{\mu\nu} - \frac{1}{6}G_{5,X}(\phi, X)\left[(\Box\phi)^3 + 2\phi_\mu{}^\nu\phi_\nu{}^\alpha\phi_\alpha{}^\mu - 3\phi_{\mu\nu}\phi^{\mu\nu}\Box\phi\right], \tag{2.7}$$

where $\Box$ is d'Alembert operator, $X = \partial_\mu\phi\partial^\mu\phi$ is the kinetic term of the field ϕ and G_i $(i = 2, \ldots 5)$ are arbitrary functions of the field.

Generally speaking, the number of propagating degrees of freedom can not be increased arbitrarily. Indeed, there exists a theorem, the Ostrogradski theorem [188], according to which a theory that has more than one degree of freedom is unstable. The consequence is a negative kinetic term of the additional degree of freedom which generates, in this way, a ghost field.

However, it was recently recognized that Horndeski's theory can be safely extended, namely, that it is possible to build up theories which exhibit equations of motion of higher (than second) order derivatives, but whose true propagating degrees of freedom obey second-order equations which are free from Ostrogradski instabilities. These new theories have been called, for such reasons, Beyond Horndeski theories [189–194]. Within this theoretical context the four Lagrangians of the Horndeski theory, Eq. 2.3, can be extended to include other two terms

$$\begin{aligned}\mathscr{L}_4^{bH} &= F_4(X,\phi)\varepsilon^{\mu\nu\rho}{}_\sigma\varepsilon^{\mu'\nu'\rho'}{}_\sigma\phi_\mu\phi_{\mu'}\phi_{\nu\nu'}\phi_{\rho\rho'} \\ \mathscr{L}_5^{bH} &= F_5(X,\phi)\varepsilon^{\mu\nu\rho\sigma}\varepsilon^{\mu'\nu'\rho'\sigma'}\phi_\mu\phi_{\mu'}\phi_{\nu\nu'}\phi_{\rho\rho'}\phi_{\sigma\sigma'},\end{aligned} \tag{2.8}$$

which depend on the two further additional functions $F_4(X,\phi)$ and $F_5(X,\phi)$, with $\varepsilon^{\mu\nu\rho}{}_\sigma$ being the anti-symmetric Levi-Civita tensor.

Very soon it was realized that even a further generalization of Beyond Horndeski's theories was possible, leading to the definition of the Degenerate Higher Order Scalar Tensor (DHOST) theories [195–199], which will be our main tool in this work.

The most general action which can be defined to describe these theories, including both quadratic and cubic order terms (in the second-order derivatives),

can be written as

$$S_{DHOST} = \int \sqrt{-g}\Big[F_{(2)}(X,\phi)^{(4)}R + P(X,\phi) + Q(X,\phi)\Box\phi + \sum_{i=1}^{5} A_i(X,\phi)\mathscr{L}^{(2)}_{i,\phi} + \\ + F_{(3)}(X,\phi)G_{\mu\nu}\phi^{\mu\nu} + \sum_{i=1}^{10} B_i(X,\phi)\mathscr{L}^{(3)}_{i,\phi}\Big]\,. \tag{2.9}$$

This action contains nineteen functions of the scalar field ϕ and its kinetic term X; five Lagrangians are quadratic, and ten are cubic in the scalar field ϕ [196, 200]. From Eq. 2.9, it is possible to see how some well-known cases are naturally included in this action:

- if $F_{(2)}(X,\phi) = M_{Pl}^2/2$ (with the Planck mass being $M_{Pl}^2 = (8\pi G)^{-1}$) and all the other functions vanish, we get the usual Hilbert-Einstein action of GR;
- we can recover the Brans-Dicke theory [201] if

$$F_{(2)}(X,\phi) \equiv F_{(2)}(\phi) = \frac{\phi}{16\pi}, \quad P(X,\phi) \equiv P(\phi) = -\frac{\omega}{16\pi\phi}; \tag{2.10}$$

- The quadratic part of Horndeski's theory is retrieved with

$$F_{(2)}(X,\phi) = G_4(X,\phi), \quad A_1(X,\phi) = -A_2(X,\phi) = 2G_{4,X} \\ A_3 = A_4 = A_5 = 0, \tag{2.11}$$

  while the cubic part with

$$F_{(3)}(X,\phi) = G_5(X,\phi), \quad 3B_1 = -B_2 = \frac{2}{3}B_3 = G_{5,X}\,. \tag{2.12}$$

With the exception of the quadratic and cubic Lagrangians in the scalar field ϕ (and of $P(X,\phi)$ and $Q(X,\phi)$), all the other functions appearing in Eq. 2.9 can not be chosen arbitrarily: in order to prevent Ostrogradski instabilities the functions $F_{(2)}$, A_i, $F_{(3)}$, and B_i have to satisfy some degeneracy conditions. Indeed, if the so-called kinetic matrix (the Hessian matrix constructed from the kinetic terms of the Lagrangians) is degenerate, then such a degeneracy translates into a series of constraints which automatically cancel the extra degree of freedom and thus the instabilities. Exactly from this property, the DHOST theories take their name.

A detailed explanation of this formalism is beyond the scope of this work and can be found in [196, 202]. Here we only present some general features that will be applicable to the particular DHOST model we have utilized and compared against observational data in our works. As a consequence of this degeneracy, for example, from the above action restricted to the case of quadratic higher-order Lagrangian (the cubic case is explained in [200]), one can find three conditions linking the A_i functions

$$A_1 + A_2 = 0, \quad A_3 + A_4 = 0, \quad A_5 = 0. \tag{2.13}$$

Both Horndeski and Beyond Horndeski theories satisfy the above conditions. Using the same degeneracy conditions, it is also possible to classify DHOST theories [195, 196, 203, 204]. In particular, the DHOST model which we will use is based on the condition $A_1 + A_2 = 0$.

Moreover, the recent multi-messenger observation of gravitational waves [180, 205] has put stronger constraints on ETGs [206, 207] ruling out many of them. Theories such as the DHOST which we will use, successfully pass these constraints. Indeed, the speed of gravitational waves c_{GW} can be defined (for brevity, from now on, since we are focusing on quadratic DHOSTs, we will assume $F \equiv F_{(2)}$) as [208]

$$c_{GW} = \frac{F}{F - XA_1}. \tag{2.14}$$

If we fix $c_{GW} = 1$ [205], therefore $A_1 = 0$ and the remaining functions A_4 and A_5 can, thus, be expressed in terms of $A_3(X, \phi)$ and $F(X, \phi)$.

The model that we have analyzed belongs to the class specified by the constraint $A_2 = -A_1$. In this class, it is then possible to identify two different subclasses, depending on the form of the non-minimal coupling between the Ricci scalar R and the scalar field ϕ:

- $F \neq XA_1$: the functions A_2, A_4, and A_5 can be re-expressed in terms of three A_1, A_3, and F which are now arbitrary

$$\begin{aligned} A_4 = \frac{1}{8(F - XA_1)^2}[&-16XA_1^3 + 4(3F + 16XF_X)A_1^2 - X^2FA_3^2 \\ &- (16X^2F_X - 12XF)A_1A_3 - 16F_X(3F + 4XF_X)A_1 \\ &+ 8F(XF_X - F)A_3 + 48FF_X^2] \end{aligned} \tag{2.15}$$

and

$$A_5 = \frac{(4F_X - 2A_1 + XA_3)(-2A_1^2 - 3XA_1A_3 + 4F_XA_1 + 4FA_3)}{8(F - XA_1)^2} \tag{2.16}$$

- $F = XA_1$: within this second subclass, the function A_3 can be re-expressed as

$$A_3 = \frac{2(F - 2XF_X)}{X^2} \tag{2.17}$$

with F, A_4, and A_5 which are arbitrary.

2.1 Phenomenology with DHOST theories

The Effective Field Theory (EFT) formalism enables us to study the evolution of the cosmological background and linear perturbations in a model-independent way. This formalism was used for the first time in [209], to study a possible coupling between a ghost condensate and gravity. It was later applied to inflation [210–212], quintessence model [213], and then to DE and modified gravity models [214–216] (for other approaches see [217–220]).

The foundation of this approach is in the so-called unitary gauge [221] that consists of choosing a time coordinate such that the perturbation $\delta\phi(t,\vec{x})$ of, for example, a certain scalar degree of freedom $\phi(t,\vec{x})$ vanishes. As a consequence, the EFT action does not show any explicit dependence on the scalar field terms, but it is written in terms of the so-called EFT functions (a more detailed description is provided in [222]). The applicability of the EFT approach ranges from cosmological scales down to scales at which we cannot adopt the classical description of gravity. Moreover, the EFT formulation can even be expanded by including non-linear scales [223–227].

In the literature, there exist several versions of the EFT action [214, 215, 217, 228–230] diversified based on notation, number of operators and order of perturbations. Here, we will consider the most general EFT action up to the second

order in perturbation (following the notation adopted in [214])

$$\begin{aligned} S_{EFT} = \frac{1}{2}\int d^4x\sqrt{-g}\big[&M_{pl}^2 f(t)R - 2\Lambda(t) - 2c(t)g^{00} \\ &+ M_2^4(t)(\delta g^{00})^2 - \bar{m}_1^3(t)\delta g^{00}\delta K - \bar{M}_2^2(t)\delta K^2 \\ &- \bar{M}_3^2(t)\delta K_\mu{}^\nu \delta K^\mu{}_\nu + \mu_1^2(t)\delta g^{00}\delta R + m_2^2(t)h^{\mu\nu}\partial_\mu g^{00}\partial_\nu g^{00} \\ &+ ...\big) + S_m \end{aligned} \tag{2.18}$$

where: M_{Pl}^2 is the Planck mass; g is the determinant of the metric $g_{\mu\nu}$; R and δR are, respectively the Ricci scalar and the perturbation of the Ricci scalar; S_m is the matter action; $\{f,\Lambda,c,M_i,m_i,\bar{M}_i,\bar{m}_i,\mu_i\}$ are the EFT-functions, time-dependent functions that guarantee the symmetry of the action [222]; the dots ... account for higher order terms into the action. The action Eq. 2.18 is organized such that all the EFT functions which appear in the first line describe the background, whilst the functions in the other two lines offer a description of the linear perturbations only. In particular, $f(t)$ (or running Planck mass) underlines the coupling between matter and the scalar field ϕ. Possible parameterization of these functions are shown in [222]. The functions $\Lambda(t)$ and $c(t)$ can be expressed in terms of the background DE density and pressure [214]; $\{M_i,m_i,\bar{M}_i,\bar{m}_i,\mu_i\}$ are mass parameters. More exhaustive details about these parameters and their physical meaning are presented in [214, 215, 217, 222, 228–230].

The proficiency of the EFT approach is related to the connection it can establish with most of the proposed gravitational theories of gravity. For example: Brans-Dicke theories are recovered from Eq. 2.18 using only the EFT background function $\{f,\Lambda,c\}$; Horndeski theories are recovered from Eq. 2.18 by imposing $\bar{M}_2^2 = -\bar{M}_3^2 = 2\mu_1^2$.

DHOST theories can be retrieved from the action Eq. 2.18 by adding three additional EFT functions [196, 197]. However, in this thesis we will consider a different but equivalent formulation of the EFT action developed to study, specifically, the properties of the Horndeski theories and their extensions [231]. Deviations from GR are parametrized by four α time-dependent functions $\{\alpha_M,\alpha_B,\alpha_K,\alpha_T\}$. To account for the extension of the Hornedski theory, i.e., Beyond Horndeski's and DHOST theories the additional α_H parameter has to be included. The advantage

of this EFT parametrization is the link between the EFT functions and physical effects.

Using this EFT framework, the DHOST action can generally be written as [215, 232]

$$S^{EFT}_{DHOST} = \int d^3x dt\, a^3 \frac{M^2}{2}\Bigg[\delta K_{ij}\delta K^{ij} - \left(1+\frac{2}{3}\alpha_L\right)\delta K^2 + (1+\alpha_T)\left(\delta^{(3)}R\frac{\delta\sqrt{h}}{a^3} + \delta_2^{(3)}R\right) + H^2\alpha_K\delta N^2 + 4H\alpha_B\delta K\delta N + (1+\alpha_H)^{(3)}R\delta N + 4\beta_1\delta K\delta\dot{N} + \beta_2\delta\dot{N}^2 + \frac{\beta_3}{a^2}(\partial_i\delta N)^2\Bigg] \tag{2.19}$$

where: a is the scale factor; δK is the variation of the trace of the extrinsic curvature; $\sqrt{h}$ is the square root of the determinant of the three-dimensional metric induced on the three-dimensional hypersurfaces; $\delta_2^{(3)}$ is the second-order term in the expansion of the Ricci scalar ${}^{(3)}R$; δN and $\delta\dot{N}$ are the variations concerning the lapse function and the time derivative of the lapse function respectively. Furthermore, the action Eq. 2.19 depends on additional nine time-dependent functions. In particular, M, α_T, α_K, and α_B are enough to completely characterize the Horndeski theory [231]. Beyond Horndeski's theories require the additional parameter α_H [216]. DHOST theories include also α_L and β_i [232].

Before moving further, few words have to be spent describing the meaning of these nine parameters since some of them have been constrained in our works:

- α_M, the running Planck mass: evolution rate of the effective Planck mass

$$\alpha_M = \frac{1}{H}\frac{d\ln M^2}{d\ln t}. \tag{2.20}$$

  At the cosmological level, this parameter influences the growth of cosmological perturbations and also influences the propagation of gravitational waves;

- α_B, the braiding: quantifies the mixing between the kinetic terms of the scalar degree of freedom and the metric. It can impact the sound speed of the scalar field mimicking dark energy, and can thus be related to possible dark energy clustering;

- α_K, the kineticity: corresponds to the kinetic energy of the scalar perturbation and affects the propagation of the dark energy field;

- α_T, the tensor speeding excess: described the deviation of the speed of propagation of the gravitational waves from the speed of light

$$c_T^2 = 1 + \alpha_T \tag{2.21}$$

Within the Horndeski gravitational scenario, these four parameters can be conceived as independent physical properties of dark energy. In addition, once a particular gravitational model is assumed, the α_i parameters are determined by the Lagrangian and the scalar degree of freedom ϕ (a list of examples is represented by [233–237]). On the other hand, theories which go beyond Horndeski require an additional parameter, α_H, which quantifies the departure from Horndeski theory, vanishes for Horndeski theories and becomes non-zero for Beyond Horndeski or DHOST theories.

Finally, DHOST theories also introduce α_L, corresponding to the detuning between the extrinsic curvature terms $\delta K_{ij}\delta K^{ij}$ and K^2; and the parameters β_1 and β_2, analogous to α_B and α_K for the additional degree of freedom present in higher-order theories, and β_3 which is related to the gradient of energy of the additional degree of freedom.

Degeneracy conditions that prevent DHOST theories from developing ghosts imply that the β_i parameters are not independent, but need to satisfy two different sets of conditions[232]

$$I: \quad \alpha_L = 0, \quad \beta_2 = -6\beta_1^2, \quad \beta_3 = -2\beta_1[2(1+\alpha_H) + \beta_1(1+\alpha_T)]$$

$$II: \beta_1 = -(1+\alpha_L)\frac{1+\alpha_H}{1+\alpha_T}, \quad \beta_2 = -6(1+\alpha_L)\frac{(1+\alpha_H)^2}{(1+\alpha_T)^2}, \quad \beta_3 = 2\frac{(1+\alpha_H)^2}{1+\alpha_T} \tag{2.22}$$

Moreover, from the action Eq. 2.19, it is possible to study the physical degrees of freedom consisting of one scalar mode and two tensor ones. In particular, as explained in [196], from the study of the scalar mode, it is possible to understand

that DHOSTs characterized by condition *II* suffer from instability (scalar and tensor modes are not stable simultaneously), preventing them from being recognized as viable theories.

2.2 DHOST at astrophysical scales

As explained in section 1.2.2, DHOST theories (and any ETG in general) must pass Solar System constraints reducing to GR at those scales. The screening mechanism which characterises DHOST more specifically is the so-called Vainshtein screening [142].

Historically, the Vainshtein screening was introduced to solve a problem of the so-called Fierz and Pauli (FP) theory [238]. This theory introduced a $2-$spin massive particle (massive graviton) establishing the fundamentals for the development of massive gravity theories. According to the FP theory, gravitons were characterised by five degrees of freedom instead of the two defined by the GR. However, according to Einstein's theory, gravitons, as a consequence of the equivalence principle, are massless particles with two degrees of freedom corresponding to their polarization states. As expected, in [239, 240] it was shown that the FP theory was suffering from instability, according to which it was impossible to reconcile the prediction of GR in the massless limit.

To solve this issue, in 1972, Vainshtein introduced a mechanism, the so-called Vainshtein screening [142], according to which, at short distances (and high mass) the non-linearities, arising in theories like the FP one, suppress the additional degree of freedom restoring GR predictions. In general, the Vainshtein screening plays a crucial role in reconciling ETGs with observational constraints.

This mechanism introduces a radius, the Vainshtein radius r_V, where the fifth force mediated by the addition scalar degree of freedom is suppressed, and GR is restored. The Vainshtein radius r_V reads

$$r_V = \left(\frac{M}{8\pi M_{pl}\mathfrak{M}}\right)^{1/3} \tag{2.23}$$

where: M is the total mass of a matter source; M_{Pl} is the Planck mass; $\mathfrak{M}$ is a specific mass scale, for instance, $\mathfrak{M} \sim M_{pl}H_0^2$, if $\mathfrak{M}$ is the energy density associated

with the present expansion rate of the Universe. In the massive gravity case [241] $\mathfrak{M} = m^2 M_{Pl}$ with m the graviton mass. In the DGP braneworld [242] gravitational scenario, the mass scale $\mathfrak{M} = r_c^{-2} M_{Pl}$ where r_c is the scale between the four and five-dimensional gravity.

The Vainshtein screening has been studied in detail also for Horndeski's theories [243–245]. However, for Beyond Horndeski [246] and DHOST theories [247–250], the Vainshtein screening is partially broken, that is, gravity is modified *also* inside the object. This partial breaking leads to interesting possibilities, such as gravity modifications that leak at astrophysical scales mimicking the effects that we attribute to dark matter (this will be discussed in other sections).

In the weak-field regime, the deformation of the spacetime induced by a matter source, assuming also spherical symmetry, is small and described by the metric

$$ds^2 = -\left[1+2\Phi(r)\right)dt^2 + \left(1-2\Psi(r)\right]\delta_{ij}dx^i dx^j\,, \tag{2.24}$$

where $\Phi(r)$ and $\Psi(r)$ are the gravitational and the metric potential induced by a matter source with a density $\rho(r)$. These two potentials are the same in GR; however, this is generally not true when gravity is modified in ETGs.

Furthermore, the matter source also induces a small perturbation in the scalar field

$$\phi = \phi_0(t) + \delta\phi(r)\,. \tag{2.25}$$

The relations that involve $\Phi(r)$, $\Psi(r)$, $\delta\phi(r)$, and $\rho(r)$ can be determined by expanding the equations of motion, assuming $\Phi(r)$, $\Psi(r)$, $\delta\phi(r)$ to be small and neglecting the high-order terms.

The final result for DHOST, as shown in [196, 247, 249, 251], leads to the modified expressions of the gravitational and metric potentials

$$\begin{aligned}\frac{d\Phi}{dr} &= \frac{G_N M(r)}{r^2} + \Xi_1 G_N M''(r),\\ \frac{d\Psi}{dr} &= \frac{G_N M(r)}{r^2} + \Xi_2\frac{G_N M'(r)}{r} + \Xi_3 G_N M''(r)\end{aligned} \tag{2.26}$$

where: $M(r)$ is the mass of the object within the radius r, and M' and M'' are the

first and second derivative of the matter source concerning the radius r

$$\begin{aligned} M(r) &= \int_0^r dx 4\pi x^2 \rho(x), \\ M'(r) &= 4\pi x^2 \rho(r), \\ M''(r) &= 8\pi r \rho(r) + 4\pi r^2 \frac{d\rho}{dr}. \end{aligned} \tag{2.27}$$

Outside the source where the mass $M(r) \equiv M$ is constant, $M' = M'' = 0$ and consequently GR is restored (with Φ and Ψ coinciding). However, inside the matter distribution, $M(r)$ is not constant and gravity is modified according to Eq. 2.26.

As underlined in [196, 247–249, 251] the $\Xi_{1,2,3}$ parameters can be related to the functions that appear in action Eq. 2.9 or to express them in terms of the more fundamental (and practical) EFT parameters in Eq. 2.19. Their most general expression, using the formalism of [249], reads

$$\Xi_1 = \frac{(\alpha_H + c_T^2 \beta_1)^2}{c_T^2(1+\alpha_V - 4\beta_1) - \alpha_H - 1}, \tag{2.28}$$

$$\Xi_2 = -\frac{\alpha_H(\alpha_H - \alpha_V + 2(1+c_T^2)\beta_1 + \beta_1(c_T^2-1)(1+c_T^2\beta_1)}{c_T^2(1+\alpha_V - 4\beta_1) - \alpha_H - 1}, \tag{2.29}$$

$$\Xi_3 = -\frac{\beta_1(\alpha_H + c_T^2\beta_1)}{c_T^2(1+\alpha_V - 4\beta_1) - \alpha_H - 1}. \tag{2.30}$$

These three parameters are not totally independent, although, and must satisfy the relation [196]

$$\Xi_3^2 - \Xi_1^2 = \frac{1}{2}\Xi_1\Xi_2. \tag{2.31}$$

An additional parameter corresponding to the fractional difference between the effective gravitational constant G_N and the "bare" one G (related to the Planck mass $M_{pl} = (8\pi G)^{-1}$) reads

$$\gamma_0 = \left(8\pi M_{PL}^2 G_N\right)^{-1} - 1 = \alpha_V - 3\beta_1. \tag{2.32}$$

The above four definitions can be greatly simplified if we apply the strong constraints on extended theories of gravity which have been derived from the multi-messenger observation of gravitational waves [180, 205–207, 252–254]. The most decisive is the one constraining the velocity of gravitational waves c_{GW} with respect to the speed of light c [255],

$$-3\cdot 10^{-15} \leq \frac{c_{GW}}{c} - 1 \leq 7\cdot 10^{-16}. \tag{2.33}$$

This condition automatically implies

$$c_T = 1 \quad \Longrightarrow \quad \alpha_T = 0, \quad \alpha_V = -\alpha_H \,. \tag{2.34}$$

With these equalities, the Ξ_i parameters can be expressed in terms of α_H and β_1 only

$$\Xi_1 = -\frac{(\alpha_H + \beta_1)^2}{2(\alpha_H + 2\beta_1)}, \quad \Xi_2 = \alpha_H, \quad \Xi_3 = -\frac{\beta_1(\alpha_H + \beta_1)}{2(\alpha_H + 2\beta_1)}. \tag{2.35}$$

and the fractional difference between G_N and G becomes

$$\gamma_0 = -\alpha_H - 3\beta_1 \tag{2.36}$$

2.3 Observational constraints on the EFT parameters

In [256], the *Planck* collaboration has investigated models characterized by a connection between the running Planck mass constant α_M and the brading α_B (typical of models such as $f(R)$, Brans-Dicke and chameleon theories). In particular, α_M has been modelled as a power law in the scale factor with a constant amplitude $\alpha_{M,0}$ and scaling β. By combining CMB amplitudes, weak lensing data (WL), BAO and Redshift Space Distortions (RSD) stringent constraints have been imposed on the amplitude of the running Planck mass $\alpha_{M,0} < 0.097$ and on the scaling $\beta = 0.92^{+0.53}_{-0.25}$ [256] (2σ CL). Adopting the most updated *Planck* data [3], the results of the analysis show a preference for a negative value of $\alpha_{M,0}$, when only CMB data have been considered, while the combination of CMB data with WL, BAO and RSD one gives $\alpha_{M,0} = -0.015^{+0.019}_{-0.017}$ (2σ CL) [3].

Additionally, constraints on the running Planck mass can be put also considering the EFT description provided by the action Eq. 2.18. To this purpose, in [257], they delved into the effects of a running Planck mass function, denoted as $f(t)$ in the action Eq. 2.18, assuming both ΛCDM and ωCDM background. The EFT parameter Ω [257], from the $f(t)$ in the action Eq. 2.18 expanded linearly in the scale factor as $f(t) = 1 + \Omega_0^{EFT} a$, [257] embodies the effects of a varying Planck mass. The results of the analysis, which are based on several data sets

(*Planck* temperature-temperature power spectra [258, 259], WMAP low-l polarization spectra [260] and BAO [261–263]) yield $\Omega_0^{EFT} < 0.061$ for the ΛCDM background and $\Omega_0^{EFT} < 0.058$ within a ωCDM background [257] being consistent with what has been found by the *Planck* collaboration [264].

For Horndeski models the EFT functions that can be constrained are $\{f, \bar{m}_1^3, M_2^4, \bar{M}_2^2\}$, using the action Eq. 2.18, and $\{\alpha_B, \alpha_K, \alpha_M, \alpha_T\}$ in the α-basis [222]. The first set of constraints has been determined for the EFT functions in the α basis from CMB, BAO, RSD and the WiggleZ survey [265] datasets. The constraints, depicted in Figure 3 of [265], favour a larger effective Planck mass M^2 (in the action Eq. 2.19) with respect to the Planck mass, a negative value for the running Planck mass $\alpha_M < 0$, a positive value for the braiding $\alpha_B > 0$ and sub-luminal propagation of gravitational waves $c_T < 1$.

Constraints from KiDS combined with GAMA [266], which are consistent with the ΛCDM, show a preference for $\alpha_{B,M} > 0$ and the S_8 parameter consistent with Planck when the gravitational framework was represented by the Horneski model instead of ΛCDM.

As shown in [267, 268] (exploiting several cosmological probes), the constraints provided by CMB data are driven by the Integrated Sachs-Wolfe (ISW) effect leading to large values for the α_i EFT parameters. The inclusion of RSD allows for breaking the degeneracy between α_M and α_B (Figure 2 of [268]).

Furthermore, in [269], it has been shown that RSD data, concerning the growth function $f\sigma_8$, when combined with data from VIPERS [270] and SDSS [271] (that enable separate measurement of f and σ_8) can improve the constraints on the EFT parameters of about $\sim 20\%$. In addition, in [269], the tight constraint $|\dot{G}_N/G| < 0.002 H_0$ on the variation, over time, of the Newtonian constant, obtained exploiting Solar System tests translated into a prior on the running Planck mass enhancing the constraining power of the growth rate f and of the amplitude of matter fluctuation σ_8.

The findings presented in [265] emphasize that, despite considering multiple cosmological probes, the kineticity parameter α_K does not affect the other parameters' constraints. To the same topic, the outcome presented in [272], reveal that bounds on the kineticity function α_K are difficult to impose because the contribution given by α_K to the observables is always within the cosmic variance. How-

ever, also in [272], the multi-tracer techniques have been presented as a possible way to overcome the cosmic variance problem.

When the gravitational scenario is described by Beyond Horndeski theories, we have an additional parameter α_H that we can constrain using observational data. In particular, the combination of CMB, BAO and RSD has shown that α_H is degenerate with the braiding α_B and the running Planck mass α_M parameters [194]. Additionally, the marginalized distributions on α_H have shown that this parameter is not consistent with the GR limit ($\alpha_H \to 0$) for most of the cases the authors have considered [194].

DHOST theories are the further generalization of Beyond Horndeski ones. As explained in Section 2.1, the action of these theories is characterized by three additional non-completely independent parameters $\beta_{1,2,3}$ [232].

Observational constraints can be imposed on the effective field theory parameters α_H and β_1, by taking into account the dependence of the DHOST parameter Ξ_1 from these (as defined by the first equation of Eq. 2.35), exploiting late-time observations. The parameter Ξ_1 controls the deviation from the standard Newtonian potential (for non-relativistic systems), and its constraints can be extracted independently from those on Ψ. First of all, from the definition of the derivative of the gravitational potential, in (2.26), can be seen that if $\Xi_1 < 0$, gravity inside an astrophysical object is stronger (the opposite happens if $\Xi_1 > 0$). This fact can be used to establish constraints, on Ξ_1, from stellar stability arguments. A lower bound of $\Xi_1 > -1/6$ arises by requiring stars to be in the hydrostatic equilibrium [273]. Furthermore, an upper bound can also be introduced. Indeed, the mass of the smallest red dwarf should be, at least, equal to the minimum mass required to start burning hydrogen [274]. The other two parameters, appearing in equation Eq. 2.26, Ξ_2 and Ξ_3 have to be constrained simultaneously requiring relativistic observations. For example, if $\Xi_3 = 0$, a constraint on Ξ_2 has been provided in [275].

Imposing the first constrain on the fractional difference in the speed of gravitational waves (first equation in Eq. 2.34), γ_0 can also be constrained through the observations on the Hulse-Taylor pulsar [276]. Considering the results provided by [253] and based on the time measurements of the Hulse-Taylor pulsar [277]

one finds (at 2σ)

$$-7.5 \cdot 10^{-3} < \gamma_0 - 1 < 2.5 \cdot 10^{-3} \tag{2.37}$$

Combining all the existing constraints on Ξ_1 and γ_0 establishes tight limits on α_H and β_1.

However, the most stringent constraints on Ξ_1 are granted by helioseismology arguments. In [278], the authors studying the interior physics of the Sun derived

$$-1.8 \cdot 10^{-3} < \Xi_1 < 1.2 \cdot 10^{-3} \tag{2.38}$$

CHAPTER 3

Observational Data: modelling and statistical analysis

In this chapter, we provide a panoramic description of the type of astrophysical data which have been used to test the possible unification of DE and DM using the DHOST model represented by Eq. 2.9.

3.1 Galaxy clusters

Galaxy clusters are the most massive gravitationally-bound structures in the Universe for which a detailed dynamical and kinematical analysis has been performed. They are quite useful because with them multiple and independent types of observations are possible.

Indeed, on the one hand, we have observations in the optical band which are used mostly in lensing analysis. The sample we have finally chosen had the important feature of combining both strong lensing, mostly for the inner regions of the clusters, and extended weak lensing data, from the outer skirts of these gravitational structures, leading to a more precise galaxy cluster mass reconstruction [279] and tighter constraints for the concentration parameter. On the other hand,

for clusters of galaxies, we also have at our disposal X-ray observations from the hot intra-cluster gas.

The importance of having both types of data has to be sought in the existing natural tension between lensing and X-ray-based mass reconstruction approaches, which relies on the fact that these two types of data are sensitive to different phenomena and regimes. Indeed, mass reconstruction from X-ray data (whose emission is susceptible to the Newtonian gravitational potential Φ) is more prone to biasedness by non-gravitational effects [280] in the internal regions of the clusters. Instead, gravitational lensing (which also allows us to test related to the combination of potentials $\Phi+\Psi$ to which photons are sensitive) is much less sensitive to local astrophysical and non-thermal phenomena, but a bit more sensitive to the presence of matter along the line of sight. These fundamental differences can systematically lead to different mass determinations which are fundamental to take into account in GR, and even more so when dealing with ETGs.

Studies of the dark matter distributions based on observations of strong gravitational lensing effects showed a discrepancy with the results obtained by cosmological simulations (and based on GR) [281–283]. Indeed, the observation of galaxy clusters at $z > 1$ implies that their formation occurred earlier than suggested by cosmological simulations. Furthermore, galaxy clusters at intermediate redshifts $z \sim 0.3$ have been observed to have denser cores than expected. Several explanations have been proposed to explain these discrepancies between observations and cosmological simulations, such as the presence of non-Gaussianities in the initial density fluctuations. However, several models that introduce non-Gaussianity in the initial conditions have been ruled out by X-ray measurements [284]. Another possibility is the introduction of an early form of dark energy (EDE) that suppressed the formation of galaxy clusters [285–288]. Therefore, to match the number of galaxy clusters that we observe today, these objects had to start forming earlier than expected.

At the present day, the main "ingredient" of cosmological simulations is dark matter, and a possible solution to the discrepancy with observations might be to introduce baryons into cosmological simulations. However, it is reasonable to expect that their contributions (since they are a sub-dominant component of galaxy

clusters) may not be sufficient to explain the observed higher concentration parameter. Indeed, it has been shown in [289–291] that when baryons are included in cosmological simulations, they can imply a variation of $\sim 10\%$ in the concentration parameter. In our analysis, we have also taken into account the contributions coming from the Brightest Cluster Galaxy (BCG) which lies at the centre of the clusters, and from the non-BCG galaxies, scattered throughout them.

In order to take advantage of this wide variety of tests, we initially planned to use the most recent data that could be obtained from the literature but then realized that it would be most useful to look for the most *complete* data set. The data set we have used in our works [292], belong to the Cluster Lensing and Supernova Survey with Hubble (*CLASH*) programme [279]. This sample consists of 25 galaxy clusters divided into two main categories

- 20 galaxy clusters selected on the basis of their X-ray measurements, with a temperature of $T_X \geq 5$ Kpc and a small deviation from the hydrostatic equilibrium. Within the ΛCDM scheme [293], numerical simulations have suggested that $\sim 70\%$ of these clusters are relaxed, with a non-negligible fraction ($\sim 30\%$) of them unrelaxed;

- 5 galaxy clusters selected for their lensing data, which may allow the determination of high-resolution dark matter maps. However, these systems are highly massive ongoing mergers [294].

In [295], the authors studied a subsample of 16 *CLASH* galaxy clusters to reconstruct the convergence $\kappa(R)$, combining weak-lensing shear and magnification data from the Subaru telescope [296], and strong-weak lensing constraints from the Hubble Space Telescope (HST) [297]. Remarkably, both photometric data and BCG mass estimates were also available for these clusters.

3.1.1 X-ray hot gas mass reconstruction

Another important advantage in selecting and working with *CLASH* clusters, is that they were selected (for dedicated observations) also taking into account the fact that archival X-ray data were available for them [280] for the X-ray analysis.

X-ray estimates of the masses of galaxy clusters are based on the collisionless Boltzmann equation with the basic assumptions of spherical symmetry and hydrostatic equilibrium. With these assumptions, the collisionless Boltzmann equation can be used to express the relationship between the gravitational potential, Φ, of a galaxy cluster and the temperature, T_{gas}, and the density, ρ_{gas}, of the hot gas,

$$-\frac{\mathrm{d}\Phi(r)}{\mathrm{d}r} = \frac{kT_{\rm gas}(r)}{\mu m_p r}\left[\frac{\mathrm{d}\ln\rho_{\rm gas}(r)}{\mathrm{d}\ln r} + \frac{\mathrm{d}\ln T_{\rm gas}(r)}{\mathrm{d}\ln r}\right] . \tag{3.1}$$

In GR, the derivative of the gravitational potential is related to the total mass of the system under exam by

$$\frac{d\Phi}{dr} = \frac{G_N M_{tot}(r)}{r^2} , \tag{3.2}$$

so that, by substituting this result in Eq. 3.1 it is possible to determine the galaxy cluster's total mass

$$\begin{aligned} M_{\rm tot}(r) &= M_{\rm gas}(r) + M_{\rm gal}(r) + M_{\rm BCG}(r) + M_{\rm DM}(r) \\ &= -\frac{kT_{\rm gas}(r)}{\mu m_p G_N} r\left[\frac{\mathrm{d}\ln\rho_{\rm gas}(r)}{\mathrm{d}\ln r} + \frac{\mathrm{d}\ln T_{\rm gas}(r)}{\mathrm{d}\ln r}\right] . \end{aligned} \tag{3.3}$$

For the *CLASH* clusters which we have used, the hot-gas density and temperature profiles have been retrieved by observational data from *Chandra* telescope in [280]. Consequently, the total mass can be inferred from Eq. 3.3. Additionally, after measuring the gas mass, M_{gas} from the same observations, and adding the information coming from other baryonic components (BCG, M_{BCG}, and galaxies, M_{gal}), one can also eventually infer the mass of the DM component M_{DM}.

Crucial for our analysis in the DHOST scenario is thus the observationally estimated total cluster mass which can be compared to the theoretically expected one, from the following relation:

$$M_{\rm tot}^{\rm obs} = \frac{r^2}{G_N}\frac{\mathrm{d}\Phi}{\mathrm{d}r} , \tag{3.4}$$

where the right-hand side, within the context of the DHOST gravitational scenario chosen for investigation, is given by Eq. 2.26.

3.1.2 Gravitational lensing

Galaxy clusters can act as, and are actually one of the best examples of, gravitational lenses. Hence, gravitational lensing is a powerful tool to be exploited to map/reconstruct the mass distribution of clusters.

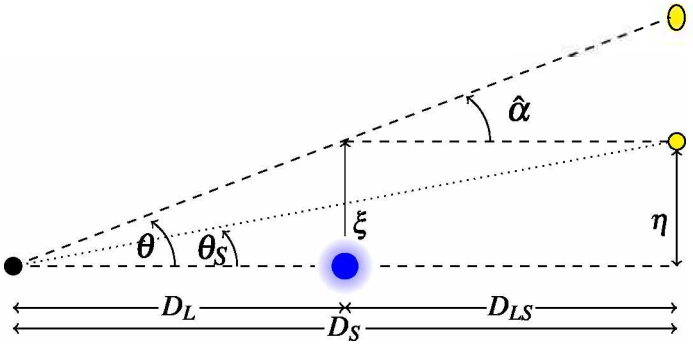

Figure 3.1: Typical lensing configuration. The gravitational lens represented by a galaxy cluster is pictured by the blue circle. The light blue shaded area around it represents the gravitational potential generated by the lens. The yellow circle represents the source (e.g. a distant galaxy), while the yellow ellipses represent the observed apparent positions of the source distorted by the lensing effects.

According to the typical lensing configuration, represented in Fig. 3.1, $\vec{\theta}_s$ is the angular position of the source (with respect to the lens); $\vec{\theta}$ is the angular position of the image; and $\vec{\hat{\alpha}}$ is the deflection angle, given by

$$\hat{\alpha} = \frac{2}{c^2}\int_{-\infty}^{+\infty} dz \vec{\nabla}_\perp \Phi \tag{3.5}$$

where $\vec{\nabla}_\perp$ is the two-dimensional gradient in the transverse plane and z specifies the coordinate along the line of sight. The angular diameter distances between observer and lens, lens and source, and observer and source are D_L, D_{LS}, and D_S, respectively.

If $\vec{\theta}$, $\vec{\theta}_s$ and $\vec{\hat{\alpha}}$ are small, in the limit of $\sin(\theta) \approx \theta$, there is a simple but fundamental equation that comes from geometrical considerations, the *lens equation*:

$$\vec{\theta} D_S = \vec{\theta}_s D_S + \vec{\hat{\alpha}} D_{LS} \, . \tag{3.6}$$

The lens equation can be recast as

$$\vec{\theta} = \vec{\theta}_s + \vec{\alpha}(\vec{\theta}) \, , \tag{3.7}$$

where $\vec{\alpha} = D_{ls}/D_s\hat{\vec{\alpha}}$ is the scaled deflection angle, and we highlighted the dependence of $\vec{\alpha}$ from $\vec{\theta}$ since this is the core of the lensing effects.

It is common practice to express all relations in terms of dimensionless quantities. From Fig. 3.1, we see that $\vec{\xi}$ and $\vec{\eta}$ are the physical lengths on the lens and source plane, but it is more common to work with dimensionless quantities. Indeed, we can define the dimensionless position of the image on the lens plane, the dimensionless source position on the lens plane and the scaled deflection angle, respectively, as

$$\vec{x} = \frac{D_L}{\vec{\xi}_0}\vec{\theta}\,, \tag{3.8}$$

$$\vec{y} = \frac{D_L}{\vec{\xi}_0}\vec{\theta}_s\,, \tag{3.9}$$

$$\vec{\alpha}(\vec{x}) = \frac{D_L D_{LS}}{D_S \xi_0}\hat{\vec{\alpha}}(\xi_0\vec{x})\,, \tag{3.10}$$

where $\vec{\xi}_0$ is a characteristic length on the lens plane whose value and nature depend on the mass models that are used to describe the lens. Eventually, using these dimensionless quantities, the lens equation, Eq. 3.6, will become

$$\vec{y} = \vec{x} - \vec{\alpha}(\vec{x})\,. \tag{3.11}$$

Since the scales (and in particular the width) on which the lens physically extends are much smaller than the typical distances between the observer and the lens and the lens and the source, the lens can be schematically modelled as a two-dimensional mass distribution, in the so-called thin-lens approximation. Thus, instead of defining the lens by its volume mass density, $\rho(r)$, with r being the three-dimensional distance from the centre of the lens, we work with the surface mass density, defined as [298]

$$\Sigma(\vec{\xi}) = 2\int_0^\infty \rho(\vec{\xi}, z)\,dz, \tag{3.12}$$

where z is the line-of-sight direction.

A relation between the scaled deflection angle and the effective lensing potential, namely the projection of the three-dimensional Newtonian potential on the

lens plane, can be established

$$\Phi_{lens} = \frac{2}{c^2}\frac{D_{ls}}{D_s D_l}\int_{-\infty}^{+\infty} dz\Phi(R,z)\,, \tag{3.13}$$

$$\vec{\alpha} = \vec{\nabla}_\theta \Phi_{lens}\,, \tag{3.14}$$

where $R = D_l\vec{\theta}$ corresponds to the two-dimensional radius projected onto the lens plane and $\nabla_\theta = D_l\vec{\nabla}$. By taking the Laplacian of the scaled deflection potential Φ_{lens}, one can obtain the lensing convergence $\kappa(R)$

$$\kappa(R) = \frac{1}{c^2}\frac{D_{ls}D_l}{D_s}\int_{-\infty}^{+\infty} dz\Delta_r\Phi(R,z)\,, \tag{3.15}$$

where: $r = \sqrt{R^2+z^2}$ is the three-dimensional radius and $\Delta_r = \frac{2}{r}\frac{\partial}{\partial r} + \frac{\partial^2}{\partial^2 r}$ is the radial part of the Laplacian operator.

The convergence, Eq. 3.15 can be related to the density distribution of the lens through the Poisson equation. Using

$$\Delta\Phi = 4\pi G_N \rho(r)\,, \tag{3.16}$$

we have

$$\kappa(R) = \frac{4\pi G_N}{c^2}\frac{D_{ls}D_l}{D_s}\int_{-\infty}^{+\infty} dz\rho(R,z) \equiv \frac{\Sigma}{\Sigma_c}\,, \tag{3.17}$$

where Σ is the two-dimensional projected mass density of the lens and Σ_c is the critical surface density

$$\Sigma_c = \frac{c^2}{4\pi G}\frac{D_s}{D_{ls}D_l}\,. \tag{3.18}$$

All the above definitions have been determined within the GR description of gravity according to which there is an equality between the gravitational and metric potentials $\Phi = \Psi$. However, when gravity is modified, for instance, as specified by Eq. 2.26, $\Phi(r)$ and $\Psi(r)$, in general, do not coincide. Hence, the convergence definition Eq. 3.15 must be generalized to

$$\kappa(R) = \frac{1}{c^2}\frac{D_{ls}D_l}{D_s}\int_{-\infty}^{+\infty} dz\Delta_r\left(\frac{\Phi(R,z)+\Psi(R,z)}{2}\right)\,. \tag{3.19}$$

Nonetheless, an important point should be stressed. The determination of $\kappa(R)$ is strictly tied to the background specification. Indeed, the cosmological background

enters in the determination of the angular diameter distance through the Hubble parameter $H(z)$

$$D_A = \frac{c}{1+z}\int_0^z \frac{dz'}{H(z)}, \tag{3.20}$$

where the Hubble parameter $H(z)$ is determined from the first Friedmann equation and thus depends on the cosmological model. When a gravity modification is cast to extend GR, Friedmann equations (and consequently the Hubble parameter) have to be modified (a non-exhaustive list of examples is represented by [121, 126, 299]. However, in our works, as we were not interested in a cosmological analysis of the DHOST model represented by (2.26), we have assumed that the global behaviour of these models on cosmological scales was equivalent to that of a standard ΛCDM background, whose Hubble parameter was reported in the previous chapter in Eq. (1.8). Both qualitative and quantitative motivations behind this choice can be found in [206], where the EFT parametrization of cosmological perturbations is made by expanding the action around the standard FRW background, and in [300, 301], in which the authors determine constraints on the DHOST theories using CMB data from *Planck* [3] adopting also a ΛCDM background.

3.1.3 Mass modeling of galaxy clusters

In galaxy clusters, DM represents the most abundant component amounting to $\sim 30\%$ (at ~ 5 kpc) and $\sim 60\%$ (at ~ 5 Mpc) of the total mass. Hot gas (as X-rays) ranges from $\sim 5\%$ to $\sim 40\%$ of the total mass in the same ranges. However, it is essential to point out that in the innermost region of galaxy clusters, the BCGs contribution is far from being considered negligible. Indeed, at $10-20$ kpc, their mass can be up to $\sim 50\%$ of the total mass, thus comparable to DM, while At $50-100$ kpc, BCGs are subdominant ($\sim 10\%$) with respect to DM but comparable to X-rays. On the contrary, the contribution provided by non-BCG galaxies is always subdominant compared to all the other components ($\sim 1-2\%$ in the range $20-300$ kpc). Although this component has the lowest weight in the calculation of the total mass, it has been included for completeness in our analysis.

Dark matter

According to cosmological simulations, the DM distribution in galaxy clusters can be described by a functional form that steepens with the distance from the cluster centre. Among these functional forms that describe the dark matter density we have the Navarro-Frenk-White (NFW) profile [163, 302] and the Einasto one [164]. In the last ten years, lensing-based observations of galaxy clusters have shown that their total masses are well described by cuspy profiles [295, 296, 303–307] such as the NFW and Einasto ones.

We have used the standard spherically symmetric NFW density function [163]

$$\rho_{DM}(r) = \frac{\rho_s}{\frac{r}{r_s}\left(1+\frac{r}{r_s}\right)^2}, \tag{3.21}$$

where ρ_s and r_s are the NFW density and scale radius, respectively. The NFW density ρ_s can be expressed in terms of the concentration parameter c_Δ

$$\rho_s = \frac{\Delta}{3}\frac{c_\Delta^3}{\log(1+c_\Delta) - \frac{c_\Delta}{1+c_\Delta}}\rho_c, \tag{3.22}$$

where the concentration parameter c_Δ is evaluated at the spherical radius r_Δ which encloses a density which is Δ-times the critical density of the Universe ρ_c,

$$\rho_c = \frac{3H^2(z)}{8\pi G_N}, \tag{3.23}$$

where $H(z)$ is the Hubble parameter Eq. 1.8.

The mass associated to Eq. 3.21 reads

$$M_{DM}(r) = 4\pi\rho_s r_s^3\left[\log\left(1+\frac{r}{r_s}\right) - \frac{r}{r+r_s}\right], \tag{3.24}$$

while the mass enclosed in the spherical radius r_Δ is given by

$$M_\Delta = \frac{4\pi}{3}\Delta\rho_c r_\Delta^3. \tag{3.25}$$

There are several choices for $\Delta = \{200, 500, 2500\}$. Although one of the most common is 200, because it is almost equal to the virialised radius, our choice was $\Delta = 500$, with a radius r_{500} corresponding approximately to half of the virialised radius, motivated by the fitting relation we used following [308] to parameterise the non-BCG component, as will be explained in the following pages.

Hot-gas

The X-ray hot gas component has been parametrized, following [280], with a double β-model [309]

$$\rho_{gas}(r) = \rho_{e,0}\left(\frac{r}{r_0}\right)^{-\alpha}\left[1+\left(\frac{r}{r_{e,0}}\right)^2\right]^{-3\beta_0/2} + \rho_{e,1}\left[\left(\frac{r}{r_{e,1}}\right)^2\right]^{-3\beta_1/2}, \quad (3.26)$$

where: $\rho_{e,0}$ and $\rho_{e,1}$ are the density normalization constants of the two β-model terms in Eq. 3.26; $r_{e,0}$ and $r_{e,1}$ are the scale radii; r_0 is the scale radius of the power-law truncating term. All the parameters appearing in Eq. 3.26 $\{\rho_{e,0}, \rho_{e,1}, r_{e,0}, r_{e,1}, r_0, \alpha, \beta_0, \beta_1\}$ have not been considered as free parameters in our analysis, but they have been fixed to their best-fit values in a preliminary step.

Although the assumed density describing the gas component is that described by Eq. 3.26, the vast majority of clusters have been successfully fitted using a single truncated β-model, namely, the first term in Eq. 3.26) (with the single exception of *MACSJ*1720, for which the double β-model is preferable). This choice is motivated by the fact that for several clusters the available data points were few or limited, so that we did not have enough information to perform a fully statistically reliable analysis of the previous expression.

Brightest cluster galaxy

BCGs reside at or near the centre of the gravitational potential of hosting galaxy clusters. Stellar mass estimations for the BCGs of *CLASH* galaxy clusters, can be found in several works [310, 311]. The main difference between [310, 311] is represented by the fact that in [310], the authors did not decompose the BCG component from the low-brightness non-BCG stellar one. On the other hand, in [311], such decomposition has been considered. These approaches translate into a difference of about $\sim 30\%$ in the BCG mass estimation. In our work [292], we have considered the BCG component separated from the stellar ones, and thus we have used the mass estimation described in [311].

Several possibilities can be considered to model the density function of the BCG component [312, 313]. In [312], the authors model the surface brightness of the BCG component using a single Sérsic profile [314]. In [313], both the single and the double Sérsic profiles (and also other possibilities) were used. The final

choice for modelling the BCG mass density function, in [292], was the double Sérsic profile [313] as the fits taking into account a central region and an outer envelope, were of better quality than those ones obtained with a single Sérsic profile.

The Sérsic profile is described by

$$I(R) = I_0 \exp\left[-\left(\frac{R}{a_s}\right)^{1/n}\right], \tag{3.27}$$

where I_0 is the central surface brightness, a_s is the Sérsic scale parameter, and n is the Sérsic index. The Sérsic profile can also be re-written as [313]

$$I(R) = I_e \exp\left[-b_n\left(\frac{R}{R_e}\right)^{1/n} - 1\right], \tag{3.28}$$

with I_e the intensity at the half-light radius, R_e and b_n a parameter defined in terms of the Sérsic index, $b_n = 2n - 0.33$ [315]. It is straightforward to show that the two definitions of surface brightness are equivalent with the substitution $a_s = R_e/(b_n)^n$.

The deprojection of the surface brightness $I(R)$, described by Eq. 3.27, leads to the luminosity density $l(r)$. However, an analytical expression for it does not exist. Indeed, it is only possible to get $l(r)$ invoking approximations as the one proposed by [316]

$$l(r) = l_1 \tilde{l}(r/a_s), \tag{3.29}$$

with

$$\begin{aligned} l(x) &\simeq x^{-p_n} \exp(-x^{1/n}) \\ l_1 &= \frac{L_{\rm tot}}{4\pi n \Gamma[(3-p)n] a_s^3}, \end{aligned} \tag{3.30}$$

with the function p_n defined as [317]

$$p_n \simeq 1.0 - \frac{0.6097}{n} + \frac{0.05463}{n^2}, \tag{3.31}$$

and the total luminosity L_{tot} as depending from the apparent magnitude m

$$L_{tot} \propto 10^{-0.4m}. \tag{3.32}$$

The required photometric parameters for the mass modeling $\{R_e, n, m\}$ are enlisted in Table 2 of [313]. Finally, we model the BCG component as

$$\rho_{BCG}(r) \propto \mathscr{A}\left[\tilde{l}\left(\frac{r}{R_{e,int}}\right) + \tilde{l}\left(\frac{r}{R_{e,ext}}\right)\right], \tag{3.33}$$

where the subscripts *int* and *ext* refer to the BCG's internal region and the external envelope; $\mathscr{A}$ encloses all the remaining constant terms such as the mass-to-light ratio, fundamental to ensure and quantify the correct conversion luminosity to mass. The value of this constant has been fixed equalling the total BCG mass, calculated at $r = 50$ kpc (integrating equation Eq. 3.33) to the mass estimate determined in [311].

Galaxies

Determining the mass density of non-BGC galaxies requires some preliminary steps. The first stage is the introduction of the cold baryonic fraction f_c (estimated in [308] for a sample of 91 galaxy clusters with $0.25 < z < 1.25$), defined as the ratio between the stellar mass M_* (consisting in the sum of the BCG and non-BCG galaxies masses within r_{500}) and the baryonic one $M_{bar} = M_* + M_{gas}$

$$f_c = \frac{M_*}{M_* + M_{gas}}, \tag{3.34}$$

where the gas mass, M_{gas} is estimated from X-ray observations. In [308], the cold baryonic fraction f_c has been obtained from a subsample of galaxy clusters in the redshift range $0.25 \leq z \leq 1.25$ with measurements of the stellar mass M_*. The resulting data, then, have been fitted using the relation

$$f_c = \mathscr{A}_f \left(\frac{M_{500}}{M_{piv}}\right)^{\mathbf{B}_f} \left(\frac{1+z}{1+z_{piv}}\right)^{\mathbf{C}_f}, \tag{3.35}$$

where M_{piv} and z_{piv} are the reference mass and redshift of the selected cluster sample. In addition, the stacked radial profile of f_c is represented, not analytically, but by a black line in Figure 11 of [308]. From that, we numerically extract its mathematical behaviours.

When we introduced the modelling of the DM component in the previous section, we stated that the DM free parameters were $\{c_{500}, r_{500}\}$. It is clear now

why we have adopted this choice with respect to other more common values, like 200. Moreover, one can see from Eq. 3.35 that the value of the cold baryonic fraction is also related to the knowledge of M_{500} (or equivalently r_{500}). In [292], the procedure adopted to determine the radial trend of the cold baryonic fraction consists of the following steps:

1. extract $\bar{f}_c(r)$, namely, the radial dependence of the stacked $f_c(r)$ shown in Figure 11 of [308]. The logarithm of $\bar{f}_c$ has been expressed as a third-order polynomial in the variable $\log r$, ensuring the best agreement with the data in [308];

2. the average cold baryonic fraction of each galaxy cluster has been determined using Eq. 3.35;

3. Finally, to get the radial profile for f_c a shift of $\bar{f}_c$ has been performed

$$f_c(r) = \bar{f}_c(r) + d\,, \tag{3.36}$$

where the displacement d is defined as

$$d = f_c + \bar{f}_c(r_{500})\,. \tag{3.37}$$

Once $f_c(r)$ has been found, the mass of the galaxy component (excluding the BCGs) is provided by Eq. 3.34

$$M_{gal}(r) = \frac{f_c(r)}{1-f_c(r)} M_{gas} - M_{BCG}(r)\,. \tag{3.38}$$

It is now straightforward to find the density of the galaxy component from Eq. 3.38 as

$$\rho_{gal}(r) = \frac{f_c(r)}{1-f_c(r)}\rho_{gas} + \frac{M_{\rm gas}(<r)}{4\pi r^2}\left[\frac{f_c(r)}{1-f_c(r)}\right]' - \rho_{BCG}(r)\,, \tag{3.39}$$

where the prime denotes the first order derivative of $f_c(r)/(1-f_c(r))$ with respect to r.

3.2 Ultra-diffuse galaxies

Low Surface Brightness galaxies (LSB) [318] are galaxies dominated by an exponential disk characterized by a value for the central surface brightness below the Freeman value $\mu_B = 21.65$ mag arcsec^{-2} [319]. This family of galaxies is characterized by properties such as luminosity, colours, and dynamics that are still under debate.

The Dragonfly Telephoto Array [320] has been developed to study specifically LSB galaxies with a low surface brightness below $\mu_B = 30$ mag arcsec^{-2}. This surface brightness is markedly beyond the limit of any other existing wide-field telescope. In [321], the Dragonfly Telephoto Array has been exploited to study the outskirts of the spiral galaxy M101. In [322] authors reported the identification of seven objects with a surface brightness of $\mu_g = 25.5 - 27.5$ mag arcsec^{-2}. These seven galaxies share similar properties (such as effective radius, absolute magnitude, median surface brightness and colour) of known galaxies in the Local Group like Sextans I and Phoenix.

The same instruments have also been used for the identification of low surface brightness objects in the Coma Cluster. While observing the Coma Cluster, it has been found a family of forty-seven galaxies with very low surface brightness [174], which seemed not to be already included in any existing catalogue [323, 324]. However, after some initial quest, it was concluded that they did not represent a new category of galaxies and some of them were actually already catalogued in [325].

Indeed, they were finally considered a subset of a specific galactic family, that of dwarf spheroidal and elliptical galaxies [326]. These galaxies are characterized by a central surface brightness $\mu_0 = 24 - 26$ mag arcsec^{-2}, a size similar to the Milky Way, and luminosity analogous to that of elliptical galaxies [327] and have been named as Ultra-Diffuse Galaxies (UDG).

UDGs can be localized in dense environments [174, 328, 329], in galaxy groups [330, 331], and in cosmic voids [332, 333]. Different environments imply different formation scenarios. For instance, UDGs could represent the final result of tidal stripping processes. In [334, 335], the authors introduced the possibility that UDGs are dwarf galaxies formed from dark matter halos characterized by

high-spins. In addition, the low amount of gas shown by UDGs might point out that these galaxies lost their gas component after forming the first population of stars. This loss could be the consequence of astrophysical phenomena like supernovae, AGN feedback [336, 337], "galaxy harassment" [320], and quenching at high redshift [338, 339].

Additionally, the unusually high number of globular clusters (GCs) in UDGs [340, 341], suggest that massive dark matter halos are hosting these galaxies. This seems to be the case of, for example, Dragonfly 44, characterized by a high number of GCs ($\sim$ 100 according to [342] while a lower number was given in [343]) and with a halo mass estimated to be $M_h \sim 99\%$ of the total one. However, it was later revealed that another UDG, NGC1052-DF2 (DF2), also observed with the Dragonfly telescope, shows a lack of dark matter ($M_h \sim 1\%$ of M_{tot}) [175]. In the same group of galaxies, also another UDG, NGC1052-DF4 (DF4) displays, as DF2, a low amount of dark matter.

The absence of DM seems strange, since dark matter is the crucial component of any gravitationally bound structure according to the current galaxy formation paradigm, although hydrodynamical simulations show that it would be possible to form galaxies like DF2 and DF4 within the gravitational paradigm represented by the ΛCDM model [344–346]. Furthermore, a galaxy like DF2 could fit the standard paradigm if it were at a lower distance [347]. However, this possibility seems to have been ruled out by the determination of the distance of DF2 using the Tip of the Red Giant Branch method [348]. In a more recent paper [349], the authors suggest that galaxies such as DF2 and DF4 could belong to a family of eleven galaxies with similar properties (above all, the dark matter deficit) that have formed as a result of a Bullet-Cluster-like mechanism.

The determination of the dynamical mass of such UDGs from kinematic data is therefore crucial for distinguishing between different formation processes. However, due to their low surface brightness (and low signal-to-noise ratio), the mass determination of these galaxies using stellar velocity dispersion data is not affordable. A viable way to reconstruct the total mass of UDGs is to study the dynamics of the associated globular clusters.

3.2.1 Internal kinematics

The internal kinematics of UDGs can be studied through the Jeans equation with the assumptions of spherical symmetry and a collisionless trace population

$$\frac{d(l(r)\sigma_r^2(r))}{dr} + \frac{\beta(r)}{r}(l(r)\sigma_r^2(r)) = l(r)\frac{d\Phi(r)}{dr}, \tag{3.40}$$

where $l(r)$ is the luminosity density measured in $L_\odot/\mathrm{kpc}^3$ and $\beta(r)$ is the so-called velocity anisotropy parameter [350]

$$\beta(r) = 1 - \frac{\sigma_t^2(r)}{\sigma_r^2(r)}. \tag{3.41}$$

In the above definition, σ_r is the radial component of the velocity dispersion and σ_t represents the tangential component of the velocity dispersion tensor, which is defined as a combination of the angular velocity dispersion components ($\sigma_{\theta,\phi}$)

$$\sigma_t^2 = \frac{\sigma_\theta^2 + \sigma_\phi^2}{2}. \tag{3.42}$$

If $\beta = 0 \longrightarrow \sigma_t = \sigma_r$, the system is defined as fully isotropic; if $\beta = 1 \longrightarrow \sigma_t = 0$, the system is considered fully radial; if $\beta \to -\infty \longrightarrow \sigma_r \to 0$, we have a purely tangential scheme.

In Eq. 3.40, the information about gravity is stored in the gravitational potential Φ at the right-hand side. The Jeans equation, then, ensures studying the internal kinematics of galaxies in any gravitational scenario as, for instance, the one specified by the first equation of Eq. 2.26 introduced within the DHOST model.

Within GR, Eq. 3.40 can be easily solved, leading to [351]

$$l(r)\sigma_r^2(r) = \frac{1}{f(r)}\int_r^\infty ds\, f(s)l(s)\frac{M(s)}{s^2}, \tag{3.43}$$

with

$$\frac{d\log f(r)}{d\log r} = 2\beta(r). \tag{3.44}$$

The function $f(r)$ depends on the chosen parametrization for the anisotropy parameter $\beta(r)$. For instance, with a constant anisotropy, the function $f(r)$ reduces to $f(r) = r^{2\beta}$ (other examples are enlisted in detail in [351]).

We can then deproject Eq. 3.43 along the line of sight, defining in this way the true observable quantity, the velocity dispersion along the line of sight σ_{los}

$$\sigma^2_{los}(R) = \frac{2}{I(R)} \int_R^\infty dr\, r \frac{l(r)\sigma^2_r(r)}{\sqrt{r^2 - R^2}} - R^2 \int_R^\infty dr\, \beta(r) \frac{l(r)\sigma^2_r(r)}{r\sqrt{r^2 - R^2}}, \tag{3.45}$$

where R is the projected two-dimensional radius, and $I(R)$ is the stellar surface brightness. Eventually, using Eq. 3.43 in Eq. 3.45, one can recast the velocity dispersion as a function of the galaxy mass distribution as

$$\sigma^2_{los}(R) = \frac{2G_N}{I(R)} \int_R^\infty dr K\left(\frac{r}{R}\right) l(r) \frac{M(r)}{r}, \tag{3.46}$$

where $K(r/R)$ is the so-called Kernel function whose expression depends on the specific parametrization chosen for $\beta(r)$ (more details are given in [351]).

We can now properly and easily generalise Eq. 3.46 for the DHOST gravity modification introduced by Eqs. 2.26. The first step is to notice that the first of Eq. 2.26 can be re-written as the derivative of a Newton-like gravitational potential

$$\frac{d\Phi}{dr} = \frac{G_N M_{eff}(r)}{r^2}, \tag{3.47}$$

introducing, therefore, an "effective" mass

$$M_{eff}(r) = M(r) + r^2 \Xi_1 M''(r), \tag{3.48}$$

accounting for the modification to the mass distribution induced by the DHOST model Eq. 2.26. With the definition Eq. 3.48 the velocity dispersion along the line of sight Eq. 3.46 then becomes

$$\sigma^2_{los}(R) = \frac{2G_N}{I(R)} \int_R^\infty dr K\left(\frac{r}{R}\right) l(r) \frac{M_{eff}(r)}{r}, \tag{3.49}$$

which can be clearly used to analyse UDGs data in the DHOST scenario.

3.2.2 Mass modelling of Ultra-diffuse galaxies

The UDGs observed with the Dragonfly Array telescope are poor-gas galaxies. Therefore, their total mass has been modelled as the sum of the DM and the stellar components only. Moreover, two scenarios have been considered to underline

the connection between the DM and the stellar component. Indeed, according to the actual galaxy formation paradigm, there should be a correlation between their corresponding masses. Such a link can be defined through the so-called Stellar-to-Halo-mass relation (SHMR). A second less conservative possibility is to consider the dark matter and the stellar component completely decoupled.

Dark Matter

For the description of the DM component in UDGs, we have considered a generalized NFW profile [165, 352]

$$\rho_{gNFW}(r) = \rho_s \left(\frac{r}{r_s}\right)^{-\gamma} \left(1+\frac{r}{r_s}\right)^{\gamma-3}, \tag{3.50}$$

where ρ_s and r_s are the gNFW parameters and γ is the inner log-slope. Eq. 3.50 reduces to the standard NFW density if $\gamma = 1$. The choice of a generalized NFW profile, as defined by Eq. 3.50 is motivated by the fact that it has more freedom to recover a larger number of inner profiles than the simpler NFW one. The mass of the dark matter component is simply derived by integrating Eq. 3.50

$$M_{DM}(<r) = \frac{4\pi\rho_s r_s^3}{3-\gamma}\left(\frac{r}{r_s}\right)^{3-\gamma} {}_2F_1\left[3-\gamma, 3-\gamma, 4-\gamma, -\frac{r}{r_s}\right], \tag{3.51}$$

where ${}_2F_1$ stands for the hypergeometric function.

Rather than use $\{\rho_s, r_s\}$ as free parameters, the dark matter component has then been parametrized in terms of the concentration parameter c_Δ, and the mass M_Δ enclosed in the spherical radius r_Δ. For UDGs, $\Delta = 200$ means that M_{200} is the mass within r_{200} inside which the average density is 200 times the critical density ρ_c of the Universe, evaluated at the redshift of the given object. For NGC 1052-DF2, and NGC 1052-DF4 we have $z = 0.004963$, derived from the NED database[1]; for Dragonfly 44 we have used the same redshift of the Coma Cluster, $z = 0.023156$ [353].

After the introduction of the concentration parameter c_{200}, the gNFW scale density can be rewritten as

$$\rho_s = \frac{200}{3}\rho_c(z)\frac{(3-\gamma)(c_{200})^\gamma}{{}_2F_1\left[3-\gamma, 3-\gamma, 4-\gamma, -c_{200}\right]}. \tag{3.52}$$

[1] https://ned.ipac.caltech.edu/

Stellar component

The stellar components of the three UDGs under consideration have been modelled using a single Sérsic profile. As previously explained in section 3.1.3, it is possible to derive, through an approximation, the luminosity density from the surface brightness, Eq. 3.27, and to express it as

$$l(r) = l_1 l(r) = \frac{L_{\text{tot}}}{4\pi n \Gamma[(3-p)n] a_s^3} \left(\frac{r}{a_s}\right)^{-p_n} \exp\left[-\left(\frac{r}{a_s}\right)^{1/n}\right], \tag{3.53}$$

with

$$a_s = \frac{R_{eff}}{(b_n)^n}, \tag{3.54}$$

$$L_{tot} = 10^{-0.4\left[m-\mu(D)-M_{S,V_{606}}\right]}, \tag{3.55}$$

where: R_{eff}, is the half-to-light radius; n is the Sérsic index; m is the galaxy apparent magnitude; $\mu(D)$ is the distance modulus; and $M_{S,V_{606}}$ is the absolute magnitude of the Sun in the V_{606} photometric band.

The luminosity density is then converted to mass density by multiplying Eq. 3.53 for the mass-to-light ratio Υ_*

$$\rho_*(r) = \Upsilon_* l(r). \tag{3.56}$$

Then, the stellar mass profile can be determined by performing the integration of equation Eq. 3.56 leading to

$$M_*(<r) = 2\pi n \Upsilon_* I_0 \left(\frac{R_{eff}}{b_n^n}\right)^2 \frac{\Gamma(2n)}{\Gamma[(3-p_n)n]} \times \tag{3.57}$$

$$\left\{\Gamma[(3-p_n)n] - \gamma\left[(3-p_n)n, b_n\left(\frac{r}{R_{eff}}\right)^{1/n}\right]\right\}, \tag{3.58}$$

where $\Gamma(z)$ and $\gamma(z,x)$ are the total and the upper incomplete gamma functions, respectively. For the three UDGs, the quantities that will be used to model the stellar masses are:

- NGC 1052-DF2: from the photometric analysis presented in [175], $n = 0.6$, $R_{eff} = 22.6$", and $I_0 = 24.4$ mag arcsec^{-2} in the V_{606} band. At a distance $D = 20$ Mpc [175], the galaxy absolute magnitude is $M = -15.4$, and the total luminosity $L_{tot} = 1.12 \cdot 10^8$ L$_\odot$;

- NGC 1052-DF4: from [176], $n = 0.79$, $R_{eff} \sim 16.58$", and the axis ratio $b/a = 0.89$. At a distance $D = 20$ Mpc [175], the galaxy absolute magnitude is the galaxy absolute magnitude is $M_V = -15 - 0$, and $L_{tot} = 7.7 \cdot 10^7$ $L_\odot$;

- Dragonfly 44: from the analysis carried out in [343, 354], $n = 0.94$, $R_{eff} = 9.69$", the axis ratio $b/a = 0.68$, and central surface brightness $I_0 = 24.1$ mag arcsec^{-2}. The galaxy has been assumed to be at the same distance as the Coma cluster $D = 100$ Mpc, at which the absolute magnitude is $M_V = -16.2$, and the total luminosity is $L_{tot} = 2.33 \cdot 10^8$ $L_\odot$.

Anisotropy parameter

The Jeans equation, Eq. 3.40, is affected by a degeneracy between radial velocity dispersion and velocity anisotropy. It is thus necessary to make some assumptions on the possible functional form of $\beta(r)$, which is not an observable quantity, to break such degeneracy. The easiest possibility is to assume $\beta(r)$ constant; however, several other options can be found in the literature [351]. For instance, in [355], the authors introduced a velocity anisotropy profile to fit the kinematic data of the Canadian Network for Observational Cosmology clusters

$$\beta(r) = 2\beta_m \frac{r}{r^2 + r_a^2} r_a, \tag{3.59}$$

with $\beta_m = 0.65$, and $r_a = 2r_v$. This profile fitted well the anisotropy of subhaloes from N-body simulations in a flat low-density ΛCDM scenario [356]. Another anisotropy profile is represented by

$$\beta(r) = \frac{1}{2} \frac{r}{r + r_a}, \tag{3.60}$$

with $r_a = 0.18$. Another commonly used $\beta(r)$ is the so-called Osipkov-Merrit anisotropy [357, 358]

$$\beta(r) = \frac{r^2}{r^2 + r_a^2}. \tag{3.61}$$

However, as can be seen from Fig. 2 of [351], the Osipkov-Merrit anisotropy profile is not able to properly fit the data coming from simulations for $r \to r_{200}$. In addition, it converges too fast to zero at smaller radii.

Furthermore, in [359], a radial anisotropy profile has been introduced, proving to be particularly appropriate for the UDGs [360]

$$\beta(r) = \beta_0 + (\beta_\infty - \beta_0)\frac{r}{r + r_a}, \tag{3.62}$$

where: $\beta_0 \equiv \beta(r = 0)$ is the inner anisotropy, and $\beta_\infty \equiv \beta(r \to \infty)$ the outer one; r_a is the radius scale parameter. From equation Eq. 3.62, it can be seen that this anisotropy profile reduces to a constant anisotropy $\beta \equiv \beta_0$ if and only if the inner and the outer terms coincide;

All the above velocity anisotropy profiles generate a specific Kernel function $K(r/R)$, Eq. 3.46 (further details with all the calculations are provided in the appendix of [351]).

Stellar-to-halo-mass relation (SHMR)

DM represents an essential ingredient for galaxies which are supposed to form due to the cooling and then condensation of gas at the centre of potential wells of virialized dark matter halos [361]. Therefore, a connection between galaxies and hosting DM halos should exist and is named stellar-to-halo mass relation (SHMR). Indeed, properties of the galaxies, such as luminosity and stellar mass, are supposed to be related to the DM halo mass. Such a connection can be studied in several ways. A first way of linking the galaxy population and the DM component is possible through the direct observation of the galaxy kinematics [362], from gravitational lensing [363], or X-rays observations [364]. A second possibility is to build hydrodynamical simulations involving both the gas and the DM component or using semi-analytical models of galaxy formation [365–369].

Extensive galaxy surveys allowed the development of other methods connecting the hosting DM halo with the galaxy population using a statistical approach. Examples are represented by the so-called halo occupation distribution method [370, 371] and by the conditional luminosity formalism [370]. However, these two methods are usually used at low redshift. To avoid this limitation and, therefore, to study the link between DM and galaxies at high redshift, a correspondence between their distributions should be established.

The most common mathematical model of the SHMR is a double power-law [370, 372]. Nonetheless, if low stellar masses data ($M_* \leq 10^7$ $M_\odot$) are included,

a double power law results in a poor fit of the stellar mass function. Therefore, other possibilities have to be exploited. In [373] (following the parametrization given in [374]), the average stellar mass has been defined as

$$< \log \mathscr{M}_* >= \log_{10}(\varepsilon M_0) + g(x) - g(0), \tag{3.63}$$

where

$$g(x) = -\log_{10}(10^{\alpha x}+1) + \delta \frac{(\log_{10}(1+e^x))^\gamma}{1+e^{-10^{-x}}}, \tag{3.64}$$

with $x = \log_{10}(M_{vir}/M_0)$. All the parameters that appear in Eq. 3.63 are redshift-dependent [373]:

$$\begin{aligned}
&\log_{10}(\varepsilon(z)) = \varepsilon_0 + \mathscr{P}(\varepsilon_1, \varepsilon_2, z)\cdot Q(z) + \mathscr{P}(\varepsilon_2, 0, z),\\
&\log_{10}(M_0(z)) = M_{0,0} + \mathscr{P}(M_{0,1}, M_{0,2}, z)\cdot Q(z),\\
&\alpha(z) = \alpha_0 + \mathscr{P}(\alpha_1, \alpha_2, z)\cdot Q(z),\\
&\delta(z) = \delta_0 + \mathscr{P}(\delta_1, \delta_2, z)\cdot Q(z),\\
&\gamma(z) = \alpha_0 + \mathscr{P}(\gamma, 0, z)\cdot Q(z),
\end{aligned} \tag{3.65}$$

with

$$\begin{aligned}
&\mathscr{P}(x,y,z) = y\cdot z - \frac{x\cdot z}{1+z},\\
&Q(z) = e^{-4(1+z)^2}.
\end{aligned} \tag{3.66}$$

The exponential function $Q(z)$ allows separating the low-redshift parameters from the high-redshift ones. In addition, similarly to what was done in [374], the parameters appearing in Eq. 3.65 are tuned to fit three different redshift ranges: one for low-reshift values; one for parametrizing intermediate redshifts; a third one for scaling high-redshift values.

3.3 Statistical analysis: a primer

When it comes to statistical inference, i.e. how to extract valuable physical information from astrophysical or cosmological data, there are two main (and controversial) approaches: the frequentist and the Bayesian. In our work, we have followed the Bayesian approach for several reasons.

First, in the frequentist approach, the definition of probability is based on the repeatability of a reproducible experiment, from which the frequency of possible outcomes is extracted over a series of trials. In cosmology, this repeatability is clearly lost. Moreover, in any experiment, any measurement result cannot be taken as the "true" expected value, because it is plagued by statistical and systematic errors. While the former can disappear in the presence of a large number of observations, the latter are unavoidable and problematic to deal with within the frequentist approach [375, 376]. Bayesian inference, on the other hand, assumes that probability expresses a degree of belief in a proposition based on the available knowledge of the experimenter. It does not require an experiment to be reproducible and repeatable and allows any prior knowledge about it to be introduced in a mathematical form [377].

Bayesian inference has its core in the Bayes theorem [378] stated as

$$\mathscr{P}(\theta|d) = \frac{\mathscr{L}(d|\theta)\pi(\theta)}{\mathscr{E}(d)}, \tag{3.67}$$

where:

- $\mathscr{P}(\theta|d)$, is the posterior probability (for brevity, posterior) which represents our degree of belief about the parameters θ having a certain set of data d, and which is the function we aim to reconstruct;
- $\mathscr{L}(d|\theta)$ is the likelihood probability function (from now on it will be referred to as likelihood), which represents the probability of having the data d given a certain set of parameters θ;
- $\pi(\theta)$ is the prior probability function (or simply prior) which encloses the initial knowledge of the parameters θ before getting the data and the key ingredient of Bayesian inference;
- the denominator of Eq. 3.67 is called the Bayesian Evidence and it is defined as the average of the likelihood over the prior volume. It plays a fundamental role in model selection.

Now, while the frequentist and Bayesian approaches may seem similar from an operational point of view, they are conceptually very different. Indeed, while in

both the frequentist and Bayesian approaches the so-called best-fit parameters of the chosen model that best describe the data are found by maximising the likelihood, in the Bayesian approach this search is constrained by the choice of the prior and what one really focuses on is the posterior, which contains the fully relevant physical information. The two approaches are equivalent only if the priors are uniform (or flat). Indeed, with this choice, $\mathscr{P}(\theta|d) \propto \mathscr{L}(d|\theta)$.

If one assumes that the measurements are normally distributed around their real value (this is most of the time true, but not always), then the likelihood can be written as

$$\mathscr{L}(d|\theta) \propto \exp\left[-\frac{\chi^2(\theta)}{2}\right], \tag{3.68}$$

where $\chi^2(\theta)$ is the so-called *chi-squared function*. In the most general case, thus, maximizing $\mathscr{L}(d|\theta)$ corresponds to minimizing $\chi^2(\theta)$, defined as

$$\chi^2(\theta) = \Delta d \cdot \mathbf{C}^{-1} \cdot \Delta d^T, \tag{3.69}$$

with $\Delta d \equiv d^{obs} - d(\theta)$, where d^{obs} is the observed data vector and $\mathbf{C}^{-1}$ is the inverse of the covariant matrix, which contains the information about the experimental errors.

3.3.1 Markov Chains Monte Carlo

From an operational point of view, Bayesian inference can be summarised in four basic steps: *i)* define a set of parameters θ; *ii)* specify the priors for the parameters θ; *iii)* construct the likelihood (the form of which depends on how the data have been collected); *iv)* derive the posterior probability of the parameters by maximising the likelihood (or equivalently, by minimising the χ^2). For the last step, we use a numerical method known as Markov Chain Monte Carlo (MCMC) [377, 379, 380].

Several examples of MCMC methods for posterior computation can be found in the literature [381], but the main goal of any MCMC algorithm is to build a sequence (or chain) of points ("samples") in the given parameter space. Without going into too much detail, the crucial property of a properly constructed MCMC is that the density of the sampled point should be a reconstruction of the posterior distribution, $\mathscr{P}(\theta|d)$, in which we are interested. The "Markov nature" of the

chains is reached when the sequence of random variables (the Monte Carlo definition comes from this randomness) is such that the probability of the $(t+1)$–th element in the chain depends only on the value of the t–th element. When this happens, the chains should converge to a stationary state (i.e. one that does not change with t) in which successive elements of the chain are sampled from the target distribution, which in our case would correspond to the posterior $\mathscr{P}(\theta|d)$.

One of the most used algorithms for MCMCs is the Metropolis-Hastings [382, 383]. A crucial role in this algorithm is due to the proposal density function, $q(\theta'|\theta)$, which rules how subsequent trial points are randomly selected, basically being the conditional probability to have θ' given θ. The steps to follow in a Metropolis-Hastings MCMC are the following ones:

1. start with an initial random point θ;

2. generate a new point θ' sampled from the chosen proposal distribution $q(\theta'|\theta)$;

3. the transition kernel $T(\theta,\theta')$, namely the conditional probability to move from one state to another, must satisfy the condition $\mathscr{P}(\theta'|d)T(\theta',\theta) = \mathscr{P}(\theta|d)T(\theta,\theta')$ in order to guarantee that the MCMC will eventually recover the posterior distribution $\mathscr{P}(\theta|d)$;

4. the previous condition can be obtained if we compute the acceptance ratio α, which tells if θ' can be accepted or not, as

$$\alpha(\theta,\theta') = min\left(\frac{\mathscr{P}(\theta'|d)\, q(\theta',\theta)}{\mathscr{P}(\theta|d)\, q(\theta,\theta')},1\right) \tag{3.70}$$

   where $T(\theta,\theta') = \alpha(\theta,\theta')q(\theta,\theta')$;

5. the acceptance or the rejection is made by sampling a random point within a uniform distribution $u \in [0,1)$: θ' will be accepted if $u < \alpha$; otherwise, it will be rejected. If θ' has been accepted, the point will be stored and the next step of the chain will start from it. On the other hand, if rejected, the algorithm stores θ, which will be the start also of the next step.

Note that the general assumption for the proposal density is a simple symmetric density such as a Gaussian centred on the current point θ with a step size proportional to the corresponding covariance matrix. Thus, in this case, at each step, the Metropolis-Hastings method simply compares the posterior probability of the target density at the two points, θ and θ'.

Theoretically speaking, a MCMC based on the previous algorithm will describe exactly the posterior. But this will be surely achieved only asymptotically, in the limit of $n \to \infty$ steps. This is clearly unfeasible and impracticable, and in all realistic cases, we have to cut the MCMC at some stage. Thus, it is important to have statistical tools to check if the MCMC has reached the so-called *convergence*, namely if it has collected a sample of θ points from the parameters space large enough to guarantee an unbiased reconstruction of the posterior. The diagnostics to be used are many [384, 385]; but we have chosen to follow the method devised in [386] where, after conducting a spectral analysis on the sample created by a single chain, we can get information about the reached (or not) convergence.

3.3.2 Model selection

The main goal of our research was to test a hypothesis, the unification of dark matter and dark energy within a DHOST scenario. However, simply fitting this model to the data, even if it were better than the standard GR scenario, would not have been a satisfactory result. To establish the reliability of a new model on solid (statistical) grounds, we need to rely on strong statistical tools, which in Bayesian inference go beyond simply improving the χ^2 (or the reduced χ^2, which is the χ^2 divided by the degrees of freedom of the given problem). To understand how to proceed, we first rewrite the Bayes theorem to make explicit a dependency that is generally overlooked:

$$\mathscr{P}(\theta, \mathscr{M}|d) = \frac{\mathscr{L}(d|\theta, \mathscr{M})\pi(\theta, \mathscr{M})}{\mathscr{E}(d|\mathscr{M})} \tag{3.71}$$

where all the probability functions that appear in Eq. 3.71 are explicitly referred to a specific model $\mathscr{M}$ (in our case, the model could be GR or the DHOST). In Eq. 3.71, the key quantity for model selection, having at disposal the data set d, is

the Bayesian Evidence

$$\mathscr{E}(d|\mathscr{M}) = \int_{V_{\mathscr{M}}} d\theta \mathscr{L}(d|\theta,\mathscr{M})\pi(\theta,\mathscr{M}) \tag{3.72}$$

where $V_{\mathscr{M}}$ is the priors volume. From Eq. 3.71 it is clear that the Evidence is the normalization factor which sets the area of the posterior distribution (or, equivalently, the total probability) equal to one. On the one hand, the value of the Evidence is pointless when performing a fit. On the other, it becomes crucial when we want to compare the statistical validity of two different models (given the same data). Indeed, the comparison is performed by calculating the Bayes Factor, namely, the ratio of the posterior probabilities of the two models, which is equivalent to the ratio of their Evidences multiplied by the ratio of the prior on the (different) model parameters. From Eq. 3.72 we can deduce that even if models with a larger number of parameters may produce better fits to the data, on the other hand, we have the Evidence, which is proportional to the volume occupied by the posterior relative to that occupied by the prior, and will thus favour models which are simpler (i.e. with a lower number of parameters) but with greater predictive power, provided they give a good enough fit the data.

The difficulty in calculating $\mathscr{E}(d|\mathscr{M})$ lies in the fact that the definition Eq. 3.72 represents a multi-dimensional integral that is difficult to solve. However, this multi-dimensional integration can be simplified into a one-dimensional integration using the Nested Sampling algorithm introduced by [387]. The essence of this algorithm relies upon the transformation of the multi-dimensional integral in Eq. 3.72 into a one-dimensional integral by introducing X as the fraction of the prior volume so that the infinitesimal element $dX = \pi(\theta|\mathscr{M})d\theta$. Thus, the quantity

$$X(\lambda) = \int_{\mathscr{L}(\theta)>\lambda} d\theta\, \pi(\theta), \tag{3.73}$$

corresponds to the prior mass (volume) in parameter space containing all the points with likelihood greater than a certain value λ. As λ increases, the prior mass decreases from 1 to 0, so, by writing the inverse function as $\mathscr{L}(X)$, the Bayesian Evidence can be finally written as a one-dimensional integral,

$$\mathscr{E}(d|\mathscr{M}) = \int_0^1 dX \mathscr{L}(X), \tag{3.74}$$

in which the integrand is positive and decreasing.

At this point, we only need to evaluate the likelihood as $\mathscr{L}_j = \mathscr{L}(X_j)$, where the X_j are a sequence of decreasing values between 0 and 1, and the Evidence can be computed by applying a simple trapezoid rule

$$\mathscr{E} = \sum_j \mathscr{E}_j, \text{ with } \mathscr{E} = \frac{\mathscr{L}_j}{2}(X_{j-1} - X_{j+1}). \tag{3.75}$$

The full algorithm [388, 389] is made of the following steps:

- sample N points randomly from within the prior and compute the corresponding likelihoods. We initialize $\{\mathscr{L} = 0, X_0 = 1\}$;
- sort the sample points by likelihood and select the point with the lowest likelihood, attributing to it a prior volume, X_j. This volume will be set randomly to get uncertainty following the probability distribution $N t_i^{N-1}$, where i is the i-th step in the algorithm, $t \in (0,1)$, and corresponding to a volume decrease $X_j/X_{j-1} = t$;
- increment the evidence by $\mathscr{E}_j = L_j(X_{j-1} - X_{j+1})/2.$;
- discard the lowest likelihood point and replace it with a new point, uniformly distributed within the remaining prior volume $(0, X_j)$ and satisfying the condition $\mathscr{L} > \mathscr{L}_j$;
- repeat the steps until the evidence has been estimated to some desired accuracy.

This algorithm is of course stochastic thus, we run it ~ 100 times obtaining a distribution of values from which we extract the best value of the Evidence as the median of the distribution with the corresponding error.

Once the Bayesian Evidence has been computed, one can write the Bayes Factor $\mathscr{B}_{ij}$ defined as the ratio between the Evidence for the model $\mathscr{M}_i$ with the Evidence for the model $\mathscr{M}_j$

$$\mathscr{B}_{ij} = \frac{\mathscr{E}(d|\mathscr{M}_i)}{\mathscr{E}(d|\mathscr{M}_j)}, \tag{3.76}$$

where, in our works, the subscript i refers to the DHOST model while j to GR. This quantity is usually interpreted using an empirical scale known as the Jeffrey scale [390]

Bayes Factor	$\log \mathscr{B}_{ij}$	Strength of Evidence
$\mathscr{B}_{ij} < 1$	$\log \mathscr{B}_{ij} < 0$	Disfavoured
$1 \leq \mathscr{B}_{ij} < 3$	$0 \leq \log \mathscr{B}_{ij} < 1.1$	Weak
$3 \leq \mathscr{B}_{ij} < 20$	$1.1 \leq \log \mathscr{B}_{ij} < 3$	Definite
$20 \leq \mathscr{B}_{ij} < 150$	$3 \leq \log \mathscr{B}_{ij} < 5$	Strong
$\mathscr{B}_{ij} \geq 150$	$\log \mathscr{B}_{ij} \geq 5$	Very Strong

However, as underlined in [391], the Bayesian Evidence and the Bayes Factor are prior-dependent quantities. Consequently, changing priors to parametrize the initial knowledge about a particular set of parameters θ could alter the decision related to consistency (or tension) between two models.

A proper comparison between the two models should rely on prior-independent quantities. For that purpose, in [392–394], the author introduced a new quantity, the suspiciousness

$$\log S_{ij} = \log \mathscr{B}_{ij} + D_{KL,i} - D_{KL,j}\,, \tag{3.77}$$

where $D_{KL,i}/D_{KL,j}$ is the Kullback-Leibler (KL) divergence for model $\mathscr{M}_i/\mathscr{M}_j$ [395]

$$D_{KL,i} = \int d\theta\, \mathscr{P}(\theta, \mathscr{M}_i|d) \log \frac{\mathscr{L}(d|\theta, \mathscr{M}_i)}{\mathscr{E}(d|\mathscr{M}_i)}\,. \tag{3.78}$$

The KL divergence, which quantifies the information gain from the data through prior and posterior, is also a prior-dependent quantity. Using the definition of the Bayesian Evidence and that of the KL divergence, one can prove that the suspiciousness Eq. 3.77 is a prior-independent quantity. Indeed, $\log \mathscr{B}_{ij}$ and the difference $D_{KL,i} - D_{KL,j}$ transform similarly under changes of prior distributions, therefore the dependence from priors vanishes. We calculated the KL divergence with the same Nested algorithm described above.

Positive values of $\log S_{ij}$ should be interpreted as a sign of consistency between two models, while negative ones as an indication of tension (in [392–394] authors derive the same considerations applied to different data samples).

CHAPTER 4

Exploring DHOST Theories in Galaxy Clusters

In this chapter we will present the results we have obtained, starting from the scale of clusters of galaxies.

In the literature, it is possible to find papers that test modified gravity models that present a breaking of the screening mechanism. For example, in [396, 397] the authors tested the possibility of describing DM as a gravitational effect induced as a consequence of breaking the Vainshtein screening mechanism of a Galileon theory [275]. They have tested this hypothesis on the *CLASH* sample. In both cases, their results show that it may be possible for the specific Galileon model to describe DE on cosmological scales and DM on astrophysical scales. In [292] we tried to improve the previous studies. First, we considered a DHOST model, which is a more general description than the one tested in [396, 397]. Secondly, while in [396, 397] the cluster masses were modelled only as the sum of the DM and X-ray components, in [292] we have also included the contributions coming from the BCG and other galactic components.

Figure 4.1 shows the mass function for each component of two representative clusters from the *CLASH* sample, MACSJ1149 and MACSJ0744 (as a proxy for

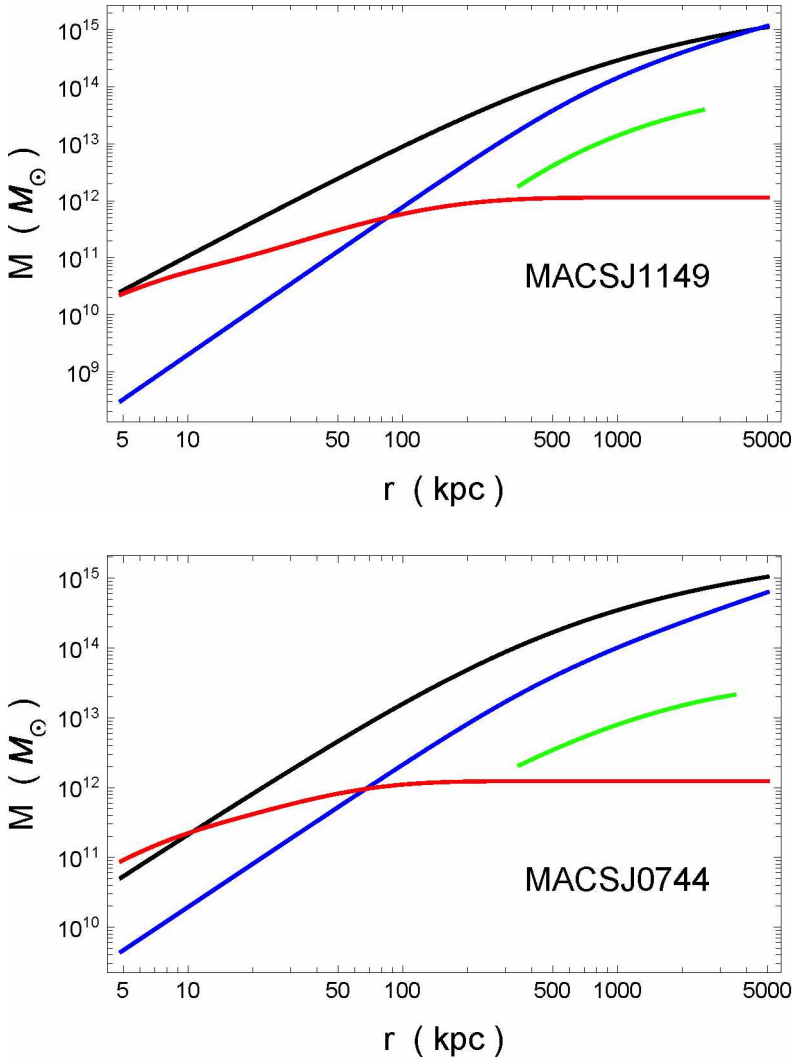

Figure 4.1: Galaxy cluster mass modelling, as in [292]. Solid lines represent the best-fit profiles of, respectively, NFW dark matter (black), X-ray gas (blue), BCG (red), and non-BCG galaxies (green).

all other clusters in the sample), as a function of distance from the cluster centre. The black and blue lines represent the DM (whose density is parameterised by Eq. 3.21) and the X-ray component (described by Eq. 3.26). These two components (especially DM) are the most abundant. However, at very small scales (close to the cluster centre) the BCG component (red lines) and the associated effects are comparable to those produced by the DM component. Moreover, close

to the cluster centre, the BCG is dominant with respect to the X-ray component. Its contribution at scales of $50-100$ kpc is subdominant compared to the DM, but still comparable to the X-ray. On the other hand, the contribution of the non-BCG galaxy component is more diffuse compared to the BCG, and largely subdominant compared to the other components ($\sim 1-2\%$ in the range $20-300$ kpc).

In order to constrain the parameters of the DHOST model, we have defined the χ^2 function associated with each probe (X-rays and lensing) of the *CLASH* subsample. For the X-ray data, the χ^2 is defined

$$\chi^2_{\rm gas} = \sum_{i=1}^{\mathcal{N}} \frac{\left[M^{\rm theo}_{\rm tot}(r_i,\theta) - M^{\rm obs}_{\rm tot}(r_i)\right]^2}{\sigma^2_{\rm obs}(r_i)}, \tag{4.1}$$

where: $\mathcal{N}$ is the number of data points for each cluster [280]; r_i is the distance from the galaxy cluster's centre; θ is the vector of free parameters; M^{theo}_{tot} is the theoretical total galaxy cluster mass and M^{obs}_{tot} is the observationally determined total cluster mass, respectively right and left-hand sides of Eq. 3.4; σ_{obs} is the error associated to the total mass.

For the gravitational lensing probe, the χ^2 function is

$$\chi^2_{\rm lens} = (\kappa^{\rm theo}(\theta) - \kappa^{\rm obs}) \cdot \mathbf{C}^{-1} \cdot (\kappa^{\rm theo}(\theta) - \kappa^{\rm obs}), \tag{4.2}$$

where: κ_{obs} is the observed convergence data vector; κ_{theo} is the theoretical convergence defined by equation Eq. 3.15; $\mathbf{C}$ is the total covariance matrix [294, 295].

When considering GR, the vector of free parameters is $\theta = \{c_{500,r_{500}}\}$, while when the DHOST model is analyzed, the free parameters will be $\theta = \{c_{500}, r_{500}, \alpha_H, \beta_1\}$. The total χ^2 function, consisting in χ^2_{lens} when the analysis is carried out with only lensing observations or $\chi^2_{tot} = \chi^2_{lens} + \chi^2_{hot-gas}$ for a joint analysis of the probes, has been minimized using the Metropolis-Hastings algorithm described in the previous chapter.

To assess the statistical validity of the DHOST model against GR, we have subsequently calculated the Bayesian Evidence (Eq. 3.71) for the DHOST, $\mathscr{E}(\mathscr{M}_i)$, and for GR, $\mathscr{E}(\mathscr{M}_j)$, using the Nested Sampling algorithm [387] cited in the previous pages. Finally, the statistical comparison between DHOST and GR has been achieved by determining the Bayes Ratio ($\mathscr{B}_{i,j} = \mathscr{E}(\mathscr{M}_j)/\mathscr{E}(\mathscr{M}_j)$) whose interpretation is provided by Jeffrey's empirical scale.

The final constraints on the NFW parameters $\theta = \{c_{500}, r_{500}\}$ which we got, are shown for the full *CLASH* sample in Table 4.1, where the clusters have been ordered by redshift z. In the left part of Table 4.1 we present the results achieved in the GR framework; the central part is dedicated to the constraints obtained for the NFW parameters and the EFT ones, α_H and β_1, when the DHOST model is mimicking only DE; and the right part has the constraints on the NFW parameters and EFT ones when the DHOST model also plays the role of an "effective" DM component. Table 4.2, instead, shows the χ^2 for the analysis (X-ray+gravitational lensing and lensing only) within the GR framework and the χ^2 and the model comparison between the DHOST models, respectively, as DE and DE + DM with respect to GR.

4.1 GR: comparison with previous works

The first step in our analysis was to compare our data with GR. This is important firstly because GR will be our reference model against which we can compare and estimate the statistical viability of the DHOST model. Secondly, it allows us to compare our modelling and statistical analysis algorithm with results from the literature for the same sample.

We compare our results with those obtained in [295], [398], and [399], recalling that in those works only lensing data were considered and thus a single NFW component fit was performed. Given that our parameter set $\{c_{500}, r_{500}\}$ is not always chosen as the fitting set, with alternatives such as $\{c_{200}, r_{200}\}$ or $\{c_{200}, M_{200}\}$ often being adopted, we have decided to convert both our parameter estimates and those of [398] and [399] into the characteristic NFW parameters $\{\rho_s, r_s\}$ for a more direct comparison. The results are shown in Fig. 4.2. We see that our estimates for ρ_s (i.e. c_{500}) are in excellent agreement within the 1σ uncertainty with the results of [398] and [399]. On the other hand, for r_s (which depends on both c_{500} and r_{500}) we see a larger deviation: our r_s estimates are generally smaller than those of [398] and [399]. Only three clusters (MACSJ0329, MACSJ1149 and MACSJ0744) are not in agreement at the 3σ confidence level with the results of [399], who performed a non-spherical triaxial NFW fit.

Table 4.1: Results from the statistical analysis. *CLASH* clusters are ordered by redshift. For each cluster, we provide 1σ constraints on each parameter in the top line, and their values in the minimum of the χ^2 in the bottom one. Units: cluster radii are in kpc. For the cases of DHOST with no NFW component, we apply a Gaussian prior on r_{500} derived from the corresponding GR cases. Lensing-selected *CLASH* clusters are indicated by stars.

	GR				DHOST+NFW				DHOST - no NFW		
	X-ray+lensing		lensing		X-ray+lensing				lensing		
name	c_{500}	r_{500}	c_{500}	r_{500}	c_{500}	r_{500}	α_H	β_1	r_{500}	α_H	β_1
A209	$1.77^{+0.33}_{-0.28}$	1262^{+75}_{-67}	$1.44^{+0.51}_{-0.39}$	1189^{+100}_{-105}	$0.73^{+0.83}_{-0.46}$	1186^{+122}_{-320}	$-0.20^{+0.17}_{-0.19}$	$-1.34^{+1.30}_{-2.39}$	1189^{+107}_{-103}	$7.99^{+1.43}_{-1.47}$	$-7.99^{+3.14}_{-4.00}$
	1.74	1269	1.33	1219	1.88	1272	−0.17	0.38	1189	8.63	−5.69
A2261	$4.49^{+0.27}_{-0.26}$	1162^{+23}_{-22}	$2.37^{+0.81}_{-0.62}$	1321^{+100}_{-101}	$2.73^{+1.05}_{-0.86}$	1244^{+31}_{-53}	$-0.06^{+0.17}_{-0.15}$	$-1.09^{+0.83}_{-1.16}$	1320^{+99}_{-101}	$6.49^{+1.60}_{-1.24}$	$-21.50^{+2.63}_{-2.92}$
	4.49	1162	2.22	1348	2.78	1263	−0.09	−1.01	1319	7.10	−18.43
RXJ2129	$3.56^{+0.13}_{-0.12}$	1132^{+17}_{-18}	$4.34^{+1.87}_{-1.36}$	864^{+88}_{-90}	$0.99^{+0.30}_{-0.23}$	1073^{+89}_{-105}	$-0.50^{+0.16}_{-0.16}$	$-3.02^{+1.12}_{-1.21}$	867^{+91}_{-91}	$3.02^{+1.18}_{-1.33}$	$-32.98^{+4.84}_{-5.00}$
	3.55	1132	4.03	889	1.31	1169	−0.48	−1.81	867	3.74	−25.52
A611	$2.35^{+0.16}_{-0.15}$	1275^{+36}_{-33}	$2.71^{+1.24}_{-0.89}$	1131^{+108}_{-119}	$1.17^{+1.01}_{-0.27}$	1280^{+31}_{-34}	$-0.17^{+0.16}_{-0.16}$	$-1.19^{+1.15}_{-0.63}$	1131^{+117}_{-119}	$8.37^{+2.31}_{-1.77}$	$-25.12^{+10.75}_{-8.67}$
	2.35	1276	2.41	1171	0.97	1272	−0.20	−1.60	1130	9.49	−18.56
MS2137	$4.34^{+0.20}_{-0.19}$	$1000.^{+28}_{-26}$	$2.50^{+2.57}_{-1.27}$	923^{+135}_{-133}	$7.85^{+0.49}_{-0.52}$	775^{+29}_{-25}	$0.42^{+0.16}_{-0.16}$	$-0.14^{+0.04}_{-0.03}$	924^{+133}_{-131}	$-0.55^{+1.51}_{-1.41}$	$-66.36^{+8.83}_{-6.78}$
	4.35	999	1.57	1013	7.73	783	0.11	−0.05	922	0.99	−55.93
RXJ2248	$2.17^{+0.16}_{-0.15}$	1547^{+47}_{-42}	$3.04^{+2.05}_{-1.26}$	956^{+119}_{-116}	$2.67^{+0.54}_{-0.51}$	1552^{+105}_{-96}	$-0.71^{+0.10}_{-0.10}$	$0.47^{+0.07}_{-0.08}$	959^{+116}_{-119}	$4.62^{+0.79}_{-0.87}$	$-6.26^{+2.86}_{-2.58}$
	2.17	1549	2.53	1005	2.98	1499	−0.72	0.45	956	4.60	−6.23
MACSJ1115	$2.76^{+0.17}_{-0.17}$	1189^{+41}_{-39}	$1.72^{+0.80}_{-0.54}$	1021^{+93}_{-98}	$1.07^{+0.57}_{-0.58}$	1220^{+83}_{-227}	$-0.49^{+0.15}_{-0.19}$	$-1.19^{+1.12}_{-2.42}$	1019^{+98}_{-99}	$2.70^{+1.77}_{-1.62}$	$-18.07^{+9.77}_{-4.26}$
	2.76	1188	1.52	1055	2.58	1243	−0.48	0.48	1019	4.30	−8.67
MACSJ1720	$3.60^{+0.27}_{-0.27}$	1059^{+37}_{-35}	$2.95^{+1.46}_{-0.98}$	953^{+92}_{-97}	$1.69^{+0.80}_{-0.47}$	1112^{+50}_{-65}	$-0.30^{+0.16}_{-0.16}$	$-1.32^{+1.11}_{-1.14}$	954^{+97}_{-97}	$8.59^{+1.32}_{-1.07}$	$-11.87^{+3.47}_{-2.89}$
	3.59	1060	2.62	984	1.71	1139	−0.32	−1.25	950	8.35	−11.74
MACSJ0416*	$1.99^{+0.41}_{-0.33}$	951^{+63}_{-66}	$1.75^{+0.67}_{-0.49}$	865^{+79}_{-84}	$0.43^{+0.61}_{-0.21}$	853^{+146}_{-176}	$-0.34^{+0.25}_{-0.28}$	$-2.30^{+1.54}_{-1.44}$	869^{+77}_{-81}	$7.44^{+0.97}_{-1.00}$	$-4.29^{+0.62}_{-0.63}$
	1.94	960	1.61	888	0.26	761	−0.49	−3.04	870	7.31	−4.20
MACSJ0429	$3.79^{+0.43}_{-0.40}$	960^{+60}_{-56}	$3.77^{+2.11}_{-1.42}$	827^{+101}_{-97}	$1.04^{+0.79}_{-0.41}$	1013^{+121}_{-166}	$-0.52^{+0.23}_{-0.29}$	$-2.42^{+1.71}_{-2.17}$	838^{+100}_{-100}	$0.88^{+3.06}_{-5.56}$	$-16.34^{+10.18}_{-19.30}$
	3.77	962	3.24	863	3.92	1012	−0.47	0.31	833	5.28	−1.44
MACSJ1206	$2.89^{+0.34}_{-0.30}$	1201^{+41}_{-40}	$3.07^{+1.99}_{-1.14}$	904^{+89}_{-94}	$0.86^{+0.35}_{-0.35}$	1269^{+71}_{-182}	$-0.65^{+0.13}_{-0.14}$	$-1.26^{+0.71}_{-1.47}$	904^{+96}_{-96}	$3.52^{+0.84}_{-0.86}$	$-14.99^{+3.88}_{-5.10}$
	2.87	1204	2.58	942	0.83	1269	−0.64	−1.36	904	3.93	−10.89
MACSJ0329	$3.10^{+0.23}_{-0.22}$	946^{+34}_{-33}	$5.62^{+2.16}_{-1.68}$	783^{+65}_{-66}	$1.27^{+2.07}_{-0.47}$	927^{+80}_{-99}	$-0.45^{+0.21}_{-0.18}$	$-1.32^{+1.53}_{-2.01}$	785^{+65}_{-64}	$-27.31^{+1.33}_{-1.75}$	$-86.34^{+3.04}_{-5.44}$
	3.10	946	5.18	798	4.11	900	−0.27	0.15	784	−29.47	−93.20
RXJ1347	$4.04^{+0.12}_{-0.11}$	1508^{+23}_{-22}	$1.65^{+0.79}_{-0.56}$	1167^{+98}_{-107}	$1.83^{+0.21}_{-0.29}$	1681^{+29}_{-38}	$-0.72^{+0.09}_{-0.09}$	$-0.43^{+0.48}_{-0.67}$	1162^{+108}_{-107}	$5.53^{+0.92}_{-0.95}$	$-3.57^{+1.54}_{-1.94}$
	4.04	1509	1.45	1202	1.99	1696	−0.72	−0.21	1169	6.14	−1.74
MACSJ1149*	$2.02^{+0.72}_{-0.52}$	861^{+61}_{-64}	$1.59^{+1.17}_{-0.63}$	713^{+83}_{-98}	$2.26^{+6.56}_{-1.18}$	410^{+126}_{-82}	$1.18^{+0.43}_{-0.48}$	$-0.61^{+0.25}_{-0.24}$	$710.^{+99}_{-96}$	$1.76^{+0.53}_{-0.53}$	$-6.67^{+1.07}_{-1.24}$
	1.87	879	1.20	753	1.45	716	0.065	−0.033	711	1.94	−5.40
MACSJ0647*	$4.53^{+1.44}_{-1.09}$	876^{+67}_{-65}	$2.53^{+1.92}_{-1.03}$	791^{+83}_{-90}	$1.05^{+0.91}_{-0.48}$	1237^{+127}_{-111}	$-0.87^{+0.19}_{-0.21}$	$-1.36^{+0.82}_{-0.65}$	790^{+91}_{-90}	$6.36^{+1.13}_{-1.21}$	$-4.37^{+1.62}_{-2.27}$
	4.26	894	2.04	830	0.75	1319	−0.98	−1.42	793	6.55	−4.59
MACSJ0744	$2.84^{+0.50}_{-0.44}$	888^{+37}_{-36}	$2.61^{+1.70}_{-1.00}$	748^{+72}_{-74}	$1.03^{+1.12}_{-0.59}$	894^{+65}_{-190}	$-0.42^{+0.19}_{-0.18}$	$-1.50^{+1.43}_{-2.35}$	748^{+74}_{-74}	$5.02^{+0.89}_{-0.88}$	$-4.34^{+2.00}_{-4.95}$
	2.82	891	2.09	777	2.95	919	−0.47	0.32	747	4.55	−10.42

Table 4.2: *First column*: galaxy cluster name ordered by z. *Second column*: minimum χ^2 values, within GR, for the mass reconstruction performed, respectively, with a joint analysis of X-rays and lensing observations, and lensing only. *Third column*: minimum χ^2 values, Bayesian ratio $\mathscr{B}_{GR}^{DHOST}$ and $\ln \mathscr{B}_{GR}^{DHOST}$ for DHOST (joint analysis) replacing DE. *Fourth column*: minimum χ^2 values, Bayesian ratio $\mathscr{B}_{GR}^{DHOST}$ and $\ln \mathscr{B}_{GR}^{DHOST}$ for DHOST (lensing only) replacing DE and DM.

	GR		DHOST+NFW			DHOST - no NFW		
	X-ray+lensing	lensing	X-ray+lensing			lensing		
name	χ^2	χ^2	χ^2	$\mathscr{B}_{GR}^{DHOST}$	$\ln \mathscr{B}_{GR}^{DHOST}$	χ^2	$\mathscr{B}_{GR}^{DHOST}$	$\ln \mathscr{B}_{GR}^{DHOST}$
A209	10.69	8.64	8.50	$1.56^{+0.05}_{-0.04}$	$0.44^{+0.03}_{-0.03}$	11.02	$0.222^{+0.007}_{-0.005}$	$-1.51^{+0.03}_{-0.02}$
A2261	11.33	5.43	9.64	$1.08^{+0.03}_{-0.03}$	$0.08^{+0.03}_{-0.02}$	10.00	$0.072^{+0.002}_{-0.002}$	$-2.63^{+0.02}_{-0.02}$
RXJ2129	20.90	7.28	7.94	254^{+8}_{-8}	$5.54^{+0.03}_{-0.03}$	8.29	$0.43^{+0.01}_{-0.01}$	$-0.86^{+0.02}_{-0.02}$
A611	5.84	3.41	4.18	$1.07^{+0.03}_{-0.02}$	$0.06^{+0.03}_{-0.02}$	4.04	$0.53^{+0.01}_{-0.01}$	$-0.63^{+0.02}_{-0.02}$
MS2137	34.38	7.74	13.51	$\left(1.77^{+0.06}_{-0.05}\right)\cdot 10^4$	$9.78^{+0.03}_{-0.03}$	5.18	$2.87^{+0.08}_{-0.06}$	$1.05^{+0.03}_{-0.02}$
RXJ2248	58.93	4.54	6.99	$\left(7.62^{+0.20}_{-0.17}\right)\cdot 10^{10}$	$25.06^{+0.03}_{-0.02}$	5.91	$0.363^{+0.008}_{-0.010}$	$-1.01^{+0.02}_{-0.03}$
MACSJ1115	19.67	7.12	7.21	235^{+5}_{-7}	$5.46^{+0.02}_{-0.03}$	15.50	$\left(1.15^{+0.02}_{-0.03}\right)\cdot 10^{-2}$	$-4.47^{+0.02}_{-0.03}$
MACSJ1720	10.44	5.00	5.93	$6.20^{+0.19}_{-0.17}$	$1.82^{+0.03}_{-0.03}$	4.99	$0.74^{+0.02}_{-0.02}$	$-0.30^{+0.02}_{-0.03}$
MACSJ0416*	14.86	8.47	9.38	$32.6^{+1.0}_{-1.0}$	$3.48^{+0.03}_{-0.03}$	12.04	$0.127^{+0.004}_{-0.003}$	$-2.06^{+0.03}_{-0.02}$
MACSJ0429	11.76	5.98	6.50	$8.90^{+0.27}_{-0.27}$	$2.19^{+0.03}_{-0.03}$	16.10	$\left(1.03^{+0.03}_{-0.03}\right)\cdot 10^{-2}$	$-4.58^{+0.02}_{-0.03}$
MACSJ1206	31.93	8.07	7.95	$\left(67.4^{+2.4}_{-1.5}\right)\cdot 10^3$	$11.12^{+0.03}_{-0.02}$	7.14	$1.21^{+0.04}_{-0.02}$	$0.19^{+0.03}_{-0.02}$
MACSJ0329	20.76	10.53	11.17	$72.8^{+2.6}_{-2.0}$	$4.29^{+0.04}_{-0.03}$	35.82	$\left(2.18^{+0.06}_{-0.06}\right)\cdot 10^{-6}$	$-13.04^{+0.02}_{-0.03}$
RXJ1347	70.82	3.67	6.40	$\left(1.27^{+0.03}_{-0.02}\right)\cdot 10^{14}$	$32.48^{+0.03}_{-0.02}$	5.31	$0.50^{+0.01}_{-0.01}$	$-0.69^{+0.03}_{-0.03}$
MACSJ1149*	31.20	8.06	8.81	$\left(16.98^{+0.61}_{-0.34}\right)\cdot 10^3$	$9.74^{+0.04}_{-0.02}$	8.93	$0.52^{+0.01}_{-0.01}$	$-0.66^{+0.03}_{-0.03}$
MACSJ0647*	24.92	6.16	5.81	$\left(3.61^{+0.12}_{-0.09}\right)\cdot 10^3$	$8.19^{+0.03}_{-0.03}$	11.78	$\left(4.56^{+0.09}_{-0.10}\right)\cdot 10^{-2}$	$-3.09^{+0.02}_{-0.02}$
MACSJ0744	17.13	9.93	10.01	190^{+4}_{-4}	$5.25^{+0.02}_{-0.02}$	10.90	$0.46^{+0.01}_{-0.01}$	$-0.77^{+0.03}_{-0.03}$

It should be stressed that it has been verified that this difference is not due to statistical bias in the MCMC algorithm: the results are statistically consistent, the chains converge, and the posteriors of the parameters do not show any pathological behaviour. In addition, Figs. 4.5 and 4.6 clearly show visually that there is no problem (within GR) to fit lensing data over the whole range of scales from 10 kpc to ~ 5 Mpc.

Although the NFW component is the dominant contribution, we cannot neglect other mass components, as shown in Fig. 4.1. For example, in the innermost part of the cluster (approximately, $r \lesssim 10-20$ kpc), the BCG component can be comparable and even dominant with respect to DM [400, 401]. The only compo-

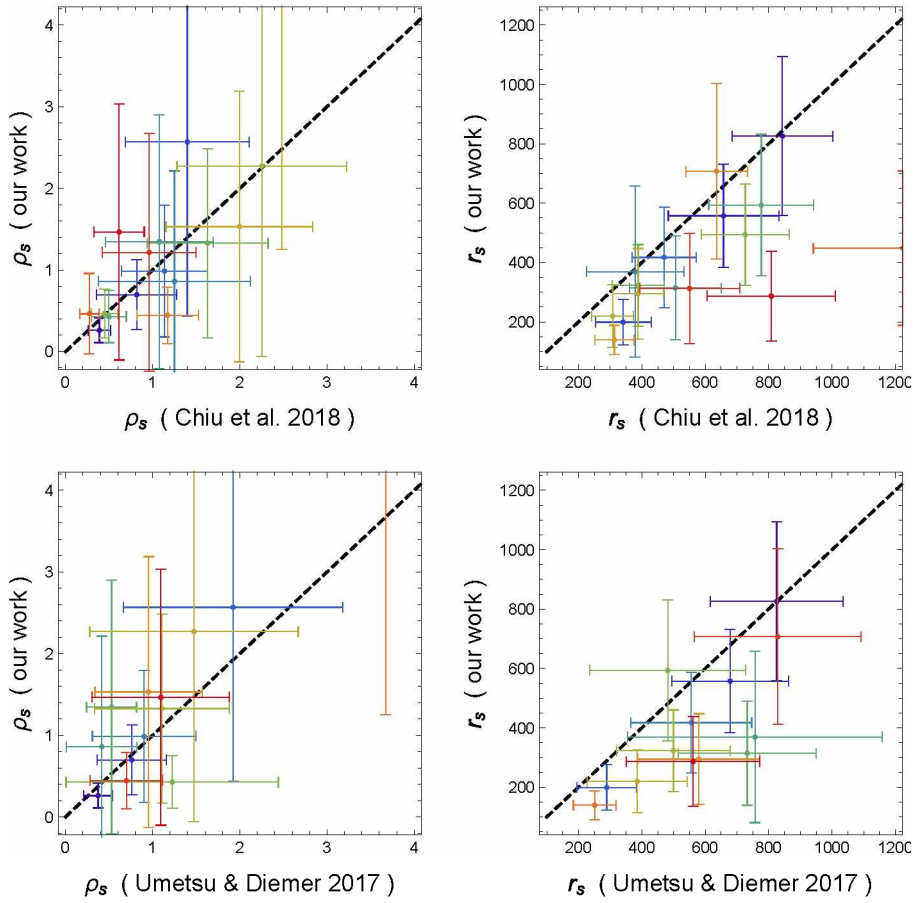

Figure 4.2: Comparison of NFW parameters from our analysis with those derived in [398] and [399].

nent that is directly related to r_{500}, apart from the DM component, is the non-BCG galaxy contribution. Here the r_{500} radius essentially plays the role of a scaling parameter that can increase or decrease the relative galaxy contribution. Non-BCG galaxies have a large influence in the radial range $50 - 200$ kpc, although they are subdominant with respect to both DM and hot gas.

Finally, and importantly, the physics of the gas within the cluster could introduce a bias in the final estimate: as the density is derived from X-ray observations, the gas mass modelling can be affected by the non-local processes described in the previous chapter. In this way, those clusters where there is a mismatch between X-ray and lensing masses could lead to slightly different estimates for r_{500}. This

seems to be the case, for example, for MACSJ1149 and MACSJ0744: as shown in Figs. 4.5 and 4.6, from a comparison of GR with combined data (dashed blue lines) and GR with lensing only (solid blue lines), we see how the above clusters show a difference in the convergence profile in the inner regions ($r < 100$ kpc). Note that MACSJ1149 is a highly disturbed CLASH cluster selected by lensing [402, 403], while MACSJ0744 is the highest redshift cluster in our sample. Both clusters have been reported to show signs of merger activity [402–404].

Continuing the comparison, within GR, between a joint analysis of X-ray and lensing and lensing-only probes, we see from the top two panels in Fig. 4.3 that there is no statistically meaningful difference for the c_{500} parameter, while there is a more pronounced bias in the r_{500} estimates, although almost all clusters agree at the $< 3\sigma$ level. However, this trend is to be expected and is a signature of the above-mentioned disagreement between lensing and X-ray-based mass deductions.

4.2 DHOST: galaxy cluster's mass reconstruction

The main objective of [292] was to test, with the most complete observational data, the reliability of the DHOST model, as expressed in Eqs. (2.26). Two different scenarios were considered:

1. DHOST model as an alternative to DE. In this case, the total galaxy cluster mass has been parametrized as $M_{tot}(r) = M_{BCG}(r) + M_{non-BCG}(r) + M_{gas}(r) + M_{DM}(r)$.

2. DHOST model as a unified description of both DE and DM as a consequence of the partial breaking of the Vainshtein screening mechanism. According to this theoretical scheme, DM is a gravitational effect induced at astrophysical scales by the DHOST model. Therefore, the total galaxy cluster mass now has been parametrized without assuming a DM component $M_{tot}(r) = M_{BCG}(r) + M_{non-BCG(r)} + M_{gas}(r)$.

Regarding the first scenario, we should first point out that an analysis using only lensing data (i.e. $\chi^2 = \chi^2_{\rm lens}$) was not possible: possibly the observational errors

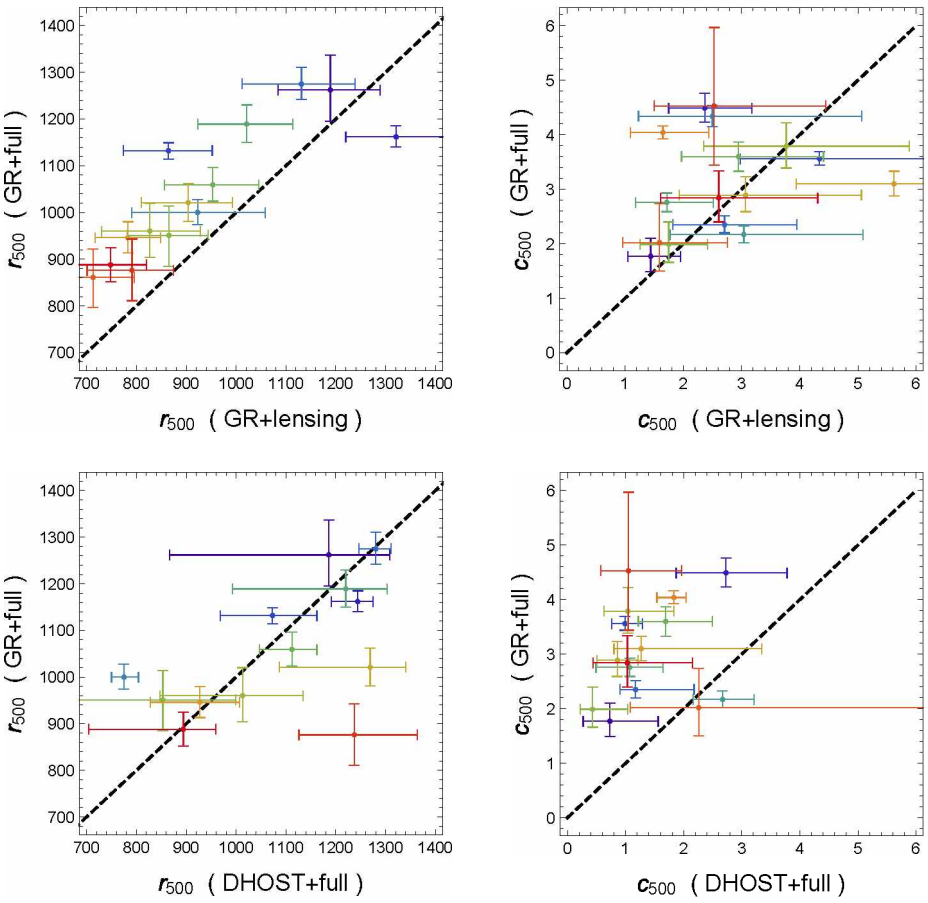

Figure 4.3: Comparison of NFW parameters from GR analysis with those derived when DHOST mimicking dark energy is considered.

are still too large to optimally constrain the model. On the other hand, using full data sets including X-ray information ($\chi^2 = \chi^2_{\rm lens} + \chi^2_{\rm gas}$), we obtain more significant results. It should be noted that X-ray data have a much higher statistical precision than lensing data. On the other hand, the X-ray approach relies on the assumption of strict hydrostatic equilibrium, which may explain the apparent discrepancy between the two data sets. Indeed, in the context of ΛCDM, a mean hydrostatic mass bias of $b \equiv 1 - M_{\rm X}/M_{\rm lens} = (12 \pm 7)\%$ [280] was found for the CLASH sample at $r = 500$ kpc with respect to the weak-lensing mass estimates of [405]. This is consistent with the typical level of hydrostatic mass bias (5%–20%) expected for cluster-scale haloes in ΛCDM cosmologies [406, 407].

The results for the first scenario, using the full available datasets, are listed in the second group of columns in Table 4.1. We report both median values (top rows) and those corresponding to the minimum in the χ^2 function (bottom rows). From a Bayesian perspective, and given the stochastic nature of MCMC sampling, the minimum χ^2 values do not have much statistical significance, but we have chosen to show them as an indication of possible asymmetry in the posterior distribution and possible asymmetry between the median and minimum estimates.

From the lower panels of Fig. 4.3 we see for the NFW parameters how we obtain $> 3\sigma$ deviations for r_{500} in only three cases, while we systematically obtain lower c_{500} values compared to the GR case (in 14 out of 16 clusters). This result suggests that the NFW dark matter halos in the DHOST scenario are less concentrated and less massive in the inner regions of the clusters than in the GR case, due to the partially broken screening mechanism effects.

There is a crucial point to be made here. As can be seen from Figs. (4.5), (4.6), (4.7), and (4.8), the DHOST model, together with an NFW dark matter component, fits the data quite well and can "solve" the tension between X-ray and lensing that naturally arises in a GR context. This can be seen quite clearly for the cases of RXJ2248, MACSJ1115, MACSJ1720, and MACSJ0429, where the DHOST+NFW model (red line) fits the GR+NFW with lensing only (solid blue line) much better than the GR+NFW with full data (dashed blue line) at smaller scales ($r < 100$ kpc), while the situation is reversed at larger scales ($r > 1$ Mpc). Somehow the additional terms resulting from the broken screening mechanism can find an adjustment between the different contributions, leading to a reasonably better fit to the data. This point is then further confirmed by Table 4.2, which shows the Bayes Factors of the DHOST model with respect to GR. We can see that in the case of the DHOST+NFW model, the logarithm of the Bayes factor is always positive, ranging from inconclusive evidence in favour of DHOST (for values ~ 1) to a much more conclusive positive assessment (for values > 5).

However, it should be emphasised that we cannot simply rely on the statistical significance of models to reliably assess the validity of gravity theories, because cluster-based tests involve an inherent equilibrium assumption [408, 409]. For example, [410] analysed 2 CLASH clusters, MACSJ1206 and RXJ2248, in the context of $f(R)$ theories [123] using combined galaxy kinematics and gravitational

lensing data. They found that while the results for MACSJ1206 are consistent with GR predictions, for RXJ2248 there is a tension with the standard GR scenario. Indeed, a detailed dynamical study of RXJ2248 found that the cluster is far from a relaxed system, with observational evidence for non-Gaussian velocity dispersion along the line of sight and a recent off-axis merger event associated with the elongated shape of the X-ray emission [411]. These observational features suggest that the assumption of hydrostatic equilibrium for RXJ2248 is likely to be invalid.

Finally, we consider the scenario where the DHOST model, together with its broken screening effects, is assumed to behave as DM and DE at galaxy cluster scales. In this case, no NFW component is considered. Note that this model still includes the r_{500} parameter, which describes the non-BCG galactic component through the cold baryon fraction (Sec. 3.1.3). Since we do not have a full NFW profile to constrain in this case, we opt to apply a Gaussian prior to r_{500} derived from the same corresponding GR scenario (i.e. with lensing-only data). This is a completely different approach to the literature, so any comparison with the constraints shown above should be taken with caution.

Firstly, it must be emphasised that a good fit is not possible using full data sets ($\chi^2 = \chi^2_{\rm lens} + \chi^2_{\rm gas}$): our Markov chains could not achieve convergence and the resulting posteriors of the parameters are highly irregular, making any parameter inference difficult. In contrast, modelling with lensing-only data ($\chi^2 = \chi^2_{\rm lens}$) gives a reasonable fit, probably due to the much larger degrees of freedom given by the larger lensing errors compared to the X-ray data.

Excluded from Fig. 4.3 are the two cases of MS2137 and MACSJ0329, which have some problematic profile fitting issues, as can be seen by inspecting the green lines and the curved profiles that appear at $r < 500$ kpc (Figs. (4.6) and (4.7)). Other clusters also show some problematic behaviour, such as MACSJ0647 (Fig. 4.8), for which we are unable to fit the data at $r > 1$ Mpc.

In general, it has been found that such an approach is unable to describe the observed lensing profiles at large cluster-centre distances. Indeed, the Bayesian Evidence ratios suggest that this model is significantly disfavoured with respect to the GR.

4.3 EFT paramaters constraints

The DHOST model we are considering can be fully characterised by the EFT parameters $\{\alpha_H, \beta_1\}$. In the left panel of Fig. 4.4, we compare our results with those derived from astrophysical constraints [249, 278]. The blue regions show the constraints derived from stellar physics considerations, such as hydrostatic equilibrium conditions or the minimum mass of the observed red dwarf stars; the red line is derived from the 2σ limits on γ_0 from the Hulse-Taylor pulsar; the combination of these two constraints produces the region bounded by the blue (vertical and horizontal) dashed lines. When helioseismology is taken into account, we obtain the 2σ confidence green regions, which in combination with the prior on γ_0 gives the region bounded by the green (vertical and horizontal) dashed lines. Much looser constraints can be derived from cosmological data [194, 412, 413] not shown in the figure.

We can then see that the parameter α_H is quite well constrained and consistent with the previous limits, while β_1 is only marginally within the 1σ confidence limit for most clusters. More interestingly, our estimates for both parameters are only marginally consistent with zero (GR limit) in most cases, at least at the 2σ level.

When the DHOST model, as a consequence of the partial breaking of the Vainshtein screening, also plays the role of DM, both EFT parameters are consistent with zero at the 3σ level, and they marginally agree with stellar constraints, excluding the Hulse-Taylor pulsar priors.

4.4 Lesson about DHOST from clusters of galaxies

This chapter mainly highlights the results of[292], whose main goal was to test a specific DHOST model that exhibits a partial breaking of the Vainshtein screening mechanism. The driving idea was the intriguing possibility that the gravitational effects induced by this modification of GR, due to the partial breaking of the screening mechanism, could leak out at the scale of galaxy clusters, also playing the role of DM. According to this scheme, the DHOST model could have been seen as a way to unify DE and DM into a single theoretical background.

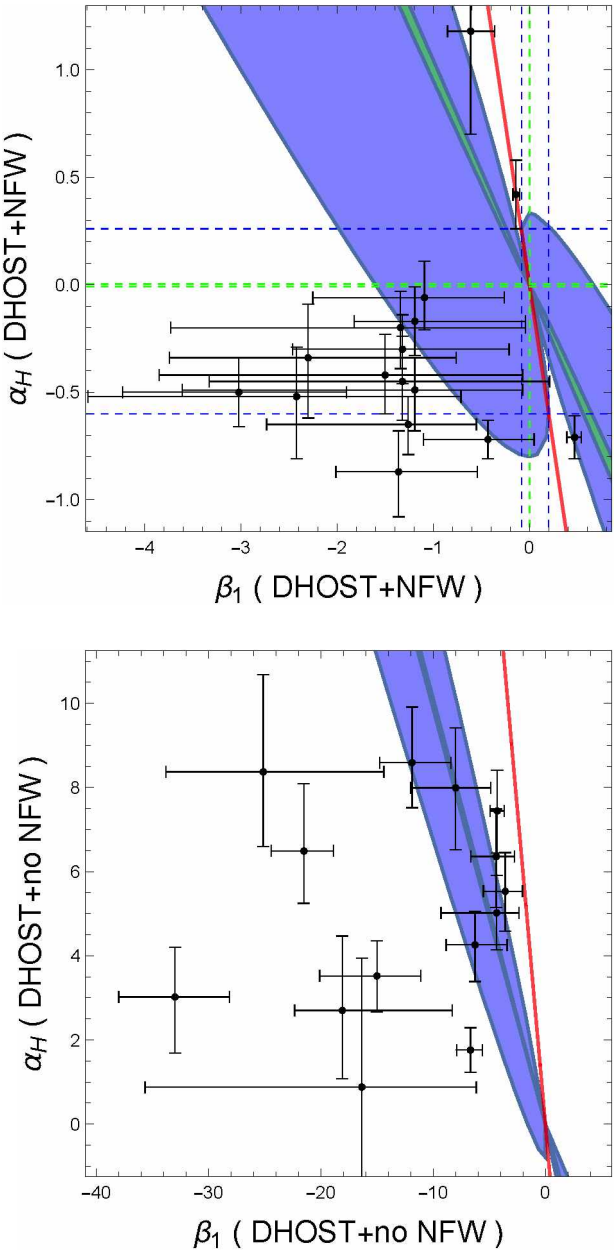

Figure 4.4: Comparison of ETF parameters constraints from our DHOST analysis with results from [249, 278]. *Top plot*: results assuming DHOST mimicking the DE component; *bottom plot*: results assuming DHOST mimicking DE and DM. Blue regions represent constraints from stellar physics considerations [249]; the red line represents the 2σ constraints on γ_0 from the Hulse-Taylor pulsar; blue (vertical and horizontal) dashed lines are the combination of these two constraints; the 2σ constraints from helioseismology arguments are shown as green regions; their combination with the 2σ constraints on γ_0 produce the green (vertical, horizontal) dashed lines.

The specific theory we have chosen to test in [292] is characterised by the second-order equations of motion introduced in [248], and is thus free of Ostrogradski instabilities. As shown in Eqs. 2.26, this model is described by modified versions of the gravitational and metric potentials, introducing four parameters $\{\Xi_1, \Xi_2, \Xi_3, \gamma_0\}$. These four parameters can be written in terms of more fundamental quantities using an EFT description. By adding the fundamental constraints derived from the multi-messenger observation of GW [180, 205, 207, 246, 253, 254] their final definition is given by Eqs. 2.35 and 2.36.

The DHOST model presented above has been tested on a sample of 16 high-mass clusters targeted by the *CLASH* programme [402] using a combination of two complementary probes: X-ray [280] and strong and weak gravitational lensing [295] observations. In addition, a multi-component approach has been used, modelling as many mass components as possible using observational results from the literature. We were able to account for the hot gas, BCG and non-BCG diffuse stellar contributions.

When the DHOST model is assumed to act only as a DE, the results show slight Bayesian Evidence in favour of this model over GR for the majority of the clusters in our sample. More importantly, in this scenario, we no longer have any tension between the X-ray hydrostatic and lensing mass measurements. Equivalently, we could say that the DHOST model, apart from providing a better fit to the data than GR, is somehow able to reconcile such a discrepancy in a new theoretical approach. However, it should also be noted that the apparent discrepancy found in a GR context is likely to arise from the working hypothesis of hydrostatic equilibrium, which is not strictly satisfied in cluster haloes in the ΛCDM framework [280, 406, 407]. Indeed, about half of the sample clusters selected in this study are expected to be unrelaxed according to the cosmological numerical simulations of [403].

When the DHOST model is assumed to play the role of both DM and DE through the partial breaking of the Vainshtein screening mechanism at cluster scales, the results show that this model is disfavoured compared to GR. Indeed, the Bayes factors are negative and can be interpreted as evidence against such a DHOST model compared to GR.

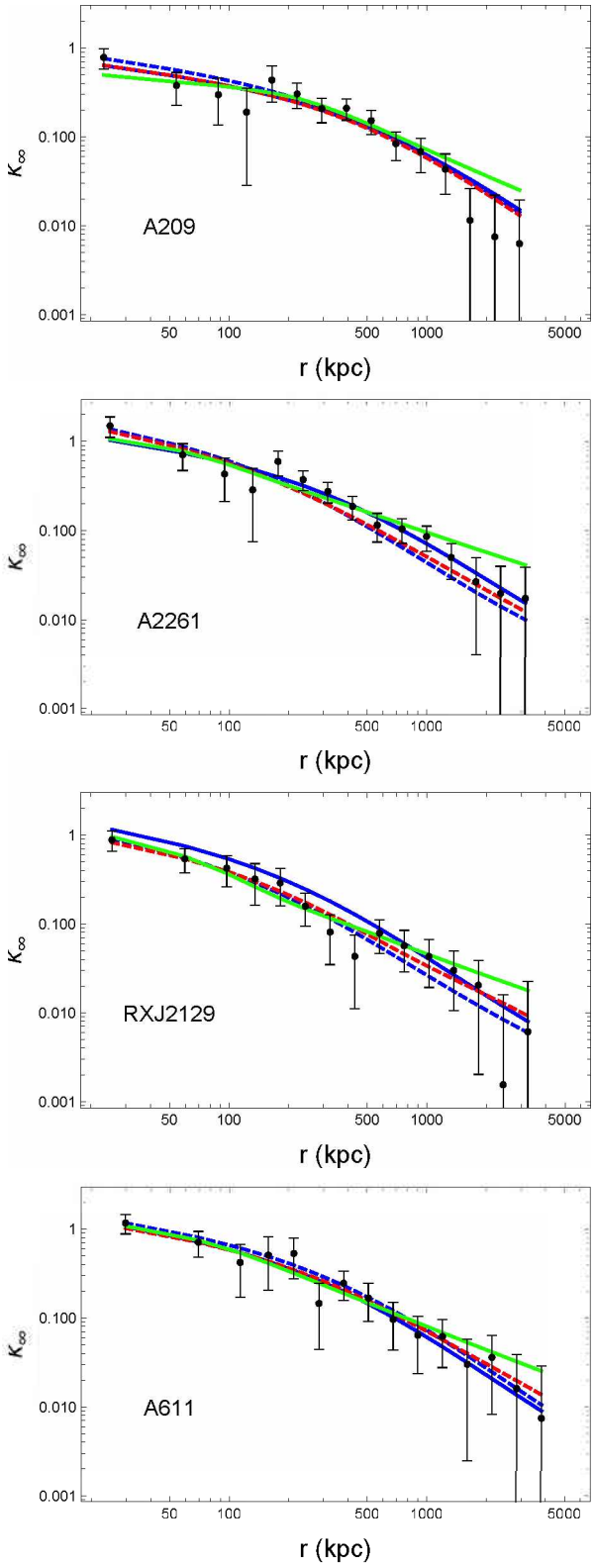

Figure 4.5: Convergence profiles reconstructed from gravitational lensing. Colour code: black points - observational data from [295]; blue dashed - GR (all), blue solid - GR (lensing); dashed red - DHOST + NFW (all); green - DHOST (no NFW, lensing).

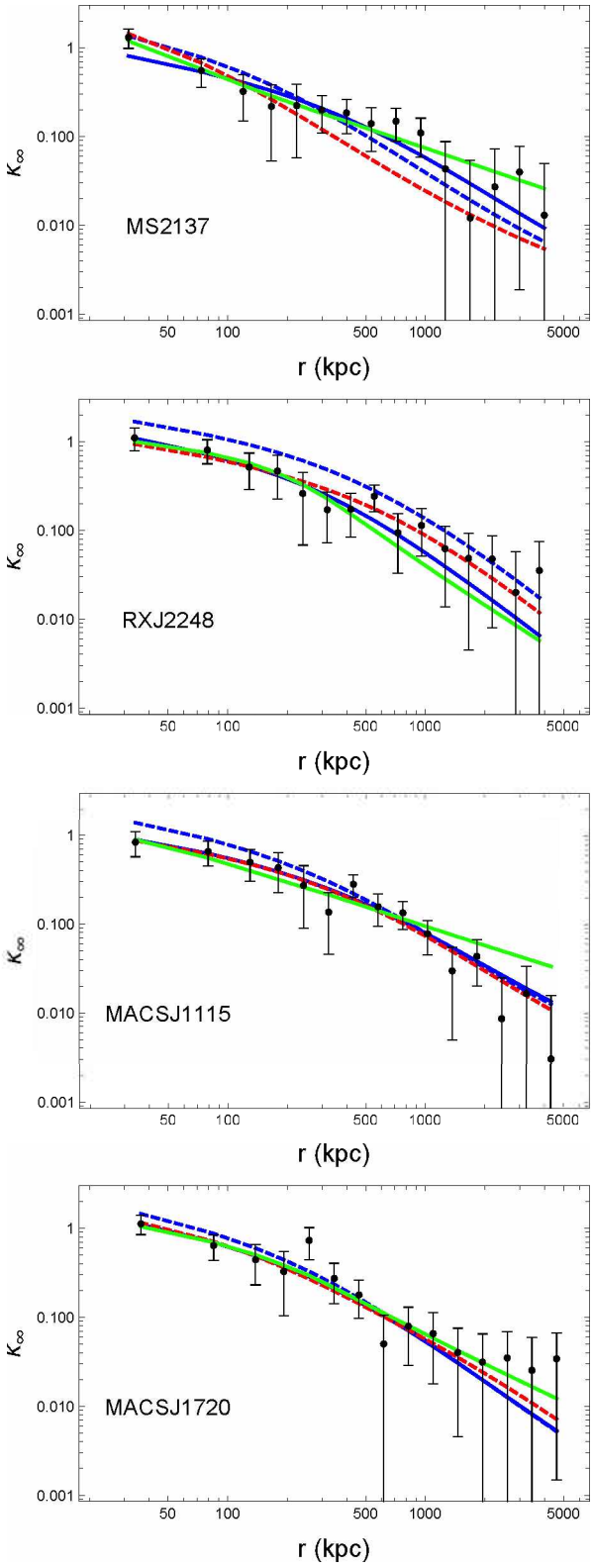

Figure 4.6: Same as Fig. 4.5.

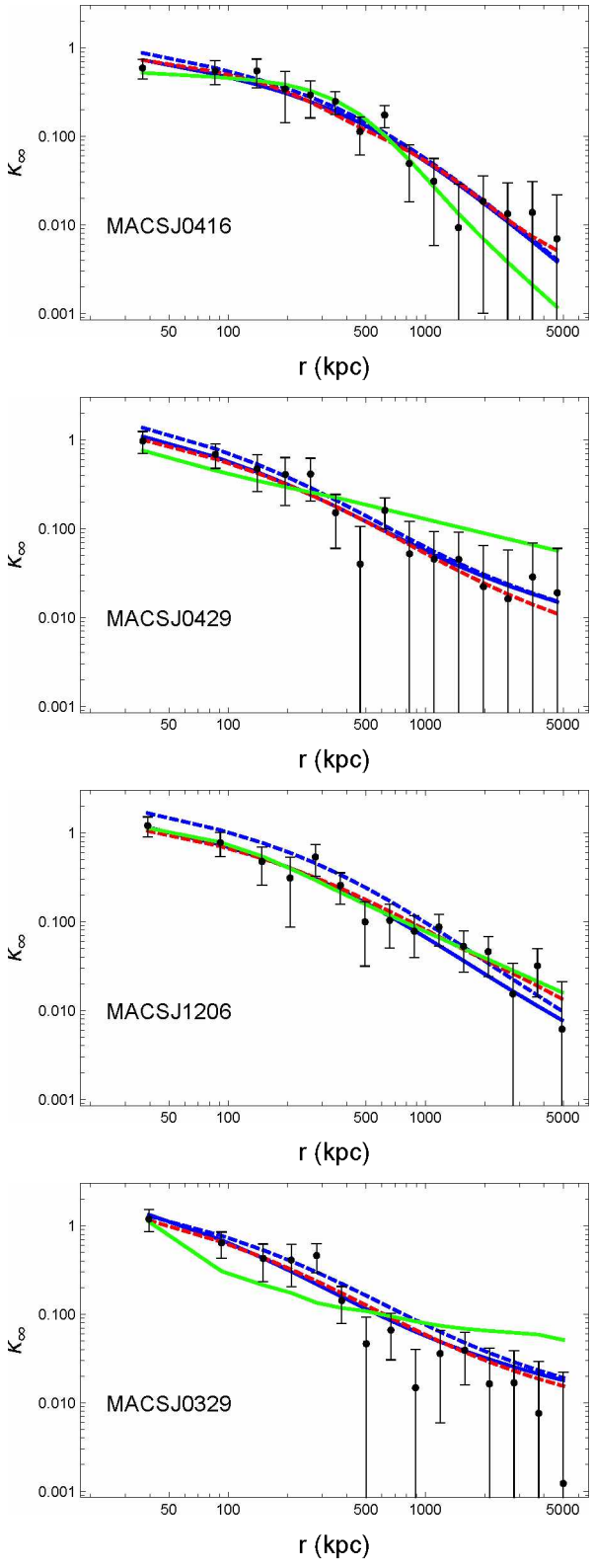

Figure 4.7: Same as Fig. 4.5.

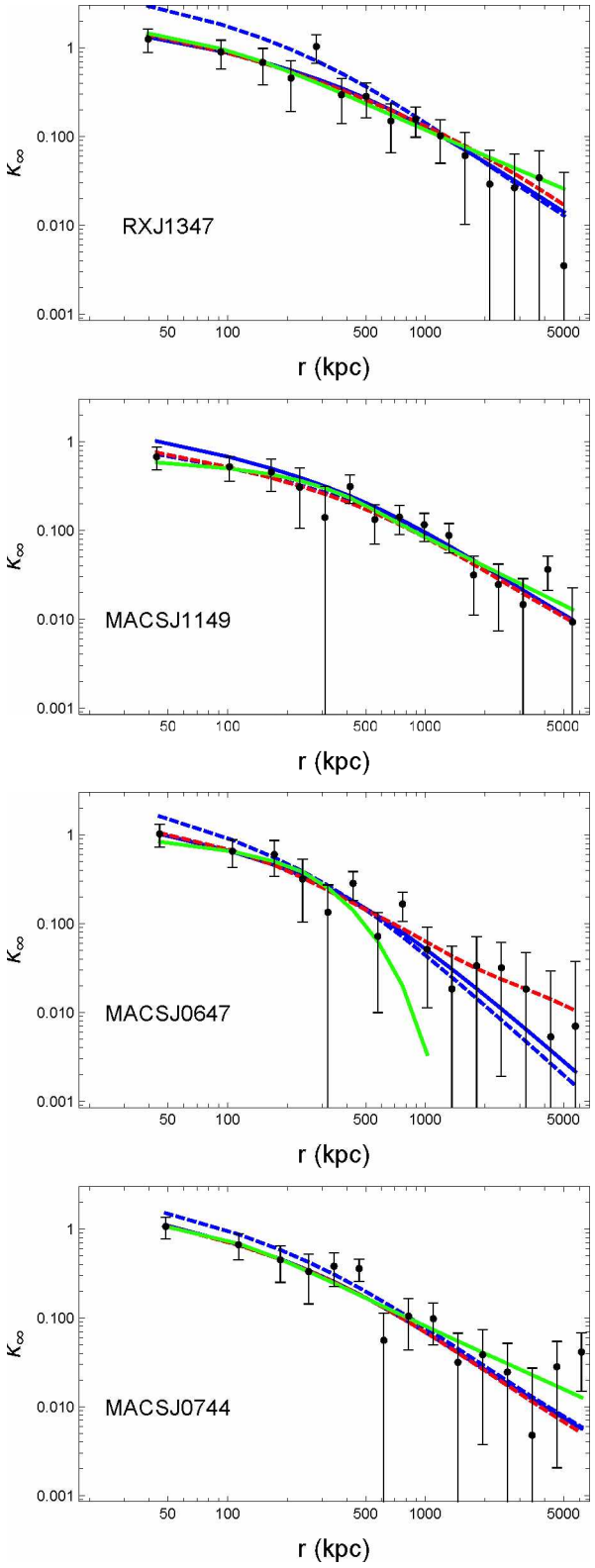

Figure 4.8: Same as Fig. 4.5.

CHAPTER 5

Exploring DHOST Theories in ultra-dwarf galaxies

In this chapter we move from the cluster scale to the galactic scale and present the results for three ultra-diffuse galaxies, NGC 1052-DF2 (DF2), NGC 1052-DF4 (DF4), and Dragonfly 44 (DF44), detected with the Dragonfly telescope array [174]. These three galaxies represent opposite systems in terms of DM content. In fact, DF2 [175] and DF4 [176] have been shown to be DM-deficient galaxies ($\sim$ 1% of their mass is DM), while DF44 is a DM-dominated galaxy ($\sim$ 99% of its mass is DM) [342].

DM is the fundamental ingredient for galaxies to exist, so galaxies lacking DM could be considered outliers in the actual galaxy formation paradigm. However, possible explanations within the standard cosmological scenario have been discussed in Sec. 3.2 of Chapter 3. Even if there are several explanations that, within the ΛCDM paradigm, justify the small amount of DM shown by DF2 and DF4 (e.g. hydrodynamical simulations [344–346], lower distance [347], non-Gaussian data [414]), alternative models have also been explored to explain galaxies like DF2 and DF4. These two galaxies, in particular, have become (in)famous as the "lacking DM galaxies" and such a lack of DM content has even been considered a

crucial deathblow for ETGs, since *"...a dark matter signature should always be detected, as it is an unavoidable consequence of the presence of ordinary matter"* [175].

Some efforts have been made to explain the dynamics of DF2 using the MOdified Newtonian Dynamics (MOND) paradigm [415]. However, as explained in [175], the velocity dispersion of DF2 reconstructed using its globular clusters with the MOND turned out to be double the 90% upper limit of the observed ones. Furthermore, in [416, 417] the authors tried to study the ETGs DF2 and DF44 with other modifications of gravity, such as the one introduced within a MOND scenario by an External Field Effect (EFE) [418, 419], Weyl conformal gravity [420, 421] and a scalar-tensor vector theory (MOG) [422]. The results highlighted in [417] state that the internal kinematics of UDGS, such as DF2 and DF44, can be explained by MOG and the MOND with (EFE) [419, 423], while Weyl conformal gravity fits the data acceptably, concluding that NGC1052-DF2 does not imply a dead end for ETGs.

In [354], the authors study the dynamics of DF44 assuming the GR framework and "fuzzy" dark matter [424] as an alternative to the GR framework.

To discriminate between different formation scenarios and different modifications of gravity, the crucial physical quantity is the dynamical mass of the galaxy. The mass of UDGs can be efficiently reconstructed using the dynamics of globular clusters, which are gravitationally bound to galaxies (this is not possible with stellar velocity dispersion due to its low signal-to-noise ratio).

In our works, [425, 426], the driving idea was to test whether the DHOST model, expressed by Eqs. 2.26, as a replacement for DM, in galaxies with low amounts of DM, such as DF2 and DF4, and galaxies dominated by DM, such as DF44, was able to describe the internal kinematics of these galaxies. To constraint the parameter $\theta = \{c_{200}, M_{200}, \gamma, D, \Upsilon\}$ (in GR), and $\theta = \{c_{200}, M_{200}, \gamma, D, \Upsilon, \Xi_1\}$ (in the DHOST scenario), I have defined the χ^2 functions associated to the data (radial velocities or velocity dispersions). For the UDGs DF2 and DF4 we have

$$\chi^2(\theta) = \sum_i^{\mathcal{N}_{data}} \frac{(v_i - v_{sys})^2}{\sigma_i^2} + \ln\left(2\pi\sigma_i^2\right) , \tag{5.1}$$

where: $\mathcal{N}_{data}$ is the total number of GCs associated to DF2 and DF4; v_{sys} is the systemic velocity of DF2 and DF4; v_i represents the observed velocity of the GCs of DF2 and DF4; $\sigma_i^2 = \sigma_{los,i}^2(\theta) + \sigma_{v_i}^2$ is the total error associated to each v_i where σ_i^2 is observed uncertainty, and $\sigma_{los,i}^2(\theta)$ is the velocity dispersion.

For the third UDG, DF44, the observational data are the effective velocity dispersions, therefore, the χ^2 reads

$$\chi^2(\theta) = \sum_{i=1}^{\mathcal{N}_{data}} \left(\frac{\sigma_{eff,i} - \sigma_{los,i}(\theta)}{\delta\sigma_i} \right)^2 + \ln(2\pi\delta\sigma_i^2) \,, \tag{5.2}$$

where: $\mathcal{N}_{data}$ is the number of observational data; $\sigma_{eff} = \sqrt{v_i^2 + \sigma_i^2}$ is the effective velocity dispersion.

In addition, we apply the following priors related to the stellar component:

- for DF2 and DF4 a Gaussian prior on the distance $D = 22.1 \pm 1.2$ Mpc whose value has been measured using the method of the Tip of the Red Giant Branch [427]. For DF44, a Gaussian prior $D = 102 \pm 14$ Mpc obtained through the Surface Brightness Fluctuation method [428, 429];

- a Gaussian prior, for DF2 and DF4, on the light-to-mass ratio $\Upsilon_* = 2.0 \pm 0.5 M_\odot/L_\odot$ [175]. For DF44, a normal prior on the light-to-mass ratio $\log\Upsilon_* = 1.5$ with 0.1 dex scatter[354];

- a Gaussian prior on the systemic velocity $v_{sys} = 1801.6 \pm 5.$ km s^{-1} [430] for DF2 and $v_{sys} = 1444.6 \pm 7.75$ km s^{-1} [176] for DF4;

- normal priors on the anisotropy parameters $-\log(1-\beta_i) = 0 \pm 0.5$ within the range $[-10, 1]$.

In addition, the velocity dispersion has to be a physical quantity, and then the control $\sigma_{los} > 0$ has also been added.

The actual galaxy formation scenario states that galaxies are embedded in DM haloes that are, in general, larger than the distance data provided. Thus, to ensure a physical meaning on the constraints on DM parameters, priors on them ($\theta = \{c_{200}, M_{200}, \gamma\}$) have been added:

- a log-normal prior on the concentration parameter c_{200} arising from the $c-M$ relation [431] (assuming the cosmology of *Planck15*) with a scatter of 0.16 dex;
- two different scenarios have been considered parametrizing the relation between the stellar and the DM component. In the first one, DM is linked to the stellar one through the Stellar-to-Halo-mass relation (SHMR) [373] described in Sec. 3.2.2, resulting in a log-normal prior whose median is provided by the SHMR with a deviation of 0.3 dex. In the second case, DM is decoupled from the stellar component, with just a flat uniform prior into the range $\log M_{200}/M_{\odot} = [2,15]$;
- a flat prior to the inner log-slope parameter $\gamma \in [0,2]$ has also been taken into account.

Then, the final $\chi^2_{tot} = \chi^2_{DM} + \chi^2_*$, when DM has been assumed, and $\chi^2_{tot} = \chi^2_*$, when the DHOST model replaces DM, has been minimized using the Metropolis-Hastings algorithm. Model comparison has been carried out through the calculation of the Bayes ratio $\mathscr{B}_{i,j}$ and suspiciousness $\log S_{ij}$.

5.1 NGC 1052-DF2

All the scenarios that have been considered, depending on the mass components involved and the priors applied are presented in Table 5.1.

The first step has been to analyse the GR scenario, which is our reference model against which we can compare and the statistical validity of the DHOST model described by Eq. 2.26. More precisely, our reference scenario is the GR case with only stellar contribution and a constant anisotropy profile. Note that in [430] there is always a DM component, so the stellar-only scenario is described here for the first time. In the top panel of Fig. 5.1 we can easily see, even just by visual inspection, how we can fit the data with stars only, with a spatially averaged total dispersion $\sigma \sim 10.53$ km s^{-1}. Statistically, i.e. in terms of Bayes Factors and suspiciousness, this scenario is the best fit to the observations. From Table 5.1 we see that there is no deviation from the applied priors, and the constant anisotropy profile shows a preference for highly tangential modes.

In the top panel of Fig. 5.2 we have the same scenario, but we allow for a radial variation of the anisotropy function. From Table 5.1 we can see that there is no statistically significant difference compared to the previous case. We see an increase in the velocity offset at small scales, while at large scales we have the same decreasing profile, although the spatially averaged dispersion velocity is still consistent with the data, being $\sigma \sim 11.10\,\mathrm{km\,s^{-1}}$. The β parameters are quite well constrained, still indicating a highly tangential anisotropy profile, while the radius parameter r_a is unconstrained. Moreover, we see that from a Bayesian point of view, this scenario is disfavoured with respect to our chosen reference one: not in a significant way for Jeffrey's scale, but already in a "statistical tension" regime, albeit very mild, when looking at the suspiciousness.

Table 5.1: Results from the statistical analysis of NGC1052-DF2. For each parameter we provide the median and the 1σ constraints; unconstrained parameters are in italic font. The parameters are, from left to right: distance D; mass-to-light ratio Υ; systemic velocity v_{sys}; anisotropy function parameters, depending on the model assumed, constant (β_c) or radial from [360] ($\beta_0, \beta_\infty, r_a$); gNFW concentration c_{200}, mass M_{200}, and inner log-slope γ; DHOST characteristic scaling Ξ_1; Bayes Factor $\mathscr{B}^i_j$; its logarithm; and the suspiciousness $\log S^i_j$.

	GR													
	D	$\Upsilon_\star$	v_{sys}	β_c	β_0	β_∞	r_a	c_{200}	$\log M_{200}$	γ	Ξ_1	$\mathscr{B}^i_j$	$\log \mathscr{B}^i_j$	$\log S^i_j$
	Mpc		km s^{-1}				kpc		$M_\odot$					
Star only	$22.09^{+1.23}_{-1.18}$	$1.81^{+0.47}_{-0.46}$	$1804.08^{+2.61}_{-2.55}$	$-3.64^{+2.33}_{-3.20}$	–	–	–	–	–	–	–	*1*	*0*	*0*
	$22.11^{+1.21}_{-1.18}$	$1.62^{+0.47}_{-0.45}$	$1804.28^{+2.98}_{-3.02}$	–	$-3.55^{+1.92}_{-2.79}$	$-1.23^{+1.27}_{-2.18}$	*22.0*	–	–	–	–	$0.42^{+0.01}_{-0.01}$	$-0.88^{+0.03}_{-0.04}$	$-0.61^{+0.04}_{-0.03}$
SHMR+NFW	$21.86^{+1.21}_{-1.19}$	$1.59^{+0.50}_{-0.50}$	$1801.93^{+3.85}_{-3.81}$	$-1.92^{+1.81}_{-3.56}$	–	–	–	$8.16^{+3.40}_{-2.29}$	$10.82^{+0.16}_{-0.18}$	< 0.41	–	$0.060^{+0.003}_{-0.002}$	$-2.82^{+0.04}_{-0.03}$	$-2.33^{+0.07}_{-0.05}$
	$21.83^{+1.22}_{-1.21}$	$1.56^{+0.51}_{-0.50}$	$1802.27^{+4.01}_{-4.15}$	–	$-1.21^{+1.05}_{-2.23}$	$-0.64^{+0.92}_{-2.11}$	*19.1*	$7.82^{+3.22}_{-2.23}$	$10.81^{+0.16}_{-0.18}$	< 0.37	–	$0.028^{+0.001}_{-0.001}$	$-3.58^{+0.04}_{-0.04}$	$-2.85^{+0.06}_{-0.06}$
no SHMR+NFW	$22.15^{+1.18}_{-1.20}$	$1.78^{+0.47}_{-0.46}$	$1804.01^{+2.72}_{-2.74}$	$-3.34^{+2.19}_{-3.26}$	–	–	–	$24.11^{+12.15}_{-8.54}$	< 6.78	*0.02*	–	$0.65^{+0.02}_{-0.02}$	$-0.44^{+0.04}_{-0.03}$	$-0.30^{+0.03}_{-0.03}$
	$22.12^{+1.20}_{-1.22}$	$1.64^{+0.49}_{-0.47}$	$1804.22^{+3.11}_{-3.05}$	–	$-3.43^{+1.94}_{-2.84}$	$-1.24^{+1.30}_{-2.27}$	*22.5*	$25.22^{+12.47}_{-8.39}$	< 6.06	*0.62*	–	$0.279^{+0.007}_{-0.008}$	$-1.28^{+0.03}_{-0.03}$	$-0.92^{+0.05}_{-0.05}$
	DHOST (as dark energy)													
	D	$\Upsilon_\star$	v_{sys}	β_c	β_0	β_∞	r_a	c_{200}	$\log M_{200}$	γ	Ξ_1	$\mathscr{B}^i_j$	$\log \mathscr{B}^i_j$	$\log S^i_j$
	Mpc		km s^{-1}				kpc		$M_\odot$					
SHMR+NFW	$21.91^{+1.19}_{-1.26}$	$1.61^{+0.50}_{-0.53}$	$1802.07^{+3.86}_{-3.71}$	$-1.45^{+1.59}_{-3.28}$	–	–	–	$8.76^{+3.63}_{-2.50}$	$10.82^{+0.16}_{-0.18}$	< 0.56	$-0.25^{+0.49}_{-0.21}$	$0.26^{+0.01}_{-0.01}$	$-1.35^{+0.04}_{-0.04}$	$-0.41^{+0.07}_{-0.07}$
no SHMR+NFW	$22.07^{+1.20}_{-1.17}$	$1.70^{+0.48}_{-0.49}$	$1804.20^{+2.83}_{-2.95}$	$-2.88^{+2.26}_{-3.46}$	–	–	–	$22.29^{+11.49}_{-7.78}$	< 7.87	*0.097*	$-0.29^{+0.53}_{-0.71}$	$0.63^{+0.02}_{-0.02}$	$-0.46^{+0.03}_{-0.03}$	$-0.25^{+0.02}_{-0.03}$
	DHOST (as dark matter)													
	D	$\Upsilon_\star$	v_{sys}	β_c	β_0	β_∞	r_a	c_{200}	$\log M_{200}$	γ	Ξ_1	$\mathscr{B}^i_j$	$\log \mathscr{B}^i_j$	$\log S^i_j$
	Mpc		km s^{-1}				kpc		$M_\odot$					
Star only	$22.14^{+1.21}_{-1.20}$	$1.81^{+0.47}_{-0.45}$	$1804.10^{+2.68}_{-2.67}$	$-3.25^{+2.32}_{-3.21}$	–	–	–	–	–	–	$-0.15^{+0.34}_{-0.32}$	$1.05^{+0.03}_{-0.03}$	$0.04^{+0.03}_{-0.03}$	$0.10^{+0.03}_{-0.03}$
	$22.04^{+1.18}_{-1.18}$	$1.61^{+0.51}_{-0.48}$	$1804.35^{+3.03}_{-2.98}$	–	$-3.30^{+1.93}_{-2.87}$	$-0.99^{+1.14}_{-2.32}$	*22.32*	–	–	–	$-0.29^{+0.47}_{-0.49}$	$0.43^{+0.02}_{-0.01}$	$-0.84^{+0.04}_{-0.03}$	$-0.52^{+0.04}_{-0.03}$

If we include a gNFW for the DM component in the GR scenario, things change drastically and are strongly related to the presence of the SHMR prior. All cases are shown in Figs. 5.1 and 5.2. The first major differences between the SHMR and no-SHMR cases are a slight shift towards a smaller distance, a smaller

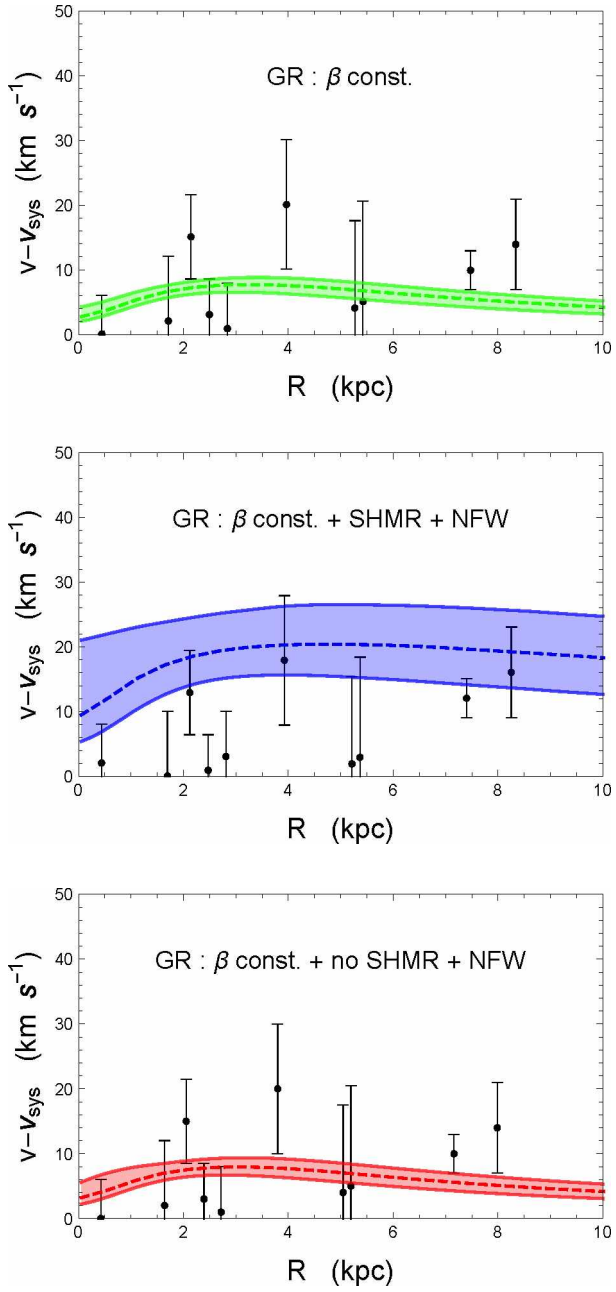

Figure 5.1: Profiles of $v - v_{sys}$ of NGC1052-DF2 as a baryonic galaxy with a constant velocity anisotropy profile. Black dots with error bars represents observational data, $v_i - v_{sys}$, with uncertainties, σ_{v_i}. Green dashed lines with shaded regions show the median and the 1σ confidence region of the σ_{los} coming from Eq. (3.46).

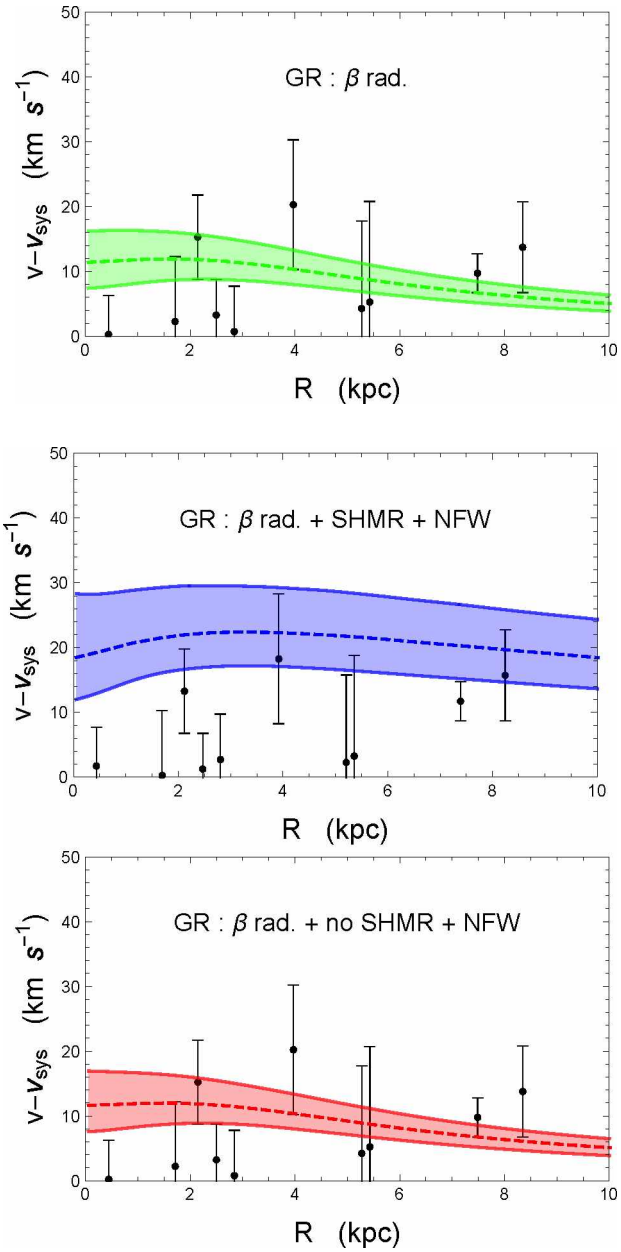

Figure 5.2: Same as Fig. 5.1 but for the radial variation of the anisotropy parameter described by [360].

mass-to-light ratio and a lower systemic velocity in the former case, although they are still statistically consistent with each other. In addition, the anisotropy parameters are less negative but still fully tangential. In the SHMR case, the spatially averaged dispersion is $\sigma \sim 17$ km s^{-1}, in agreement with most of the data, while in the no-SHMR case, we have $\sigma \sim 11$ km s^{-1}, much more in agreement with the observations.

Looking more closely at the DM parameters, we see the greatest net differences. The SHMR case has perfect Gaussian constraints on both c_{200} and M_{200}, while for γ we can only set an upper bound since it is consistent with zero. Note that the median we obtain for $c_{200} \sim 8$, is not exactly the median we would expect from the $c-M$ relation of [431] using the resulting M_{200} MCMC outputs, which would be $c_{200} \sim 11$. However, given the uncertainties, they are still statistically consistent. Nevertheless, the SHMR case is both strongly disfavoured and in strong tension with the reference scenario.

The situation is different when the SHMR assumption is relaxed and we do not impose such a prior. All parameters are perfectly consistent with the reference case, but the DM now has quite different properties: a very high concentration, $c_{200} \sim 24$; a very low mass content, $\log M_{200} < 7 M_{\odot}$; and γ unconstrained, with a uniform distribution over the entire allowed range. Note that the constraint on M_{200} is only an upper bound.

We also show in Table 5.1 that such a scenario is in only slight tension with the reference star-only case. This is equivalent to saying that the absence of DM at such scales in NGC1052-DF2 is a more than highly statistically valid hypothesis. We would also like to point out that we have allowed for the possibility that the gNFW somehow fails to properly describe the galaxy's DM halo (if any). We have therefore also relied on another DM model, the Einasto profile [164],

$$\rho_{Ein}(r) = \rho_s \exp\left\{-\frac{2}{\gamma}\left[\left(\frac{r}{r_s}\right)^{\gamma} - 1\right]\right\}, \tag{5.3}$$

which is another three-parameter model which successfully applies to galactic scales, but absolutely no qualitative difference has come out.

We now turn our attention to the DHOST model as the main goal is to test and possibly demonstrate its viability in describing the kinematic data of NGC1052-DF2. We first consider the scenario where the DHOST theory plays the role of

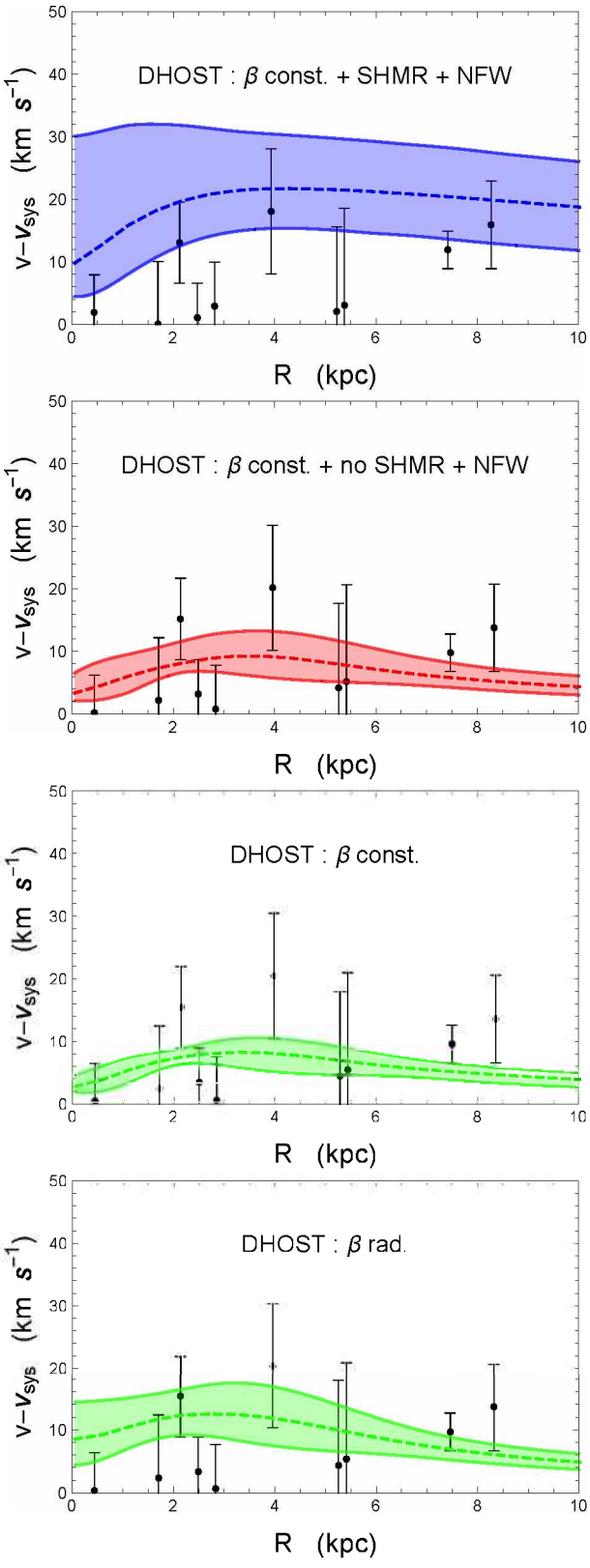

Figure 5.3: Same as Fig. 5.1 but for the DHOST model.

DE, the effects of which could be felt on galactic scales by breaking the screening mechanism. In this case, we still need to include a DM component in the matter budget, which is always parameterised by a gNFW model.

As can be seen from Table 5.1 and the two upper panels of Fig. 5.3, the presence of the DHOST model does not significantly alter the results we obtain in the GR case, which are in fact statistically equivalent. In fact, the value of the DHOST parameter Ξ_1 is equal to zero: as expected, DE does not play a relevant role on galactic scales. On the other hand, we see that the addition of the DHOST model slightly increases both the Bayes Factor and the suspiciousness with respect to the GR+DM case: even if they remain slightly disadvantaged, the tension is somewhat alleviated, and this effect is most noticeable when the SHMR prior is applied.

The same conclusions can be drawn in the case where the DHOST plays both the role of DE at cosmological scales and fully mimics the DM at galactic scales. The results are shown in Table 5.1 and in the two bottom panels of Fig. 5.3. The most interesting thing to note is that although the parameters are more or less statistically equivalent to the GR star-only case, and although the characteristic DHOST parameter has a non-zero median but is consistent with the GR limit at the 1σ confidence level, we have an increase in both the Bayes Factor and the suspiciousness. In the case of constant anisotropy, the Bayes Factor is even slightly positive, although by a negligible amount, for which we cannot conclude with certainty that it should be preferred over the GR-based reference case. Suspiciousness also becomes positive (the only case among all those considered), which means that it is fully consistent and not in tension with our reference model.

This is the main conclusion and goal of our work, [425]: we have shown that even in a galaxy with a very low DM content, or even with no DM at all, DHOST theories cannot be discarded, but can be as successful as GR in explaining the observational data. Thus, NGC1052-DF2 has not dealt a deathblow to DHOST theories, which can still be investigated as reliable candidates for ETGs. Another interesting and important point is that in the case where DHOST also plays the role of DM, given only a limited number of physically reasonable priors, the chains automatically place a sharp upper bound on the possible values of the characteristic DHOST parameters, namely $\Xi_1 \leq 0.5$ with a confidence level of 2σ.

5.2 NGC 1052-DF4

The UDG NGC 1052-DF4 (DF4) is the "twin" galaxy of NGC 1052-DF2 being characterized by a lack of DM, at least, within the range of distances specified by the data [176]. All the results of our analysis may be found in Table 5.2.

The results of the case with GR and only a baryonic component are effectively similar to those found for DF2 [426], namely the kinematics apparently do not require any DM to be supported, as can be seen in the top panel of Fig. 5.4. Independently of the functional form, the anisotropy parameters β point to a more tangential anisotropy profile, although the constant anisotropy profile seems to be slightly favoured, as can be seen from the values of the Bayes Factors and the suspiciousness (last two columns of table 5.2). The spatially averaged velocity dispersion is $\sigma \sim 6$ km s^{-1} for the case of constant anisotropy and $\sigma \sim 5.9$ km s^{-1} for the case of radial anisotropy, both consistent with the estimate of $\sigma \sim 7$ km s^{-1} in [176].

When a DM component is added to the matter budget, we need to distinguish the results according to the presence or absence of the SHMR prior. Looking at the middle panels of Figs. 5.4 and 5.5, when the SHMR prior is assumed, the velocity dispersion profile fails to fit the data over the full range of distances for both anisotropy cases, with a spatially averaged value of $\sigma \sim 11 - 13$ km s^{-1}. The agreement with the data improves when the prior on the SHMR is relaxed and the stellar and DM components are decoupled. Indeed, allowing a smaller amount of DM leads to less tension with the data, as can be seen from the lower panels of Figs. 5.4 and 5.5. In addition, when the anisotropy parameter is constant, the resulting velocity dispersion profile is in better agreement with the data in the innermost region than that with the radial $\beta(r)$ given by Eq. 3.62.

Looking more closely at the gNFW parameter values, we can see that DF4 behaves almost as perfectly as DF2. In the SHMR case, we have: perfect Gaussian constraints on c_{200} and M_{200}; only an upper bound on γ which is consistent with zero; and the median of $c_{200} \sim 8$ does not exactly match the median we would expect from the theoretical $c - M$ relation of [431], indicating some hidden tension. When the SHMR prior is removed, the concentration parameter $c_{200_c} \sim$ grows, the

Table 5.2: Results from the statistical analysis of NGC1052-DF4. For each parameter we provide the median and the 1σ constraints; unconstrained parameters are in italic font. The parameters are, from left to right: distance D; mass-to-light ratio Υ; systemic velocity v_{sys}; anisotropy function parameters, depending on the model assumed, constant (β_c) or radial from [360] $(\beta_0, \beta_\infty, r_a)$; gNFW concentration c_{200}, mass M_{200}, and inner log-slope γ; DHOST characteristic scaling Ξ_1; Bayes Factor $\mathscr{B}^i_j$; logarithm of the Bayes Factor $\log \mathscr{B}^i_j$; and the suspiciousness $\log S^i_j$.

	GR												
	D	Υ_*	v_{sys}	β_c	β_0	β_∞	r_a	c_{200}	$\log M_{200}$	γ	Ξ_1	$\log \mathscr{B}^i_j$	$\log S^i_j$
	Mpc		km/s				kpc		$M_\odot$				
Stars only	$22.05^{+1.17}_{-1.19}$	$1.93^{+0.49}_{-0.49}$	$1445.92^{+2.30}_{-2.26}$	> -3.06	–	–	–	–	–	–	–	0	0
	$22.04^{+1.23}_{-1.23}$	$1.81^{+0.51}_{-0.51}$	$1445.56^{+2.91}_{-2.99}$	–	> -3.37	> -1.54	*50.47*	–	–	–	–	$-0.43^{+0.02}_{-0.02}$	$-0.10^{+0.05}_{-0.05}$
SHMR + gNFW	$21.90^{+1.17}_{-1.18}$	$1.91^{+0.49}_{-0.52}$	$1445.78^{+4.59}_{-4.59}$	> -1.98	–	–	–	$8.87^{+3.83}_{-2.61}$	$10.77^{+0.15}_{-0.17}$	< 0.48	–	$-2.25^{+0.02}_{-0.02}$	$-1.69^{+0.07}_{-0.05}$
	$21.83^{+1.24}_{-1.12}$	$1.89^{+0.52}_{-0.51}$	$1445.55^{+5.01}_{-5.10}$	–	> -1.88	> -1.12	*49.57*	$8.53^{+3.69}_{-2.34}$	$10.78^{+0.16}_{-0.16}$	< 0.45	–	$-2.60^{+0.02}_{-0.02}$	$-1.83^{+0.07}_{-0.10}$
NO SHMR + gNFW	$22.03^{+1.23}_{-1.15}$	$1.92^{+0.50}_{-0.49}$	$1446.04^{+2.39}_{-2.40}$	> -3.18	–	–	–	$25.63^{+11.61}_{-8.35}$	< 6.08	*1.00*	–	$-0.21^{+0.01}_{-0.01}$	$-0.08^{+0.02}_{-0.03}$
	$21.99^{+1.20}_{-1.17}$	$1.83^{+0.52}_{-0.50}$	$1445.63^{+3.04}_{-3.13}$	–	> -3.42	> -1.48	*47.81*	$25.72^{+12.83}_{-8.48}$	< 5.85	*0.99*	–	$-0.65^{+0.01}_{-0.01}$	$-0.13^{+0.06}_{-0.06}$
	DHOST (as dark energy)												
	D	Υ_*	v_{sys}	β_c	β_0	β_∞	r_a	c_{200}	$\log M_{200}$	γ	Ξ_1	$\log \mathscr{B}^i_j$	$\log S^i_j$
	Mpc		km/s				kpc		$M_\odot$				
SHMR + gNFW	$21.98^{+1.21}_{-1.27}$	$1.91^{+0.50}_{-0.49}$	$1445.90^{+4.46}_{-4.51}$	> -1.70	–	–	–	$9.55^{+4.57}_{-3.04}$	$10.75^{+0.16}_{-0.17}$	*0.71*	$-0.06^{+1.52}_{-0.34}$	$-1.72^{+0.03}_{-0.02}$	$-0.04^{+0.02}_{-0.02}$
	$21.84^{+1.24}_{-1.12}$	$1.93^{+0.53}_{-0.54}$	$1446.04^{+4.77}_{-4.84}$	–	> -2.19	> -1.25	*47.93*	$8.49^{+4.07}_{-2.60}$	$10.77^{+0.16}_{-0.17}$	< 0.57	$-0.25^{+0.54}_{-0.19}$	$-2.03^{+0.02}_{-0.02}$	$-0.43^{+0.16}_{-0.13}$
NO SHMR + gNFW	$22.01^{+1.22}_{-1.21}$	$1.90^{+0.51}_{-0.49}$	$1445.90^{+2.35}_{-2.48}$	> -2.87	–	–	–	$25.68^{+12.15}_{-8.43}$	< 6.48	*1.03*	$-0.09^{+0.48}_{-0.60}$	$-0.24^{+0.02}_{-0.02}$	$-0.04^{+0.04}_{-0.04}$
	$21.99^{+1.22}_{-1.20}$	$1.82^{+0.51}_{-0.50}$	$1445.53^{+2.97}_{-2.98}$	–	> -3.34	> -1.46	*48.05*	$25.44^{+11.92}_{-8.36}$	< 6.23	*0.99*	$-0.22^{+0.62}_{-0.70}$	$-0.58^{+0.02}_{-0.02}$	$-0.09^{+0.06}_{-0.06}$
	DHOST (as dark matter)												
	D	Υ_*	v_{sys}	β_c	β_0	β_∞	r_a	c_{200}	$\log M_{200}$	γ	Ξ_1	$\log \mathscr{B}^i_j$	$\log S^i_j$
	Mpc		km/s				kpc		$M_\odot$				
Stars only	$22.09^{+1.20}_{-1.22}$	$1.92^{+0.49}_{-0.49}$	$1445.89^{+2.29}_{-2.31}$	> -2.22	–	–	–	–	–	–	$-0.11^{+0.48}_{-0.62}$	$0.03^{+0.02}_{-0.01}$	$0.04^{-0.04}_{-0.04}$
	$21.95^{+1.55}_{-2.63}$	$1.82^{+0.52}_{-0.51}$	$1445.69^{+2.91}_{-2.89}$	–	> -3.24	> -1.36	*47.68*	–	–	–	$-0.18^{+0.53}_{-0.61}$	$-0.37^{+0.01}_{-0.01}$	$-0.02^{+0.06}_{-0.04}$

virial mass $\log M_{200}/M_\odot \sim 6$ decreases and is only upper bounded, and γ is unconstrained. We can reinforce our conclusions by looking at the Bayes Factor and Suspiciousness: the SHMR scenario is strongly disfavoured, while the absence of the SHMR prior is consistent with the reference scenario. Both results strongly suggest an absence or large deficiency of DM in the investigated areas.

We now turn to the cases where the gravitational scenario is described by the DHOST model. When the DHOST model describes only DE, we need to include

DM in the matter budget, and as we can see from Table 5.2, there is no significant difference compared to the corresponding GR cases. The presence of a DE effect from the DHOST model has no relevant role in changing the values of the fitting parameters. It is also possible to see that the results are almost completely analogous (considering the 1σ confidence levels) to those in GR by looking at the middle and bottom panels of Fig. 5.6 and 5.7. If we look at the values of the DHOST parameter Ξ_1, they are perfectly consistent with the GR limit. Once again, this is not unexpected, as we do not expect DE to play a significant role on galactic scales.

However, an important difference between the GR and DE DHOST cases becomes apparent when we look at the last columns of Table 5.2: we can see that both the Bayesian Factor and the suspiciousness are improved in the DHOST scenario compared to the GR framework. In particular, the most significant changes are in the application of the SHMR prior, which is now only slightly disfavoured and consistent within 1σ with the reference GR case. Thus, the DHOST effect somehow mitigates or plays a role in the internal kinematics of DF4, easing the tension with GR.

Finally, we come to the scenario we are most interested in, i.e. when, as a result of the Vainshtein screening, the DHOST model could mimic all the effects typically attributed to the DM. The results are summarised in the lower part of Table 5.2 and shown in the upper panels of Figs. 5.6 and 5.7. If we compare the results with those obtained within the GR framework, we can see that the DHOST model hardly implies any substantial change in the values of the parameters. We can also see that the DHOST parameter Ξ_1 is still consistent with the GR limit at the 1σ confidence level. From the last columns of Table 5.2, the constant anisotropy scenario is characterized by a positive Bayesian Ratio and a slightly positive suspiciousness, thus being perfectly equivalent to the GR case in terms of statistical reliability. The case with radial anisotropy instead has a slight improvement which also makes it consistent within 1σ with the reference case.

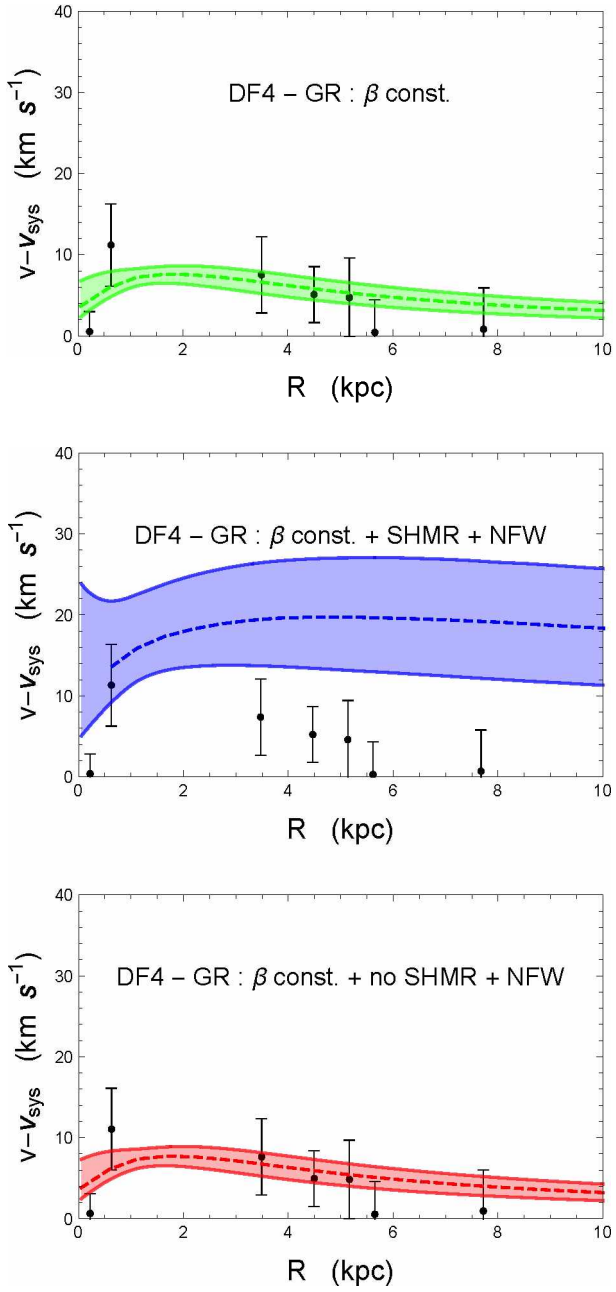

Figure 5.4: Profiles of the velocity offset of NGC1052-DF4 with GR and a constant velocity anisotropy profile. Black dots and bars are observational data, $v_i - v_{sys}$, with uncertainties, σ_{v_i}. Coloured dashed lines and shaded regions are respectively the median and the 1σ confidence region of the σ_{los} profile derived from Eq. (3.46).

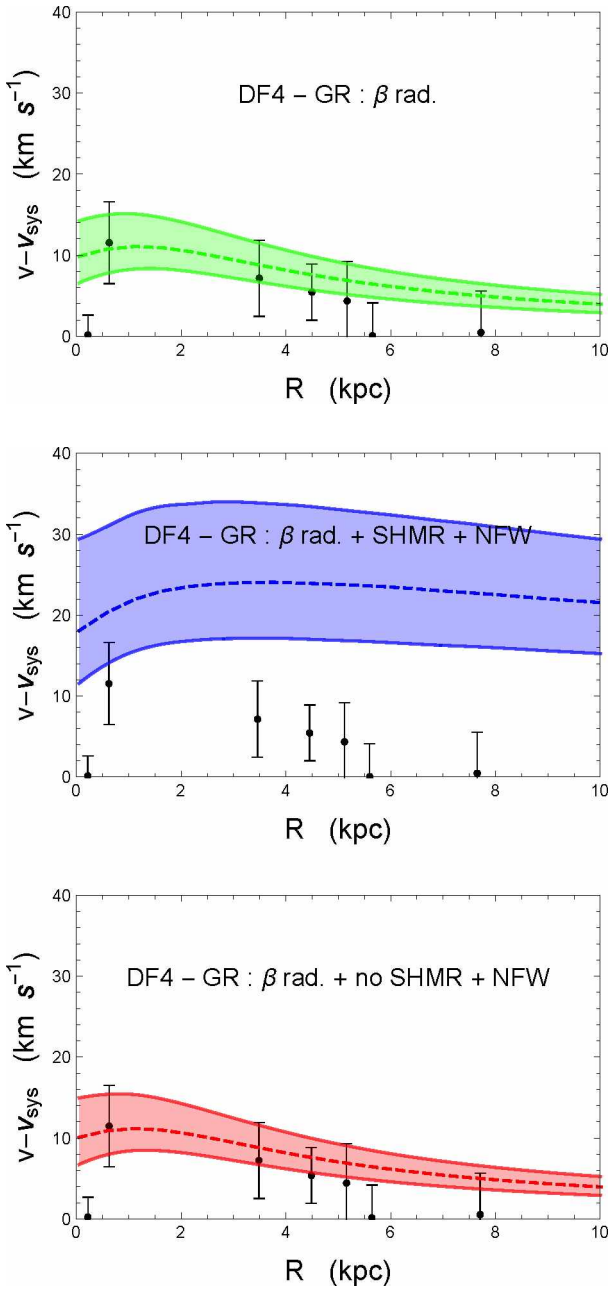

Figure 5.5: Same as Fig. 5.4 but with a radial velocity profile.

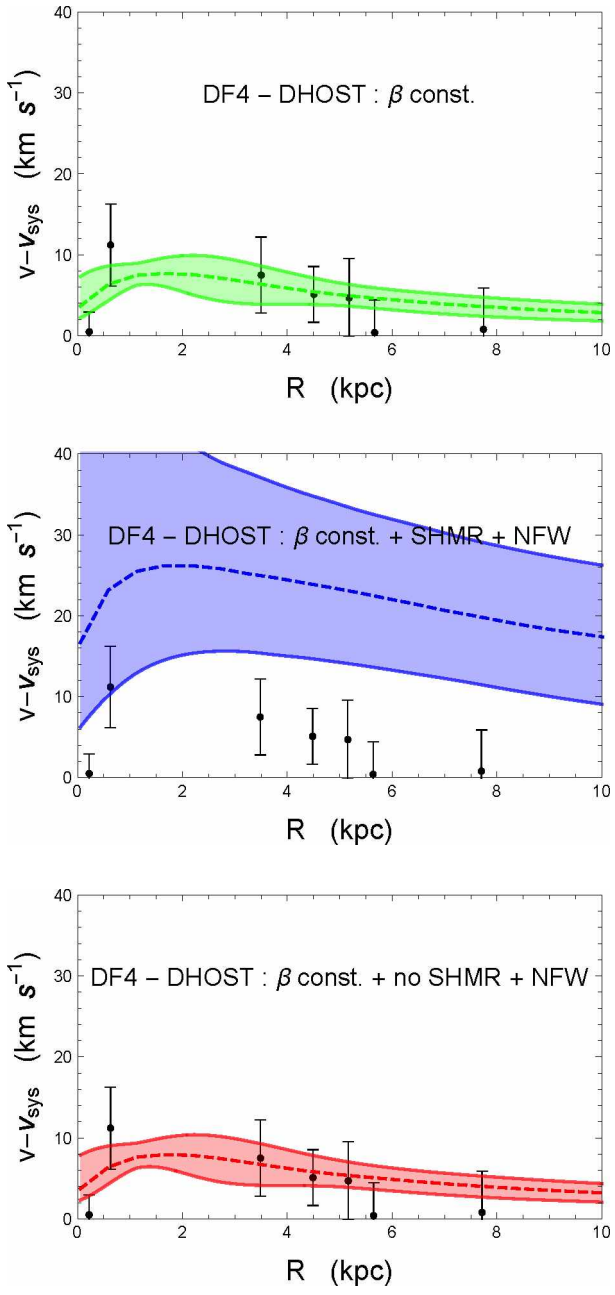

Figure 5.6: Same as Fig. 5.4 but for the DHOST model.

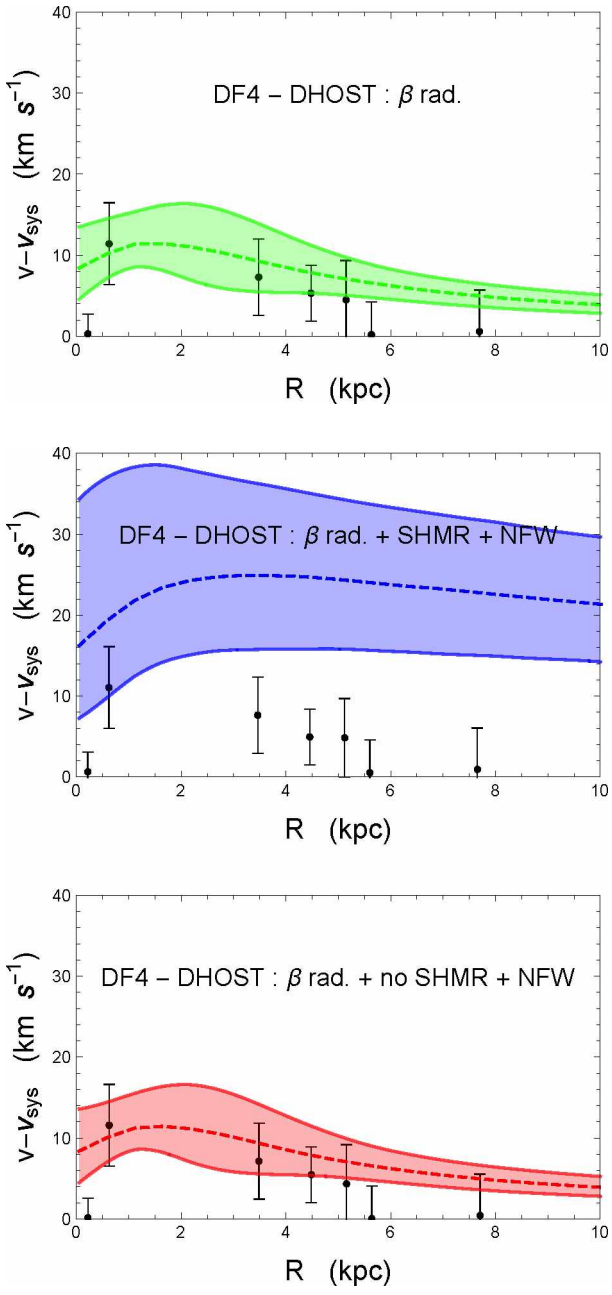

Figure 5.7: Same as Fig. 5.5 but for the DHOST model.

5.3 Dragonfly 44

Dragonfly 44 (DF44) [342, 343, 354] was revealed to be a dark matter-dominated galaxy with $M_{halo} \sim 99\%$ of the total mass. Constraints on the free parameters (GR and DHOST) are in Tables 5.3 and 5.4.

Table 5.3: Results from the statistical analysis of DF44. For each parameter we provide the median and the 1σ constraints; unconstrained parameters are in italic font. The parameters are, from left to right: distance D; mass-to-light ratio Υ; anisotropy function parameters, depending on the model assumed, constant (β_c) or radial from [360] $(\beta_0, \beta_\infty, r_a)$; gNFW concentration c_{200}, mass M_{200}, and inner log-slope γ; DHOST characteristic scaling Ξ_1; logarithm of the Bayes Factor $\log \mathscr{B}^i_j$; the suspiciousness $\log S^i_j$.

	GR											
	D	Υ_*	β_c	β_0	β_∞	r_a	c_{200}	$\log M_{200}$	γ	Ξ_1	$\log \mathscr{B}^i_j$	$\log S^i_j$
	Mpc					kpc		$M_\odot$				
Stars only	$153.98^{+10.98}_{-10.79}$	$9.10^{+0.59}_{-0.79}$	$0.17^{+0.11}_{-0.13}$	–	–	–	–	–	–	–	$-21.45^{+0.01}_{-0.01}$	$-21.75^{+0.03}_{-0.02}$
	$111.99^{+12.61}_{-12.13}$	$2.15^{+0.41}_{-0.32}$	–	$-0.43^{+1.40}_{-1.03}$	$-0.27^{+0.69}_{-1.06}$	*56.62*	–	–	–	–	$-2.06^{+0.01}_{-0.01}$	$-2.23^{+0.04}_{-0.04}$
SHMR+gNFW	$99.28^{+13.23}_{-13.59}$	$1.55^{+0.39}_{-0.32}$	$-0.40^{+0.28}_{-0.45}$	–	–	–	$10.71^{+3.21}_{-2.84}$	$10.97^{+0.15}_{-0.16}$	< 0.73	–	*0*	*0*
	$94.90^{+14.34}_{-13.53}$	$1.52^{+0.39}_{-0.32}$	–	> -3.06	> -1.77	*50.41*	$8.14^{+2.61}_{-2.08}$	$10.93^{+0.15}_{-0.16}$	< 0.45	–	$-0.24^{+0.02}_{-0.01}$	$-0.07^{+0.05}_{-0.07}$
NO SHMR+gNFW	$100.23^{+14.69}_{-13.72}$	$1.62^{+0.42}_{-0.34}$	> -1.29	–	–	–	$11.89^{+6.94}_{-4.73}$	$10.55^{+1.36}_{-0.48}$	*0.78*	–	$0.08^{+0.02}_{-0.02}$	$0.25^{+0.06}_{-0.05}$
	$99.93^{+14.32}_{-15.32}$	$1.62^{+0.42}_{-0.35}$	–	> -4.18	> -1.97	*48.96*	$10.86^{+5.98}_{-3.94}$	$10.22^{+0.76}_{-0.66}$	< 0.60	–	$-0.22^{+0.01}_{-0.02}$	$-0.04^{+0.05}_{-0.05}$
	DHOST (as dark energy)											
	D	Υ_*	β_c	β_0	β_∞	r_a	c_{200}	$\log M_{200}$	γ	Ξ_1	$\log \mathscr{B}^i_j$	$\log S^i_j$
	Mpc					kpc		$M_\odot$				
SHMR+gNFW	$98.57^{+13.32}_{-14.08}$	$1.52^{+0.38}_{-0.31}$	$-0.32^{+0.38}_{-0.46}$	–	–	–	$9.98^{+3.52}_{-2.98}$	$10.95^{+0.15}_{-0.16}$	< 0.76	$-0.019^{+0.515}_{-0.409}$	$-0.04^{+0.01}_{-0.02}$	$0.02^{+0.05}_{-0.05}$
	$95.31^{+14.51}_{-14.78}$	$1.52^{+0.38}_{-0.31}$	–	> -2.83	> -1.36	*49.55*	$7.87^{+2.81}_{-2.12}$	$10.95^{+0.14}_{-0.17}$	< 0.52	$-0.08^{+0.30}_{-0.18}$	$-0.29^{+0.02}_{-0.01}$	$-0.03^{+0.07}_{-0.06}$
NO SHMR+gNFW	$101.62^{+14.70}_{-14.28}$	$1.51^{+0.41}_{-0.31}$	> -2.70	–	–	–	$18.85^{+8.87}_{-5.59}$	$9.08^{+0.78}_{-0.39}$	> 1.53	$-7.68^{+6.75}_{-6.27}$	$-0.07^{+0.02}_{-0.02}$	$0.09^{+0.05}_{-0.05}$
	$101.83^{+13.59}_{-13.10}$	$1.57^{+0.40}_{-0.32}$	–	> -6.81	> -2.52	*50.28*	$18.56^{+9.57}_{-6.52}$	$8.60^{+0.62}_{-0.51}$	$1.10^{+0.48}_{-0.61}$	$-1.67^{+1.08}_{-2.11}$	$-0.49^{+0.01}_{-0.02}$	$-0.15^{+0.06}_{-0.05}$
	DHOST (as dark matter)											
	D	Υ_*	β_c	β_0	β_∞	r_a	c_{200}	$\log M_{200}$	γ	Ξ_1	$\log \mathscr{B}^i_j$	$\log S^i_j$
	Mpc					kpc		$M_\odot$				
Stars only	$103.74^{+14.11}_{-13.68}$	$1.67^{+0.45}_{-0.36}$	$0.92^{+0.02}_{-0.02}$	–	–	–	–	–	–	$-17.10^{+4.66}_{-6.24}$	$-2.90^{+0.01}_{-0.01}$	$-3.09^{+0.03}_{-0.03}$
	$111.77^{+12.63}_{-12.21}$	$2.09^{+0.38}_{-0.32}$	–	$-8.49^{+1.41}_{-1.01}$	$-0.11^{+0.58}_{-0.95}$	*44.54*	–	–	–	$-0.32^{+0.16}_{-0.18}$	$-1.18^{+0.02}_{-0.02}$	$-1.27^{+0.03}_{-0.04}$

For DF44, as for DF2 and DF4, we first consider the case where the dynamical mass of the galaxy consists entirely of baryons. Looking at the top panels of Figs. 5.8 and 5.9, it is clear that the fits with the only baryonic component are

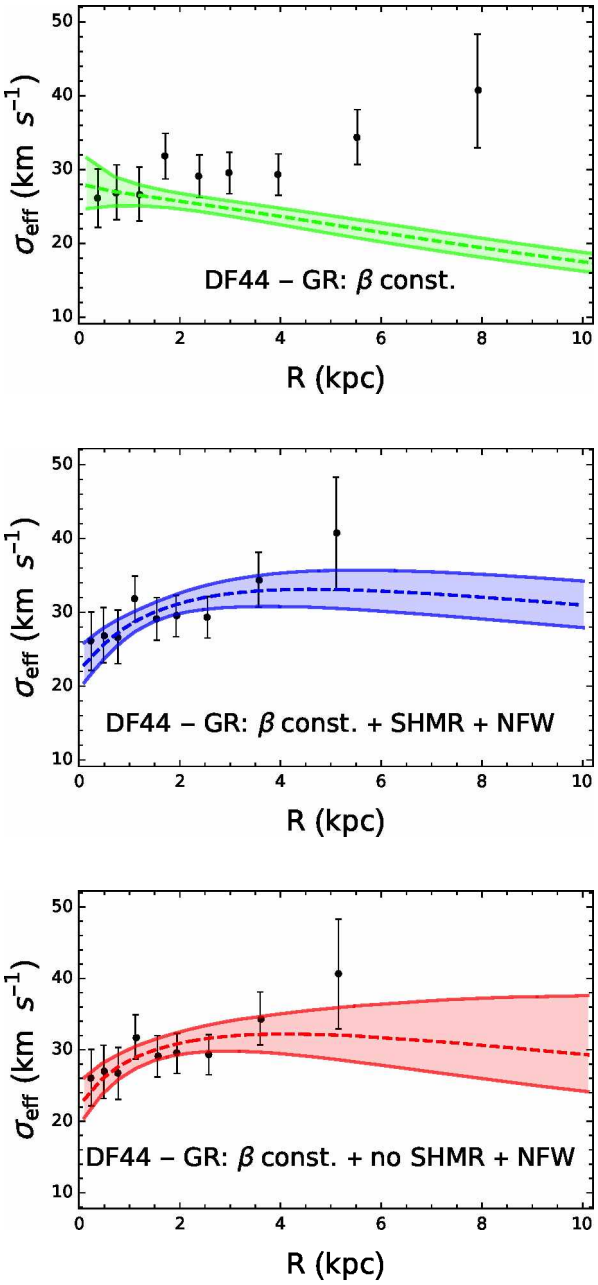

Figure 5.8: Profiles of the velocity dispersion of Dragonfly 44 with GR assuming a constant velocity anisotropy profile. Black dots and bars are observational data, $\sigma_{eff} = \left(\sigma_i^2 + v_i^2\right)^{1/2}$, with uncertainties. Coloured dashed lines and shaded regions are, respectively, the median and the 1σ confidence region of the σ_{eff} profile derived from Eq. 3.46.

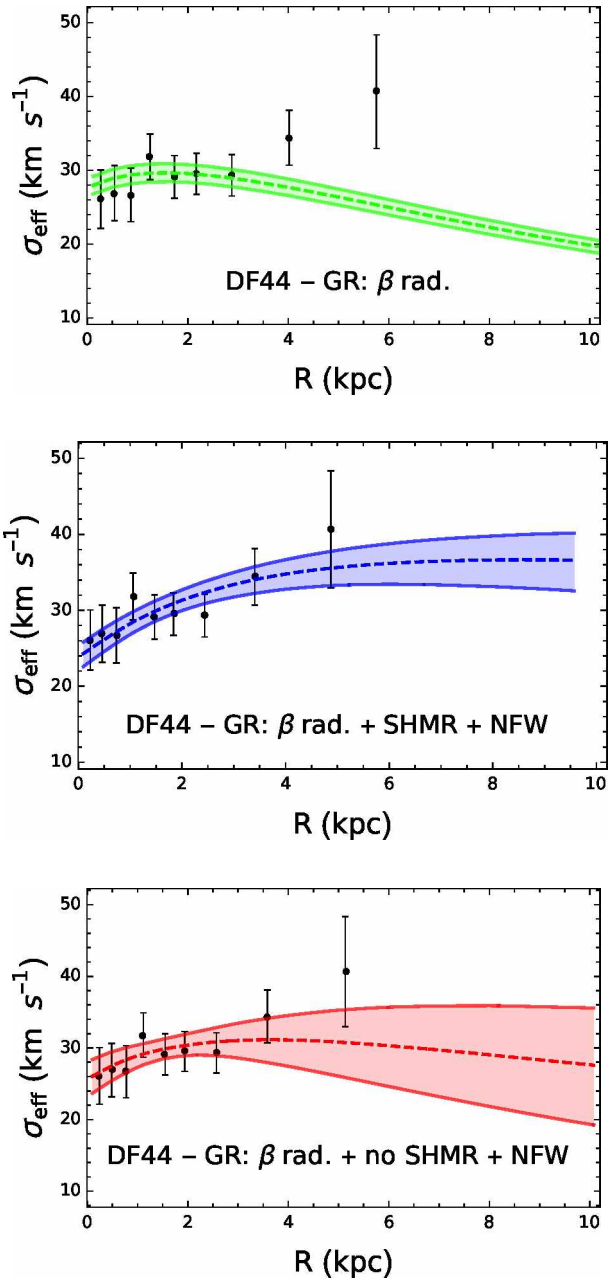

Figure 5.9: Same as Fig. 5.8 with radial velocity profile.

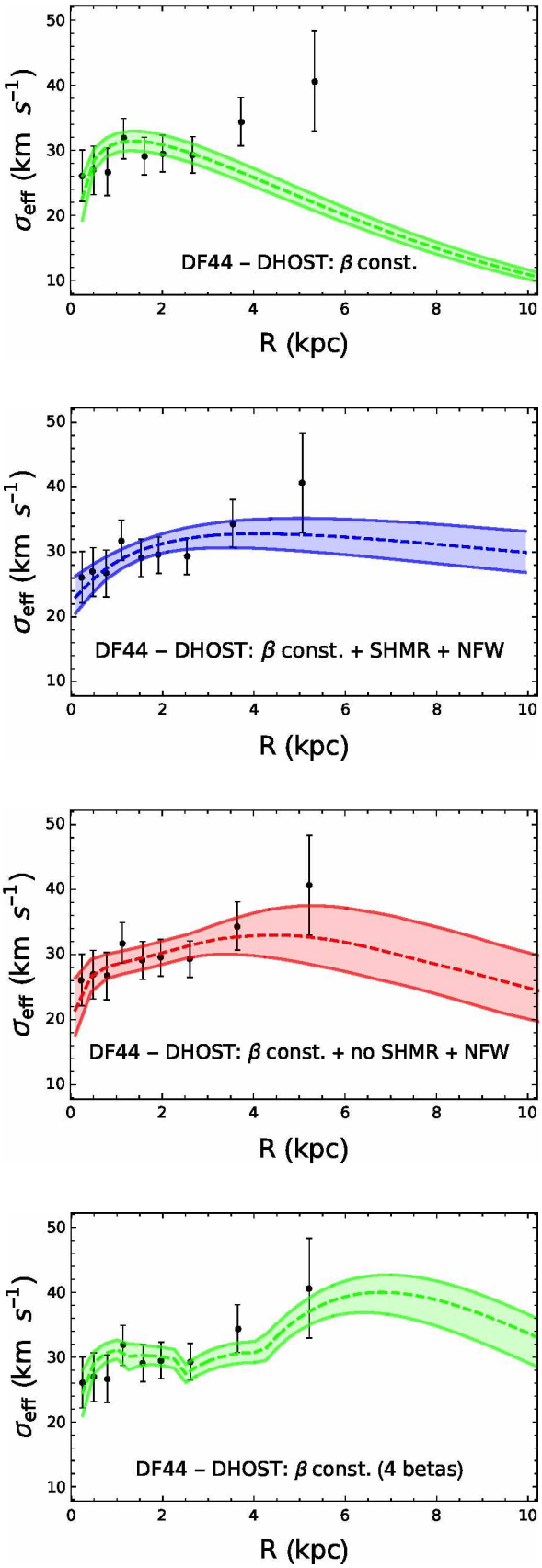

Figure 5.10: Same as Fig. 5.8 for the DHOST model.

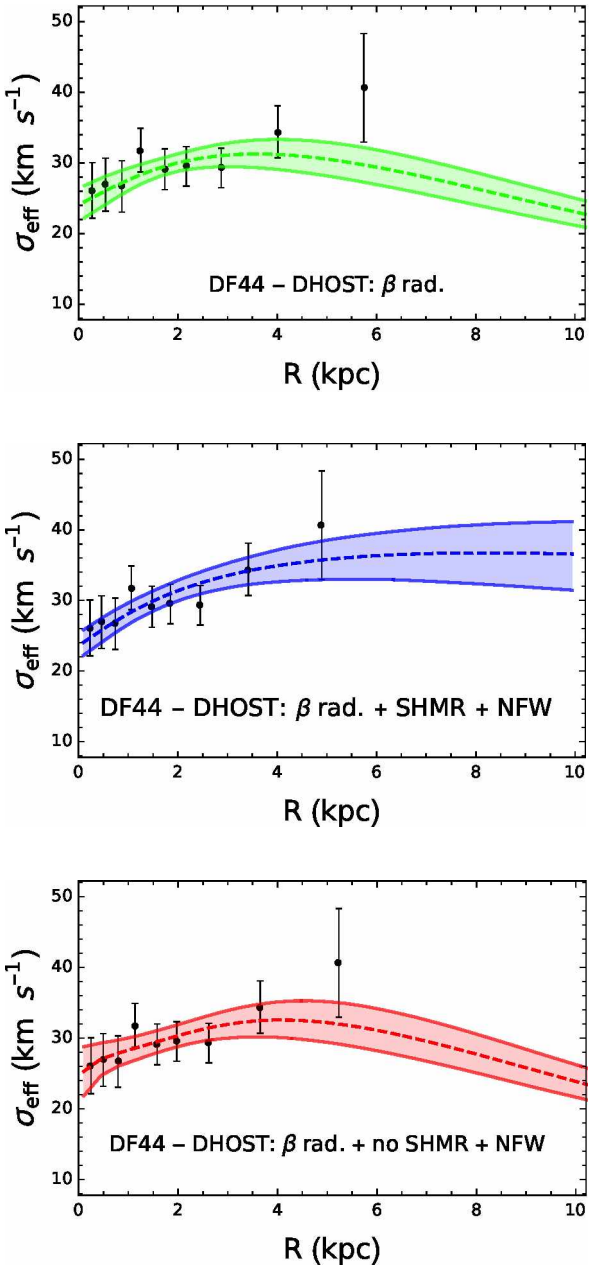

Figure 5.11: Same as Fig. 5.9 for the DHOST model.

undoubtedly poor. Looking at Table 5.3, it can be seen that the case of constant anisotropy implies a higher distance and, in particular, a mass-to-light ratio Υ_* that is not consistent with the range given in [343, 354]. The discrepancy is reduced by assuming a radial anisotropy profile, but the Bayesian indicators still underline the impossibility of the baryonic component, regardless of the specific functional form of the anisotropy, to reproduce the observational data.

When DM is included in the mass budget, the GR case with a constant anisotropy profile points to a tangent value for β_c, in perfect agreement with the results of [354]. For DM, the comparison is not so straightforward, because in [354] only a standard NFW profile was assumed (corresponding to $\gamma = 1$). If we look at the columns of Table 4.2 with the results for the DM parameters, we may notice a first important point: if a constant anisotropy profile is assumed, the reported c_{200} value is in full agreement with the value that would result from using the $c - M$ relation of [431]. So there is no tension in this case, unlike in DF4 and DF2. The upper bound on γ is also more relaxed and less cuspy compared to that described by a standard NFW density profile.

This scenario is characterised by an increase in the velocity dispersion at larger radii, in agreement with the data, so we can state unequivocally that the presence of DM is strongly required. The spatially averaged velocity dispersion we find is $\sigma \sim 31$ km s^{-1}, in agreement with the value of $\sigma \sim 33.5$ km s^{-1} presented in [343]. When the anisotropy profile is a radial function, the β parameters $\beta_{0,\infty}$ also tend to tangential values and the scale parameter r_a is practically unconstrained, and again there seems to be a small tension between the obtained and the expected values of c_{200}. From the top panels of Fig 5.9, if we compare the velocity dispersion profiles σ_{eff}, we can see that the case with $\beta(r)$ shows a more significant increase in the velocity dispersion profile for $r \geq 5$ kpc.

If we remove the SHMR prior and allow less DM, the situation is not so different from the one described above, but it is different from DF4 and DF2. In fact, looking at Table 5.3, we can see that c_{200} and M_{200} are now in perfect agreement with literature results and theoretical expectations. The inner log-slope parameter γ seems to be essentially unconstrained for the case of constant anisotropy, while for the other case it points to a core DM halo. From the last columns of Table 5.3, the Bayes Factor and the suspiciousness underline full consistency for

the constant anisotropy case, which is even slightly favoured with respect to the case with applied SHMR. The radial anisotropy scenario does not show a different picture compared to the SHMR prior.

We now turn to the DHOST gravity scenario. Looking first at the case where DHOST only plays the role of DE, Table 5.3 highlights the fact that the presence of DHOST effects does not lead to a change in the results we previously obtained for the GR case, at least in the case where the SHMR prior is applied. Instead, when it is not included, the values of c_{200} and M_{200} show the same tension as in DF4 and DF2. In addition, the γ parameter is now completely different: whereas before we always had $\gamma < 1$, now we prefer > 1. The values of the DHOST parameter Ξ_1 are consistent with zero in the SHMR case, while they are quite large in the case of no SHMR prior, being consistent with zero only at the 2σ level.

Looking at the Bayes Factors and the suspiciousness, we see that the SHMR cases and the constant anisotropy profiles are the best candidates, with marginal or almost null disfavour with respect to the GR cases.

When the DHOST model is cast as a DM description, it can be seen from Table 4.2 that the β_c case points to a radial system, and the corresponding value of the Ξ_1 parameter is not consistent with the GR limit at the 3σ confidence level. In the case of radial anisotropy, we recover a preferentially tangential behaviour, but with a slightly large estimate for the distance and the stellar mass-to-light ratio, while the DHOST parameter is now consistent with the GR limit within a 2σ confidence level. The top panels of Figs. 5.10 and 5.11 clearly show that DHOST cannot replace DM in this context, and both the Bayesian Factor and the suspiciousness point to a strong and significant tension between this scenario and the GR reference case. A standard DM component is required and DHOST cannot effectively play its role. Finally, by looking at the Bayesian quantities $\log \mathscr{B}^i_j$ and $\log S^i_j$, we can see that the case in which the anisotropy is assumed to be constant, had the SHMR been applied, are the best scenarios, being as successful as GR in fitting the velocity dispersion data of DF44.

Nevertheless, it seems to be important and interesting to highlight here that (when we try to mimic DM with the DHOST) when a radial profile is assumed, there is a rise in the dispersion velocity at larger distances from the centre of the galaxy, for which the fit is improved with respect to the corresponding GR case

(although still statistically disfavoured with respect to the reference case which includes DM). Given the fact that the anisotropy function $\beta(r)$ is unknown, we have tried different functional forms to check if we could find one which adapted better to the data. Here we will describe quickly all the cases, but we will focus more only on what resulted to be the best one, which we show in Table 5.4 and in the bottom panel of Fig. 5.10.

Table 5.4: Results from the statistical analysis of NGC1052-DF44 with a "piecewise" anisotropy profile. For each parameter we provide the median and the 1σ constraints; unconstrained parameters are in italic font. The parameters are, from left to right: distance D; mass-to-light ratio Υ; anisotropy function parameters with a division in four bins; gNFW concentration c_{200}, mass M_{200}, and inner log-slope γ; DHOST characteristic scaling Ξ_1; logarithm of the Bayes Factor $\log \mathscr{B}^i_j$; the suspiciousness $\log S^i_j$.

	GR											
	D	Υ_*	β_1	β_2	β_3	β_4	c_{200}	$\log M_{200}$	γ	Ξ_1	$\log \mathscr{B}^i_j$	$\log S^i_j$
	Mpc							$M_\odot$				
Stars only	$152.03^{+10.96}_{-10.94}$	$8.95^{+0.65}_{-0.81}$	$0.14^{+0.13}_{-0.16}$	$0.57^{+0.16}_{-0.20}$	> -5.81	> -6.79	–	–	–	–	$-19.72^{+0.01}_{-0.01}$	$-19.90^{+0.04}_{-0.05}$
SHMR + gNFW	$98.31^{+14.11}_{-13.90}$	$1.53^{+0.39}_{-0.33}$	> -1.15	> -2.84	*−4.45*	*−4.71*	$10.36^{+3.89}_{-3.11}$	$10.93^{+0.15}_{-0.18}$	< 1.00	–	$-0.39^{+0.02}_{-0.02}$	$-0.004^{+0.072}_{-0.067}$
no SHMR + gNFW	$102.18^{+13.73}_{-14.48}$	$1.60^{+0.42}_{-0.34}$	*−4.04*	*−5.25*	*−3.70*	*−5.85*	$13.93^{+6.84}_{-4.31}$	$10.10^{+0.26}_{-0.18}$	> 1.46	–	$-0.20^{+0.01}_{-0.02}$	$-0.20^{+0.05}_{-0.04}$
	DHOST (as dark energy)											
	D	Υ_*	β_1	β_2	β_3	β_4	c_{200}	$\log M_{200}$	γ	Ξ_1	$\log \mathscr{B}^i_j$	$\log S^i_j$
	Mpc							$M_\odot$				
SHMR + gNFW	$95.27^{+13.32}_{-14.08}$	$1.48^{+0.38}_{-0.31}$	$-0.96^{+0.60}_{-0.92}$	> -3.87	*−4.58*	*−5.04*	$9.40^{+3.64}_{-2.67}$	$10.97^{+0.17}_{-0.18}$	< 0.97	$0.24^{+0.48}_{-0.42}$	$-0.54^{+0.02}_{-0.02}$	$0.04^{+0.09}_{-0.08}$
no SHMR + gNFW	$101.40^{+14.12}_{-12.88}$	$1.57^{+0.41}_{-0.31}$	*−3.98*	*−5.83*	*−4.83*	*−7.52*	$18.28^{+9.08}_{-6.99}$	$9.64^{+0.59}_{-0.61}$	> 1.88	$-1.88^{+2.19}_{-4.69}$	$-0.03^{+0.01}_{-0.02}$	$-0.005^{+0.005}_{-0.005}$
	DHOST (as dark matter)											
	D	Υ_*	β_1	β_2	β_3	β_4	c_{200}	$\log M_{200}$	γ	Ξ_1	$\log \mathscr{B}^i_j$	$\log S^i_j$
	Mpc							$M_\odot$				
Stars only	$101.33^{+13.98}_{-14.48}$	$1.54^{+0.42}_{-0.31}$	$0.93^{+0.02}_{-0.02}$	$0.90^{+0.06}_{-0.07}$	> -0.19	*−4.89*	–	–	–	$-18.50^{+4.93}_{-6.75}$	$0.07^{+0.02}_{-0.02}$	$0.10^{+0.05}_{-0.05}$

Our first check has been to examine the impact of the priors on the final results. We relaxed the Gaussian priors on $\log(1-\beta_{0,\infty})$ and we also decided to tighten the flat prior on $r_a \in [0,1]$. However these new conditions did not change, from a statistical point of view, the results already listed in Table 5.3. We then investigated the feasibility of the Osipkov-Merritt profile [357, 358]

$$\beta(r) = \beta_{OM}\frac{r^2}{r^2+r_a^2}. \tag{5.4}$$

Unlike other works [351, 432], we have left the multiplicative factor β_{OM} as a free parameter, imposing a flat prior $\beta_{OM} \in [-10, 1]$. Nevertheless, the Osipkov-Merritt profile has resulted in a poorer fit to the observational data with respect to the cases we have already considered.

Finally, we explored a "piecewise" anisotropy profile, i.e. we assumed that $\beta(r)$ could be constant or radial within different spatially separated bins. We have explored many different configurations, splitting the data from two to four bins, with the latter being the best fit and really improving on the standard scenarios considered in Table 5.4. While the assumption of a radial profile (in each bin) generally produces worse fits to data, when the anisotropy is assumed to be constant we get interesting results. Within GR, we do not really get any statistically significant change with respect to Table 4.2, with similar or sometimes slightly worse values for the Bayes Factor and the suspiciousness. The same consideration holds when we turn our attention to the DHOST gravitational scenario when it reproduces the DE effects.

The most relevant differences concern the case where the DHOST model acts as a substitute for DM. Indeed, in this case, the suspiciousness goes from a strongly negative value of ~ -3 to a slightly positive one of ~ 0.1. In more detail, the distance and the stellar-to-light mass ratio are in perfect agreement with the literature; the anisotropy profile seems to indicate a constant in the first two bins, with a decrease in the outer ones (where we have fewer points and thus only a lower limit can be fixed); and finally, the characteristic DHOST parameter, Ξ_1, is in agreement with the result in Table 5.3. Looking at the lower panel of Fig. 5.10, the DHOST model now seems to fit the observational data as well as GR.

5.4 EFT parameter constraints

In Fig. 5.12 we compare our constraints on Ξ_1, as a function of the ETG parameters α_H and β_1, with others which are in literature, the same ones described in Chapter 4. In blue, we have the constraints obtained from stellar physics arguments as conditions for dynamical equilibrium and for a minimal mass of red dwarf stars; in red, the 2σ limits on γ_0 from the Hulse–Taylor pulsar [249]; in green, the constraints provided by helioseismology arguments [278]; grey points

with error bars represent the results we got in [292] from the analysis of the CLASH galaxy clusters. The new constraints on α_H and β_1, for DF2 [425], which can be derived from our estimations for Ξ_1 are represented by brown lines for NGC1052-DF2, black for NGC1052-DF4 and purple for Dragonfly44. Dashed lines are for the case with the SHMR prior, and solid ones for the case without the SHMR prior, always assuming a constant anisotropy profile.

For DF2 one can conclude that, independently of the considered scenario (i.e. DHOST as DE only or as DM too) our constraints are consistent with GR limits and with literature. In particular with stellar scale limits (blue and green regions), and "contain" the limits from pulsars (red line), which are known to be the most stringent. There is instead a larger tension with estimations from clusters of galaxies (grey points).

For DF4 and DF44, in general, it is possible to see, when the DHOST model is assumed to play the role of DE alone (top panel of Fig. 5.12), the constraints from both galaxies span slightly broader ranges than all those covered by stellar constraints, being consistent with them. They also contain both the ΛCDM limit and the tightest constraint so far from pulsars.

In the bottom panel of Fig. 5.12 the constraints on the DHOST parameters α_H and β_1 when the DHOST model resembles also DM are shown. It is possible to notice that the constraints derived for DF4 are similar to those previously obtained for DF2. This fact is not unexpected since the galaxies are similar in several aspects, such as size, surface brightness, and DM content. But it is also clearly evident that Dragonfly 44 produces constraints that are for a large part not consistent with the other probes which have been considered so far, even in the case of four β bins, which still fit the data. This is a further indication of the difficulty of the DHOST model in describing DM in this galaxy.

5.5 Lesson about DHOST from UDGs

In this chapter, the analysis of the DHOST model introduced in [204, 248, 249] has been deepened. In [292] we started our journey at clusters of galaxies' scales; here we tried to shed light on the dynamics of the Ultra-diffuse galaxy NGC1052-

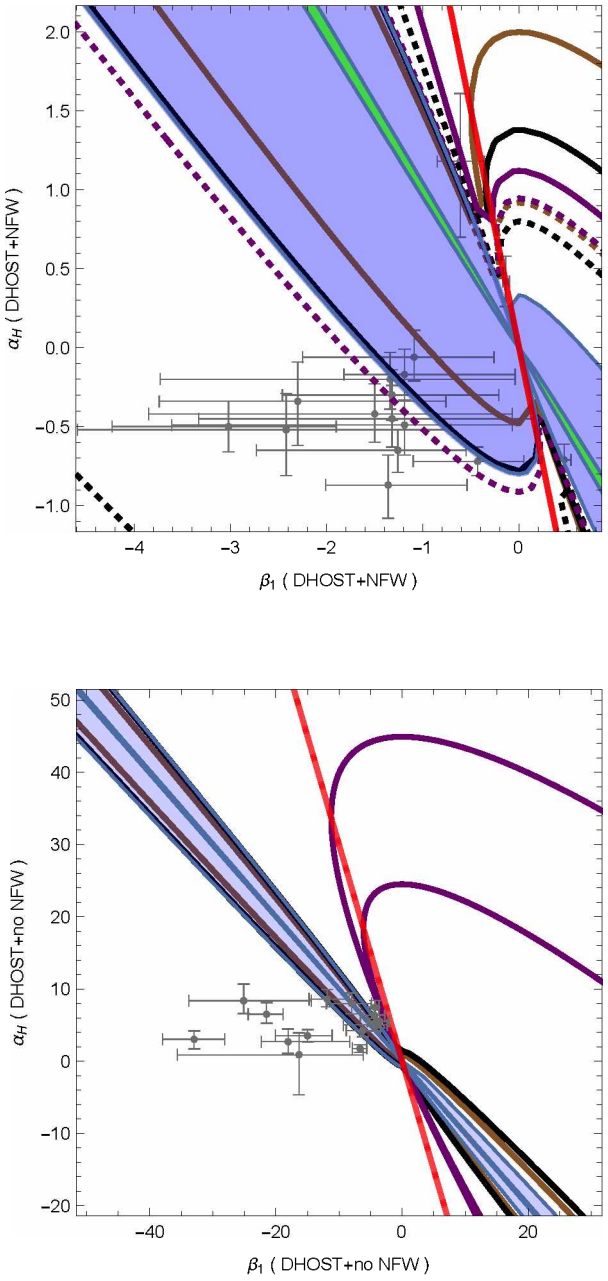

Figure 5.12: Comparison of EFT parameter constraints from our DHOST analysis [425, 426] with [249], [278] and [292]. Top panel: results under the assumption that DHOST mimics DE. Dashed lines are 1σ constraints for the case with SHMR prior; solid lines are 1σ constraints for the case without the SHMR prior. Brown lines are for NGC1052-DF2, black for NGC1052-DF4 and purple for Dragonfly44. Bottom panel: results when DHOST is assumed to play the role of both dark energy and dark matter. In all cases, we assume a constant stellar anisotropy profile. In both panels blue regions are derived from stellar physics considerations [249]; red from 2σ limits on γ_0 from the Hulse-Taylor pulsar; green from helioseismology 2σ constraints [278]. Grey points/crosses are single constraints from *CLASH* clusters from [292].

DF2 which has been claimed to be a "lacking DM galaxy" [175] and, as such, might be a potentially big problem for ETGs.

The mass of NGC1052-DF2 has been inferred using the Jeans equation, Eq. 3.40, and the total mass of the galaxy has been modelled as the sum of DM (if DM is assumed) and a stellar contribution. The DM component has been described using a generalisation of the classical Navarro-Frenk-White profile. We also consider two different models for the anisotropy parameter β: a case where it is constant, and one with a radial profile described by Eq. (3.62).

In agreement with the results of [430], when GR is assumed, the best agreement with the data is obtained when no DM is included at all. While in [430] the authors always include a DM component and conclude that it should be present in a very small amount, we also explicitly consider the case of no DM, i.e. a purely baryonic galaxy. We can conclude that, at least at the scales tested by the observations, the hypothesis of a total absence of DM can be considered a satisfactory option from a statistical point of view. In fact, the inclusion of DM only worsens all the Bayesian indices considered (Bayes Factor and suspiciousness). These results are also quite independent of the priors that can be adopted.

When the DHOST model is assumed to act only as a DE, there is a substantial equivalence between this scenario and the corresponding GR cases, which is somehow expected, because if we have a DM component, the large-scale effects of DE could be expected to be negligible at galactic scales. However, it should be noted that all the Bayesian indicators are improved with respect to the GR+DM cases. Nevertheless, the reference case of GR with only stars is still the most favoured, statistically speaking.

Finally, the DHOST model has been assumed to fully mimic DM: considering a constant anisotropy profile, we even get both a positive Bayes Factor and a positive suspicion. Although they are only slightly larger than zero (but different from it at least at 1σ), they indicate that NGC1052-DF2 can be described quite satisfactorily by our DHOST model, as successfully as by GR.

The mass properties and modelling of NGC1052-DF4 and Dragonfly 44 were carried out as for DF2. In addition, the same DHOST scenarios were analysed.

For NGC1052-DF4, the results are equivalent to those for NGC1052-DF2 [426], of which it can be considered as a twin: the case of a baryonic galaxy

with constant anisotropy is statistically preferred over all other scenarios. The introduction of DM has the net effect of worsening the Bayesian tools. This is particularly evident in cases where a correlation between the stellar and the DM counterpart, in the form of the SHMR prior, has been considered. The discrepancy is less when the stellar and DM components are decoupled. When the DHOST model acts only as a DE, it does not produce significant differences compared to the corresponding GR cases. The main effect is an improvement in the Bayesian indicators for all anisotropy parameter cases, more evident for the SHMR scenario. In general, we have agreement with GR at the 1σ confidence level. When the DHOST model also acts as a replacement for DM, we find that DHOST and GR are still statistically equivalent, with basically no tension.

Thus, combining our results from both NGC1052-DF2 and NGC1052-DF4, we can conclude that the DHOST model may be successful in describing the dynamics of highly DM-deficient or almost completely baryonic galaxies. However, this does not allow us to make an unequivocal claim in favour of the DHOST model. We can only conclude that, in the absence of DM, the DHOST model with only a stellar mass component is consistently able to reproduce the internal dynamics of such galaxies.

For galaxies such as Dragonfly 44, which appear to be dominated by DM, the results are quite different. In general, the best agreement with the data is obtained when GR describes the gravity, with a constant anisotropy scenario and with the stellar and DM components decoupled.

When the DHOST is considered as a DE component, there are no significant differences with respect to the corresponding GR cases. Thus, at least as a DE, DHOST is statistically equivalent to GR. However, when the DHOST model tries to replace the DM, the Bayesian indicators show a high tension for both the constant (β_c) and the radial anisotropy described by Eq. (3.62) compared to the GR reference case. Therefore, we can conclude that the DHOST model is not able to replace DM in a system like DF44. However, if the anisotropy parameter is a "piecewise" function, allowing different constant values within different bins, the situation may change, with the DHOST model now seemingly able to play the role of DM for a dark matter dominated galaxy.

Unfortunately, if we look at the analysis from the more fundamental perspective of the EFT approach and parameters, the situation in the case of Dragonfly 44 is not so easily resolved. While the results of the NGC1052-DF2 and NGC1052-DF4 analyses are perfectly consistent with the constraints imposed by more stringent and precise probes at stellar scales, regardless of the presence or absence of a DM component, Dragonfly 44 is more problematic. If we take our DHOST model as DE only, the agreement is quite good; but if we try to replace DM, the constraints on the EFT parameters are completely inconsistent with the stellar limits. So this scenario seems to be discarded.

CHAPTER 6

Conclusions and Final remarks

In this thesis, we have reported the results of a series of scientific articles aimed at investigating a possible unification of the dark matter and dark energy components, which make up $\sim 95\%$ of the energy/matter budget of our Universe, in a scenario described by an extended theory of gravity. Modifications of Einstein's general theory of relativity have mostly been introduced to replace dark energy, but not dark matter. Moreover, all these theories face the challenge of reproducing the results of General Relativity at those scales at which this theory has been extensively tested and found to be valid. The "safe" mechanism that allows these theories to mimic dark energy at cosmological scales and reduce to General Relativity (at Solar system scales) is called the "screening mechanism".

A unification of the two dark components could be achieved if the screening mechanism, which allows to restore the standard gravitational paradigm, is broken at astrophysical scales. In this way, the effects induced by a gravitational modification could also reproduce the effects normally associated with dark matter. Therefore, there will be no need to describe dark matter as a particle, but it would become a gravitational effect induced by a modified gravity theory.

In this thesis, attention has been focused on a particular model belonging to the family of degenerate higher-order scalar tensor (DHOST) theories, which exhibits

a partial breaking of the so-called Vaishtein screening mechanism.

This rather novel and potentially powerful hypothesis has been tested over a wide range of scales of the large-scale structure of the Universe. At all the scales tested, two different scenarios have been considered:

- the DHOST model mimics the dark energy component alone;
- the DHOST model mimics both the dark energy and the dark matter component as a consequence of the partial breaking of the Vainshtein screening mechanism.

In the first scenario, a dark matter component was always assumed in the total mass budget of the studied objects. In the second scenario, which is the main novel contribution of this work, the observational data have been fitted using only the baryonic component.

The analysis, carried out at different scales, has yielded interesting results, which are shown in bold below.

Initially, the focus was on the scales of galaxy clusters, which serve as the most massive, gravitationally bounded structures in the Universe. The data sets used to test the analysis at these scales are derived from the Cluster Lensing and Supernova Survey with Hubble (*CLASH*) programme, for which both X-ray and gravitational lensing (strong and weak) observations are available. In addition, a multi-component approach has been used to parameterise the masses of the clusters, taking into account not only the contributions from dark matter and X-rays, but also from the Brightest Cluster Galaxy and other stellar non-brightest cluster galaxy components.

- **The DHOST model is slightly favoured over general relativity in reproducing effects associated with dark energy alone.**

When the DHOST model mimics dark energy, we found a slight preference for this model over General Relativity. More importantly, in this scenario the tension that exists in the standard gravitational framework between gravitational lensing and X-ray probes (because they are sensitive to different phenomena) is alleviated, resulting in a better fit to the observational data with respect to General Relativity.

However, the core scenario, according to which dark energy and dark matter could be unified as different effects induced by the same extended theory of gravity, emphasises a more negative conclusion:

- **the DHOST model cannot reproduce the effects associated with dark matter on astrophysical scales.**

The DHOST model, which by partially breaking the Vainshtein screening mechanism could also replace dark matter at galaxy cluster scales, results to be statistically disadvantaged compared to General Relativity.

The natural progression of the analysis was to galactic scales. In particular, the analysis focused on the family of the Ultra-diffuse Galaxies observed with the Dragonfly Telescope Array for which kinematic data were available. Two of them, NGC 1052-DF2 and NGC 1052-DF4, are characterised by a lack of dark matter ($M_{DM} \sim 1\%$ of their total mass), while the third, Dragonfly 44, is a dark matter-dominated galaxy with $M_{DM} \sim 99\%$ of its total mass. Thus, in addition to the above scenarios, another was considered, namely their internal kinematics supported by the stellar components alone, within the framework of General Relativity.

- **The baryonic hypothesis, within the framework of General Relativity in the absence of dark matter, gave the best agreement with the observational data in the case of NGC 1052-DF2 and NGC 1052-DF4, while for Dragonfly 44 a dark matter component is needed.**

To our knowledge, there have been no previous analyses of dark matter-poor galaxies modelled as fully baryonic systems, without including a dark matter component in the total mass budget. Therefore, the results presented here for NGC 1052-DF2 and NGC1052-DF4 are derived for the first time.

From the analysis of the internal kinematics of these galaxies, we can conclude that at the scales tested by the observational data, the hypothesis of a baryonic galaxy for NGC 1052-DF2 and NGC 1052-DF4 can be considered as fully satisfactory from a statistical point of view. On the other hand, for a dark matter-dominated galaxy such as Dragonfly 44, the best scenario within the framework of general relativity is to consider both a dark matter and a stellar component, completely decoupled, assuming a constant anisotropy for the stellar counterpart.

- **The DHOST model as dark energy does not lead to significant changes compared to the corresponding cases of General Relativity.**

As expected, if we still consider a dark matter component in the total mass budget, the large-scale effects associated with the dark energy component are expected to be negligible. Statistically, however, the Bayesian Ratio and the suspiciousness in this case are greatly improved compared to the corresponding General Relativity cases.

- **DHOST model as dark matter is as successful as General Relativity in describing the dynamics of galaxies lacking dark matter while for dark matter-dominated galaxies, the results are more uncertain.**

We show that for galaxies such as NGC 1052-DF2 and NGC 1052-DF4, the scenario in which dark matter can be interpreted as a gravitational effect induced by the DHOST modification of gravity, due to the partial breaking of the Vainshtein screening mechanism, can sustain the dynamics of these galaxies just as successfully as General Relativity.

If we try to apply the same scenario to an antithetic galaxy with respect to the previous two, dominated by dark matter, such as Dragonfly 44, with a constant stellar anisotropy profile, we can conclude that the DHOST model cannot play the role of dark matter. However, if we consider a more sophisticated piecewise parametrization of the anisotropy, constant in each radial bin considered (we have considered a case of four bins), the conclusion is quite different. Indeed, in this case, the DHOST model as dark matter seems to be able to describe the dynamics of a dark matter-dominated galaxy like Dragonfly 44.

- **Effective Field Theory parameters constraints are generally consistent with broader stellar constraints, with the DHOST model failing to produce physically consistent results in the case of Dragonfly 44.**

As for the values of the Effective Field Theory parameters, at galaxy cluster scales the combined use of the two potentials Φ and Ψ allows us to place constraints on both α_H and β_1 separately. The parameter α_H shows constraints compatible with the existing ones derived mainly from stellar scales, while β_1 is only marginally in

agreement with them, at the 1σ confidence level, for the vast majority of clusters. In general, the estimates for both parameters are marginally compatible with the General Relativity limit (α_H,$\beta_1 \to 0$) for most clusters, at least at the 2σ level. At galactic scales, the constraints span somewhat wider ranges than those set by the stellar arguments but still produce results that are fully consistent with them. They also include both the ΛCDM limit and the Hulse-Taylor pulsar constraints.

These results hold in the case where the DHOST model plays only the role of dark energy. When the DHOST model also mimics the dark matter component, the derived constraints on the EFT parameters at galaxy cluster scales are in 3σ agreement with the GR limit, and only marginally in agreement with the stellar and Hulse-Taylor pulsar constraints. For dark matter deficient galaxies, such as NGC 1052-DF2 and NGC 1052-DF4, the limits at α_H and β_1 are consistent with the stellar arguments. However, the case of Dragonfly 44 is more problematic. Indeed, the constraints on the effective field theory parameters are incompatible with the limits on these parameters set by stellar arguments. This result leads us to conclude that the DHOST model as an "effective" component of dark matter seems to have to be discarded for a galaxy like Dragonfly 44.

At the end of this work, we can ask again the question we posed in the introduction: "*Can we unify dark energy and dark matter in a single theoretical background due to the partial breaking of the Vainsthein screening?* In this thesis we have shown that this scenario seems to work only for highly deficient dark matter galaxies, while for clusters and dark matter-dominated galaxies such as Dragonfly 44 a dark matter component should always be considered. Therefore, our answer to the question should be negative. However, further investigation may shed light on the possible unification of the two dark components in a single theoretical background.

Streszczenie rozprawy doktorskiej

Uniwersytet Szczeciński
Instytut Fizyki

mgr Enrico Laudato

Tytuł rozprawy doktorskie: **A DHOST model to unify them all**

promotor: dr hab. Vincenzo Salzano, prof. US

Obecnie, szczególną uwagę poświęcono Rozszerzonym Teoriom Grawitacji z dodatkowymi stopniami swobody, których efekty mogą być tłumione w małych skalach (np. w Układzie Słonecznym) przez mechanizmy ekranujące, przywracające Ogólną Teorię Względności.

W niniejszej rozprawie rozważaliśmy model należący do rodziny zdegenerowanych teorii skalarno-tensorowych wyższego rzędu (DHOST), dla których mechanizm Vainshteina jest częściowo złamany. Przetestowaliśmy, na ile ta własność pozwala, w ramach rozważanego modelu, naśladować zarówno ciemną energię na skalach kosmologicznych, jak i ciemną materię na skalach astrofizycznych. Model ten został zastosowany do gromad galaktyk oraz do ultra-rozproszonych galaktyk (UDGs).

W skali gromady galaktyk próbka 16 gromad galaktyk należących do programu Cluster Lensing and Supernova survey with Hubble (CLASH) została zbadana zużyciem pomiarów promieniowania rentgenowskiego oraz obserwacji silnego i słabego soczewkowania grawitacyjnego. Masy zostały zamodelowane z uwzględnieniem wkładu wszystkich składników: gorącego gazu i galaktyk.

W skali galaktycznej, zbadano wewnętrzną kinematykę trzech galaktyk ultra-rozproszonych (UDG), zidentyfikowanych za pomocą Dragonfly Telescope Array. Masy zostały zamodelowane jako suma ciemnej materii i komponentu gwiazdowego.

Z bayesowskiego punktu widzenia, dla zdecydowanej większości gromad, model DHOST naśladujący składnik ciemnej energii wykazuje łagodnie lepszą zgodność z obserwacjami w porównaniu z Ogólną Teorią Względności. Dodatkowo, istniejące napięcie pomiędzy obserwacjami rentgenowskimi i soczewkowania zostało złagodzone. W przypadku UDGs scenariusz ten jest zasadniczo równoważny z Ogólną Teorią Względności, ponieważ w skalach galaktycznych efekty ciemnej energii są w dużej mierze drugorzędne.

Gdy model DHOST odgrywa również rolę ciemnej materii, ze względu na częściowe łamanie ekranowania Vainsteina, wyniki pokazują, że w skalach gromad galaktyk scenariusz ten jest statystycznie mniej korzystny w porównaniu z Ogólną Teorią Względności, podczas gdy jest statystycznie równoważny z Ogólną Teorią Względności w skalach galaktyk dla galaktyk pozbawionych ciemnej materii.

Słowa kluczowe: soczewkowanie grawitacyjne, kosmologia, ciemna materia, ciemna energia, rozszerzone teorie grawitacji.

Data, podpis

Summary of the Doctoral Thesis

University of Szczecin
Institute of Physics

Enrico Laudato M.Sc.

PhD Thesis entitled: **A DHOST model to unify them all**

supervisor: dr hab. Vincenzo Salzano, prof. US

Recently, special attention has been given to Extended Theories of Gravity with additional degrees of freedom and whose cosmological effects can be suppressed at small scales by some screening mechanism, thus restoring General Relativity.

In this thesis, we have considered a model belonging to the family of Degenerate Higher Orders Scalar Tensor theories, for which the corresponding (Vainshtein) screening mechanism is partially broken. We have tested whether this property allows it to mimic both dark energy on cosmological scales and dark matter on astrophysical scales. This model has been applied to galaxy clusters and to ultra-diffuse galaxies (UDGs).

At galaxy cluster scales a sample of 16 clusters from the Cluster Lensing and Supernova Survey with Hubble (CLASH) programme has been studied using both X-ray and strong and weak gravitational lensing observations. The masses have been modelled including the contributions from all components, the hot gas and the galaxies. At galactic scales, the internal kinematics of three UDGs, identified

with the Dragonfly Telescope Array, have been studied. The masses have been modelled as the sum of the dark matter and stellar components.

From a Bayesian point of view, the DHOST model, which mimics the dark energy component, shows a slight preference over General Relativity for the vast majority of clusters. In addition, the existing tension between the X-ray and lensing probes has been alleviated. For the UDGs, this scenario is essentially equivalent to General Relativity, since dark energy effects are largely subdominant on galactic scales.

When the DHOST model also plays the role of dark matter due to the partial breaking of the Vainstein screening, the results show that at galaxy cluster scales this scenario is statistically disfavoured compared to General Relativity, while at galactic scales it is statistically equivalent to General Relativity in the absence of dark matter galaxies.

Keywords: gravitational lensing, cosmology, dark matter, dark energy, extended theories of gravity.

Date, signature

Bibliography

[1] Adam G. Riess et al. "Observational evidence from supernovae for an accelerating universe and a cosmological constant". In: *Astron. J.* 116 (1998), pp. 1009–1038. DOI: 10.1086/300499. arXiv: astro-ph/9805201.

[2] S. Perlmutter et al. "Measurements of Ω and Λ from 42 high redshift supernovae". In: *Astrophys. J.* 517 (1999), pp. 565–586. DOI: 10.1086/307221. arXiv: astro-ph/9812133.

[3] N. Aghanim et al. "Planck 2018 results. VI. Cosmological parameters". In: *Astron. Astrophys.* 641 (2020). [Erratum: Astron.Astrophys. 652, C4 (2021)], A6. DOI: 10.1051/0004-6361/201833910. arXiv: 1807.06209 [astro-ph.CO].

[4] T. M. C. Abbott et al. "Dark Energy Survey Year 3 results: A 2.7% measurement of baryon acoustic oscillation distance scale at redshift 0.835". In: *Phys. Rev. D* 105.4 (2022), p. 043512. DOI: 10.1103/PhysRevD.105.043512. arXiv: 2107.04646 [astro-ph.CO].

[5] T. M. C. Abbott et al. "First Cosmology Results using Type Ia Supernovae from the Dark Energy Survey: Constraints on Cosmological Parameters". In: *Astrophys. J. Lett.* 872.2 (2019), p. L30. DOI: 10.3847/2041-8213/ab04fa. arXiv: 1811.02374 [astro-ph.CO].

[6] T. M. C. Abbott et al. "Dark Energy Survey Year 3 results: Cosmological constraints from galaxy clustering and weak lensing". In: *Phys. Rev. D* 105.2 (2022), p. 023520. DOI: 10.1103/PhysRevD.105.023520. arXiv: 2105.13549 [astro-ph.CO].

[7] Shadab Alam et al. "Completed SDSS-IV extended Baryon Oscillation Spectroscopic Survey: Cosmological implications from two decades of spectroscopic surveys at the Apache Point Observatory". In: *Phys. Rev. D* 103.8 (2021), p. 083533. DOI: 10.1103/PhysRevD.103.083533. arXiv: 2007.08991 [astro-ph.CO].

[8] F. Zwicky. "On the Masses of Nebulae and of Clusters of Nebulae". In: *Astrophys. J.* 86 (1937), pp. 217–246. DOI: 10.1086/143864.

[9] Vera C. Rubin and Jr. Ford W. Kent. "Rotation of the Andromeda Nebula from a Spectroscopic Survey of Emission Regions". In: ApJ 159 (Feb. 1970), p. 379. DOI: 10.1086/150317.

[10] Pavan Kumar Aluri et al. "Is the observable Universe consistent with the cosmological principle?" In: *Class. Quant. Grav.* 40.9 (2023), p. 094001. DOI: 10.1088/1361-6382/acbefc. arXiv: 2207.05765 [astro-ph.CO].

[11] Eleonora Di Valentino et al. "In the realm of the Hubble tension—a review of solutions". In: *Class. Quant. Grav.* 38.15 (2021), p. 153001. DOI: 10.1088/1361-6382/ac086d. arXiv: 2103.01183 [astro-ph.CO].

[12] Adam G. Riess et al. "A Comprehensive Measurement of the Local Value of the Hubble Constant with 1 km s^{-1} Mpc^{-1} Uncertainty from the Hubble Space Telescope and the SH0ES Team". In: *Astrophys. J. Lett.* 934.1 (2022), p. L7. DOI: 10.3847/2041-8213/ac5c5b. arXiv: 2112.04510 [astro-ph.CO].

[13] Adam G. Riess and Louise Breuval. "The Local Value of H_0". In: Aug. 2023. arXiv: 2308.10954 [astro-ph.CO].

[14] G. Hinshaw et al. "Nine-Year Wilkinson Microwave Anisotropy Probe (WMAP) Observations: Cosmological Parameter Results". In: *arXiv e-prints*, arXiv:1212.5226 (Dec. 2012), arXiv:1212.5226. DOI: 10.48550/arXiv.1212.5226. arXiv: 1212.5226 [astro-ph.CO].

[15] J. W. Henning et al. "Measurements of the Temperature and E-Mode Polarization of the CMB from 500 Square Degrees of SPTpol Data". In: *Astrophys. J.* 852.2 (2018), p. 97. DOI: 10.3847/1538-4357/aa9ff4. arXiv: 1707.09353 [astro-ph.CO].

[16] D. Dutcher et al. "Measurements of the E-mode polarization and temperature-E-mode correlation of the CMB from SPT-3G 2018 data". In: *Phys. Rev. D* 104.2 (2021), p. 022003. DOI: 10.1103/PhysRevD.104.022003. arXiv: 2101.01684 [astro-ph.CO].

[17] Simone Aiola et al. "The Atacama Cosmology Telescope: DR4 Maps and Cosmological Parameters". In: *JCAP* 12 (2020), p. 047. DOI: 10.1088/1475-7516/2020/12/047. arXiv: 2007.07288 [astro-ph.CO].

[18] Ke Wang and Qing-Guo Huang. "Implications for cosmology from Ground-based Cosmic Microwave Background observations". In: *JCAP* 06 (2020), p. 045. DOI: 10.1088/1475-7516/2020/06/045. arXiv: 1912.05491 [astro-ph.CO].

[19] Ryan J. Cooke, Max Pettini, and Charles C. Steidel. "One Percent Determination of the Primordial Deuterium Abundance". In: *Astrophys. J.* 855.2 (2018), p. 102. DOI: 10.3847/1538-4357/aaab53. arXiv: 1710.11129 [astro-ph.CO].

[20] Mikhail M. Ivanov, Marko Simonović, and Matias Zaldarriaga. "Cosmological Parameters from the BOSS Galaxy Power Spectrum". In: *JCAP* 05 (2020), p. 042. DOI: 10.1088/1475-7516/2020/05/042. arXiv: 1909.05277 [astro-ph.CO].

[21] Guido D'Amico et al. "The Cosmological Analysis of the SDSS/BOSS data from the Effective Field Theory of Large-Scale Structure". In: *JCAP* 05 (2020), p. 005. DOI: 10.1088/1475-7516/2020/05/005. arXiv: 1909.05271 [astro-ph.CO].

[22] Brent Follin and Lloyd Knox. "Insensitivity of the distance ladder Hubble constant determination to Cepheid calibration modelling choices". In: *Mon. Not. Roy. Astron. Soc.* 477.4 (2018), pp. 4534–4542. DOI: 10.1093/mnras/sty720. arXiv: 1707.01175 [astro-ph.CO].

[23] G. Pietrzynski et al. "A distance to the Large Magellanic Cloud that is precise to one per cent". In: *arXiv e-prints*, arXiv:1903.08096 (Mar. 2019), arXiv:1903.08096. DOI: 10.48550/arXiv.1903.08096. arXiv: 1903.08096 [astro-ph.GA].

[24] M. J. Reid, D. W. Pesce, and A. G. Riess. "An Improved Distance to NGC 4258 and its Implications for the Hubble Constant". In: *Astrophys. J. Lett.* 886.2 (2019), p. L27. DOI: 10.3847/2041-8213/ab552d. arXiv: 1908.05625 [astro-ph.GA].

[25] Wenlong Yuan et al. "Absolute Calibration of Cepheid Period-Luminosity Relations in NGC 4258". In: *arXiv e-prints*, arXiv:2203.06681 (Mar. 2022), arXiv:2203.06681. DOI: 10.48550/arXiv.2203.06681. arXiv: 2203.06681 [astro-ph.GA].

[26] Wilmar Cardona, Martin Kunz, and Valeria Pettorino. "Determining H_0 with Bayesian hyper-parameters". In: *JCAP* 03 (2017), p. 056. DOI: 10.1088/1475-7516/2017/03/056. arXiv: 1611.06088 [astro-ph.CO].

[27] David Camarena and Valerio Marra. "Local determination of the Hubble constant and the deceleration parameter". In: *Phys. Rev. Res.* 2.1 (2020), p. 013028. DOI: 10.1103/PhysRevResearch.2.013028. arXiv: 1906.11814 [astro-ph.CO].

[28] Suhail Dhawan, Saurabh W. Jha, and Bruno Leibundgut. "Measuring the Hubble constant with Type Ia supernovae as near-infrared standard candles". In: *Astron. Astrophys.* 609 (2018), A72. DOI: 10.1051/0004-6361/201731501. arXiv: 1707.00715 [astro-ph.CO].

[29] Christopher R. Burns et al. "The Carnegie Supernova Project: Absolute Calibration and the Hubble Constant". In: *Astrophys. J.* 869.1 (2018), p. 56. DOI: 10.3847/1538-4357/aae51c. arXiv: 1809.06381 [astro-ph.CO].

[30] John Soltis, Stefano Casertano, and Adam G. Riess. "The Parallax of ω Centauri Measured from Gaia EDR3 and a Direct, Geometric Calibration of the Tip of the Red Giant Branch and the Hubble Constant". In: *Astrophys. J. Lett.* 908.1 (2021), p. L5. DOI: 10.3847/2041-8213/abdbad. arXiv: 2012.09196 [astro-ph.GA].

[31] Wendy L. Freedman et al. "Calibration of the Tip of the Red Giant Branch (TRGB)". In: (Feb. 2020). DOI: 10.3847/1538-4357/ab7339. arXiv: 2002.01550 [astro-ph.GA].

[32] Wendy L. Freedman et al. "The Carnegie-Chicago Hubble Program. VIII. An Independent Determination of the Hubble Constant Based on the Tip of the Red Giant Branch". In: *Astrophys. J.* 882 (2019), p. 34. DOI: 10.3847/1538-4357/ab2f73. arXiv: 1907.05922 [astro-ph.CO].

[33] Wenlong Yuan et al. "Consistent Calibration of the Tip of the Red Giant Branch in the Large Magellanic Cloud on the Hubble Space Telescope Photometric System and a Redetermination of the Hubble Constant". In: *Astrophys. J.* 886 (2019), p. 61. DOI: 10.3847/1538-4357/ab4bc9. arXiv: 1908.00993 [astro-ph.GA].

[34] In Sung Jang and Myung Gyoon Lee. "The Tip of the Red Giant Branch Distances to Type Ia Supernova Host Galaxies. IV. Color Dependence and Zero-point Calibration". In: ApJ 835.1, 28 (Jan. 2017), p. 28. DOI: 10.3847/1538-4357/835/1/28. arXiv: 1611.05040 [astro-ph.GA].

[35] Caroline D. Huang et al. "Hubble Space Telescope Observations of Mira Variables in the Type Ia Supernova Host NGC 1559: An Alternative Candle to Measure the Hubble Constant". In: (Aug. 2019). DOI: 10.3847/1538-4357/ab5dbd. arXiv: 1908.10883 [astro-ph.CO].

[36] John P. Blakeslee et al. "The Hubble Constant from Infrared Surface Brightness Fluctuation Distances". In: *Astrophys. J.* 911.1 (2021), p. 65. DOI: 10.3847/1538-4357/abe86a. arXiv: 2101.02221 [astro-ph.CO].

[37] Nandita Khetan et al. "A new measurement of the Hubble constant using Type Ia supernovae calibrated with surface brightness fluctuations". In: *Astron. Astrophys.* 647 (2021), A72. DOI: 10.1051/0004-6361/202039196. arXiv: 2008.07754 [astro-ph.CO].

[38] Ehsan Kourkchi et al. "Cosmicflows-4: The Calibration of Optical and Infrared Tully–Fisher Relations". In: *Astrophys. J.* 896.1 (2020), p. 3. DOI: 10.3847/1538-4357/ab901c. arXiv: 2004.14499 [astro-ph.GA].

[39] James Schombert, Stacy McGaugh, and Federico Lelli. "Using the Baryonic Tully–Fisher Relation to Measure H o". In: *Astron. J.* 160.2 (2020), p. 71. DOI: 10.3847/1538-3881/ab9d88. arXiv: 2006.08615 [astro-ph.CO].

[40] T. de Jaeger et al. "A measurement of the Hubble constant from Type II supernovae". In: *Mon. Not. Roy. Astron. Soc.* 496.3 (2020), pp. 3402–3411. DOI: 10.1093/mnras/staa1801. arXiv: 2006.03412 [astro-ph.CO].

[41] D. W. Pesce et al. "The Megamaser Cosmology Project. XIII. Combined Hubble constant constraints". In: *Astrophys. J. Lett.* 891.1 (2020), p. L1. DOI: 10.3847/2041-8213/ab75f0. arXiv: 2001.09213 [astro-ph.CO].

[42] S. Birrer et al. "H0LiCOW - IX. Cosmographic analysis of the doubly imaged quasar SDSS 1206+4332 and a new measurement of the Hubble constant". In: *Mon. Not. Roy. Astron. Soc.* 484 (2019), p. 4726. DOI: 10.1093/mnras/stz200. arXiv: 1809.01274 [astro-ph.CO].

[43] Kenneth C. Wong et al. "H0LiCOW – XIII. A 2.4 per cent measurement of H0 from lensed quasars: 5.3σ tension between early- and late-Universe probes". In: *Mon. Not. Roy. Astron. Soc.* 498.1 (2020), pp. 1420–1439. DOI: 10.1093/mnras/stz3094. arXiv: 1907.04869 [astro-ph.CO].

[44] Raul Jimenez and Abraham Loeb. "Constraining cosmological parameters based on relative galaxy ages". In: *Astrophys. J.* 573 (2002), pp. 37–42. DOI: 10.1086/340549. arXiv: astro-ph/0106145.

[45] Michele Moresco et al. "Constraining the expansion rate of the Universe using low-redshift ellipticals as cosmic chronometers". In: *JCAP* 03 (2011), p. 045. DOI: 10.1088/1475-7516/2011/03/045. arXiv: 1010.0831 [astro-ph.CO].

[46] M. Moresco et al. "Improved constraints on the expansion rate of the Universe up to z~1.1 from the spectroscopic evolution of cosmic chronometers". In: *JCAP* 08 (2012), p. 006. DOI: 10.1088/1475-7516/2012/08/006. arXiv: 1201.3609 [astro-ph.CO].

[47] Yun Chen, Suresh Kumar, and Bharat Ratra. "Determining the Hubble constant from Hubble parameter measurements". In: *Astrophys. J.* 835.1 (2017), p. 86. DOI: 10.3847/1538-4357/835/1/86. arXiv: 1606.07316 [astro-ph.CO].

[48] Michele Moresco et al. "Constraining the expansion rate of the Universe using low-redshift ellipticals as cosmic chronometers". In: J. Cosmology Astropart. Phys. 2011.3, 045 (Mar. 2011), p. 045. DOI: 10.1088/1475-7516/2011/03/045. arXiv: 1010.0831 [astro-ph.CO].

[49] Hai Yu, Bharat Ratra, and Fa-Yin Wang. "Hubble Parameter and Baryon Acoustic Oscillation Measurement Constraints on the Hubble Constant, the Deviation from the Spatially Flat ΛCDM Model, the Deceleration–Acceleration Transition Redshift, and Spatial Curvature". In: *Astrophys. J.* 856.1 (2018), p. 3. DOI: 10.3847/1538-4357/aab0a2. arXiv: 1711.03437 [astro-ph.CO].

[50] Adrià Gómez-Valent and Luca Amendola. "H_0 from cosmic chronometers and Type Ia supernovae, with Gaussian Processes and the novel Weighted Polynomial Regression method". In: *JCAP* 04 (2018), p. 051. DOI: 10.1088/1475-7516/2018/04/051. arXiv: 1802.01505 [astro-ph.CO].

[51] Balakrishna S. Haridasu et al. "An improved model-independent assessment of the late-time cosmic expansion". In: *JCAP* 10 (2018), p. 015. DOI: 10.1088/1475-7516/2018/10/015. arXiv: 1805.03595 [astro-ph.CO].

[52] Koushik Dutta et al. "Cosmology with low-redshift observations: No signal for new physics". In: *Phys. Rev. D* 100.10 (2019), p. 103501. DOI: 10.1103/PhysRevD.100.103501. arXiv: 1908.07267 [astro-ph.CO].

[53] C. Krishnan et al. "Is there an early Universe solution to Hubble tension?" In: *Phys. Rev. D* 102.10 (2020), p. 103525. DOI: 10.1103/PhysRevD.102.103525. arXiv: 2002.06044 [astro-ph.CO].

[54] Fabrizio Renzi and Alessandra Silvestri. "Hubble speed from first principles". In: *Phys. Rev. D* 107.2 (2023), p. 023520. DOI: 10.1103/PhysRevD.107.023520. arXiv: 2011.10559 [astro-ph.CO].

[55] Rafael C. Nunes and Armando Bernui. "BAO signatures in the 2-point angular correlations and the Hubble tension". In: *Eur. Phys. J. C* 80.11 (2020), p. 1025. DOI: 10.1140/epjc/s10052-020-08601-8. arXiv: 2008.03259 [astro-ph.CO].

[56] Xue Zhang and Qing-Guo Huang. "Hubble constant and sound horizon from the late-time Universe". In: *Phys. Rev. D* 103.4 (2021), p. 043513. DOI: 10.1103/PhysRevD.103.043513. arXiv: 2006.16692 [astro-ph.CO].

[57] B. P. Abbott et al. "A gravitational-wave standard siren measurement of the Hubble constant". In: *Nature* 551.7678 (2017), pp. 85–88. DOI: 10.1038/nature24471. arXiv: 1710.05835 [astro-ph.CO].

[58] Suvodip Mukherjee et al. "Velocity correction for Hubble constant measurements from standard sirens". In: *Astron. Astrophys.* 646 (2021), A65. DOI: 10.1051/0004-6361/201936724. arXiv: 1909.08627 [astro-ph.CO].

[59] M. Fishbach et al. "A Standard Siren Measurement of the Hubble Constant from GW170817 without the Electromagnetic Counterpart". In: *Astrophys. J. Lett.* 871.1 (2019), p. L13. DOI: 10.3847/2041-8213/aaf96e. arXiv: 1807.05667 [astro-ph.CO].

[60] M. Soares-Santos et al. "First Measurement of the Hubble Constant from a Dark Standard Siren using the Dark Energy Survey Galaxies and the LIGO/Virgo Binary–Black-hole Merger GW170814". In: *Astrophys. J. Lett.* 876.1 (2019), p. L7. DOI: 10.3847/2041-8213/ab14f1. arXiv: 1901.01540 [astro-ph.CO].

[61] W. Ballard et al. "A Dark Siren Measurement of the Hubble Constant with the LIGO/Virgo Gravitational Wave Event GW190412 and DESI Galaxies". In: *Res. Notes AAS* 7.11 (2023), p. 250. DOI: 10.3847/2515-5172/ad0eda. arXiv: 2311.13062 [astro-ph.CO].

[62] V. Alfradique et al. "A dark siren measurement of the Hubble constant using gravitational wave events from the first three LIGO/Virgo observing runs and DELVE". In: (Oct. 2023). arXiv: 2310.13695 [astro-ph.CO].

[63] Paolo Cremonese and Vincenzo Salzano. "High accuracy on H_0 constraints from gravitational wave lensing events". In: *Phys. Dark Univ.* 28 (2020), p. 100517. DOI: 10.1016/j.dark.2020.100517. arXiv: 1911.11786 [astro-ph.CO].

[64] Marika Asgari et al. "KiDS-1000 Cosmology: Cosmic shear constraints and comparison between two point statistics". In: *Astron. Astrophys.* 645 (2021), A104. DOI: 10.1051/0004-6361/202039070. arXiv: 2007.15633 [astro-ph.CO].

[65] G. F. Lesci et al. "AMICO galaxy clusters in KiDS-DR3: Cosmological constraints from counts and stacked weak lensing". In: *Astron. Astrophys.* 659 (2022), A88. DOI: 10.1051/0004-6361/202040194. arXiv: 2012.12273 [astro-ph.CO].

[66] Shi-Fan Chen, Zvonimir Vlah, and Martin White. "A new analysis of galaxy 2-point functions in the BOSS survey, including full-shape information and post-reconstruction BAO". In: *JCAP* 02.02 (2022), p. 008. DOI: 10.1088/1475-7516/2022/02/008. arXiv: 2110.05530 [astro-ph.CO].

[67] David J. Bacon, Alexandre R. Refregier, and Richard S. Ellis. "Detection of weak gravitational lensing by large-scale structure". In: MNRAS 318.2 (Oct. 2000), pp. 625–640. DOI: 10.1046/j.1365-8711.2000.03851.x. arXiv: astro-ph/0003008 [astro-ph].

[68] Nick Kaiser, Gillian Wilson, and Gerard A. Luppino. "Large scale cosmic shear measurements". In: (Mar. 2000). arXiv: astro-ph/0003338.

[69] L. Van Waerbeke et al. "Detection of correlated galaxy ellipticities from CFHT data: first evidence for gravitational lensing by large-scale structures". In: A&A 358 (June 2000), pp. 30–44. DOI: 10.48550/arXiv.astro-ph/0002500. arXiv: astro-ph/0002500 [astro-ph].

[70] David M. Wittman et al. "Detection of weak gravitational lensing distortions of distant galaxies by cosmic dark matter at large scales". In: Nature 405.6783 (May 2000), pp. 143–148. DOI: 10.1038/35012001. arXiv: astro-ph/0003014 [astro-ph].

[71] Niall MacCrann et al. "Cosmic discordance: are Planck CMB and CFHTLenS weak lensing measurements out of tune?" In: MNRAS 451.3 (Aug. 2015), pp. 2877–2888. DOI: 10.1093/mnras/stv1154. arXiv: 1408.4742 [astro-ph.CO].

[72] Konrad Kuijken et al. "Gravitational Lensing Analysis of the Kilo Degree Survey". In: *Mon. Not. Roy. Astron. Soc.* 454.4 (2015), pp. 3500–3532. DOI: 10.1093/mnras/stv2140. arXiv: 1507.00738 [astro-ph.CO].

[73] H. Hildebrandt et al. "KiDS-450: Cosmological parameter constraints from tomographic weak gravitational lensing". In: *Mon. Not. Roy. Astron. Soc.* 465 (2017), p. 1454. DOI: 10.1093/mnras/stw2805. arXiv: 1606.05338 [astro-ph.CO].

[74] I. Fenech Conti et al. "Calibration of weak-lensing shear in the Kilo-Degree Survey". In: *Mon. Not. Roy. Astron. Soc.* 467.2 (2017), pp. 1627–1651. DOI: 10.1093/mnras/stx200. arXiv: 1606.05337 [astro-ph.CO].

[75] Shahab Joudaki et al. "KiDS-450: Testing extensions to the standard cosmological model". In: *Mon. Not. Roy. Astron. Soc.* 471.2 (2017), pp. 1259–1279. DOI: 10.1093/mnras/stx998. arXiv: 1610.04606 [astro-ph.CO].

[76] Shahab Joudaki et al. "KiDS-450 + 2dFLenS: Cosmological parameter constraints from weak gravitational lensing tomography and overlapping redshift-space galaxy clustering". In: *Mon. Not. Roy. Astron. Soc.* 474.4 (2018), pp. 4894–4924. DOI: 10.1093/mnras/stx2820. arXiv: 1707.06627 [astro-ph.CO].

[77] H. Hildebrandt et al. "KiDS+VIKING-450: Cosmic shear tomography with optical and infrared data". In: *Astron. Astrophys.* 633 (2020), A69. DOI: 10.1051/0004-6361/201834878. arXiv: 1812.06076 [astro-ph.CO].

[78] Catherine Heymans et al. "KiDS-1000 Cosmology: Multi-probe weak gravitational lensing and spectroscopic galaxy clustering constraints". In: *Astron. Astrophys.* 646 (2021), A140. DOI: 10.1051/0004-6361/202039063. arXiv: 2007.15632 [astro-ph.CO].

[79] S. Joudaki et al. "KiDS+VIKING-450 and DES-Y1 combined: Cosmology with cosmic shear". In: *Astron. Astrophys.* 638 (2020), p. L1. DOI: 10.1051/0004-6361/201936154. arXiv: 1906.09262 [astro-ph.CO].

[80] Marika Asgari et al. "KiDS+VIKING-450 and DES-Y1 combined: Mitigating baryon feedback uncertainty with COSEBIs". In: *Astron. Astrophys.* 634 (2020), A127. DOI: 10.1051/0004-6361/201936512. arXiv: 1910.05336 [astro-ph.CO].

[81] Fabio Bellagamba et al. "AMICO: optimized detection of galaxy clusters in photometric surveys". In: *Mon. Not. Roy. Astron. Soc.* 473.4 (2018), pp. 5221–5236. DOI: 10.1093/mnras/stx2701. arXiv: 1705.03029 [astro-ph.CO].

[82] Nathalie Palanque-Delabrouille et al. "Hints, neutrino bounds and WDM constraints from SDSS DR14 Lyman-α and Planck full-survey data". In: *JCAP* 04 (2020), p. 038. DOI: 10.1088/1475-7516/2020/04/038. arXiv: 1911.09073 [astro-ph.CO].

[83] Steven Weinberg. "The cosmological constant problem". In: *Rev. Mod. Phys.* 61 (1 Jan. 1989), pp. 1–23. DOI: 10.1103/RevModPhys.61.1. URL: https://link.aps.org/doi/10.1103/RevModPhys.61.1.

[84] Philip Bull et al. "Beyond ΛCDM: Problems, solutions, and the road ahead". In: *Phys. Dark Univ.* 12 (2016), pp. 56–99. DOI: 10.1016/j.dark.2016.02.001. arXiv: 1512.05356 [astro-ph.CO].

[85] Edmund J. Copeland, M. Sami, and Shinji Tsujikawa. "Dynamics of dark energy". In: *Int. J. Mod. Phys. D* 15 (2006), pp. 1753–1936. DOI: 10.1142/S021827180600942X. arXiv: hep-th/0603057.

[86] Michel Chevallier and David Polarski. "Accelerating universes with scaling dark matter". In: *Int. J. Mod. Phys. D* 10 (2001), pp. 213–224. DOI: 10.1142/S0218271801000822. arXiv: gr-qc/0009008.

[87] Eric V. Linder. "Exploring the expansion history of the universe". In: *Phys. Rev. Lett.* 90 (2003), p. 091301. DOI: 10.1103/PhysRevLett.90.091301. arXiv: astro-ph/0208512.

[88] Harvinder Kaur Jassal, J. S. Bagla, and T. Padmanabhan. "Observational constraints on low redshift evolution of dark energy: How consistent are different observations?" In: *Phys. Rev. D* 72 (2005), p. 103503. DOI: 10.1103/PhysRevD.72.103503. arXiv: astro-ph/0506748.

[89] G. Efstathiou. "Constraining the equation of state of the universe from distant type Ia supernovae and cosmic microwave background anisotropies". In: *Mon. Not. Roy. Astron. Soc.* 310 (1999), pp. 842–850. DOI: 10.1046/j.1365-8711.1999.02997.x. arXiv: astro-ph/9904356.

[90] E. M. Barboza Jr. and J. S. Alcaniz. "A parametric model for dark energy". In: *Phys. Lett. B* 666 (2008), pp. 415–419. DOI: 10.1016/j.physletb.2008.08.012. arXiv: 0805.1713 [astro-ph].

[91] Takeshi Chiba, Takahiro Okabe, and Masahide Yamaguchi. "Kinetically driven quintessence". In: *Phys. Rev. D* 62 (2000), p. 023511. DOI: 10.1103/PhysRevD.62.023511. arXiv: astro-ph/9912463.

[92] R. R. Caldwell. "A Phantom menace?" In: *Phys. Lett. B* 545 (2002), pp. 23–29. DOI: 10.1016/S0370-2693(02)02589-3. arXiv: astro-ph/9908168.

[93] Eleonora Di Valentino, Ankan Mukherjee, and Anjan A. Sen. "Dark Energy with Phantom Crossing and the H_0 Tension". In: *Entropy* 23.4 (2021), p. 404. DOI: 10.3390/e23040404. arXiv: 2005.12587 [astro-ph.CO].

[94] Marc Kamionkowski, Josef Pradler, and Devin G. E. Walker. "Dark energy from the string axiverse". In: *Phys. Rev. Lett.* 113.25 (2014), p. 251302. DOI: 10.1103/PhysRevLett.113.251302. arXiv: 1409.0549 [hep-ph].

[95] Anton Chudaykin, Dmitry Gorbunov, and Nikita Nedelko. "Combined analysis of Planck and SPTPol data favors the early dark energy models". In: *JCAP* 08 (2020), p. 013. DOI: 10.1088/1475-7516/2020/08/013. arXiv: 2004.13046 [astro-ph.CO].

[96] Prateek Agrawal et al. "Rock 'n' Roll Solutions to the Hubble Tension". In: (Apr. 2019). arXiv: 1904.01016 [astro-ph.CO].

[97] Tristan L. Smith, Vivian Poulin, and Mustafa A. Amin. "Oscillating scalar fields and the Hubble tension: a resolution with novel signatures". In: *Phys. Rev. D* 101.6 (2020), p. 063523. DOI: 10.1103/PhysRevD.101.063523. arXiv: 1908.06995 [astro-ph.CO].

[98] Stephon Alexander and Evan McDonough. "Axion-Dilaton Destabilization and the Hubble Tension". In: *Phys. Lett. B* 797 (2019), p. 134830. DOI: 10.1016/j.physletb.2019.134830. arXiv: 1904.08912 [astro-ph.CO].

[99] Gen Ye and Yun-Song Piao. "Is the Hubble tension a hint of AdS phase around recombination?" In: *Phys. Rev. D* 101.8 (2020), p. 083507. DOI: 10.1103/PhysRevD.101.083507. arXiv: 2001.02451 [astro-ph.CO].

[100] Meng-Xiang Lin et al. "Acoustic Dark Energy: Potential Conversion of the Hubble Tension". In: *Phys. Rev. D* 100.6 (2019), p. 063542. DOI: 10.1103/PhysRevD.100.063542. arXiv: 1905.12618 [astro-ph.CO].

[101] David Lovelock. "The Einstein Tensor and Its Generalizations". In: *Journal of Mathematical Physics* 12.3 (Oct. 2003), pp. 498–501. ISSN: 0022-2488. DOI: 10.1063/1.1665613. eprint: https://pubs.aip.org/aip/jmp/article-pdf/12/3/498/10951642/498_1_online.pdf. URL: https://doi.org/10.1063/1.1665613.

[102] David Lovelock. "The Four-Dimensionality of Space and the Einstein Tensor". In: *Journal of Mathematical Physics* 13.6 (Oct. 2003), pp. 874–876. ISSN: 0022-2488. DOI: 10.1063/1.1666069. eprint: https://pubs.aip.org/aip/jmp/article-pdf/13/6/874/10952017/874_1_online.pdf. URL: https://doi.org/10.1063/1.1666069.

[103] Kazuya Koyama. "Cosmological Tests of Modified Gravity". In: *Rept. Prog. Phys.* 79.4 (2016), p. 046902. DOI: 10.1088/0034-4885/79/4/046902. arXiv: 1504.04623 [astro-ph.CO].

[104] Fulvio Sbisà. "Classical and quantum ghosts". In: *Eur. J. Phys.* 36 (2015), p. 015009. DOI: 10.1088/0143-0807/36/1/015009. arXiv: 1406.4550 [hep-th].

[105] Justin Khoury and Amanda Weltman. "Chameleon cosmology". In: *Phys. Rev. D* 69 (2004), p. 044026. DOI: 10.1103/PhysRevD.69.044026. arXiv: astro-ph/0309411.

[106] Justin Khoury and Amanda Weltman. "Chameleon fields: Awaiting surprises for tests of gravity in space". In: *Phys. Rev. Lett.* 93 (2004), p. 171104. DOI: 10.1103/PhysRevLett.93.171104. arXiv: astro-ph/0309300.

[107] Kurt Hinterbichler and Justin Khoury. "Screening Long-Range Forces through Local Symmetry Restoration". In: *Phys. Rev. Lett.* 104 (23 June 2010), p. 231301. DOI: 10.1103/PhysRevLett.104.231301. URL: https://link.aps.org/doi/10.1103/PhysRevLett.104.231301.

[108] Philippe Brax et al. "Dilaton and modified gravity". In: *Phys. Rev. D* 82 (6 Sept. 2010), p. 063519. DOI: 10.1103/PhysRevD.82.063519. URL: https://link.aps.org/doi/10.1103/PhysRevD.82.063519.

[109] Alberto Nicolis, Riccardo Rattazzi, and Enrico Trincherini. "The Galileon as a local modification of gravity". In: *Phys. Rev. D* 79 (2009), p. 064036. DOI: 10.1103/PhysRevD.79.064036. arXiv: 0811.2197 [hep-th].

[110] Christopher Eling, Ted Jacobson, and David Mattingly. "Einstein-Aether theory". In: *Deserfest: A Celebration of the Life and Works of Stanley Deser*. Oct. 2004, pp. 163–179. arXiv: gr-qc/0410001.

[111] Ted Jacobson. "Einstein-aether gravity: A Status report". In: *PoS* QG-PH (2007), p. 020. DOI: 10.22323/1.043.0020. arXiv: 0801.1547 [gr-qc].

[112] Kurt Hinterbichler. "Theoretical Aspects of Massive Gravity". In: *Rev. Mod. Phys.* 84 (2012), pp. 671–710. DOI: 10.1103/RevModPhys.84.671. arXiv: 1105.3735 [hep-th].

[113] Claudia de Rham. "Massive Gravity". In: *Living Rev. Rel.* 17 (2014), p. 7. DOI: 10.12942/lrr-2014-7. arXiv: 1401.4173 [hep-th].

[114] M. Banados, P. G. Ferreira, and C. Skordis. "Eddington-Born-Infeld gravity and the large scale structure of the Universe". In: *Phys. Rev. D* 79 (2009), p. 063511. DOI: 10.1103/PhysRevD.79.063511. arXiv: 0811.1272 [astro-ph].

[115] Antonio De Felice et al. "Minimal Theory of Bigravity: construction and cosmology". In: *JCAP* 04 (2021), p. 015. DOI: 10.1088/1475-7516/2021/04/015. arXiv: 2012.01073 [gr-qc].

[116] Lavinia Heisenberg. "Scalar-Vector-Tensor Gravity Theories". In: *JCAP* 10 (2018), p. 054. DOI: 10.1088/1475-7516/2018/10/054. arXiv: 1801.01523 [gr-qc].

[117] Lavinia Heisenberg, Ryotaro Kase, and Shinji Tsujikawa. "Cosmology in scalar-vector-tensor theories". In: *Phys. Rev. D* 98.2 (2018), p. 024038. DOI: 10.1103/PhysRevD.98.024038. arXiv: 1805.01066 [gr-qc].

[118] Alexei A. Starobinsky. "A New Type of Isotropic Cosmological Models Without Singularity". In: *Phys. Lett. B* 91 (1980). Ed. by I. M. Khalatnikov and V. P. Mineev, pp. 99–102. DOI: 10.1016/0370-2693(80)90670-X.

[119] Salvatore Capozziello. "Curvature quintessence". In: *Int. J. Mod. Phys. D* 11 (2002), pp. 483–492. DOI: 10.1142/S0218271802002025. arXiv: gr-qc/0201033.

[120] Shin'ichi Nojiri and Sergei D. Odintsov. "Modified $f(R)$ gravity consistent with realistic cosmology: From a matter dominated epoch to a dark energy universe". In: *Phys. Rev. D* 74 (8 Oct. 2006), p. 086005. DOI: 10.1103/PhysRevD.74.086005. URL: https://link.aps.org/doi/10.1103/PhysRevD.74.086005.

[121] Antonio De Felice and Shinji Tsujikawa. "f(R) theories". In: *Living Rev. Rel.* 13 (2010), p. 3. DOI: 10.12942/lrr-2010-3. arXiv: 1002.4928 [gr-qc].

[122] Thomas P. Sotiriou and Valerio Faraoni. "$f(R)$ theories of gravity". In: *Rev. Mod. Phys.* 82 (1 Mar. 2010), pp. 451–497. DOI: 10.1103/RevModPhys.82.451. URL: https://link.aps.org/doi/10.1103/RevModPhys.82.451.

[123] Salvatore Capozziello and Mariafelicia De Laurentis. "Extended Theories of Gravity". In: *Phys. Rept.* 509 (2011), pp. 167–321. DOI: 10.1016/j.physrep.2011.09.003. arXiv: 1108.6266 [gr-qc].

[124] Lavinia Heisenberg. "Review on $f(Q)$ Gravity". In: (Sept. 2023). arXiv: 2309.15958 [gr-qc].

[125] Yi-Fu Cai et al. "f(T) teleparallel gravity and cosmology". In: *Rept. Prog. Phys.* 79.10 (2016), p. 106901. DOI: 10.1088/0034-4885/79/10/106901. arXiv: 1511.07586 [gr-qc].

[126] Shinji Mukohyama. "Horava-Lifshitz Cosmology: A Review". In: *Class. Quant. Grav.* 27 (2010), p. 223101. DOI: 10.1088/0264-9381/27/22/223101. arXiv: 1007.5199 [hep-th].

[127] Philip D. Mannheim. "Making the Case for Conformal Gravity". In: *Found. Phys.* 42 (2012), pp. 388–420. DOI: 10.1007/s10701-011-9608-6. arXiv: 1101.2186 [hep-th].

[128] Stanley Deser and R. P. Woodard. "Nonlocal Cosmology". In: *Phys. Rev. Lett.* 99 (2007), p. 111301. DOI: 10.1103/PhysRevLett.99.111301. arXiv: 0706.2151 [astro-ph].

[129] Salvatore Capozziello and Francesco Bajardi. "Nonlocal gravity cosmology: An overview". In: *Int. J. Mod. Phys. D* 31.06 (2022), p. 2230009. DOI: 10.1142/S0218271822300099. arXiv: 2201.04512 [gr-qc].

[130] Sebastian Bahamonde, Salvatore Capozziello, and Konstantinos F. Dialektopoulos. "Constraining Generalized Non-local Cosmology from Noether Symmetries". In: *Eur. Phys. J. C* 77.11 (2017), p. 722. DOI: 10.1140/epjc/s10052-017-5283-x. arXiv: 1708.06310 [gr-qc].

[131] Leonardo Modesto. "Super-renormalizable Gravity". In: *13th Marcel Grossmann Meeting on Recent Developments in Theoretical and Experimental General Relativity, Astrophysics, and Relativistic Field Theories*. 2015, pp. 1128–1130. DOI: 10.1142/9789814623995_0098. arXiv: 1302.6348 [hep-th].

[132] Fabio Briscese et al. "Inflation in (Super-)renormalizable Gravity". In: *Phys. Rev. D* 87.8 (2013), p. 083507. DOI: 10.1103/PhysRevD.87.083507. arXiv: 1212.3611 [hep-th].

[133] G. R. Dvali, Gregory Gabadadze, and Massimo Porrati. "4-D gravity on a brane in 5-D Minkowski space". In: *Phys. Lett. B* 485 (2000), pp. 208–214. DOI: 10.1016/S0370-2693(00)00669-9. arXiv: hep-th/0005016.

[134] G. R. Dvali and Gregory Gabadadze. "Gravity on a brane in infinite volume extra space". In: *Phys. Rev. D* 63 (2001), p. 065007. DOI: 10.1103/PhysRevD.63.065007. arXiv: hep-th/0008054.

[135] Pedro G. S. Fernandes et al. "The 4D Einstein–Gauss–Bonnet theory of gravity: a review". In: *Class. Quant. Grav.* 39.6 (2022), p. 063001. DOI: 10.1088/1361-6382/ac500a. arXiv: 2202.13908 [gr-qc].

[136] J. M. Overduin and P. S. Wesson. "Kaluza-Klein gravity". In: *Phys. Rept.* 283 (1997), pp. 303–380. DOI: 10.1016/S0370-1573(96)00046-4. arXiv: gr-qc/9805018.

[137] Claudia de Rham et al. "Cascading Gravity and Degravitation". In: *JCAP* 02 (2008), p. 011. DOI: 10.1088/1475-7516/2008/02/011. arXiv: 0712.2821 [hep-th].

[138] S. S. Shapiro et al. "Measurement of the Solar Gravitational Deflection of Radio Waves using Geodetic Very-Long-Baseline Interferometry Data, 1979–1999". In: *Phys. Rev. Lett.* 92 (12 Mar. 2004), p. 121101. DOI: 10.1103/PhysRevLett.92.121101. URL: https://link.aps.org/doi/10.1103/PhysRevLett.92.121101.

[139] B. Bertotti, L. Iess, and P. Tortora. "A test of general relativity using radio links with the Cassini spacecraft". In: *Nature* 425 (2003), pp. 374–376. DOI: 10.1038/nature01997.

[140] Austin Joyce et al. "Beyond the Cosmological Standard Model". In: *Phys. Rept.* 568 (2015), pp. 1–98. DOI: 10.1016/j.physrep.2014.12.002. arXiv: 1407.0059 [astro-ph.CO].

[141] E. Babichev, C. Deffayet, and R. Ziour. "k-Mouflage gravity". In: *Int. J. Mod. Phys. D* 18 (2009), pp. 2147–2154. DOI: 10.1142/S0218271809016107. arXiv: 0905.2943 [hep-th].

[142] A. I. Vainshtein. "To the problem of nonvanishing gravitation mass". In: *Phys. Lett. B* 39 (1972), pp. 393–394. DOI: 10.1016/0370-2693(72)90147-5.

[143] V. C. Rubin, Jr. Ford W. K., and N. Thonnard. "Extended rotation curves of high-luminosity spiral galaxies. IV. Systematic dynamical properties, Sa -> Sc." In: *Astrophys. J.l* 225 (Nov. 1978), pp. L107–L111. DOI: 10.1086/182804.

[144] Gianfranco Bertone, Dan Hooper, and Joseph Silk. "Particle dark matter: Evidence, candidates and constraints". In: *Phys. Rept.* 405 (2005), pp. 279–390. DOI: 10.1016/j.physrep.2004.08.031. arXiv: hep-ph/0404175.

[145] Giorgio Arcadi et al. "The waning of the WIMP? A review of models, searches, and constraints". In: *Eur. Phys. J. C* 78.3 (2018), p. 203. DOI: 10.1140/epjc/s10052-018-5662-y. arXiv: 1703.07364 [hep-ph].

[146] Lasha Berezhiani and Justin Khoury. "Theory of dark matter superfluidity". In: *Phys. Rev. D* 92 (10 Nov. 2015), p. 103510. DOI: 10.1103/PhysRevD.92.103510. URL: https://link.aps.org/doi/10.1103/PhysRevD.92.103510.

[147] R. D. Peccei and Helen R. Quinn. "CP Conservation in the Presence of Pseudoparticles". In: *Phys. Rev. Lett.* 38 (25 June 1977), pp. 1440–1443. DOI: 10.1103/PhysRevLett.38.1440. URL: https://link.aps.org/doi/10.1103/PhysRevLett.38.1440.

[148] Gaia Lanfranchi, Maxim Pospelov, and Philip Schuster. "The Search for Feebly Interacting Particles". In: *Ann. Rev. Nucl. Part. Sci.* 71 (2021), pp. 279–313. DOI: 10.1146/annurev-nucl-102419-055056. arXiv: 2011.02157 [hep-ph].

[149] Riccardo Catena and Laura Covi. "SUSY dark matter(s)". In: *Eur. Phys. J. C* 74 (2014), p. 2703. DOI: 10.1140/epjc/s10052-013-2703-4. arXiv: 1310.4776 [hep-ph].

[150] Matteo Viel et al. "Constraining warm dark matter candidates including sterile neutrinos and light gravitinos with WMAP and the Lyman-alpha forest". In: *Phys. Rev. D* 71 (2005), p. 063534. DOI: 10.1103/PhysRevD.71.063534. arXiv: astro-ph/0501562.

[151] Matteo Viel et al. "Warm dark matter as a solution to the small scale crisis: New constraints from high redshift Lyman-α forest data". In: *Phys. Rev. D* 88 (2013), p. 043502. DOI: 10.1103/PhysRevD.88.043502. arXiv: 1306.2314 [astro-ph.CO].

[152] E. Aprile et al. "Projected WIMP sensitivity of the XENONnT dark matter experiment". In: *JCAP* 11 (2020), p. 031. DOI: 10.1088/1475-7516/2020/11/031. arXiv: 2007.08796 [physics.ins-det].

[153] Stefan Heimersheim et al. "Cannibalism hinders growth: Cannibal Dark Matter and the S_8 tension". In: *JCAP* 12 (2020), p. 016. DOI: 10.1088/1475-7516/2020/12/016. arXiv: 2008.08486 [astro-ph.CO].

[154] Guillermo Franco Abellán et al. "Implications of the S_8 tension for decaying dark matter with warm decay products". In: *Phys. Rev. D* 105.6 (2022), p. 063525. DOI: 10.1103/PhysRevD.105.063525. arXiv: 2008.09615 [astro-ph.CO].

[155] E. Aprile et al. "Excess electronic recoil events in XENON1T". In: Phys. Rev. D 102.7, 072004 (Oct. 2020), p. 072004. DOI: 10.1103/PhysRevD.102.072004. arXiv: 2006.09721 [hep-ex].

[156] Kristjan Kannike et al. "Dark Matter and the XENON1T electron recoil excess". In: *Phys. Rev. D* 102.9 (2020), p. 095002. DOI: 10.1103/PhysRevD.102.095002. arXiv: 2006.10735 [hep-ph].

[157] Stefano Camera, Matteo Martinelli, and Daniele Bertacca. "Does quartessence ease cosmic tensions?" In: *Phys. Dark Univ.* 23 (2019), p. 100247. DOI: 10.1016/j.dark.2018.11.008. arXiv: 1704.06277 [astro-ph.CO].

[158] W. J. G. de Blok. "The Core-Cusp Problem". In: *Advances in Astronomy* 2010, 789293 (Jan. 2010), p. 789293. DOI: 10.1155/2010/789293. arXiv: 0910.3538 [astro-ph.CO].

[159] Lauren H. Cooke et al. "Cuspy dark matter density profiles in massive dwarf galaxies". In: MNRAS 512.1 (May 2022), pp. 1012–1031. DOI: 10.1093/mnras/stac588. arXiv: 2203.00694 [astro-ph.GA].

[160] Ricardo A. Flores and Joel R. Primack. "Observational and theoretical constraints on singular dark matter halos". In: *Astrophys. J. Lett.* 427 (1994), pp. L1–4. DOI: 10.1086/187350. arXiv: astro-ph/9402004.

[161] B. Moore. "Evidence against dissipationless dark matter from observations of galaxy haloes". In: *Nature* 370 (1994), p. 629. DOI: 10.1038/370629a0.

[162] Federico Lelli. "Gas dynamics in dwarf galaxies as testbeds for dark matter and galaxy evolution". In: *Nature Astron.* 6 (2022), pp. 35–47. DOI: 10.1038/s41550-021-01562-2. arXiv: 2201.11752 [astro-ph.GA].

[163] Julio F. Navarro, Carlos S. Frenk, and Simon D. M. White. "The Structure of cold dark matter halos". In: *Astrophys. J.* 462 (1996), pp. 563–575. DOI: 10.1086/177173. arXiv: astro-ph/9508025.

[164] J. Einasto. "On the Construction of a Composite Model for the Galaxy and on the Determination of the System of Galactic Parameters". In: *Trudy Astrofizicheskogo Instituta Alma-Ata* 5 (Jan. 1965), pp. 87–100.

[165] Ben Moore et al. "Cold collapse and the core catastrophe". In: *Mon. Not. Roy. Astron. Soc.* 310 (1999), pp. 1147–1152. DOI: 10.1046/j.1365-8711.1999.03039.x. arXiv: astro-ph/9903164.

[166] Lars Hernquist. "An Analytical Model for Spherical Galaxies and Bulges". In: ApJ 356 (June 1990), p. 359. DOI: 10.1086/168845.

[167] Hongsheng Zhao. "Analytical models for galactic nuclei". In: MNRAS 278.2 (Jan. 1996), pp. 488–496. DOI: 10.1093/mnras/278.2.488. arXiv: astro-ph/9509122 [astro-ph].

[168] M. Davis et al. "The evolution of large-scale structure in a universe dominated by cold dark matter". In: ApJ 292 (May 1985), pp. 371–394. DOI: 10.1086/163168.

[169] N. C. Amorisco and N. W. Evans. "Dark matter cores and cusps: the case of multiple stellar populations in dwarf spheroidals". In: MNRAS 419.1 (Jan. 2012), pp. 184–196. DOI: 10.1111/j.1365-2966.2011.19684.x. arXiv: 1106.1062 [astro-ph.CO].

[170] G Kauffmann, Simon D. M. White, and B. Guiderdoni. "The Formation and Evolution of Galaxies Within Merging Dark Matter Haloes". In: *Mon. Not. Roy. Astron. Soc.* 264 (1993), p. 201.

[171] Anatoly A. Klypin et al. "Where are the missing Galactic satellites?" In: *Astrophys. J.* 522 (1999), pp. 82–92. DOI: 10.1086/307643. arXiv: astro-ph/9901240.

[172] Mario Mateo. "Dwarf galaxies of the Local Group". In: *Ann. Rev. Astron. Astrophys.* 36 (1998), pp. 435–506. DOI: 10.1146/annurev.astro.36.1.435. arXiv: astro-ph/9810070.

[173] B. Moore et al. "Dark matter substructure within galactic halos". In: *Astrophys. J. Lett.* 524 (1999), pp. L19–L22. DOI: 10.1086/312287. arXiv: astro-ph/9907411.

[174] Pieter van Dokkum et al. "Forty-Seven Milky Way-Sized, Extremely Diffuse Galaxies in the Coma Cluster". In: *Astrophys. J. Lett.* 798.2 (2015), p. L45. DOI: 10.1088/2041-8205/798/2/L45. arXiv: 1410.8141 [astro-ph.GA].

[175] Pieter van Dokkum et al. "A galaxy lacking dark matter". In: *Nature* 555.7698 (2018), pp. 629–632. DOI: 10.1038/nature25767. arXiv: 1803.10237 [astro-ph.GA].

[176] Pieter van Dokkum et al. "A Second Galaxy Missing Dark Matter in the NGC 1052 Group". In: ApJ 874.1, L5 (Mar. 2019), p. L5. DOI: 10.3847/2041-8213/ab0d92. arXiv: 1901.05973 [astro-ph.GA].

[177] Anže Slosar et al. "Dark Energy and Modified Gravity". In: (2019). arXiv: 1903.12016 [astro-ph.CO].

[178] David H. Weinberg et al. "Observational Probes of Cosmic Acceleration". In: *Phys. Rept.* 530 (2013), pp. 87–255. DOI: 10.1016/j.physrep.2013.05.001. arXiv: 1201.2434 [astro-ph.CO].

[179] B. P. Abbott et al. "GW170817: Observation of Gravitational Waves from a Binary Neutron Star Inspiral". In: *Phys. Rev. Lett.* 119.16 (2017), p. 161101. DOI: 10.1103/PhysRevLett.119.161101. arXiv: 1710.05832 [gr-qc].

[180] B. P. Abbott et al. "Multi-messenger Observations of a Binary Neutron Star Merger". In: *Astrophys. J. Lett.* 848.2 (2017), p. L12. DOI: 10.3847/2041-8213/aa91c9. arXiv: 1710.05833 [astro-ph.HE].

[181] Timothy Clifton et al. "Modified Gravity and Cosmology". In: *Phys. Rept.* 513 (2012), pp. 1–189. DOI: 10.1016/j.physrep.2012.01.001. arXiv: 1106.2476 [astro-ph.CO].

[182] Mustapha Ishak. "Testing General Relativity in Cosmology". In: *Living Rev. Rel.* 22.1 (2019), p. 1. DOI: 10.1007/s41114-018-0017-4. arXiv: 1806.10122 [astro-ph.CO].

[183] Tsutomu Kobayashi, Yuki Watanabe, and Daisuke Yamauchi. "Breaking of Vainshtein screening in scalar-tensor theories beyond Horndeski". In: *Phys. Rev. D* 91 (6 Mar. 2015), p. 064013. DOI: 10.1103/PhysRevD.91.064013. URL: https://link.aps.org/doi/10.1103/PhysRevD.91.064013.

[184] Gilles Esposito-Farese and D. Polarski. "Scalar tensor gravity in an accelerating universe". In: *Phys. Rev. D* 63 (2001), p. 063504. DOI: 10.1103/PhysRevD.63.063504. arXiv: gr-qc/0009034.

[185] Gregory Walter Horndeski. "Second-order scalar-tensor field equations in a four-dimensional space". In: *Int. J. Theor. Phys.* 10 (1974), pp. 363–384. DOI: 10.1007/BF01807638.

[186] C. Deffayet, Gilles Esposito-Farese, and A. Vikman. "Covariant Galileon". In: *Phys. Rev. D* 79 (2009), p. 084003. DOI: 10.1103/PhysRevD.79.084003. arXiv: 0901.1314 [hep-th].

[187] C. Deffayet, S. Deser, and G. Esposito-Farese. "Generalized Galileons: All scalar models whose curved background extensions maintain second-order field equations and stress-tensors". In: *Phys. Rev. D* 80 (2009), p. 064015. DOI: 10.1103/PhysRevD.80.064015. arXiv: 0906.1967 [gr-qc].

[188] Richard P. Woodard. "Ostrogradsky's theorem on Hamiltonian instability". In: *Scholarpedia* 10.8 (2015), p. 32243. DOI: 10.4249/scholarpedia.32243. arXiv: 1506.02210 [hep-th].

[189] Jérôme Gleyzes et al. "Healthy theories beyond Horndeski". In: *Phys. Rev. Lett.* 114.21 (2015), p. 211101. DOI: 10.1103/PhysRevLett.114.211101. arXiv: 1404.6495 [hep-th].

[190] Jérôme Gleyzes et al. "Exploring gravitational theories beyond Horndeski". In: *JCAP* 02 (2015), p. 018. DOI: 10.1088/1475-7516/2015/02/018. arXiv: 1408.1952 [astro-ph.CO].

[191] Chunshan Lin et al. "Hamiltonian structure of scalar-tensor theories beyond Horndeski". In: *JCAP* 10 (2014), p. 071. DOI: 10.1088/1475-7516/2014/10/071. arXiv: 1408.0670 [hep-th].

[192] Cedric Deffayet, Gilles Esposito-Farese, and Daniele A. Steer. "Counting the degrees of freedom of generalized Galileons". In: *Phys. Rev. D* 92 (2015), p. 084013. DOI: 10.1103/PhysRevD.92.084013. arXiv: 1506.01974 [gr-qc].

[193] Jérôme Gleyzes et al. "New Class of Consistent Scalar-Tensor Theories". In: *Phys. Rev. Lett.* 114 (21 May 2015), p. 211101. DOI: 10.1103/PhysRevLett.114.211101. URL: https://link.aps.org/doi/10.1103/PhysRevLett.114.211101.

[194] Dina Traykova, Emilio Bellini, and Pedro G. Ferreira. "The phenomenology of beyond Horndeski gravity". In: *JCAP* 08 (2019), p. 035. DOI: 10.1088/1475-7516/2019/08/035. arXiv: 1902.10687 [astro-ph.CO].

[195] David Langlois and Karim Noui. "Degenerate higher derivative theories beyond Horndeski: evading the Ostrogradski instability". In: *JCAP* 02 (2016), p. 034. DOI: 10.1088/1475-7516/2016/02/034. arXiv: 1510.06930 [gr-qc].

[196] David Langlois. "Dark energy and modified gravity in degenerate higher-order scalar–tensor (DHOST) theories: A review". In: *Int. J. Mod. Phys. D* 28.05 (2019), p. 1942006. DOI: 10.1142/S0218271819420069. arXiv: 1811.06271 [gr-qc].

[197] David Langlois et al. "Mimetic gravity as DHOST theories". In: *JCAP* 02 (2019), p. 036. DOI: 10.1088/1475-7516/2019/02/036. arXiv: 1802.03394 [gr-qc].

[198] David Langlois, Karim Noui, and Hugo Roussille. "Quadratic degenerate higher-order scalar-tensor theories revisited". In: *Phys. Rev. D* 103.8 (2021), p. 084022. DOI: 10.1103/PhysRevD.103.084022. arXiv: 2012.10218 [gr-qc].

[199] M. Crisostomi et al. "Cosmological evolution in DHOST theories". In: *JCAP* 01 (2019), p. 030. DOI: 10.1088/1475-7516/2019/01/030. arXiv: 1810.12070 [hep-th].

[200] Jibril Ben Achour et al. "Degenerate higher order scalar-tensor theories beyond Horndeski up to cubic order". In: *JHEP* 12 (2016), p. 100. DOI: 10.1007/JHEP12(2016)100. arXiv: 1608.08135 [hep-th].

[201] C. Brans and R. H. Dicke. "Mach's Principle and a Relativistic Theory of Gravitation". In: *Phys. Rev.* 124 (3 Nov. 1961), pp. 925–935. DOI: 10.1103/PhysRev.124.925. URL: https://link.aps.org/doi/10.1103/PhysRev.124.925.

[202] Tsutomu Kobayashi. "Horndeski theory and beyond: a review". In: *Rept. Prog. Phys.* 82.8 (2019), p. 086901. DOI: 10.1088/1361-6633/ab2429. arXiv: 1901.07183 [gr-qc].

[203] Jibril Ben Achour, David Langlois, and Karim Noui. "Degenerate higher order scalar-tensor theories beyond Horndeski and disformal transformations". In: *Phys. Rev. D* 93 (12 June 2016), p. 124005. DOI: 10.1103/PhysRevD.93.124005. URL: https://link.aps.org/doi/10.1103/PhysRevD.93.124005.

[204] Marco Crisostomi, Kazuya Koyama, and Gianmassimo Tasinato. "Extended Scalar-Tensor Theories of Gravity". In: *JCAP* 04 (2016), p. 044. DOI: 10.1088/1475-7516/2016/04/044. arXiv: 1602.03119 [hep-th].

[205] B. P. Abbott et al. "GW170817: Observation of Gravitational Waves from a Binary Neutron Star Inspiral". In: *Phys. Rev. Lett.* 119.16 (2017), p. 161101. DOI: 10.1103/PhysRevLett.119.161101. arXiv: 1710.05832 [gr-qc].

[206] Paolo Creminelli and Filippo Vernizzi. "Dark Energy after GW170817 and GRB170817A". In: *Phys. Rev. Lett.* 119.25 (2017), p. 251302. DOI: 10.1103/PhysRevLett.119.251302. arXiv: 1710.05877 [astro-ph.CO].

[207] Jose María Ezquiaga and Miguel Zumalacárregui. "Dark Energy After GW170817: Dead Ends and the Road Ahead". In: *Phys. Rev. Lett.* 119 (25 Dec. 2017), p. 251304. DOI: 10.1103/PhysRevLett.119.251304. URL: https://link.aps.org/doi/10.1103/PhysRevLett.119.251304.

[208] Claudia de Rham and Andrew Matas. "Ostrogradsky in Theories with Multiple Fields". In: *JCAP* 06 (2016), p. 041. DOI: 10.1088/1475-7516/2016/06/041. arXiv: 1604.08638 [hep-th].

[209] Nima Arkani-Hamed et al. "Ghost condensation and a consistent infrared modification of gravity". In: *JHEP* 05 (2004), p. 074. DOI: 10.1088/1126-6708/2004/05/074. arXiv: hep-th/0312099.

[210] Paolo Creminelli et al. "Starting the Universe: Stable Violation of the Null Energy Condition and Non-standard Cosmologies". In: *JHEP* 12 (2006), p. 080. DOI: 10.1088/1126-6708/2006/12/080. arXiv: hep-th/0606090.

[211] Clifford Cheung et al. "The Effective Field Theory of Inflation". In: *JHEP* 03 (2008), p. 014. DOI: 10.1088/1126-6708/2008/03/014. arXiv: 0709.0293 [hep-th].

[212] Lorenzo Bordin et al. "Simplifying the EFT of Inflation: generalized disformal transformations and redundant couplings". In: *JCAP* 09 (2017), p. 043. DOI: 10.1088/1475-7516/2017/09/043. arXiv: 1706.03758 [astro-ph.CO].

[213] Paolo Creminelli et al. "The Effective Theory of Quintessence: the w<-1 Side Unveiled". In: *JCAP* 02 (2009), p. 018. DOI: 10.1088/1475-7516/2009/02/018. arXiv: 0811.0827 [astro-ph].

[214] Giulia Gubitosi, Federico Piazza, and Filippo Vernizzi. "The Effective Field Theory of Dark Energy". In: *JCAP* 02 (2013), p. 032. DOI: 10.1088/1475-7516/2013/02/032. arXiv: 1210.0201 [hep-th].

[215] Jerome Gleyzes et al. "Essential Building Blocks of Dark Energy". In: *JCAP* 08 (2013), p. 025. DOI: 10.1088/1475-7516/2013/08/025. arXiv: 1304.4840 [hep-th].

[216] Jérôme Gleyzes, David Langlois, and Filippo Vernizzi. "A unifying description of dark energy". In: *Int. J. Mod. Phys. D* 23.13 (2015), p. 1443010. DOI: 10.1142/S021827181443010X. arXiv: 1411.3712 [hep-th].

[217] Jolyon K. Bloomfield et al. "Dark energy or modified gravity? An effective field theory approach". In: *JCAP* 08 (2013), p. 010. DOI: 10.1088/1475-7516/2013/08/010. arXiv: 1211.7054 [astro-ph.CO].

[218] Jolyon Bloomfield. "A Simplified Approach to General Scalar-Tensor Theories". In: *JCAP* 12 (2013), p. 044. DOI: 10.1088/1475-7516/2013/12/044. arXiv: 1304.6712 [astro-ph.CO].

[219] Tessa Baker, Pedro G. Ferreira, and Constantinos Skordis. "The Parameterized Post-Friedmann framework for theories of modified gravity: concepts, formalism and examples". In: *Phys. Rev. D* 87.2 (2013), p. 024015. DOI: 10.1103/PhysRevD.87.024015. arXiv: 1209.2117 [astro-ph.CO].

[220] Richard A. Battye and Jonathan A. Pearson. "Effective action approach to cosmological perturbations in dark energy and modified gravity". In: *JCAP* 07 (2012), p. 019. DOI: 10.1088/1475-7516/2012/07/019. arXiv: 1203.0398 [hep-th].

[221] Hideo Kodama and Misao Sasaki. "Cosmological Perturbation Theory". In: *Progress of Theoretical Physics Supplement* 78 (Jan. 1984), pp. 1–166. ISSN: 0375-9687. DOI: 10.1143/PTPS.78.1. eprint: https://academic.oup.com/ptps/article-pdf/doi/10.1143/PTPS.78.1/5321391/78-1.pdf. URL: https://doi.org/10.1143/PTPS.78.1.

[222] Noemi Frusciante and Louis Perenon. "Effective field theory of dark energy: A review". In: *Phys. Rept.* 857 (2020), pp. 1–63. DOI: 10.1016/j.physrep.2020.02.004. arXiv: 1907.03150 [astro-ph.CO].

[223] Noemi Frusciante and Georgios Papadomanolakis. "Tackling non-linearities with the effective field theory of dark energy and modified gravity". In: *JCAP* 12 (2017), p. 014. DOI: 10.1088/1475-7516/2017/12/014. arXiv: 1706.02719 [gr-qc].

[224] Daisuke Yamauchi, Shuichiro Yokoyama, and Hiroyuki Tashiro. "Constraining modified theories of gravity with the galaxy bispectrum". In: *Phys. Rev. D* 96.12 (2017), p. 123516. DOI: 10.1103/PhysRevD.96.123516. arXiv: 1709.03243 [astro-ph.CO].

[225] Giulia Cusin, Matthew Lewandowski, and Filippo Vernizzi. "Nonlinear Effective Theory of Dark Energy". In: *JCAP* 04 (2018), p. 061. DOI: 10.1088/1475-7516/2018/04/061. arXiv: 1712.02782 [astro-ph.CO].

[226] Giulia Cusin, Matthew Lewandowski, and Filippo Vernizzi. "Dark Energy and Modified Gravity in the Effective Field Theory of Large-Scale Structure". In: *JCAP* 04 (2018), p. 005. DOI: 10.1088/1475-7516/2018/04/005. arXiv: 1712.02783 [astro-ph.CO].

[227] Joe Kennedy, Lucas Lombriser, and Andy Taylor. "Screening and degenerate kinetic self-acceleration from the nonlinear freedom of reconstructed Horndeski theories". In: *Phys. Rev. D* 100.4 (2019), p. 044034. DOI: 10.1103/PhysRevD.100.044034. arXiv: 1902.09853 [gr-qc].

[228] Federico Piazza, Heinrich Steigerwald, and Christian Marinoni. "Phenomenology of dark energy: exploring the space of theories with future redshift surveys". In: *JCAP* 05 (2014), p. 043. DOI: 10.1088/1475-7516/2014/05/043. arXiv: 1312.6111 [astro-ph.CO].

[229] Bin Hu et al. "EFTCAMB/EFTCosmoMC: Numerical Notes v3.0". In: (May 2014). arXiv: 1405.3590 [astro-ph.IM].

[230] Shinji Tsujikawa. "The effective field theory of inflation/dark energy and the Horndeski theory". In: *Lect. Notes Phys.* 892 (2015). Ed. by Eleftherios Papantonopoulos, pp. 97–136. DOI: 10.1007/978-3-319-10070-8_4. arXiv: 1404.2684 [gr-qc].

[231] Emilio Bellini and Ignacy Sawicki. "Maximal freedom at minimum cost: linear large-scale structure in general modifications of gravity". In: *JCAP* 07 (2014), p. 050. DOI: 10.1088/1475-7516/2014/07/050. arXiv: 1404.3713 [astro-ph.CO].

[232] David Langlois et al. "Effective Description of Higher-Order Scalar-Tensor Theories". In: *JCAP* 05 (2017), p. 033. DOI: 10.1088/1475-7516/2017/05/033. arXiv: 1703.03797 [hep-th].

[233] Nathan Chow and Justin Khoury. "Galileon Cosmology". In: *Phys. Rev. D* 80 (2009), p. 024037. DOI: 10.1103/PhysRevD.80.024037. arXiv: 0905.1325 [hep-th].

[234] Ignacy Sawicki et al. "Consistent perturbations in an imperfect fluid". In: *JCAP* 01 (2013), p. 004. DOI: 10.1088/1475-7516/2013/01/004. arXiv: 1208.4855 [astro-ph.CO].

[235] Dan N. Vollick. "1/R Curvature corrections as the source of the cosmological acceleration". In: *Phys. Rev. D* 68 (2003), p. 063510. DOI: 10.1103/PhysRevD.68.063510. arXiv: astro-ph/0306630.

[236] Antonio De Felice, David F. Mota, and Shinji Tsujikawa. "Matter instabilities in general Gauss-Bonnet gravity". In: *Phys. Rev. D* 81 (2010), p. 023532. DOI: 10.1103/PhysRevD.81.023532. arXiv: 0911.1811 [gr-qc].

[237] Bharat Ratra and P. J. E. Peebles. "Cosmological consequences of a rolling homogeneous scalar field". In: *Phys. Rev. D* 37 (12 June 1988), pp. 3406–3427. DOI: 10.1103/PhysRevD.37.3406. URL: https://link.aps.org/doi/10.1103/PhysRevD.37.3406.

[238] M. Fierz and W. Pauli. "On relativistic wave equations for particles of arbitrary spin in an electromagnetic field". In: *Proc. Roy. Soc. Lond. A* 173 (1939), pp. 211–232. DOI: 10.1098/rspa.1939.0140.

[239] H. van Dam and M. J. G. Veltman. "Massive and massless Yang-Mills and gravitational fields". In: *Nucl. Phys. B* 22 (1970), pp. 397–411. DOI: 10.1016/0550-3213(70)90416-5.

[240] V. I. Zakharov. "Linearized gravitation theory and the graviton mass". In: *JETP Lett.* 12 (1970), p. 312.

[241] Claudia de Rham et al. "Cosmic Acceleration and the Helicity-0 Graviton". In: *Phys. Rev. D* 83 (2011), p. 103516. DOI: 10.1103/PhysRevD.83.103516. arXiv: 1010.1780 [hep-th].

[242] Alberto Nicolis and Riccardo Rattazzi. "Classical and quantum consistency of the DGP model". In: *JHEP* 06 (2004), p. 059. DOI: 10.1088/1126-6708/2004/06/059. arXiv: hep-th/0404159.

[243] Rampei Kimura, Tsutomu Kobayashi, and Kazuhiro Yamamoto. "Vainshtein screening in a cosmological background in the most general second-order scalar-tensor theory". In: *Phys. Rev. D* 85 (2012), p. 024023. DOI: 10.1103/PhysRevD.85.024023. arXiv: 1111.6749 [astro-ph.CO].

[244] Tatsuya Narikawa et al. "Testing general scalar-tensor gravity and massive gravity with cluster lensing". In: *Phys. Rev. D* 87 (2013), p. 124006. DOI: 10.1103/PhysRevD.87.124006. arXiv: 1302.2311 [astro-ph.CO].

[245] Kazuya Koyama, Gustavo Niz, and Gianmassimo Tasinato. "Effective theory for the Vainshtein mechanism from the Horndeski action". In: *Phys. Rev. D* 88 (2013), p. 021502. DOI: 10.1103/PhysRevD.88.021502. arXiv: 1305.0279 [hep-th].

[246] Jeremy Sakstein and Bhuvnesh Jain. "Implications of the Neutron Star Merger GW170817 for Cosmological Scalar-Tensor Theories". In: *Phys. Rev. Lett.* 119.25 (2017), p. 251303. DOI: 10.1103/PhysRevLett.119.251303. arXiv: 1710.05893 [astro-ph.CO].

[247] David Langlois et al. "Scalar-tensor theories and modified gravity in the wake of GW170817". In: *Phys. Rev. D* 97.6 (2018), p. 061501. DOI: 10.1103/PhysRevD.97.061501. arXiv: 1711.07403 [gr-qc].

[248] Marco Crisostomi and Kazuya Koyama. "Vainshtein mechanism after GW170817". In: *Phys. Rev. D* 97.2 (2018), p. 021301. DOI: 10.1103/PhysRevD.97.021301. arXiv: 1711.06661 [astro-ph.CO].

[249] Alexandru Dima and Filippo Vernizzi. "Vainshtein Screening in Scalar-Tensor Theories before and after GW170817: Constraints on Theories beyond Horndeski". In: *Phys. Rev. D* 97.10 (2018), p. 101302. DOI: 10.1103/PhysRevD.97.101302. arXiv: 1712.04731 [gr-qc].

[250] Nicola Bartolo et al. "Cosmic structures and gravitational waves in ghost-free scalar-tensor theories of gravity". In: *JCAP* 05 (2018), p. 048. DOI: 10.1088/1475-7516/2018/05/048. arXiv: 1712.04002 [gr-qc].

[251] Vincenzo F. Cardone et al. "Jointly fitting weak lensing, x-ray, and Sunyaev-Zel'dovich data to constrain scalar-tensor theories with clusters of galaxies". In: *Phys. Rev. D* 103 (6 Mar. 2021), p. 064065. DOI: 10.1103/PhysRevD.103.064065. URL: https://link.aps.org/doi/10.1103/PhysRevD.103.064065.

[252] Jeremy Sakstein and Bhuvnesh Jain. "Implications of the Neutron Star Merger GW170817 for Cosmological Scalar-Tensor Theories". In: *Phys. Rev. Lett.* 119 (25 Dec. 2017), p. 251303. DOI: 10.1103/PhysRevLett.119.251303. URL: https://link.aps.org/doi/10.1103/PhysRevLett.119.251303.

[253] T. Baker et al. "Strong Constraints on Cosmological Gravity from GW170817 and GRB 170817A". In: *Phys. Rev. Lett.* 119 (25 Dec. 2017), p. 251301. DOI: 10.1103/PhysRevLett.119.251301. URL: https://link.aps.org/doi/10.1103/PhysRevLett.119.251301.

[254] Tessa Baker and Ian Harrison. "Constraining Scalar-Tensor Modified Gravity with Gravitational Waves and Large Scale Structure Surveys". In: *JCAP* 01 (2021), p. 068. DOI: 10.1088/1475-7516/2021/01/068. arXiv: 2007.13791 [astro-ph.CO].

[255] B. P. Abbott et al. "Gravitational Waves and Gamma-rays from a Binary Neutron Star Merger: GW170817 and GRB 170817A". In: *Astrophys. J. Lett.* 848.2 (2017), p. L13. DOI: 10.3847/2041-8213/aa920c. arXiv: 1710.05834 [astro-ph.HE].

[256] P. A. R. Ade et al. "Planck 2015 results. XIII. Cosmological parameters". In: *Astron. Astrophys.* 594 (2016), A13. DOI: 10.1051/0004-6361/201525830. arXiv: 1502.01589 [astro-ph.CO].

[257] Marco Raveri et al. "Effective Field Theory of Cosmic Acceleration: constraining dark energy with CMB data". In: *Phys. Rev. D* 90.4 (2014), p. 043513. DOI: 10.1103/PhysRevD.90.043513. arXiv: 1405.1022 [astro-ph.CO].

[258] P. A. R. Ade et al. "Planck 2013 results. XV. CMB power spectra and likelihood". In: *Astron. Astrophys.* 571 (2014), A15. DOI: 10.1051/0004-6361/201321573. arXiv: 1303.5075 [astro-ph.CO].

[259] P. A. R. Ade et al. "Planck 2013 results. XVI. Cosmological parameters". In: *Astron. Astrophys.* 571 (2014), A16. DOI: 10.1051/0004-6361/201321591. arXiv: 1303.5076 [astro-ph.CO].

[260] G. Hinshaw et al. "Nine-year Wilkinson Microwave Anisotropy Probe (WMAP) Observations: Cosmological Parameter Results". In: ApJS 208.2, 19 (Oct. 2013), p. 19. DOI: 10.1088/0067-0049/208/2/19. arXiv: 1212.5226 [astro-ph.CO].

[261] Will J. Percival et al. "Baryon acoustic oscillations in the Sloan Digital Sky Survey Data Release 7 galaxy sample". In: MNRAS 401.4 (Feb. 2010), pp. 2148–2168. DOI: 10.1111/j.1365-2966.2009.15812.x. arXiv: 0907.1660 [astro-ph.CO].

[262] Nikhil Padmanabhan et al. "A 2 per cent distance to z = 0.35 by reconstructing baryon acoustic oscillations - I. Methods and application to the Sloan Digital Sky Survey". In: MNRAS 427.3 (Dec. 2012), pp. 2132–2145. DOI: 10.1111/j.1365-2966.2012.21888.x. arXiv: 1202.0090 [astro-ph.CO].

[263] Lauren Anderson et al. "The clustering of galaxies in the SDSS-III Baryon Oscillation Spectroscopic Survey: baryon acoustic oscillations in the Data Release 9 spectroscopic galaxy sample". In: MNRAS 427.4 (Dec. 2012), pp. 3435–3467. DOI: 10.1111/j.1365-2966.2012.22066.x. arXiv: 1203.6594 [astro-ph.CO].

[264] P. A. R. Ade et al. "Planck 2015 results. XIV. Dark energy and modified gravity". In: *Astron. Astrophys.* 594 (2016), A14. DOI: 10.1051/0004-6361/201525814. arXiv: 1502.01590 [astro-ph.CO].

[265] Emilio Bellini et al. "Constraints on deviations from ΛCDM within Horndeski gravity". In: *JCAP* 02 (2016). [Erratum: JCAP 06, E01 (2016)], p. 053. DOI: 10.1088/1475-7516/2016/06/E01. arXiv: 1509.07816 [astro-ph.CO].

[266] A. Spurio Mancini et al. "KiDS + GAMA: constraints on horndeski gravity from combined large-scale structure probes". In: *Mon. Not. Roy. Astron. Soc.* 490.2 (2019), pp. 2155–2177. DOI: 10.1093/mnras/stz2581. arXiv: 1901.03686 [astro-ph.CO].

[267] C. D. Kreisch and E. Komatsu. "Cosmological Constraints on Horndeski Gravity in Light of GW170817". In: *JCAP* 12 (2018), p. 030. DOI: 10.1088/1475-7516/2018/12/030. arXiv: 1712.02710 [astro-ph.CO].

[268] Johannes Noller and Andrina Nicola. "Cosmological parameter constraints for Horndeski scalar-tensor gravity". In: *Phys. Rev. D* 99.10 (2019), p. 103502. DOI: 10.1103/PhysRevD.99.103502. arXiv: 1811.12928 [astro-ph.CO].

[269] Louis Perenon et al. "Optimising growth of structure constraints on modified gravity". In: *JCAP* 06 (2019), p. 020. DOI: 10.1088/1475-7516/2019/06/020. arXiv: 1901.11063 [astro-ph.CO].

[270] S. de la Torre et al. "The VIMOS Public Extragalactic Redshift Survey (VIPERS). Gravity test from the combination of redshift-space distortions and galaxy-galaxy lensing at $0.5 < z < 1.2$". In: *Astron. Astrophys.* 608 (2017), A44. DOI: 10.1051/0004-6361/201630276. arXiv: 1612.05647 [astro-ph.CO].

[271] Feng Shi et al. "Mapping the Real Space Distributions of Galaxies in SDSS DR7: II. Measuring the growth rate, clustering amplitude of matter and biases of galaxies at redshift 0.1". In: *Astrophys. J.* 861.2 (2018), p. 137. DOI: 10.3847/1538-4357/aacb20. arXiv: 1712.04163 [astro-ph.CO].

[272] Noemi Frusciante et al. "Cosmology of surviving Horndeski theory: The road ahead". In: *Phys. Rev. D* 99.6 (2019), p. 063538. DOI: 10.1103/PhysRevD.99.063538. arXiv: 1810.10521 [astro-ph.CO].

[273] Ryo Saito et al. "Modified gravity inside astrophysical bodies". In: *JCAP* 06 (2015), p. 008. DOI: 10.1088/1475-7516/2015/06/008. arXiv: 1503.01448 [gr-qc].

[274] Jeremy Sakstein. "Hydrogen Burning in Low Mass Stars Constrains Scalar-Tensor Theories of Gravity". In: *Phys. Rev. Lett.* 115 (2015), p. 201101. DOI: 10.1103/PhysRevLett.115.201101. arXiv: 1510.05964 [astro-ph.CO].

[275] Jeremy Sakstein et al. "Testing Gravity Using Galaxy Clusters: New Constraints on Beyond Horndeski Theories". In: *JCAP* 07 (2016), p. 019. DOI: 10.1088/1475-7516/2016/07/019. arXiv: 1603.06368 [astro-ph.CO].

[276] R. A. Hulse and J. H. Taylor. "Discovery of a pulsar in a binary system." In: ApJ 195 (Jan. 1975), pp. L51–L53. DOI: 10.1086/181708.

[277] J. M. Weisberg, D. J. Nice, and J. H. Taylor. "Timing Measurements of the Relativistic Binary Pulsar PSR B1913+16". In: ApJ 722.2 (Oct. 2010), pp. 1030–1034. DOI: 10.1088/0004-637X/722/2/1030. arXiv: 1011.0718 [astro-ph.GA].

[278] Ippocratis D. Saltas and Ilídio Lopes. "Obtaining Precision Constraints on Modified Gravity with Helioseismology". In: *Phys. Rev. Lett.* 123.9 (2019), p. 091103. DOI: 10.1103/PhysRevLett.123.091103. arXiv: 1909.02552 [astro-ph.CO].

[279] Marc Postman et al. "The Cluster Lensing and Supernova Survey with Hubble: An Overview". In: ApJS 199.2, 25 (Apr. 2012), p. 25. DOI: 10.1088/0067-0049/199/2/25. arXiv: 1106.3328 [astro-ph.CO].

[280] Megan Donahue et al. "CLASH-X: A Comparison of Lensing and X-ray Techniques for Measuring the Mass Profiles of Galaxy Clusters". In: *Astrophys. J.* 794.2 (2014), p. 136. DOI: 10.1088/0004-637X/794/2/136. arXiv: 1405.7876 [astro-ph.CO].

[281] Tom Broadhurst et al. "Comparison of Cluster Lensing Profiles with Lambda CDM Predictions". In: *Astrophys. J. Lett.* 685 (2008), pp. L9–L12. DOI: 10.1086/592400. arXiv: 0805.2617 [astro-ph].

[282] Masamune Oguri et al. "Subaru Weak Lensing Measurements of Four Strong Lensing Clusters: Are Lensing Clusters Overconcentrated?" In: ApJ 699.2 (July 2009), pp. 1038–1052. DOI: 10.1088/0004-637X/699/2/1038. arXiv: 0901.4372 [astro-ph.CO].

[283] M. Sereno, Ph. Jetzer, and M. Lubini. "On the overconcentration problem of strong lensing clusters". In: MNRAS 403.4 (Apr. 2010), pp. 2077–2087. DOI: 10.1111/j.1365-2966.2010.16248.x. arXiv: 1001.1696 [astro-ph.CO].

[284] Doron Lemze, Sharon Sadeh, and Yoel Rephaeli. "Cluster contribution to the X-ray background as a cosmological probe". In: MNRAS 397.4 (Aug. 2009), pp. 1876–1884. DOI: 10.1111/j.1365-2966.2009.14882.x. arXiv: 0904.1983 [astro-ph.CO].

[285] Cosimo Fedeli and Matthias Bartelmann. "Effects of early dark energy on strong cluster lensing". In: *Astron. Astrophys.* 461 (2007), pp. 49–57. DOI: 10.1051/0004-6361:20065976. arXiv: astro-ph/0607069.

[286] S. Sadeh and Y. Rephaeli. "The probability distribution of cluster formation times and implied Einstein Radii". In: *Mon. Not. Roy. Astron. Soc.* 388 (2008), p. 1759. DOI: 10.1111/j.1365-2966.2008.13501.x. arXiv: 0804.0892 [astro-ph].

[287] Matthew J. Francis, Geraint F. Lewis, and Eric V. Linder. "Can Early Dark Energy be Detected in Non-Linear Structure?" In: *Mon. Not. Roy. Astron. Soc.* 394 (2008), pp. 605–614. DOI: 10.1111/j.1365-2966.2008.14286.x. arXiv: 0808.2840 [astro-ph].

[288] Margherita Grossi and Volker Springel. "The impact of Early Dark Energy on non-linear structure formation". In: *Mon. Not. Roy. Astron. Soc.* 394 (2009), pp. 1559–1574. DOI: 10.1111/j.1365-2966.2009.14432.x. arXiv: 0809.3404 [astro-ph].

[289] Alan R. Duffy et al. "Impact of baryon physics on dark matter structures: a detailed simulation study of halo density profiles". In: MNRAS 405.4 (July 2010), pp. 2161–2178. DOI: 10.1111/j.1365-2966.2010.16613.x. arXiv: 1001.3447 [astro-ph.CO].

[290] James M. G. Mead et al. "The impact of AGN feedback and baryonic cooling on galaxy clusters as gravitational lenses". In: MNRAS 406.1 (July 2010), pp. 434–444. DOI: 10.1111/j.1365-2966.2010.16674.x. arXiv: 1001.2281 [astro-ph.CO].

[291] Lindsay J. King and James M. G. Mead. "The mass-concentration relationship of virialized haloes and its impact on cosmological observables". In: MNRAS 416.4 (Oct. 2011), pp. 2539–2549. DOI: 10.1111/j.1365-2966.2011.19009.x. arXiv: 1105.3155 [astro-ph.CO].

[292] Enrico Laudato, Vincenzo Salzano, and Keiichi Umetsu. "Multicomponent DHOST analysis in galaxy clusters". In: *Mon. Not. Roy. Astron. Soc.* 511.2 (2022), pp. 1878–1892. DOI: 10.1093/mnras/stac180. arXiv: 2110.11019 [astro-ph.CO].

[293] M. Meneghetti et al. "The MUSIC of CLASH: predictions on the concentration-mass relation". In: *Astrophys. J.* 797.1 (2014), p. 34. DOI: 10.1088/0004-637X/797/1/34. arXiv: 1404.1384 [astro-ph.CO].

[294] Keiichi Umetsu. "Cluster–galaxy weak lensing". In: *Astron. Astrophys. Rev.* 28.1 (2020), p. 7. DOI: 10.1007/s00159-020-00129-w. arXiv: 2007.00506 [astro-ph.CO].

[295] Keiichi Umetsu et al. "CLASH: Joint Analysis of Strong-Lensing, Weak-Lensing Shear and Magnification Data for 20 Galaxy Clusters". In: *Astrophys. J.* 821.2 (2016), p. 116. DOI: 10.3847/0004-637X/821/2/116. arXiv: 1507.04385 [astro-ph.CO].

[296] Keiichi Umetsu et al. "CLASH: Weak-Lensing Shear-and-Magnification Analysis of 20 Galaxy Clusters". In: *Astrophys. J.* 795.2 (2014), p. 163. DOI: 10.1088/0004-637X/795/2/163. arXiv: 1404.1375 [astro-ph.CO].

[297] Adi Zitrin et al. "Hubble Space Telescope Combined Strong and Weak Lensing Analysis of the CLASH Sample: Mass and Magnification Models and Systematic Uncertainties". In: *Astrophys. J.* 801.1 (2015), p. 44. DOI: 10.1088/0004-637X/801/1/44. arXiv: 1411.1414 [astro-ph.CO].

[298] Massimo Meneghetti. *Introduction to Gravitational Lensing*. Nov. 2016. URL: http://www.ita.uni-heidelberg.de/~massimo/sub/Lectures/gl_all.pdf.

[299] Marco Crisostomi and Kazuya Koyama. "Self-accelerating universe in scalar-tensor theories after GW170817". In: *Phys. Rev. D* 97.8 (2018), p. 084004. DOI: 10.1103/PhysRevD.97.084004. arXiv: 1712.06556 [astro-ph.CO].

[300] Takashi Hiramatsu and Daisuke Yamauchi. "Testing gravity theories with cosmic microwave background in the degenerate higher-order scalar-tensor theory". In: *Phys. Rev. D* 102.8 (2020), p. 083525. DOI: 10.1103/PhysRevD.102.083525. arXiv: 2004.09520 [astro-ph.CO].

[301] Takashi Hiramatsu. "CMB constraints on DHOST theories". In: *JCAP* 10 (2022), p. 035. DOI: 10.1088/1475-7516/2022/10/035. arXiv: 2205.11559 [astro-ph.CO].

[302] Julio F. Navarro, Carlos S. Frenk, and Simon D. M. White. "A Universal Density Profile from Hierarchical Clustering". In: ApJ 490.2 (Dec. 1997), pp. 493–508. DOI: 10.1086/304888. arXiv: astro-ph/9611107 [astro-ph].

[303] Keiichi Umetsu et al. "Cluster Mass Profiles from a Bayesian Analysis of Weak-lensing Distortion and Magnification Measurements: Applications to Subaru Data". In: ApJ 729.2, 127 (Mar. 2011), p. 127. DOI: 10.1088/0004-637X/729/2/127. arXiv: 1011.3044 [astro-ph.CO].

[304] L. J. Beraldo e Silva, M. Lima, and L. Sodre. "Testing phenomenological and theoretical models of dark matter density profiles with galaxy clusters". In: *Mon. Not. Roy. Astron. Soc.* 436 (2013), p. 2616. DOI: 10.1093/mnras/stt1761. arXiv: 1301.1684 [astro-ph.CO].

[305] Andrew B. Newman et al. "The Density Profiles of Massive, Relaxed Galaxy Clusters. I. The Total Density Over Three Decades in Radius". In: ApJ 765.1, 24 (Mar. 2013), p. 24. DOI: 10.1088/0004-637X/765/1/24. arXiv: 1209.1391 [astro-ph.CO].

[306] Nobuhiro Okabe et al. "LoCuSS: The Mass Density Profile of Massive Galaxy Clusters at z=0.2". In: *Astrophys. J. Lett.* 769 (2013), p. L35. DOI: 10.1088/2041-8205/769/2/L35. arXiv: 1302.2728 [astro-ph.CO].

[307] Mauro Sereno et al. "PSZ2LenS. Weak lensing analysis of the Planck clusters in the CFHTLenS and in the RCSLenS". In: *Mon. Not. Roy. Astron. Soc.* 472.2 (2017), pp. 1946–1971. DOI: 10.1093/mnras/stx2085. arXiv: 1703.06886 [astro-ph.CO].

[308] I. Chiu et al. "Baryon Content in a Sample of 91 Galaxy Clusters Selected by the South Pole Telescope at $0.2 < z < 1.25$". In: *Mon. Not. Roy. Astron. Soc.* 478.3 (2018), pp. 3072–3099. DOI: 10.1093/mnras/sty1284. arXiv: 1711.00917 [astro-ph.CO].

[309] A. Cavaliere and R. Fusco-Femiano. "The Distribution of Hot Gas in Clusters of Galaxies". In: *Astron. Astrophys.* 70 (Nov. 1978), p. 677.

[310] Kevin C. Cooke et al. "Star Formation in Intermediate Redshift 0.2 < z < 0.7 Brightest Cluster Galaxies". In: ApJ 833.2, 224 (Dec. 2016), p. 224. DOI: 10.3847/1538-4357/833/2/224. arXiv: 1610.05310 [astro-ph.GA].

[311] Claire Burke, Matt Hilton, and Chris Collins. "Co-evolution of BCGs and ICL using CLASH". In: *Mon. Not. Roy. Astron. Soc.* 449 (2015), p. 2353. DOI: 10.1093/mnras/stv450. arXiv: 1503.04321 [astro-ph.CO].

[312] Yong Tian et al. "The Radial Acceleration Relation in CLASH Galaxy Clusters". In: *Astrophys. J.* 896.1 (2020), p. 70. DOI: 10.3847/1538-4357/ab8e3d. arXiv: 2001.08340 [astro-ph.CO].

[313] F. Durret et al. "Link between brightest cluster galaxy properties and large scale extensions of 38 DAFT/FADA and CLASH clusters in the redshift range 0.2 < z < 0.9". In: A&A 622, A78 (Feb. 2019), A78. DOI: 10.1051/0004-6361/201834374. arXiv: 1812.03672 [astro-ph.GA].

[314] J. L. Sérsic. "Influence of the atmospheric and instrumental dispersion on the brightness distribution in a galaxy". In: *Boletin de la Asociacion Argentina de Astronomia La Plata Argentina* 6 (Feb. 1963), pp. 41–43.

[315] N. Caon, M. Capaccioli, and M. D'Onofrio. "On the shape of the light profiles of early type galaxies". In: *Mon. Not. Roy. Astron. Soc.* 265 (1993), p. 1013. DOI: 10.1093/mnras/265.4.1013. arXiv: astro-ph/9309013.

[316] P. Prugniel and F. Simien. "The fundamental plane of early-type galaxies: non-homology of the spatial structure." In: A&A 321 (May 1997), pp. 111–122.

[317] Gastao B. Lima Neto, Daniel Gerbal, and Isabel Marquez. "The specific entropy of elliptical galaxies: an explanation for profile shape distance indicators?" In: *Mon. Not. Roy. Astron. Soc.* 309 (1999), p. 481. DOI: 10.1046/j.1365-8711.1999.02849.x. arXiv: astro-ph/9905048.

[318] G. Bothun, C. Impey, and S. McGaugh. "LOW-SURFACE-BRIGHTNESS GALAXIES: HIDDEN GALAXIES REVEALED". In: *Publications of the Astronomical Society of the Pacific* 109.737 (July 1997), p. 745. DOI: 10.1086/133941. URL: https://dx.doi.org/10.1086/133941.

[319] K. C. Freeman. "On the Disks of Spiral and S0 Galaxies". In: ApJ 160 (June 1970), p. 811. DOI: 10.1086/150474.

[320] Roberto G. Abraham and Pieter G. van Dokkum. "Ultra–Low Surface Brightness Imaging with the Dragonfly Telephoto Array". In: *Publ. Astron. Soc. Pac.* 126.935 (2016), pp. 55–69. DOI: 10.1086/674875. arXiv: 1401.5473 [astro-ph.IM].

[321] Pieter G. van Dokkum, Roberto Abraham, and Allison Merritt. "First Results from the Dragonfly Telephoto Array: The Apparent Lack of a Stellar Halo in the Massive Spiral Galaxy M101". In: ApJ 782.2, L24 (Feb. 2014), p. L24. DOI: 10.1088/2041-8205/782/2/L24. arXiv: 1401.5467 [astro-ph.GA].

[322] Allison Merritt, Pieter van Dokkum, and Roberto Abraham. "The Discovery of Seven Extremely Low Surface Brightness Galaxies in the Field of the Nearby Spiral Galaxy M101". In: ApJ 787.2, L37 (June 2014), p. L37. DOI: 10.1088/2041-8205/787/2/L37. arXiv: 1406.2315 [astro-ph.GA].

[323] M. P. Ulmer et al. "Low Surface Brightness Galaxies in the Core of the Coma Cluster". In: AJ 112 (Dec. 1996), p. 2517. DOI: 10.1086/118198. arXiv: astro-ph/9610040 [astro-ph].

[324] C. Adami et al. "VizieR Online Data Catalog: A deep wide survey of faint low surface brightness galaxies in the direction of the Coma cluster of galaxies." In: *VizieR Online Data Catalog*, J/A+A/459/679 (May 2007), J/A+A/459/679. DOI: 10.26093/cds/vizier.34590679.

[325] I. D. Karachentsev et al. "Dwarf galaxy candidates found on the SERC EJ sky survey". In: A&AS 145 (Sept. 2000), pp. 415–423. DOI: 10.1051/aas:2000249.

[326] Christopher J. Conselice. "Ultra-diffuse Galaxies Are a Subset of Cluster Dwarf Elliptical/Spheroidal Galaxies". In: *Research Notes of the American Astronomical Society* 2.1, 43 (Mar. 2018), p. 43. DOI: 10.3847/2515-5172/aab7f6. arXiv: 1803.06927 [astro-ph.GA].

[327] Shiyin Shen et al. "The Size distribution of galaxies in the Sloan Digital Sky Survey". In: *Mon. Not. Roy. Astron. Soc.* 343 (2003), p. 978. DOI: 10.1046/j.1365-8711.2003.06740.x. arXiv: astro-ph/0301527.

[328] J. Christopher Mihos. "Intragroup and Intracluster Light". In: *The General Assembly of Galaxy Halos: Structure, Origin and Evolution*. Ed. by A. Bragaglia et al. Vol. 317. Aug. 2016, pp. 27–34. DOI: 10.1017/S1743921315006857. arXiv: 1510.01929 [astro-ph.GA].

[329] Roberto P. Muñoz et al. "Unveiling a Rich System of Faint Dwarf Galaxies in the Next Generation Fornax Survey". In: ApJ 813.1, L15 (Nov. 2015), p. L15. DOI: 10.1088/2041-8205/813/1/L15. arXiv: 1510.02475 [astro-ph.GA].

[330] Javier Román and Ignacio Trujillo. "Ultra-diffuse galaxies outside clusters: clues to their formation and evolution". In: MNRAS 468.4 (July 2017), pp. 4039–4047. DOI: 10.1093/mnras/stx694. arXiv: 1610.08980 [astro-ph.GA].

[331] Lukas Leisman et al. "(Almost) Dark Galaxies in the ALFALFA Survey: Isolated H I-bearing Ultra-diffuse Galaxies". In: ApJ 842.2, 133 (June 2017), p. 133. DOI: 10.3847/1538-4357/aa7575. arXiv: 1703.05293 [astro-ph.GA].

[332] Javier Román et al. "Discovery of a red ultra-diffuse galaxy in a nearby void based on its globular cluster luminosity function". In: MNRAS 486.1 (June 2019), pp. 823–835. DOI: 10.1093/mnras/stz835. arXiv: 1903.08168 [astro-ph.GA].

[333] Pavel E. Mancera Piña et al. "The evolution of ultra-diffuse galaxies in nearby galaxy clusters from the Kapteyn IAC WEAVE INT Clusters Survey". In: MNRAS 485.1 (May 2019), pp. 1036–1052. DOI: 10.1093/mnras/stz238. arXiv: 1901.07577 [astro-ph.GA].

[334] N. C. Amorisco and A. Loeb. "Ultradiffuse galaxies: the high-spin tail of the abundant dwarf galaxy population". In: MNRAS 459.1 (June 2016), pp. L51–L55. DOI: 10.1093/mnrasl/slw055. arXiv: 1603.00463 [astro-ph.GA].

[335] Yu Rong et al. "A Universe of ultradiffuse galaxies: theoretical predictions from ΛCDM simulations". In: MNRAS 470.4 (Oct. 2017), pp. 4231–4240. DOI: 10.1093/mnras/stx1440. arXiv: 1703.06147 [astro-ph.GA].

[336] Oscar Agertz and Andrey V. Kravtsov. "On the interplay between star formation and feedback in galaxy formation simulations". In: *Astrophys. J.* 804.1 (2015), p. 18. DOI: 10.1088/0004-637X/804/1/18. arXiv: 1404.2613 [astro-ph.GA].

[337] Amy E. Reines, Jenny E. Greene, and Marla Geha. "Dwarf Galaxies with Optical Signatures of Active Massive Black Holes". In: *Astrophys. J.* 775 (2013), p. 116. DOI: 10.1088/0004-637X/775/2/116. arXiv: 1308.0328 [astro-ph.CO].

[338] Yutaka Fujita. "Pre-processing of galaxies before entering a cluster". In: *Publ. Astron. Soc. Jap.* 56 (2004), p. 29. DOI: 10.1093/pasj/56.1.29. arXiv: astro-ph/0311193.

[339] C. Yozin and K. Bekki. "The quenching and survival of ultra diffuse galaxies in the Coma cluster". In: MNRAS 452.1 (Sept. 2015), pp. 937–943. DOI: 10.1093/mnras/stv1073. arXiv: 1507.05161 [astro-ph.GA].

[340] Michael A. Beasley and Ignacio Trujillo. "Globular Clusters Indicate That Ultra-diffuse Galaxies Are Dwarfs". In: ApJ 830.1, 23 (Oct. 2016), p. 23. DOI: 10.3847/0004-637X/830/1/23. arXiv: 1604.08024 [astro-ph.GA].

[341] Eric W. Peng and Sungsoon Lim. "A Rich Globular Cluster System in Dragonfly 17: Are Ultra-diffuse Galaxies Pure Stellar Halos?" In: ApJ 822.2, L31 (May 2016), p. L31. DOI: 10.3847/2041-8205/822/2/L31. arXiv: 1604.07496 [astro-ph.GA].

[342] Pieter van Dokkum et al. "A High Stellar Velocity Dispersion and ~100 Globular Clusters for the Ultra-diffuse Galaxy Dragonfly 44". In: *Astrophys. J. Lett.* 828.1 (2016), p. L6. DOI: 10.3847/2041-8205/828/1/L6. arXiv: 1606.06291 [astro-ph.GA].

[343] Pieter van Dokkum et al. "Spatially-resolved stellar kinematics of the ultra diffuse galaxy Dragonfly 44. I. Observations, kinematics, and cold dark matter halo fits". In: *Astrophys. J.* 880 (2019), p. 91. DOI: 10.3847/1538-4357/ab2914. arXiv: 1904.04838 [astro-ph.GA].

[344] Andrea V. Macciò et al. "Creating a galaxy lacking dark matter in a dark matter-dominated universe". In: MNRAS 501.1 (Feb. 2021), pp. 693–700. DOI: 10.1093/mnras/staa3716. arXiv: 2010.02245 [astro-ph.GA].

[345] Go Ogiya. "Tidal stripping as a possible origin of the ultra diffuse galaxy lacking dark matter". In: *Mon. Not. Roy. Astron. Soc.* 480.1 (2018), pp. L106–L110. DOI: 10.1093/mnrasl/sly138. arXiv: 1804.06421 [astro-ph.GA].

[346] Adi Nusser. "Orbital Decay of Globular Clusters in the Galaxy with Little Dark Matter". In: ApJ 863.2, L17 (Aug. 2018), p. L17. DOI: 10.3847/2041-8213/aad6ee. arXiv: 1806.01812 [astro-ph.GA].

[347] Ignacio Trujillo et al. "A distance of 13 Mpc resolves the claimed anomalies of the galaxy lacking dark matter". In: MNRAS 486.1 (June 2019), pp. 1192–1219. DOI: 10.1093/mnras/stz771. arXiv: 1806.10141 [astro-ph.GA].

[348] Zili Shen et al. "A Tip of the Red Giant Branch Distance of 22.1 ± 1.2 Mpc to the Dark Matter Deficient Galaxy NGC 1052-DF2 from 40 Orbits of Hubble Space Telescope Imaging". In: ApJ 914.1, L12 (June 2021), p. L12. DOI: 10.3847/2041-8213/ac0335. arXiv: 2104.03319 [astro-ph.GA].

[349] Pieter van Dokkum et al. "A trail of dark-matter-free galaxies from a bullet-dwarf collision". In: *Nature* 605.7910 (2022), pp. 435–439. DOI: 10.1038/s41586-022-04665-6. arXiv: 2205.08552 [astro-ph.GA].

[350] James Binney and Scott Tremaine. *Galactic Dynamics: Second Edition*. 2008.

[351] Gary A. Mamon and Ewa L. Lokas. "Confronting lambda-CDM with the optical observations of elliptical galaxies. 2. Weighing the dark matter component". In: *Mon. Not. Roy. Astron. Soc.* 363 (2005). [Addendum: Mon.Not.Roy.Astron.Soc. 370, 1582 (2006)], pp. 705–722. DOI: 10.1111/j.1365-2966.2005.09400.x. arXiv: astro-ph/0405491.

[352] HongSheng Zhao. "Analytical models for galactic nuclei". In: *Mon. Not. Roy. Astron. Soc.* 278 (1996), pp. 488–496. DOI: 10.1093/mnras/278.2.488. arXiv: astro-ph/9509122.

[353] Marc Wenger et al. "The simbad astronomical database". In: *Astron. Astrophys. Suppl. Ser.* 143 (2000), p. 9. DOI: 10.1051/aas:2000332. arXiv: astro-ph/0002110.

[354] Asher Wasserman et al. "Spatially Resolved Stellar Kinematics of the Ultra-Diffuse Galaxy Dragonfly 44: II. Constraints on Fuzzy Dark Matter". In: (May 2019). DOI: 10.3847/1538-4357/ab3eb9. arXiv: 1905.10373 [astro-ph.GA].

[355] Ray G. Carlberg, H. K. C. Yee, and E. Ellingson. "The Average mass and light profiles of galaxy clusters". In: *Astrophys. J.* 478 (1997), p. 462. DOI: 10.1086/303805. arXiv: astro-ph/9512087.

[356] Pedro Colín, Anatoly A. Klypin, and Andrey V. Kravtsov. "Velocity Bias in a Λ Cold Dark Matter Model". In: *The Astrophysical Journal* 539.2 (Aug. 2000), p. 561. DOI: 10.1086/309248. URL: https://dx.doi.org/10.1086/309248.

[357] L. P. Osipkov. "Spherical systems of gravitating bodies with an ellipsoidal velocity distribution". In: *Soviet Astronomy Letters* 5 (Jan. 1979), pp. 42–44.

[358] D. Merritt. "Distribution functions for spherical galaxies". In: MNRAS 214 (June 1985), 25P–28P. DOI: 10.1093/mnras/214.1.25P.

[359] Gary A. Mamon, Andrea Biviano, and Gwenaël Boué. "MAMPOSSt: Modelling Anisotropy and Mass Profiles of Observed Spherical Systems - I. Gaussian 3D velocities". In: MNRAS 429.4 (Mar. 2013), pp. 3079–3098. DOI: 10.1093/mnras/sts565. arXiv: 1212.1455 [astro-ph.CO].

[360] Hong-Xin Zhang et al. "The Next Generation Virgo Cluster Survey. VI. The Kinematics of Ultra-compact Dwarfs and Globular Clusters in M87". In: *Astrophys. J.* 802.1 (2015), p. 30. DOI: 10.1088/0004-637X/802/1/30. arXiv: 1501.03167 [astro-ph.GA].

[361] S. D. M. White and M. J. Rees. "Core condensation in heavy halos: a two-stage theory for galaxy formation and clustering." In: MNRAS 183 (May 1978), pp. 341–358. DOI: 10.1093/mnras/183.3.341.

[362] Cheng Li et al. "Internal Kinematics of Groups of Galaxies in the Sloan Digital Sky Survey Data Release 7". In: ApJ 758.1, 50 (Oct. 2012), p. 50. DOI: 10.1088/0004-637X/758/1/50. arXiv: 1206.3566 [astro-ph.CO].

[363] Malin Velander et al. "CFHTLenS: the relation between galaxy dark matter haloes and baryons from weak gravitational lensing". In: MNRAS 437.3 (Jan. 2014), pp. 2111–2136. DOI: 10.1093/mnras/stt2013. arXiv: 1304.4265 [astro-ph.CO].

[364] A. V. Kravtsov, A. A. Vikhlinin, and A. V. Meshcheryakov. "Stellar Mass—Halo Mass Relation and Star Formation Efficiency in High-Mass Halos". In: *Astronomy Letters* 44.1 (Jan. 2018), pp. 8–34. DOI: 10.1134/S1063773717120015. arXiv: 1401.7329 [astro-ph.CO].

[365] Volker Springel and Lars Hernquist. "Cosmological smoothed particle hydrodynamics simulations: a hybrid multiphase model for star formation". In: MNRAS 339.2 (Feb. 2003), pp. 289–311. DOI: 10.1046/j.1365-8711.2003.06206.x. arXiv: astro-ph/0206393 [astro-ph].

[366] D. Nelson et al. "The illustris simulation: Public data release". In: *Astronomy and Computing* 13 (Nov. 2015), pp. 12–37. DOI: 10.1016/j.ascom.2015.09.003. arXiv: 1504.00362 [astro-ph.CO].

[367] S. McAlpine et al. "The EAGLE simulations of galaxy formation: Public release of halo and galaxy catalogues". In: *Astronomy and Computing* 15 (Apr. 2016), pp. 72–89. DOI: 10.1016/j.ascom.2016.02.004. arXiv: 1510.01320 [astro-ph.GA].

[368] Rachel S. Somerville and Romeel Davé. "Physical Models of Galaxy Formation in a Cosmological Framework". In: ARA&A 53 (Aug. 2015), pp. 51–113. DOI: 10.1146/annurev-astro-082812-140951. arXiv: 1412.2712 [astro-ph.GA].

[369] Darren J. Croton et al. "Semi-Analytic Galaxy Evolution (SAGE): Model Calibration and Basic Results". In: ApJS 222.2, 22 (Feb. 2016), p. 22. DOI: 10.3847/0067-0049/222/2/22. arXiv: 1601.04709 [astro-ph.GA].

[370] Xiaohu Yang et al. "Evolution of the Galaxy-Dark Matter Connection and the Assembly of Galaxies in Dark Matter Halos". In: ApJ 752.1, 41 (June 2012), p. 41. DOI: 10.1088/0004-637X/752/1/41. arXiv: 1110.1420 [astro-ph.CO].

[371] J. Carretero et al. "An algorithm to build mock galaxy catalogues using MICE simulations". In: MNRAS 447.1 (Feb. 2015), pp. 646–670. DOI: 10.1093/mnras/stu2402. arXiv: 1411.3286 [astro-ph.GA].

[372] Benjamin P. Moster, Thorsten Naab, and Simon D. M. White. "Galactic star formation and accretion histories from matching galaxies to dark matter haloes". In: MNRAS 428.4 (Feb. 2013), pp. 3121–3138. DOI: 10.1093/mnras/sts261. arXiv: 1205.5807 [astro-ph.CO].

[373] Aldo Rodríguez-Puebla et al. "Constraining the galaxy-halo connection over the last 13.3 Gyr: star formation histories, galaxy mergers and structural properties". In: MNRAS 470.1 (Sept. 2017), pp. 651–687. DOI: 10.1093/mnras/stx1172. arXiv: 1703.04542 [astro-ph.GA].

[374] Peter S. Behroozi, Risa H. Wechsler, and Charlie Conroy. "The Average Star Formation Histories of Galaxies in Dark Matter Halos from z = 0-8". In: ApJ 770.1, 57 (June 2013), p. 57. DOI: 10.1088/0004-637X/770/1/57. arXiv: 1207.6105 [astro-ph.CO].

[375] G. D'Agostini. "Probability and Measurement Uncertainty in Physics - a Bayesian Primer". In: (1995). arXiv: hep-ph/9512295 [hep-ph].

[376] IEC ISO and BIPM OIML. "Guide to the Expression of Uncertainty in Measurement". In: *Geneva, Switzerland* 122 (1995).

[377] Roberto Trotta. "Bayesian Methods in Cosmology". In: Jan. 2017. arXiv: 1701.01467 [astro-ph.CO].

[378] David GT Denison et al. *Bayesian methods for nonlinear classification and regression*. Vol. 386. John Wiley and Sons, 2002.

[379] Sanjib Sharma. "Markov Chain Monte Carlo Methods for Bayesian Data Analysis in Astronomy". In: ARA&A 55.1 (Aug. 2017), pp. 213–259. DOI: 10.1146/annurev-astro-082214-122339. arXiv: 1706.01629 [astro-ph.IM].

[380] Luis E. Padilla et al. "Cosmological Parameter Inference with Bayesian Statistics". In: *Universe* 7.7 (2021), p. 213. DOI: 10.3390/universe7070213. arXiv: 1903.11127 [astro-ph.CO].

[381] Bernd A. Berg. "Introduction to Markov Chain Monte Carlo Simulations and their Statistical Analysis". In: (2004). arXiv: cond-mat/0410490.

[382] W. K. Hastings. "Monte Carlo sampling methods using Markov chains and their applications". In: *Biometrika* 57.1 (1970), pp. 97–109. ISSN: 0006-3444. DOI: 10.1093/biomet/57.1.97. URL: https://doi.org/10.1093/biomet/57.1.97.

[383] Nicholas Metropolis et al. "Equation of State Calculations by Fast Computing Machines". In: *The Journal of Chemical Physics* 21.6 (1953), pp. 1087–1092. DOI: 10.1063/1.1699114. eprint: https://doi.org/10.1063/1.1699114. URL: https://doi.org/10.1063/1.1699114.

[384] Adrian E. Raftery. "Bayesian Model Selection in Social Research". In: *Sociological Methodology* 25 (1995), pp. 111–163. ISSN: 00811750, 14679531. URL: http://www.jstor.org/stable/271063.

[385] Andrew Gelman and Donald B. Rubin. "Inference from Iterative Simulation Using Multiple Sequences". In: *Statist. Sci.* 7.4 (1992), pp. 457–472. DOI: 10.1214/ss/1177011136. URL: https://doi.org/10.1214/ss/1177011136.

[386] Joanna Dunkley et al. "Fast and reliable mcmc for cosmological parameter estimation". In: *Mon. Not. Roy. Astron. Soc.* 356 (2005), pp. 925–936. DOI: 10.1111/j.1365-2966.2004.08464.x. arXiv: astro-ph/0405462.

[387] John Skilling. "Nested Sampling". In: *Bayesian Inference and Maximum Entropy Methods in Science and Engineering: 24th International Workshop on Bayesian Inference and Maximum Entropy Methods in Science and Engineering*. Ed. by Rainer Fischer, Roland Preuss, and Udo Von Toussaint. Vol. 735. American Institute of Physics Conference Series. Nov. 2004, pp. 395–405. DOI: 10.1063/1.1835238.

[388] Pia Mukherjee, David Parkinson, and Andrew R. Liddle. "A nested sampling algorithm for cosmological model selection". In: *Astrophys. J.* 638 (2006), pp. L51–L54.

[389] Greg Ashton et al. "Nested sampling for physical scientists". In: *Nature* 2 (2022). DOI: 10.1038/s43586-022-00121-x. arXiv: 2205.15570 [stat.CO].

[390] Harold Jeffreys. *The Theory of Probability*. Third. Oxford University Press, 1961.

[391] Savvas Nesseris and Juan Garcia-Bellido. "Is the Jeffreys' scale a reliable tool for Bayesian model comparison in cosmology?" In: *JCAP* 08 (2013), p. 036. DOI: 10.1088/1475-7516/2013/08/036. arXiv: 1210.7652 [astro-ph.CO].

[392] Will Handley and Pablo Lemos. "Quantifying tensions in cosmological parameters: Interpreting the DES evidence ratio". In: *Phys. Rev. D* 100.4 (2019), p. 043504. DOI: 10.1103/PhysRevD.100.043504. arXiv: 1902.04029 [astro-ph.CO].

[393] Will Handley and Pablo Lemos. "Quantifying dimensionality: Bayesian cosmological model complexities". In: *Phys. Rev. D* 100.2 (2019), p. 023512. DOI: 10.1103/PhysRevD.100.023512. arXiv: 1903.06682 [astro-ph.CO].

[394] B. Joachimi et al. "When tension is just a fluctuation: How noisy data affect model comparison". In: *Astron. Astrophys.* 647 (2021), p. L5. DOI: 10.1051/0004-6361/202039560. arXiv: 2102.09547 [astro-ph.CO].

[395] S. Kullback and R. A. Leibler. "On Information and Sufficiency". In: *The Annals of Mathematical Statistics* 22.1 (1951), pp. 79–86. DOI: 10.1214/aoms/1177729694.

[396] Vincenzo Salzano et al. "No need for dark matter in galaxy clusters within Galileon theory". In: *JCAP* 10 (2016), p. 033. DOI: 10.1088/1475-7516/2016/10/033. arXiv: 1607.02606 [astro-ph.CO].

[397] Vincenzo Salzano et al. "Breaking the Vainshtein screening in clusters of galaxies". In: *Phys. Rev. D* 95.4 (2017), p. 044038. DOI: 10.1103/PhysRevD.95.044038. arXiv: 1701.03517 [astro-ph.CO].

[398] Keiichi Umetsu and Benedikt Diemer. "Lensing Constraints on the Mass Profile Shape and the Splashback Radius of Galaxy Clusters". In: *Astrophys. J.* 836.2 (2017), p. 231. DOI: 10.3847/1538-4357/aa5c90. arXiv: 1611.09366 [astro-ph.CO].

[399] I-Non Chiu et al. "CLUMP-3D: Three-dimensional Shape and Structure of 20 CLASH Galaxy Clusters from Combined Weak and Strong Lensing". In: *Astrophys. J.* 860.2 (2018), p. 126. DOI: 10.3847/1538-4357/aac4a0. arXiv: 1804.00676 [astro-ph.CO].

[400] N. Okabe et al. "Central Mass Profiles of the Nearby Cool-core Galaxy Clusters Hydra A and A478". In: *Mon. Not. Roy. Astron. Soc.* 456.4 (2016), pp. 4475–4487. DOI: 10.1093/mnras/stv2916. arXiv: 1503.04412 [astro-ph.CO].

[401] B. Sartoris et al. "CLASH-VLT: a full dynamical reconstruction of the mass profile of Abell S1063 from 1 kpc out to the virial radius". In: *Astron. Astrophys.* 637 (2020), A34. DOI: 10.1051/0004-6361/202037521. arXiv: 2003.08475 [astro-ph.CO].

[402] Marc Postman et al. "Cluster Lensing And Supernova survey with Hubble (CLASH): An Overview". In: *Astrophys. J. Suppl.* 199 (2012), p. 25. DOI: 10.1088/0067-0049/199/2/25. arXiv: 1106.3328 [astro-ph.CO].

[403] M. Meneghetti et al. "The MUSIC of CLASH: predictions on the concentration-mass relation". In: *Astrophys. J.* 797.1 (2014), p. 34. DOI: 10.1088/0004-637X/797/1/34. arXiv: 1404.1384 [astro-ph.CO].

[404] Jack Sayers et al. "CLUMP-3D: the lack of non-thermal motions in galaxy cluster cores". In: *Mon. Not. Roy. Astron. Soc.* 505.3 (2021), pp. 4338–4344. DOI: 10.1093/mnras/stab1542. arXiv: 2102.06324 [astro-ph.CO].

[405] Keiichi Umetsu et al. "CLASH: Weak-Lensing Shear-and-Magnification Analysis of 20 Galaxy Clusters". In: *Astrophys. J.* 795.2 (2014), p. 163. DOI: 10.1088/0004-637X/795/2/163. arXiv: 1404.1375 [astro-ph.CO].

[406] Daisuke Nagai, Alexey Vikhlinin, and Andrey V. Kravtsov. "Testing X-ray Measurements of Galaxy Clusters with Cosmological Simulations". In: *Astrophys. J.* 655 (2007), pp. 98–108. DOI: 10.1086/509868. arXiv: astro-ph/0609247.

[407] M. Angelinelli et al. "Turbulent pressure support and hydrostatic mass-bias in the intracluster medium". In: *Mon. Not. Roy. Astron. Soc.* 495.1 (2020), pp. 864–885. DOI: 10.1093/mnras/staa975. arXiv: 1905.04896 [astro-ph.CO].

[408] Lorenzo Pizzuti et al. "Probing Vainsthein-screening gravity with galaxy clusters using internal kinematics and strong and weak lensing". In: *arXiv e-prints*, arXiv:2112.12139 (Dec. 2021), arXiv:2112.12139. arXiv: 2112.12139 [astro-ph.CO].

[409] Balakrishna S. Haridasu et al. "Testing generalized scalar-tensor theories of gravity with clusters of galaxies". In: *arXiv e-prints*, arXiv:2111.01101 (Nov. 2021), arXiv:2111.01101. arXiv: 2111.01101 [astro-ph.CO].

[410] L. Pizzuti et al. "CLASH-VLT: constraints on $f(R)$ gravity models with galaxy clusters using lensing and kinematic analyses". In: *JCAP* 07 (2017), p. 023. DOI: 10.1088/1475-7516/2017/07/023. arXiv: 1705.05179 [astro-ph.CO].

[411] A. Mercurio et al. "CLASH-VLT: Abell~S1063. Cluster assembly history and spectroscopic catalogue". In: *Astron. Astrophys.* 656 (2021), A147. DOI: 10.1051/0004-6361/202142168. arXiv: 2109.03305 [astro-ph.GA].

[412] Shin'ichi Hirano et al. "Constraining degenerate higher-order scalar-tensor theories with linear growth of matter density fluctuations". In: *Phys. Rev. D* 99.10 (2019), p. 104051. DOI: 10.1103/PhysRevD.99.104051. arXiv: 1902.02946 [astro-ph.CO].

[413] Daisuke Yamauchi and Naonori S. Sugiyama. "Second-order peculiar velocity field as a novel probe of scalar-tensor theories". In: *Phys. Rev. D* 105.6 (2022), p. 063515. DOI: 10.1103/PhysRevD.105.063515. arXiv: 2108.02382 [astro-ph.CO].

[414] Nicolas F. Martin et al. "Current Velocity Data on Dwarf Galaxy NGC 1052-DF2 do not Constrain it to Lack Dark Matter". In: ApJ 859.1, L5 (May 2018), p. L5. DOI: 10.3847/2041-8213/aac216. arXiv: 1804.04136 [astro-ph.GA].

[415] M. Milgrom. "A modification of the newtonian dynamics : implications for galaxy systems." In: ApJ 270 (July 1983), pp. 384–389. DOI: 10.1086/161132.

[416] Tousif Islam. "Enigmatic velocity dispersions of ultradiffuse galaxies in light of modified gravity theories and the radial acceleration relation". In: *Phys. Rev. D* 102.2 (2020), p. 024068. DOI: 10.1103/PhysRevD.102.024068. arXiv: 1910.09726 [gr-qc].

[417] Tousif Islam and Koushik Dutta. "Modified Gravity Theories in Light of the Anomalous Velocity Dispersion of NGC1052-DF2". In: *Phys. Rev. D* 100.10 (2019), p. 104049. DOI: 10.1103/PhysRevD.100.104049. arXiv: 1908.07160 [gr-qc].

[418] Hosein Haghi et al. "A new formulation of the external field effect in MOND and numerical simulations of ultra-diffuse dwarf galaxies - application to NGC 1052-DF2 and NGC 1052-DF4". In: MNRAS 487.2 (Aug. 2019), pp. 2441–2454. DOI: 10.1093/mnras/stz1465. arXiv: 1906.03268 [astro-ph.GA].

[419] B. Famaey, S. McGaugh, and M. Milgrom. "MOND and the dynamics of NGC 1052–DF2". In: *Mon. Not. Roy. Astron. Soc.* 480.1 (2018), pp. 473–476. DOI: 10.1093/mnras/sty1884. arXiv: 1804.04167 [astro-ph.GA].

[420] Philip D. Mannheim and Demosthenes Kazanas. "Exact Vacuum Solution to Conformal Weyl Gravity and Galactic Rotation Curves". In: ApJ 342 (July 1989), p. 635. DOI: 10.1086/167623.

[421] Philip D. Mannheim. "Alternatives to dark matter and dark energy". In: *Prog. Part. Nucl. Phys.* 56 (2006), pp. 340–445. DOI: 10.1016/j.ppnp.2005.08.001. arXiv: astro-ph/0505266.

[422] J. W. Moffat. "Scalar-tensor-vector gravity theory". In: *JCAP* 03 (2006), p. 004. DOI: 10.1088/1475-7516/2006/03/004. arXiv: gr-qc/0506021.

[423] Hosein Haghi et al. "A new formulation of the external field effect in MOND and numerical simulations of ultra-diffuse dwarf galaxies – application to NGC 1052-DF2 and NGC 1052-DF4". In: *Mon. Not. Roy. Astron. Soc.* 487.2 (2019), pp. 2441–2454. DOI: 10.1093/mnras/stz1465. arXiv: 1906.03268.

[424] Leanne D. Duffy and Karl van Bibber. "Axions as Dark Matter Particles". In: *New J. Phys.* 11 (2009), p. 105008. DOI: 10.1088/1367-2630/11/10/105008. arXiv: 0904.3346 [hep-ph].

[425] Enrico Laudato and Vincenzo Salzano. "DHOST gravity in ultra-diffuse galaxies—Part II: NGC 1052-DF4 and Dragonfly 44". In: *Eur. Phys. J. C* 83.5 (2023), p. 402. DOI: 10.1140/epjc/s10052-023-11564-1. arXiv: 2211.08839 [gr-qc].

[426] Enrico Laudato and Vincenzo Salzano. "DHOST gravity in ultra-diffuse galaxies – part I: the case of NGC1052-DF2". In: *Eur. Phys. J. C* 82.10 (2022), p. 935. DOI: 10.1140/epjc/s10052-022-10901-0. arXiv: 2206.06284 [gr-qc].

[427] Myung Gyoon Lee, Wendy L. Freedman, and Barry F. Madore. "The Tip of the Red Giant Branch as a Distance Indicator for Resolved Galaxies". In: *apj* 417 (Nov. 1993), p. 553. DOI: 10.1086/173334.

[428] John Tonry and Donald P. Schneider. "A New Technique for Measuring Extragalactic Distances". In: *aj* 96 (Sept. 1988), p. 807. DOI: 10.1086/114847.

[429] John P. Blakeslee et al. "Surface Brightness Fluctuations in the Hubble Space Telescope ACS/WFC F814W Bandpass and an Update on Galaxy Distances". In: *apj* 724.1 (Nov. 2010), pp. 657–668. DOI: 10.1088/0004-637X/724/1/657. arXiv: 1009.3270 [astro-ph.CO].

[430] Asher Wasserman et al. "A Deficit of Dark Matter from Jeans Modeling of the Ultra-diffuse Galaxy NGC 1052-DF2". In: *Astrophys. J. Lett.* 863.2 (2018), p. L15. DOI: 10.3847/2041-8213/aad779. arXiv: 1807.07069 [astro-ph.GA].

[431] Camila A. Correa et al. "The accretion history of dark matter haloes – III. A physical model for the concentration–mass relation". In: *Mon. Not. Roy. Astron. Soc.* 452.2 (2015), pp. 1217–1232. DOI: 10.1093/mnras/stv1363. arXiv: 1502.00391 [astro-ph.CO].

[432] Gary A. Mamon, Andrea Biviano, and Gwenael Boue. "MAMPOSSt: Modelling Anisotropy and Mass Profiles of Observed Spherical Systems. I. Gaussian 3D velocities". In: *Mon. Not. Roy. Astron. Soc.* 429 (2013), p. 3079. DOI: 10.1093/mnras/sts565. arXiv: 1212.1455 [astro-ph.CO].